The application of mass spectrometry-based techniques to full thickness skin tissue: method development and biochemical analysis in health and disease

Emily Jane Bliss

University College London Great Ormond Street Institute of Child Health

Doctor of Philosophy (PhD) Thesis in Child Health - Biochemistry

Declaration

I, Emily Jane Bliss confirm that the work presented in this thesis is my own. Where information has been derived from other sources, I confirm that this has been indicated in the thesis.

Emily Bliss, November 2016

Abstract

The work presented in this thesis collates a selection of mass spectrometry-based techniques which have been applied to skin samples in order to identify biochemical changes expressed in the skin in health and disease.

The results of an immunohistochemical study into the distribution of proteins within the skin revealed calmodulin-like protein 5 (CLP5) as having a different staining pattern between control and eczema samples. Further investigation revealed the role of CLP5 as a marker of keratinocyte differentiation and highlighted the importance of the calcium ion gradient in the skin for correct transport of proteases, protease inhibitors and antimicrobial proteins. Skin protease inhibitor and protease binding studies suggested that cystatin A could be a key player in manifestations of atopic eczema in susceptible children alongside two of its binding partners: dermcidin and caspase-14.

Skin is a challenging tissue to analyse using traditional proteomic techniques due to the high lipid content, insolubility and extensive cross-linking of proteins. However, this thesis presents a mass spectrometry compatible method for its analysis and how that method has been applied to the study of hypertrophic scarring and post-operative morbidity. For hypertrophic scarring the most interesting and clinically significant perspective of this investigation was that there are changes in the endogenous profile of healthy skin that could predict whether a healthy scar or a hypertrophic scar will form after surgical injury. For the second clinical outcome (post-operative morbidity) we identified pre-operative hypoxia, antioxidant levels and reactive oxygen species (ROS) as indicators of post-operative morbidity.

To conclude this thesis presents the work of a range of mass spectrometry techniques and has applied them to the study of human skin in health and disease. It demonstrates the versatility of mass spectrometry and has highlighted areas of clinical medicine where proteomics and a personalised medicine approach could be further investigated.

Table of contents

List of figures

List of tables

Abbreviations

2D-LC	Two dimensional liquid chromatography
ACN	Acetonitrile
ADAM	A disintegrin and metalloproteinase
AE	Atopic eczema
AGP	Alpha-1-acid glycoprotein
AmBic	Ammonium bicarbonate
ASB-14	Amidosulfobetaine-14
BH	Bleomycin hydrolase
C18	Carbon-18
Ca^{2+}	Calcium ion
CD	Cluster of differentiation
Cer[EOS]	30-linoyloxytriacontanoic acid-[(2S, 3R)-1,3-dihydroxyoctadec-4-en-zyl]-amide
CHAPS	3-[(3-Cholamidopropyl)dimethylammonio]-1-propanesulfonate hydrate
$CHCL_3$	Chloroform
CID	Collision induced dissociation
CLP3	Calmodulin-like protein 3
CLP5	Calmodulin-like protein 5
CS	Cholesterol sulphate
Da	Dalton
DAB	3, 3’ diaminobenzidine
DTE	1, 4-dithioerythritol
EDTA	Ethylenediaminetetraacetic acid
EI	Electron ionisation
ESI	Electrospray ionisation
ETD	Electron transfer dissociation
FA	Formic acid
FAM213A	Family with sequence similarity 213 member A
GA	General anaesthetic
GB1	Glucocerebroside
GB3	Globotriaosylceramide
GTP	Guanosine triphosphate
Guanidine HCl	Guanidine hydrochloride
HDMSE	High-definition label-free mass spectrometry
HLA	Human leucocyte antigen
IgE	Immunoglobulin E
IHC	Immunohistochemistry

IMS	Ion mobility separation
IS	Internal standard
LA	Local anaesthetic
LC	Liquid chromatography
LEKTI	Lympho-epithelial Kazal-type-related inhibitor
m/z	Mass-to-charge ratio
MALDI	Matrix-assisted laser desorption ionisation
MAP	Microtubule associated protein
MeOH	Methanol
MRM	Multiple reaction monitoring
MS	Mass spectrometer
MS/MS	Tandem mass spectrometry
MSE	Label-free mass spectrometry
MW	Molecular weight
NaCl	Sodium chloride
PBS	Phosphate buffered saline
PCA	Principal components analysis
PLS	Papillon-Lefèvre syndrome
PPIase	Peptidylprolyl isomerase
PTM	Post-translational modification
QToF	Quadrupole time-of-flight
RAC	Reticulate acropigmentation of Kitamura
ROS	Reactive oxygen species
RT	Room temperature
SDS-PAGE	Sodium dodecyl-polyacrylamide gel electrophoresis
SPINK5	Serine protease inhibitor Kazal-type 5
SRM	Selected reaction monitoring
TFA	Triflouracetic acid
TGF-β	Transforming growth factor beta
ToF	Time-of-flight
Tris	Trisma base
Tris-HCl	Trisma hydrochloride
TW IMS	Travelling wave ion mobility separation
UDMSE	Ultrahigh-definition label-free mass spectrometry
UPLC	Ultrahigh performance liquid chromatography
VEGF	Vascular endothelial growth factor

Acknowledgements

This thesis would not have been possible without the help, care and supervision of countless people, let alone for it to exist in the form presented here. The only place I can start is with Dr Kevin Mills and his research group at the UCL Great Ormond Street Institute of Child Health, circa late 2012, with whom I was undertaking my BSc research project at the time. If it were not for Kevin's enthusiasm, encouragement and belief that I could do a PhD, the last three years of my life would have undoubtedly taken a very different path. Not only was I made to feel welcome and supported by the group but I was inspired by the breadth and scope of translational medical research.

Kevin continued to be an excellent primary supervisor providing guidance and support throughout the inevitable ups and downs of a PhD. My two subsidiary supervisors: Dr Wendy Heywood and Prof Neil Sebire have also been brilliant, contributing ideas and keeping me on the straight and narrow when I would lose focus. I would also like to thank the nanoAcquity liquid chromatography system that I had the pleasure of "looking after" during my PhD. It has taught me patience beyond what I thought was humanly possible as well as skills in plumbing, fine motor movements and DIY that I never expected to acquire!

I must also thank everyone else in the Biological Mass Spectrometry Group and Great Ormond Street Hospital Histopathology Department for keeping spirits high and for showing willing to help. I have had an unforgettable three years which is thanks to my colleagues and a testament to the diversity and 'joie de vivre' which we are lucky enough to harbour. It would not have been nearly as enjoyable if it were not for the lunches in the park, late night pub trips, hugs, laughter, outrageous music, singing and dancing, which kept a smile on my face! I will miss each and every one of you.

I have been exceptionally supported by friends and family throughout this journey for which I am incredibly grateful. Even in my most intolerable of moments you have stuck by me and in whatever way possible managed to make me feel better. To each and every one of you, I will never be able to repay your kindness and cannot express my thankfulness enough.

And finally, thanks to my paternal grandparents who although completely out of their depth when trying to understand the concept of a PhD and what it entails, they never failed to show interest and enthusiasm for my studies. It saddens me that they did not live long enough to see the completion of this project, so I dedicate this thesis to them and their unwavering love.

Chapter 1

Introduction

1 Introduction

Contents

The title of this PhD thesis is “the application of mass spectrometry-based techniques to full thickness skin tissue: method development and biochemical analysis in health and disease”. This introduction explains the concepts of mass spectrometry, skin analysis and how they can be applied to health and diseases in humans.

1.1 Mass spectrometry

The concept of mass spectrometry began in the late nineteenth century when scientists observed canal rays. These are beams of positively charged ions which can be generated in an anode ray tube.[1; 2] Further observations led to the discovery that the path of these canal rays of charged ions would be deflected when in the presence of a magnetic field relative to the particles’ mass-to-charge ratio (m/z)[3]. J. J. Thomson was awarded the Nobel Prize in Physics in 1906 for his work on the conduction of electricity by gasses[4]. Since that time developments in mass spectrometry techniques and abilities have continued to grow. Today mass spectrometry can not only be used for the measurement of electrons and charged elements, but also macromolecules, such as small mass metabolites, lipid molecules, peptides and even large mass compounds such as whole proteins. Mass spectrometers have not changed much from the same three principles of the first basic instrument designed by Thompson. Although mass spectrometers now are significantly more sophisticated and sensitive, they all rely on the same principles of creation of ions or charged particles (ionisation), separation of those ions in a vacuum (mass analyser) and detection of those ions.

1.1.1 Ionisation techniques

In order to measure the mass-to-charge ratio of a compound using either a quadrupole or a time-of-flight (ToF) mass analyser as described in sections 1.1.3 and 1.1.4 the analyte must first be ionised, i.e. become charged. There are many different ways of ionising a compound, before being subjected to a magnetic or electric field within the mass analyser.

1.1.1.1 Electrospray ionisation (ESI)

Electrospray ionisation (ESI) is an ionisation technique that can produce either positively or negatively charged ions. It was first described in 1984 by Masamichi Yamashita and John Fenn[5]; the latter was awarded the Noble Prize in Chemistry in 2002 for his work developing ESI and its application to macromolecules[6]. The technique involves delivering the analyte in liquid form through a fine needle, into the mass spectrometer. A potential difference is applied across the gap between the tip of the needle and the entrance to the mass spectrometer. The charge at the tip of the needle causes the liquid to become polarised and disperses away in a cone-like formation from the tip of the needle in droplets. A jet of nitrogen gas is used to counteract the

condensable vapour produced and also to increase the rate of solvent evaporation from the charged droplets. ESI produces a range of charged species, not just singly charged molecules. It is termed a “soft” ionisation technique because it does not cause analyte fragmentation in the same way that other “hard” ionisation techniques might.

1.1.1.2 Matrix-assisted laser desorption ionisation (MALDI)

Matrix-assisted laser desorption ionisation (MALDI) is another form of “soft” ionisation that is used mainly with time-of-flight mass analysers (section 1.1.4). It differs from ESI by producing predominantly singly charged ions rather than multiply charged ions which are more often observed in ESI. For MALDI, the samples need to be mixed with a specific matrix and applied to the surface of a metal plate. Ionisation occurs when a laser beam pulsates across the plate, the laser’s energy is absorbed by the matrix crystals causing ionisation. Once ionised, a series of oppositely charged plates are used to attract and then accelerate each ion into the time-of-flight mass analyser. Each ion is given the same amount of energy, so the ions with a lower mass-to-charge ratio travel further than the ions with a greater mass-to-charge ratio. Hence, the mass-to-charge ratio of the ion can be determined by measuring its time-of-flight.

1.1.1.3 Electron ionisation (EI)

EI is an example of a ‘hard’ ionisation technique, described as such due to the highly energetic electrons used to interact with the gas or liquid analyte for ionisation. The electrons are generated from a heated metal wire in an electric circuit by thermionic emission, which are then accelerated towards the analyte. When one of these electrons collides with an analyte compound it knocks out an electron from the compound, creating a positively charged ion. This type of ionisation also simultaneously results in extensive fragmentation of the analyte compound.

1.1.2 Peptide sequencing using tandem mass spectrometry fragmentation

Modern mass spectrometry usually uses two mass spectrometers in conjunction and is more commonly referred to as tandem mass spectrometry. This can be two of the same type of mass analyser in tandem or two different types of mass analyser for example a quadrupole (section 1.1.3) and a time-of-flight (section 1.1.4) mass analyser in tandem. When two mass analysers of the same configuration are used, for example triple quadrupole-based platforms, they are generally designated as tandem mass spectrometry (MS/MS) systems (although technically quadrupole time-of-flight and ion trap systems also fit this label). After isolation of a precursor ion mass spectrometry can also be used to fragment that precursor ion into product ions, in

order to interrogate the composition of that precursor ion. In order to achieve this there is a fragmentation cell between the two mass analysers. Different fragmentation techniques are employed in depending on the configuration of the mass analysers.

Collision-induced dissociation (CID) uses an inert gas, such as argon to collide and fragment the ionised precursor. Electron-transfer dissociation (ETD) fragments positively charged molecules of ≥2+ charge, an electron is transferred to the precursor ion which destabilises the ion and causes fragmentation. Peptide sequencing by fragmentation of peptides into product ions is a very common technique used in the study of proteins by mass spectrometry. It is used to determine the specific amino acid sequence which makes up the protein of interest. Depending on the type of fragmentation used peptides will fragment at slightly different positions.

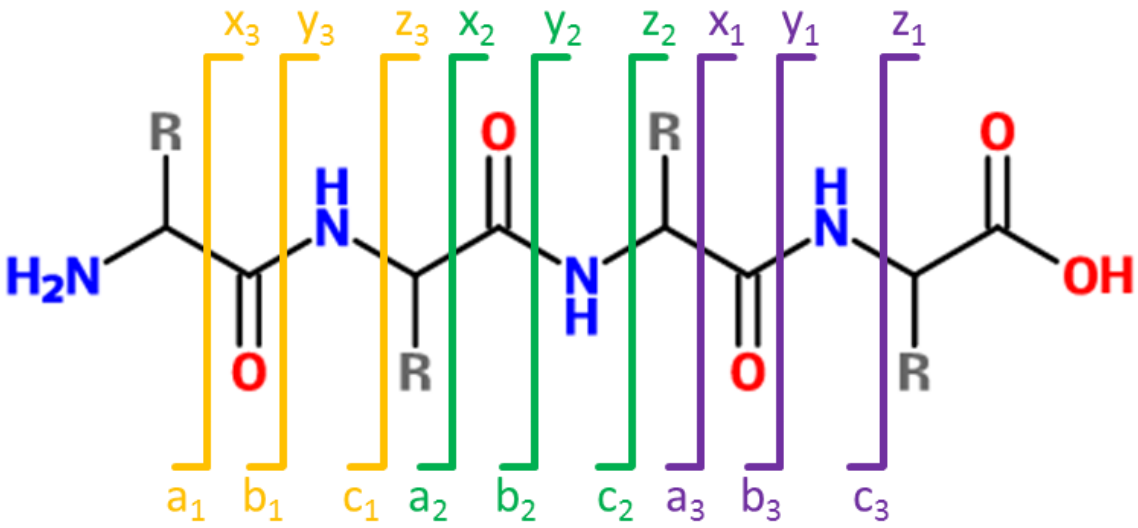

Figure 1.1. **Figure illustrating how a, b, c and x, y, z ions are formed when fragmenting a peptide sequence.** When a peptide sequence is fragmented for mass spectrometry a ions are associated with x ions, b with y and c with z. Depending on the type of fragmentation either a and x, b and y or c and z ions will be generated, depending on which bond of the peptide backbone is fragmented. a, b and c ions describe the N-terminus fragments and x, y and z ions describe the C-terminus fragments.

CID fragmentation produces b and y ions because the dissociation encourages fragmentation along the peptide bond (between the carboxyl group of one amino acid and the amino group of the adjacent amino acid) and ETD generates c and z ions because the dissociation encourages the protein backbone to fragment at the C-terminus side of the amine group[7].

1.1.3 Quadrupole mass analyser

A quadrupole describes a type of mass analyser, of ranging size depending on the mass-to-charge range for that quadrupole. A quadrupole is used to select ions of a specific mass-to-charge ratio and to divert any ions of a different mass-to-charge ratio. It comprises of four cylindrical metal rods, parallel to each other in a square formation. An oscillating radio frequency and direct current electric field are applied to the four rods this makes the ions travelling through the space between the rods oscillate in a similar manner, however only ions of the specific mass-to-charge ratio will be able to maintain their trajectory within the quadrupole.

1.1.4 Time-of-flight mass analyser

Time-of-flight (ToF) describes an analyser used in mass spectrometry to determine accurate mass of ionised compounds. This is based upon the time it takes for ions to travel a set distance within an electric field. The speed at which an ion travels the distance is determined by its mass-to-charge ratio, “lighter” ions will travel faster than “heavier” ones. The longer the path the ions need to take, the more accurate the mass measurement. Often a reflectron is used at one end of the ToF tube to redirect the ions back to the original end, thus doubling the flight path; this is described as ‘V’ mode. If the ions are reflected a total of three times it is described as ‘W’ mode. Operating in ‘W’ mode increases the resolution, however there is an approximate 50% reduction in sensitivity compared with ‘V’ mode.

The reflectron is a series of 12-20 lenses which creates an increasing ion-retarding field, the energy of the travelling ions will determine at which depth of the reflectron they will be redirected. Those ions travelling faster will penetrate further before being redirected and those ions travelling less fast will not penetrate as far before being redirected by the reflectron.

1.1.5 Post-translational modifications of proteins

Post-translational modifications (PTMs) describe any modification made to a protein after it has been transcribed. These range from minor mass changes such as the addition of a hydroxyl group (~15.99 Da), to large mass changes such as the addition of a glycan (~2000 Da). PTMs change the mass of the precursor ion and associated product ions, this needs to be taken into account when using mass spectrometry as mass changes of the analytes will affect the mass-to-charge ratio.

1.1.6 Liquid chromatography systems

Very simple pure samples can be injected directly into a mass spectrometer to determine the mass-to-charge ratio and fragmentation pattern. However, the more complex a sample, the greater the chance of other compounds having similar or the same mass-to-charge ratio as the analyte of interest in the sample. Those compounds will act in a similar manner in the magnetic or electric field so it becomes increasingly difficult to separate the individual mass-to-charge ratio information for those similar compounds.

In order to reduce the complexity of a sample a liquid chromatography (LC) separating unit may be used before the mass spectrometer. The path of a sample mixture would be that it is first injected into the LC system as a solution, adsorbed onto a stationary phase and eluted using a gradient between aqueous and organic mobile phases. Depending on the polarity of compounds within the sample mix they will elute from the stationary phase at different points on the aqueous/organic gradient. If the aqueous/organic gradient is extended for a longer period of time, there will be greater separation between compounds, ensuring that the likelihood of two compounds with the same mass-to-charge ratio entering the mass spectrometer at the same moment in time is reduced. Ionisation of the compounds will take place at the end of the LC system just before the ions enter the mass spectrometer, however with MALDI there is not usually a coupled LC system.

1.1.6.1 Two-dimensional liquid chromatography separation

Mass spectrometry can be used to analyse highly complex samples containing tens of thousands of molecules that would be observed in biological samples. However, this complexity can saturate the capacity of a mass spectrometer. To overcome this liquid chromatography systems (section 1.1.6) are used to reduce the complexity of samples entering the mass spectrometer at any one time. An additional dimension of separation can also be applied for very complex samples.

Two-dimensional liquid chromatography (2D-LC) separation further reduces the complexity of a sample by dividing it into multiple fractions using an additional column. In our laboratory these fractions are separated using two C18 reverse phase columns; one separates peptides using a high pH aqueous/organic gradient into fractions that are then eluted onto the second C18 reverse phase column and separated by a low pH aqueous/organic gradient.

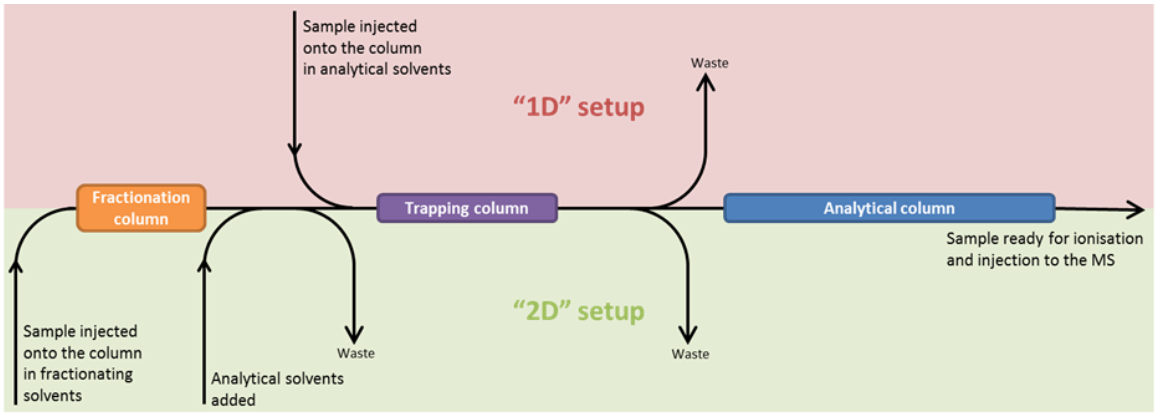

Figure 1.2. **Diagram illustrating the difference between the standard "1D" and the "2D"-LC setups.** In red the traditional "1D" setup of the LC system as described in section 1.1.6. The sample would be injected into the sampling loop, then desalted on the trapping column, before being chromatographically separated on the analytical column. In green, the "2D"-LC setup described here in section 1.1.6.1, includes the additional fractionation column where the original samples is separated into fractions according to pH, prior to desalting and chromatographic separation.

1.1.7 Label-free mass spectrometry (MS^E)

Label-free mass spectrometry (MS^E) analysis describes a method of quantifying data generated from a mass spectrometer such as a QToF mass spectrometer. It is called label-free because unlike similar techniques that require the addition of heavy labelled isotopes, MS^E does not in order to obtain quantitative results.

For MS analysis of proteins, they need to be digested into peptide fragments of suitable length (typically 6-25 amino acids long or 400-2500 m/z). Most intact proteins are too large for analysis with most commercially available mass spectrometers because they exceed the mass range and are too large to be fragmented (with the exception of low molecular weight proteins such as haemoglobin). Peptides are introduced into the mass spectrometer using liquid chromatography separation as described in sections 1.1.6 and 1.1.6.1. In MS^E mode the mass-to-charge ratio information about the ionised precursor peptide as well as the generated product ions from fragmentation are recorded. This information is obtained by using rapidly alternating low and high collision energy modes. Data from both collision energy states is acquired simultaneously, alternating between quantitation (of the precursor ion) and identification (from product ions and therefore fragmentation data) scans. The amino acid sequence from mass-to-charge ratio differences of the product ions is then "blast" searched against protein sequence databases and the protein from which the analysed peptide came from can be correctly identified.

1.1.7.1 Ion mobility mass spectrometry (IMS)

Ion mobility separation (IMS) is a technique which introduces an additional dimension of separation within the mass spectrometer for compounds which co-elute from the liquid chromatography system. There are different approaches to achieve IMS, here travelling-wave ion mobility (TW IMS) will be presented. In TW IMS the flow of ions enter the ion mobility cell where a helium gas is travelling against the ion flow. The ions meet the travelling waves of helium gas and co-eluting compounds are separated according to shape and size. Differences in shape and size of the ions mean that they pass through or over the waves of helium gas at different rates. Each ion will have a unique 'drift time' which is the time it took for that ion to pass through the ion mobility cell[8; 9].

When IMS is used in conjunction with MS^E it is described as high-definition label-free mass spectrometry ($HDMS^E$). IMS can be applied before or after precursor ion fragmentation depending on the application. If IMS is being used to separate out co-eluting precursors from the LC system then IMS will be applied before fragmentation. However, if it is being used to separate product ions of the same mass-to-charge ratio then IMS will be applied after fragmentation.

1.1.7.2 Ultra-high definition label-free mass spectrometry ($UDMS^E$)

Ultra-high definition label-free mass spectrometry ($UDMS^E$) is similar to $HDMS^E$ apart from the collision energy ramp. The nature of MS^E means that in the collision cell the collision energy is rapidly alternating between high and low collision energies: low energy maintains the intact precursor ion for quantitation and high energy to fragment the precursor into product ions for identification. Different peptide bonds require different amounts of energy to be broken, in MS^E (section 1.1.7) and $HDMS^E$ (section 1.1.7.1) a linear collision energy ramp is used during the high collision energy phase in order to achieve best fragmentation. In $UDMS^E$ it is possible to customise a non-linear gradient of collision energies during the high energy state based on the optimum fragmentation collision energy of a reference sample.

1.1.8 Tandem or triple quadrupole mass spectrometry (MS/MS)

Tandem or triple quadrupole mass spectrometry can be separated into three parts: MS_1, collision cell and MS_2. MS_1 and MS_2 are the same as the quadrupoles described in section 1.1.3. This type of tandem mass spectrometry is suited to a 'targeted' analysis more so than QToFs. Tandem mass spectrometry has superior quantitative ability compared to ToF analysers. Therefore, triple quadrupole mass spectrometers are the standard quantitative MS

used in medical and pharmaceutical industries. Tandem mass spectrometers can be operated in a variety of different scan modes: product-ion scan, precursor-ion scan, neutral-loss scan and multiple reaction monitoring (MRM). Due to the 'targeted' nature of tandem mass spectrometry analysis prior knowledge of ion masses for the compound or class of compounds being studied is required.

Product-ion scans are where the first mass analyser (MS_1) is fixed to select an ion of a specific mass-to-charge ratio, that ion is then fragmented and all the product ions detected. MRM is when MS_1 is fixed at a specific mass-to-charge ratio, that ion is fragmented and the second mass analyser (MS_2) is fixed at a second specific mass-to-charge ratio to allow a single fragment ion through. A precursor-ion scan is where MS_2 is fixed at a specific fragment ion mass-to-charge ratio and the precursor ions that fragment into that specific fragment ion are recorded. Finally a neutral-loss scan is where a neutral value x is selected and MS_2 is off-set by x m/z to detect fragment ions of x m/z less than their precursor ion.

Internal standards (ISs) can be used to enable quantification when using tandem mass spectrometry. An IS is usually of the same class as the analyte of interest but with a slightly different mass. The best ISs are those that are heavily or isotope-labelled versions of the compound being quantitated. These ISs behave exactly the same during preparation and liquid chromatography separation (they elute ever so slightly later on the chromatographic gradient) compensating for losses, changes in chromatography and ion suppression. A known amount of IS is added as early in the sample preparation process as possible. The IS can be differentiated from the compound of interest by mass difference detected by MS. Calibration curves can be used to calculate the exact amount of the analyte of interest.

1.2 Background to the skin

The skin is the largest organ covering the external surface of our body. It provides a barrier protecting the body from excessive water loss, microorganisms, physical trauma and ultra violet (UV) radiation. It is adapted highly to the environment such that individuals in equatorial regions have darker skin protecting them from UV radiation conversely individuals nearer the poles have lighter skin. Skin also thickens providing protection at sites of friction or repeated trauma, such as the feet and hands. Not only is the skin able to adapt to long term environmental factors, but it also responds to short term changes such as sweating in hot temperatures.[10] The skin has this multi-purpose ability due to its complex structure. The skin has three main layers: epidermis (uppermost layer), dermis and subcutaneous (lowermost layer).

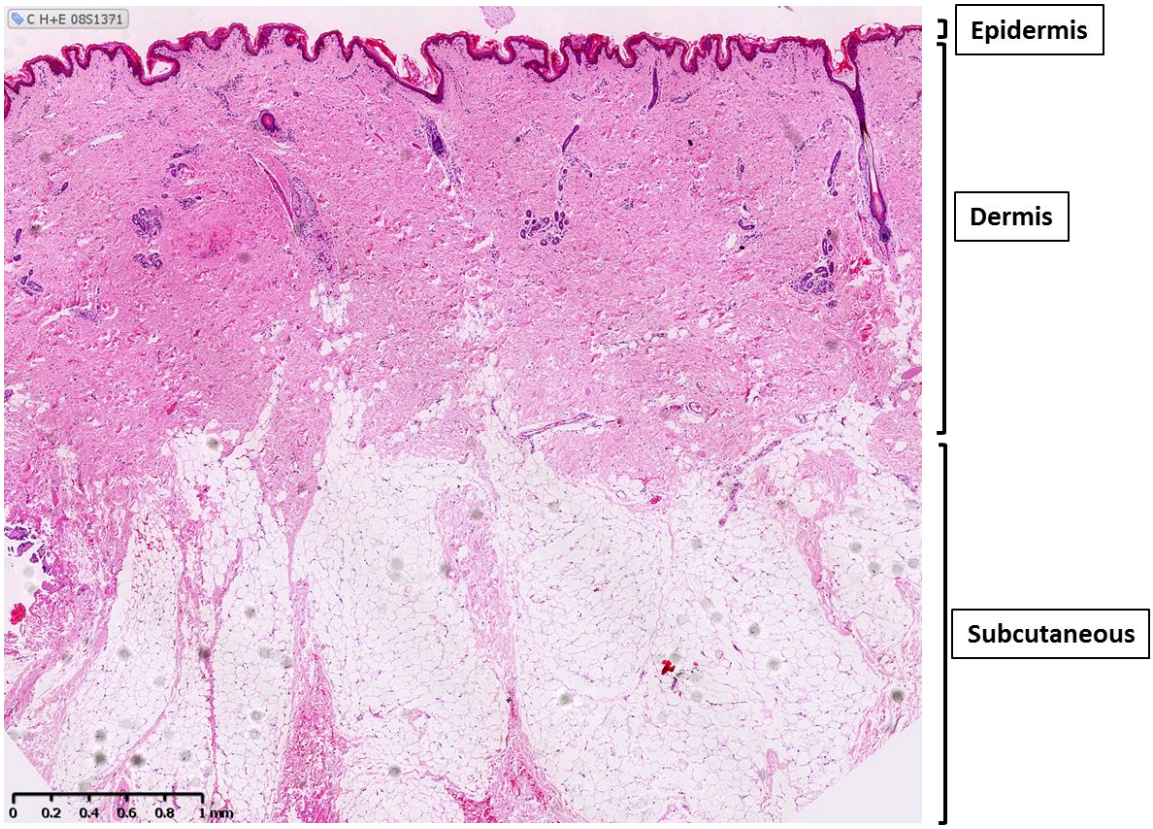

Figure 1.3. **Image showing the three major layers of skin.** The epidermis, dermis and subcutaneous layer can be distinguished using a microscope when stained using haematoxylin and eosin. The subcutaneous layer is largely fat and appears here at the bottom largely as membrane surrounded fat vacuoles. The dermis is highly innervate, contains hair follicles, glandular tissue and blood vessels. The epidermis is the most superficial and undulating layer. It is most darkly stained here due to the density of proteins in that area. The black bar represents 1mm.

The subcutaneous layer is largely fat and plays a major role in insulation. The dermis is highly vascularised, containing nervous and glandular tissue. The epidermis is the thinnest, most superficial layer. The epidermis comprises the “skin barrier” which is critical for protection from the external environment and is composed of multi-layered squamous epithelial cells. The epidermis is further subdivided into four or five layers: stratum corneum (uppermost layer), stratum lucidum (only found on the palms of the hands and the soles of the feet), stratum granulosum, stratum spinosum and stratum basale (lowermost layer).

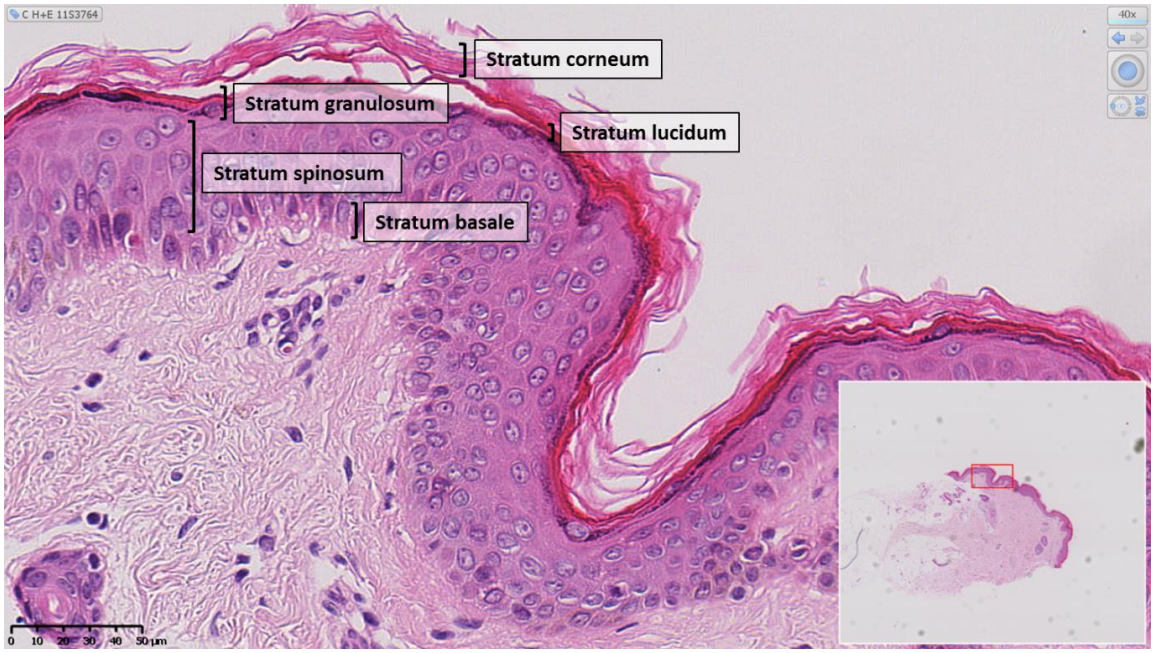

Figure 1.4. **Image showing the five layers of the epidermis.** The stratum corneum, stratum lucidum, stratum granulosum, stratum spinosum and stratum basale can be distinguished using a microscope when stained for using haematoxylin and eosin. The stratum corneum is the layer which is continuously shed, here layers of cells can be seen separating themselves from the rest of the epidermis. The stratum basale contains the germinal cells which are undifferentiated keratinocytes, these cells have a large dark nucleus. In the stratum spinosum those germinal cells become differentiated: the nucleus becomes less densely stained and eventually the cells become anucleated. The black bar represents 50µm.

1.3 The skin barrier

The term “skin barrier” refers to the epidermis and more specifically the stratum corneum. This is where the keratinocytes, which are the predominant cell type in the epidermis have become terminally differentiated into corneocytes which form a tight network through cross-linking bonds (covalent and non-covalent) as well as junctions (desmosomes) between the cells. Desmosomes are molecular complexes made up of keratin cytoskeletal filaments that have a role in adherence to neighbouring cells. This is important for the prevention of excessive water loss[11] and to provide a supportive framework for the lipid network within the skin[12]. Such lipids are fundamental in reducing water loss[13] and proper barrier function[14].[15]

When barrier function is disrupted it leads to disease as the skin fails to fulfil its roles. Examples of such diseases include ichthyosis vulgaris and Netherton syndrome. Ichthyosis vulgaris is a largely autosomal dominant disease presenting as a dry, scaly rash caused by a filaggrin loss of function mutation[16]. Filaggrin is a protein involved in protein assembly in the stratum corneum and binding keratins and microfibrils[17]. Mutations in this gene lead to breakdown of structure within the stratum corneum and therefore increased permeability of the skin barrier allowing

excessive water loss which in turn leads to the clinical symptoms of ichthyosis vulgaris[18]. Netherton syndrome is characterised by excessive skin cell shedding, redness and brittle hairs. It is caused by a mutation in the serine protease inhibitor Kazal-type 5 (*SPINK5*) gene which codes for the protease inhibitor lympho-epithelial Kazal-type-related inhibitor (LEKTI)[19]. It is postulated that the mutation in the serine protease inhibitor gene leads to an imbalance in the protease:protease inhibitor ratio in the skin, leading to excessive protein cleavage in the stratum corneum disrupting the skin barrier, thus reducing its functionality[20]. There are no cures for these diseases and treatment is focused on relieving symptoms and attempts to restore skin barrier function with emollients.

1.4 Biochemistry of the skin

Skin biochemistry is diverse and varies according to the specific part being studied. In the epidermis lipids play a role in the extracellular matrix. The stratum corneum largely comprises ceramides, cholesterol and long chain saturated fatty acids[21]. In the granular cell layer, the lipid matrix contains more phospholipids and cholesterol, alongside significant quantities of glucosylceramides and ceramides. The lipid matrix in the basal layer is mainly phosphoglycerides and sphingomyelin with a small amount of cholesterol.[22] Between the uppermost granular cells and the bottom of the stratum corneum secretory organelles called lamellar granules are found. These organelles are responsible for lipid secretion into intercellular spaces which form a network of multilamellar sheets surrounding the keratinocytes.[23] An unusual ceramide, abbreviated as Cer[EOS] (30-linoyloxytriacontanoic acid-[(2S, 3R)-1,3-dihydroxyoctadec-4-en-zyl]-amide) has been identified as playing a vital role in lipid organisation in the intracellular space of the stratum corneum[24]. This ceramide has been shown to be involved in diseases of the skin barrier. A study investigated the relationship between epidermal lipids and skin barrier impairment in 47 patients with atopic eczema (AE) and 20 age and sex-matched controls, the ceramide:cholesterol ratio was significantly lower in the AE cohort compared with controls. Patients with AE that did not have active lesions at the time of study had intermediate ceramide and cholesterol levels.[25]

Another epidermal lipid is cholesterol sulphate (CS), which regulates desquamation[26]. In culture, keratinocytes accumulate CS during maturation, differentiation-defective cell lines do not conform to this pattern[27]. One study investigated how CS is essential for keratinisation acting as a transcriptional activator for transglutaminase 1 which forms the cornified envelope[27; 28]. CS regulates the activity of serine proteases which play a fundamental role in the skin for epidermal cell adhesion and the production of antimicrobial peptides[28; 29] and it inhibits proteases which slow desquamation[30]. Its role in skin barrier diseases such as AE has been described previously along with Cer[EOS][25] however, one study reported no significant change between CS in controls compared with AE patients[25]. It has been suggested that not only do

patients with AE suffer from a ceramide disorder but also from altered fatty acid metabolism in the epidermis[31].

Biochemistry of the skin is complex, involving intricate relationships between lipids, enzymes and proteins within and surrounding keratinocytes. Despite investigations into the role of cholesterols and ceramides, other lipids and proteins are poorly studied.

1.5 The skin disease eczema

The disease of the skin barrier that is of particular interest to this project is eczema. Eczema affects approximately 15-20% of children in the UK and 2-10% of the adult population[32], although in most cases this disease is not life threatening it can have serious psychosocial implications both for the child affected and their family. Atopic eczema (AE), also known as atopic dermatitis is the most common of all the eczemas and affects up to 15% of children in the UK before the age of 7.[33] AE is a chronic inflammatory skin condition characterised by episodic outbreaks of an itchy, dry, red rash, which often presents on hands, face and skin folds. The increasing prevalence of AE is a financial burden on the NHS due to the chronic nature of the disease and secondary psychosocial implications that it can have on the patient and their family[34]. The cause of AE is still unknown, different patients report different triggers such as stress or UV light and other patients that can identify no pattern to their outbreaks.

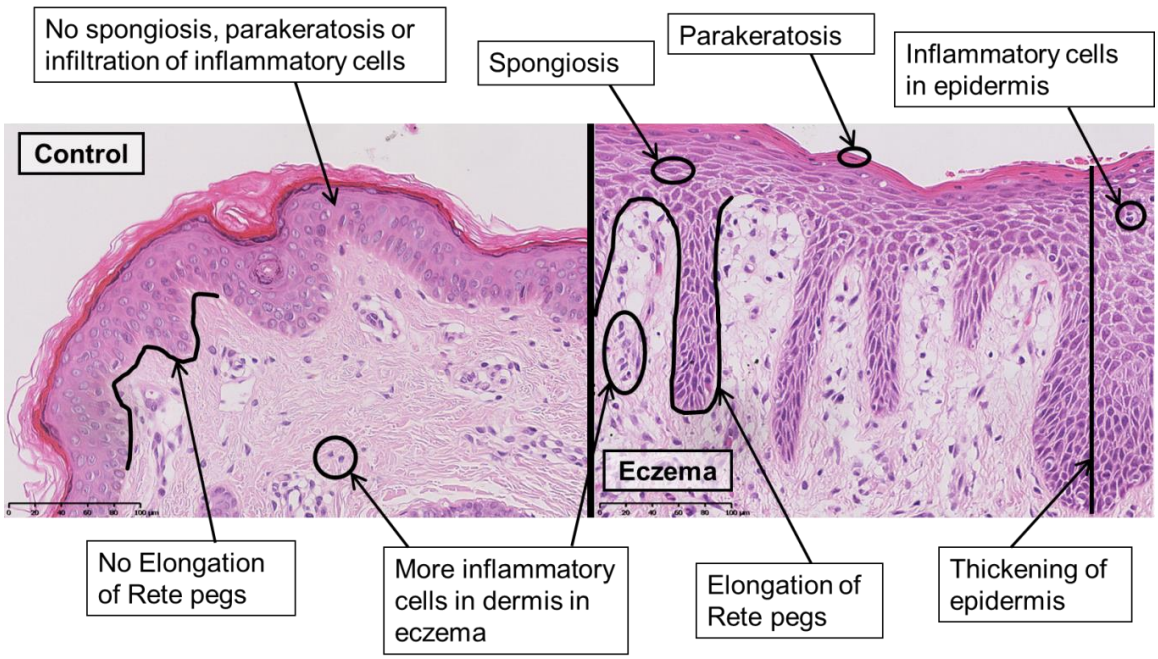

Figure 1.5. **Figure showing the histological differences between control and eczematous skin.** Figure showing the presence of more infiltrating immune cells in eczema and the 'halo'-ing effect of oedema surrounding the cells in the epidermis which is not observed in control skin. In eczema the Rete pegs are elongated and the epidermis is thicker. Tissue stained with haematoxylin and eosin, bars represent 100 µm.

Figure 1.5 shows characteristic histological differences between healthy and eczematous skin. Notably, hyperplasia, where there are increased numbers of cells in the epidermis of the eczema sample making it a thicker layer compared with the control. Rete pegs (natural undulations in the epidermal-dermal boundary) are elongated in eczema and spongiosis is observed, illustrated here as 'halo'-ing around the keratinocytes in the epidermis. This occurs due to localised oedema (fluid build-up), the 'halo'-ing is the space created between keratinocytes by the exuded fluid. Parakeratosis is also observed, which is the presence of keratinocyte nuclei in the stratum corneum, normally in the stratum corneum keratinocytes are terminally differentiated and therefore anucleated (without a nucleus) corneocytes. Nuclei in the stratum corneum suggest inefficient keratinocyte differentiation. Finally in eczema there are a greater number of inflammatory cells and they have infiltrated the epidermis which is not observed in controls.

1.5.1 Current causation hypotheses for eczema

One theory for the increasing prevalence of AE is that it is a disease arising from an impaired skin barrier, likening it to milder forms of the rare diseases described previously (section 1.3). It has been reported that the skin barrier is compromised even at unaffected sites in children prone to AE[35] and patients who have been disease-free for 5 years show resolved barrier function[36]. For the skin barrier to be functioning optimally it requires the correct lipid composition, maintained by the appropriate protein scaffold.

Other theories for the causation of AE include immunological dysregulation, the hygiene hypothesis and increased susceptibility to foreign pathogens[34]. The susceptibility to foreign pathogens hypothesis arose after observations that compared with the unaffected population, AE sufferers experience more frequent fungal and bacterial infections even at non-lesional sites. Bacterial infections such as *Staphylococcus aureus* could trigger AE through the subsequent immunological cascade that staphylococcal super-antigens can initiate.[37] The hygiene hypothesis is in response to observations that AE prevalence has increased in the past few decades, particularly in developed countries[38]. This is attributed to children's access to 'cleaner' lifestyles. In the first few hours, days and weeks of a child's life they are exposed to fewer foreign antigens that they would have been previously. This could cause environmental allergens to provoke abnormal immunological responses later on in life because tolerance was not established in early life. Immune dysregulation, also referred to as 'inside-outside' pathology is characterised by elevated serum immunoglobulin E (IgE) levels. This means that the skin is in a perpetual state of sub-clinical inflammation and IgE receptors are overstimulated therefore more likely to trigger an immune response to external antigens.[34] Finally loss of function mutations in the gene that code for filaggrin are found in 10% of the population[39] and are found

in 40% of patients with moderate to severe AE[40] suggestive that this could be the cause of AE in some patients[41].

1.5.2 Current treatment for AE

AE remains a challenging disease to treat and manage despite research into finding a cause. Common treatments include moisturising creams which relieve dryness and maintain skin hydration and topical corticosteroids which act to suppress the immune system response. The drawback of steroid treatment is that they can only be used in acute flare-ups and not for long-term treatment, due to the systemic side-effects[42; 43]. There are other less common therapies such as phototherapy, tar preparations, anti-bacterial/fungal/viral treatment and in extreme cases systemic immunosuppressive therapies are used[34]. Treatments can be effective in some cases, especially when managed closely, yet upon discharge from hospital patient compliance can decrease leading to exacerbation of the condition.

1.6 Skin aesthetics

Our skin covers the surface of our bodies, diseases affecting our skin are often noticeable. In a media-driven society, that is increasingly aesthetic and image-conscious, the psychosocial repercussions of skin disease and abnormalities are also increasing.

1.6.1 Scarring

Scarring is a healthy process that the body uses to heal after injury. However, scars can be noticeable or the wound may not heal properly and this can be challenging to deal with. Healthy, unscarred skin is macroscopically and microscopically different to scarred skin. There are various types of abnormal scar such as hypertrophic and keloid, they both present when the natural healing cessation does not happen at the end of the remodelling phase. This would normally stop further collagen production at the scar site.

1.7 What else can we learn from the skin?

Not only can the skin indicate skin disease status, but it can also be used to identify other diseases and monitor bodily processes. Jaundice can indicate liver disease, fatty depositions can indicate hyperlipidaemia and infections may indicate diabetes mellitus. The skin is highly perfused and systematic changes may be reflected in the biochemical equilibrium of the skin in real-time. For example during major surgical procedures there is concern that the body may not

be sufficiently oxygenated and this could lead to post-surgical morbidity, the skin could be used to indicate what is happening throughout the rest of the body[44].

1.8 Application of mass spectrometry to the study of skin

Mass spectrometry is an expanding and versatile technique, the applications are seemingly limitless. In the field of medical sciences, there is not a biological fluid or tissue that has not been studied by mass spectrometry. Where genetics can study genes, mass spectrometry can study the proteins, lipids or small molecules of a sample. This gives a different perspective on the data analysis, for example mass spectrometry can measure the amount of protein in a sample and take into account potential PTMs of that protein. Genetic information is not always directly correlated with amount of functional *in vivo* protein.

1.8.1 Previous studies using mass spectrometry to analyse skin tissue

There are relatively few human skin proteomic studies and datasets currently available in the literature[45; 46] compared with other human tissues or fluids. A human-specific PubMed search showed three times as many publications for "liver AND proteomics"[47] and twelve times as many for "blood AND proteomics"[48] compared with "skin AND proteomics"[49]. Skin is a challenging tissue to analyse using traditional proteomic techniques due to the high lipid content, insolubility and extensive cross-linking of proteins. This can complicate isolation and digestion of proteins. Other research groups studying skin proteomics[49] have used techniques including gel-based protein fractionation[50; 51], heavy isotope labelled assays to identify phosphorylated proteins[52] and studying secreted skin proteins, rather than skin tissue itself[53]. The latter two techniques are specific to a particular aspect of the skin proteome and do not represent the composition of the tissue as a whole.

Investigations into the skin's lipid content are similarly sparse compared with other tissues, however there are many publications documenting the major classes of lipid in the skin: MALDI-MS/MS was used to identify glycerophospholipids and sphingolipids as the major lipid component of skin[54]. Glycerophospholipids and sphingolipids were also found to be the two major lipid classes in skin by LC-MS/MS[55] and finally ceramide (a member of the sphingolipid class), free fatty acids and cholesterol were identified as the predominant lipids in the stratum corneum of the skin using a LC-MS method[56].

1.8.2 Using mass spectrometry to study human skin

Mass spectrometry is an invaluable method for assessing the composition of proteins and lipids in a biological sample. It is versatile as it can search for the most abundant proteins/lipids in a sample or it can be targeted to identify specific species of interest. Mass spectrometry can generate information about a biological samples that is not currently available by any other technique. The skin is an important organ, often overlooked in science and medicine, however, it can teach us about biological processes and underlying mechanisms of disease. Most mass spectrometry and skin analysis techniques described in this thesis have been used to study invasive skin biopsies or surgical incision sites. However, further assays would be developed into targeted tests, which are more sensitive and would require less clinical sample, such as a skin scraping or taping.

Chapter 2

Aims of this thesis

2 Aims of this thesis

The aims of this thesis were to use mass spectrometry to investigate and explore further skin tissue in health and disease. We wanted to understand more about the underlying mechanisms causing the skin disease eczema in order to improve treatment options for patients. We also wanted to study the roles of protease inhibitors and proteases in the skin as dysregulation between certain protease proteinase inhibitor partners have already been described in other skin diseases such as Netherton's syndrome so perhaps similar mechanisms could be disturbed in other skin conditions. Mass spectrometry was also used to investigate whether it is possible to identify differences in unscarred healthy tissue of individuals who will and will not develop a hypertrophic scar post-surgery. And finally to elucidate markers in the skin that may be suggestive of post-operative morbidity post-major surgery.

Chapter 3

Immunohistochemical analysis of skin biopsies to validate previous proteomic findings dysregulated in eczema

3 Immunohistochemical analysis of skin biopsies to validate previous proteomic findings dysregulated in eczema

Contents

The aim of this thesis was to develop methods to screen skin and apply those methods to investigate disease. Prior to starting this project preliminary work in our laboratory[57; 58] identified changes in proteins present in the uppermost layer of the skin in patients with eczema, and ichthyosis compared with controls. That preliminary work involved taking skin scraping samples from healthy volunteers who had eczema and those who did not, extracting the proteins, digesting them and identifying them by QToF MS. The proteins that were differentially expressed were collated and other candidates from the literature were added to form a list of proteins to be validated in this thesis. The data in this chapter validates the protein changes identified in the preliminary work using immunohistochemistry (IHC). Two skin conditions were used as models for testing this hypothesis: eczema and ichthyosis. Eczema is a common childhood disease whereby the creases of the body develop a red, itchy and raised rash. Ichthyosis covers a group of related diseases which is usually an inherited genetic disease, the affected children present early in life with an accumulation of rough scaly skin on their body.

3.1 Atopic eczema (AE)

AE as detailed in the introduction (section 1.5) is a chronic inflammatory skin condition characterised by episodic outbreaks of an itchy, dry, red rash, which often presents on hands, face and skin folds. It can be burdensome with incessant itching and repeated treatment[59]. Neither cause nor disease mechanism are entirely understood[60; 61]. In the absence of a cure[62] children persist with disease management until it subsides. The incidence of eczema is highest in children, with almost all patients no longer affected by adulthood[63; 64; 65].

3.2 Ichthyosis

Ichthyosis covers a group of Mendelian disorders of cornification. The disease sub-categories are classified according to the degree of visible scaling and or hyperkeratosis of the skin as well as onset and mode of inheritance. This group of diseases usually presents as a burdensome disease due to the large proportion of affected skin, patients are routinely tested to identify which genetic mutations are responsible for their ichthyosis.[66]

3.3 Causes of AE

As detailed in section 1.5.1 there is no certainty regarding the underlying disease mechanism of AE. This affects treatment for AE because without understanding of the disease mechanism it can only be treated reactively, rather than proactively. In order to address the pathogenesis of AE a pilot project was carried before the start of this PhD project to investigate the differential protein expression between controls, people affected by AE and people affected by ichthyosis.

3.4 Results of the pilot study

Skin scrapings reflect the composition of the outer epidermis and were taken from the elbows of volunteers for proteomic profiling, for this pilot study. The proteins were digested (method 10.2.10), the peptides subject to MS^E analysis (method 10.2.4) and the variable protein expression interrogated (method 10.2.5). It was hoped that biomarkers of disease mechanism would be identified, several candidate proteins were found. Seven were selected based on involvement in skin barrier function, fold change and likelihood to being involved in disease pathology to be validated by immunohistochemistry (IHC).

Full Protein Name	Protein Abbreviation	Reason for Inclusion
Alpha-1-acid glycoprotein 2	A1AG2_HUMAN	13.7 fold change in AE from MS data
Bleomycin hydrolase	BLMH_HUMAN	High abundance protease in skin
Calmodulin-like protein 3	CALL3_HUMAN	-16 fold change in AE from MS data
Calmodulin-like protein 5	CALL5_HUMAN	-3.2 fold change in AE from MS data
Caspase-14	CASPE_HUMAN	High abundance protease in skin
Cathepsin D	CATD_HUMAN	Skin protease
Dermcidin	DCD_HUMAN	Antimicrobial peptide in skin

Table 3.1. **Table showing the 7 proteins selected for IHC analysis.** Table showing alpha-1-acid glycoprotein, calmodulin-like proteins 3 and 5 selected from the pilot mass spectrometry experiment, plus bleomycin hydrolase, caspase-14, cathepsin D and dermcidin which were selected from the literature to be included for IHC analysis. Fold changes for alpha-1-acid glycoprotein, calmodulin-like proteins 3 and 5 are expressed relative to the control group.

3.5 Validation of selected proteins using immunohistochemistry

As part of this PhD project IHC staining was selected to validate the proteins selected in Table 3.1 as a complementary technique to the pilot mass spectrometry data. IHC staining is only a semi-quantitative technique however, unlike mass spectrometry it can show locational variation of the proteins within a skin section. IHC can detect changes of 10-100-fold, we predicted that some of the selected protein changes may be too subtle to detect. However, the location of each biomarker within the three-dimensional architecture of the skin could provide information on the integrity of the skin barrier in disease. Six histologically normal skin biopsies, 11 eczematous samples and 3 ichthyosis samples were analysed in this IHC study. Results are presented and discussed below.

3.5.1 Immunohistochemical staining of alpha-1-acid glycoprotein

Alpha-1-acid glycoprotein 2 (AGP2) is a highly glycosylated blood protein. The gene that codes for the protein AGP 2 is *ORM2* there is also *ORM1* which codes for alpha-1-acid glycoprotein 1 (AGP1), these two genes and their respective proteins are highly homologous. The protein sequences have 90% sequence homology and are often referred to in the single term of AGP[67]. There was no specific commercial antibody available for AGP2, as identified in the MS data, so an AGP antibody was purchased and used. Due to the high sequence homology it was concluded that this would not interfere significantly with the analysis. AGP is a 40 kDa, type-1 acute-phase protein with anti-inflammatory and immunomodulating properties[67] it binds protease inhibitors and is thought to alter protein binding[68]. However, its precise biological function remains unknown[69]. The glycosylation state of AGP has been linked to cancer, along with other heavily glycosylated acute phase proteins such as haptoglobin[70].

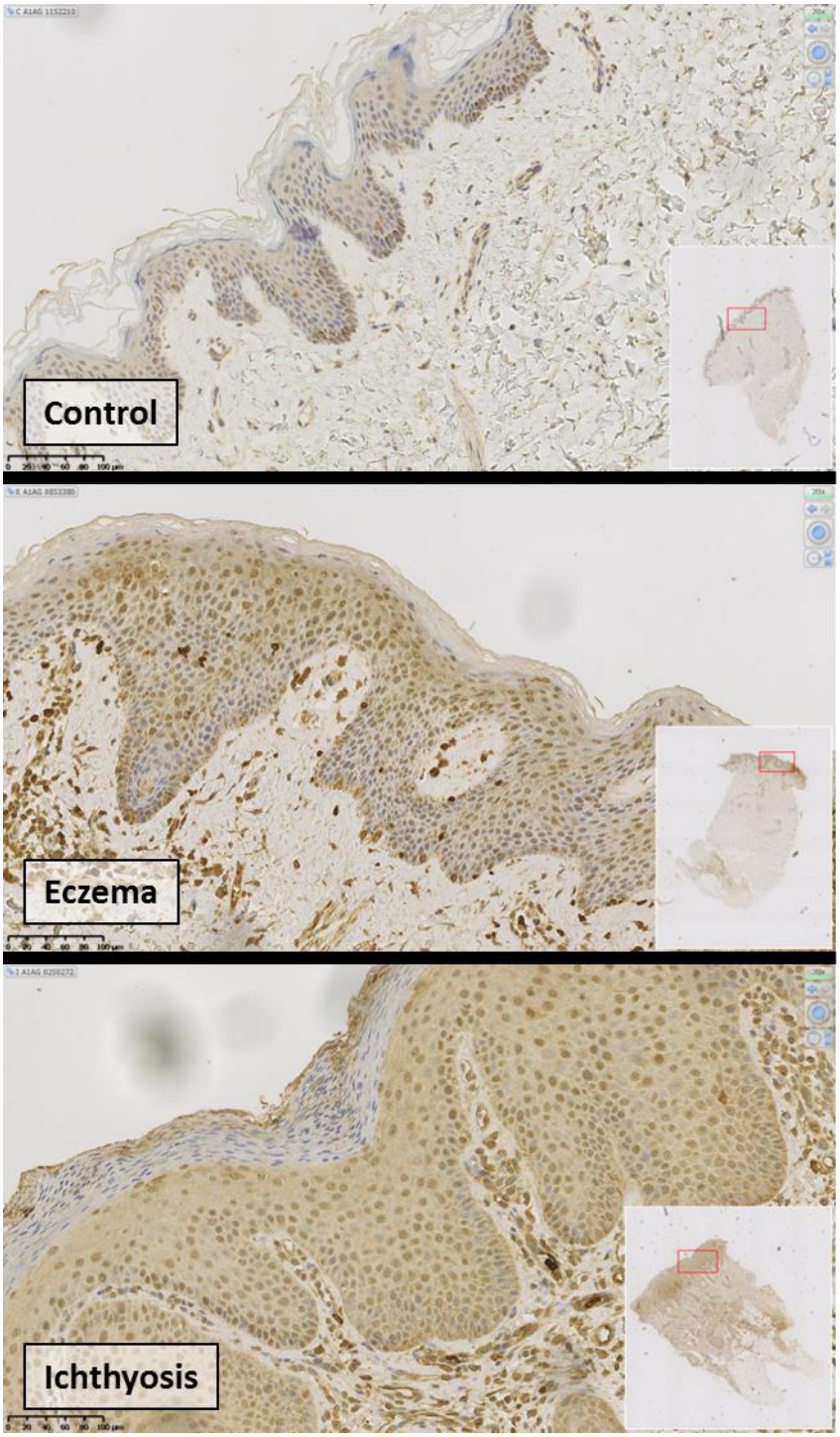

Figure 3.1. **Images showing the results of IHC staining for AGP in control, eczema and ichthyosis patients.** AGP protein is stained brown following the IHC protocol (10.2.2), the nuclei have been counterstained blue with haematoxylin solution (Mayer's), the black bar represents 100 µm.

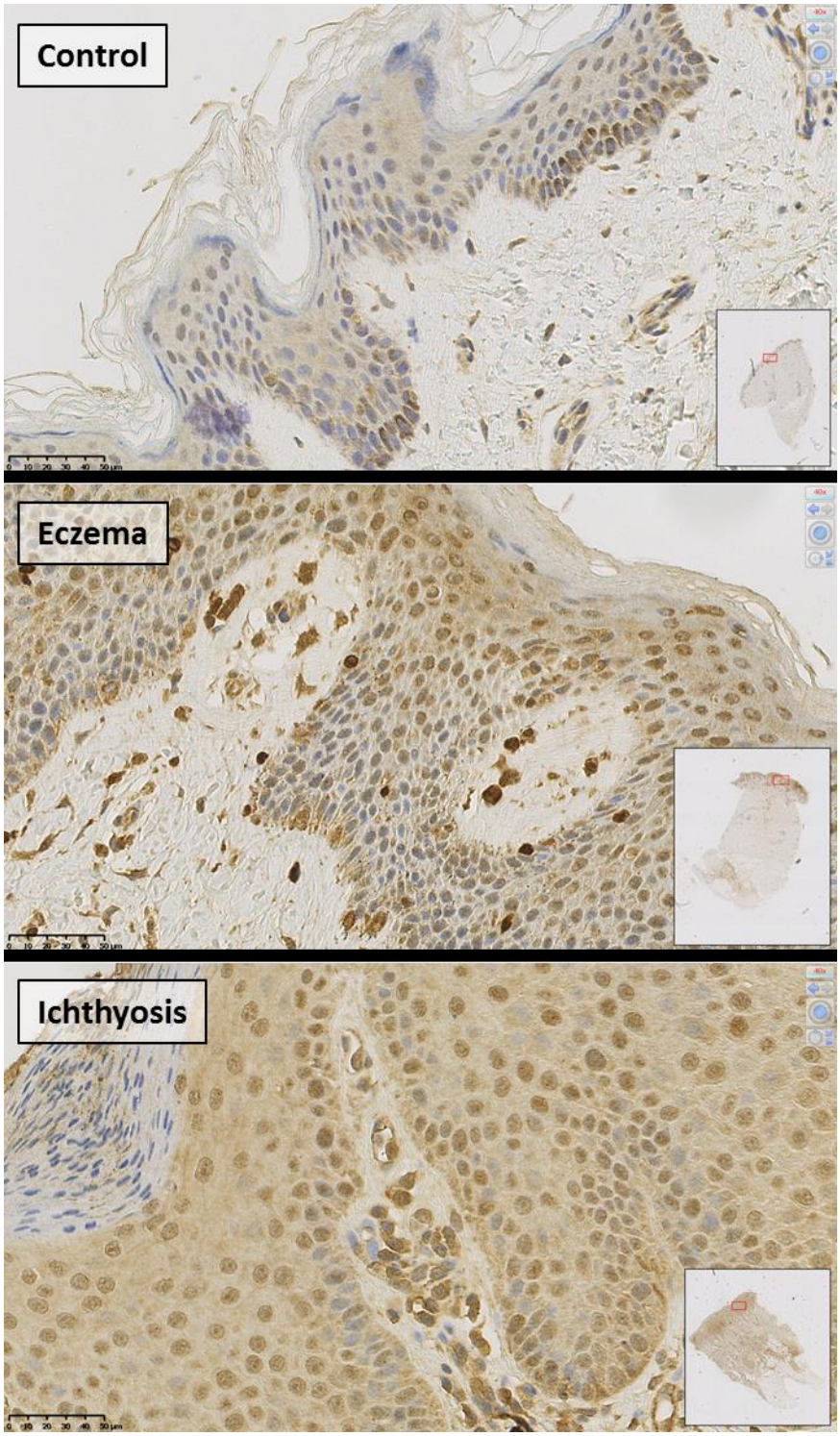

Figure 3.2. **Skin sections shown in Figure 3.1 at a higher magnification.** This series of images is at higher magnification to illustrate some of the intracellular and more subtle differences in staining patterns. Bar represents 50 µm.

These images show that in controls most of the AGP staining appears in the stratum basale, more specifically clustered around the nuclear envelope or on the peripheral chromatin within the nucleus. The eczema samples show a slightly different pattern of staining, less staining in the stratum basale and more staining as the keratinocytes become more differentiated. For

ichthyosis the staining is generally more diffuse, but there is noticeably no staining in the thickened layer of superficial skin.

It is difficult to interpret whether such differences represent disease cause or effect. AGP is a blood protein so elevated levels of AGP closer to the surface of the skin may reflect increased permeability of the skin barrier in these diseases. Furthermore, AGP is an acute phase protein whose concentration increases at sites of inflammation[71]. In the pilot MS study it was detected in unaffected skin regions of patients known to suffer from AE, suggesting that inflammation is increased throughout the skin of people who are susceptible to AE, rather than limited to lesional sites. AE is an inflammatory disease, so it would be likely that these lesions are showing signs of inflammation, whereas ichthyosis is not described as an inflammatory disease. Ichthyotic skin may cause discomfort with secondary scratching or rubbing which would trigger a local inflammatory response, increasing local levels of acute phase proteins such as AGP. AGP2 was elevated in the pilot proteomic data 13.7-fold in eczema and 7.7-fold in ichthyosis, concurring with the IHC data. It may also reflect the level of inflammation. Of the three groups most inflammation is seen in eczema patients.

3.5.2 Immunohistochemical staining of bleomycin hydrolase

Bleomycin hydrolase (BH) is a is a cysteine protease which is thought to have roles in tumour suppression, preparation of peptides for antigen presentation[72] and involvement in filaggrin citrullination which occurs in the stratum corneum alongside the protease calpain I. Citrullination is the process by which filaggrin is broken down into amino acids. The amino acids produced are responsible for maintaining and facilitating epidermal moisturisation.[73]

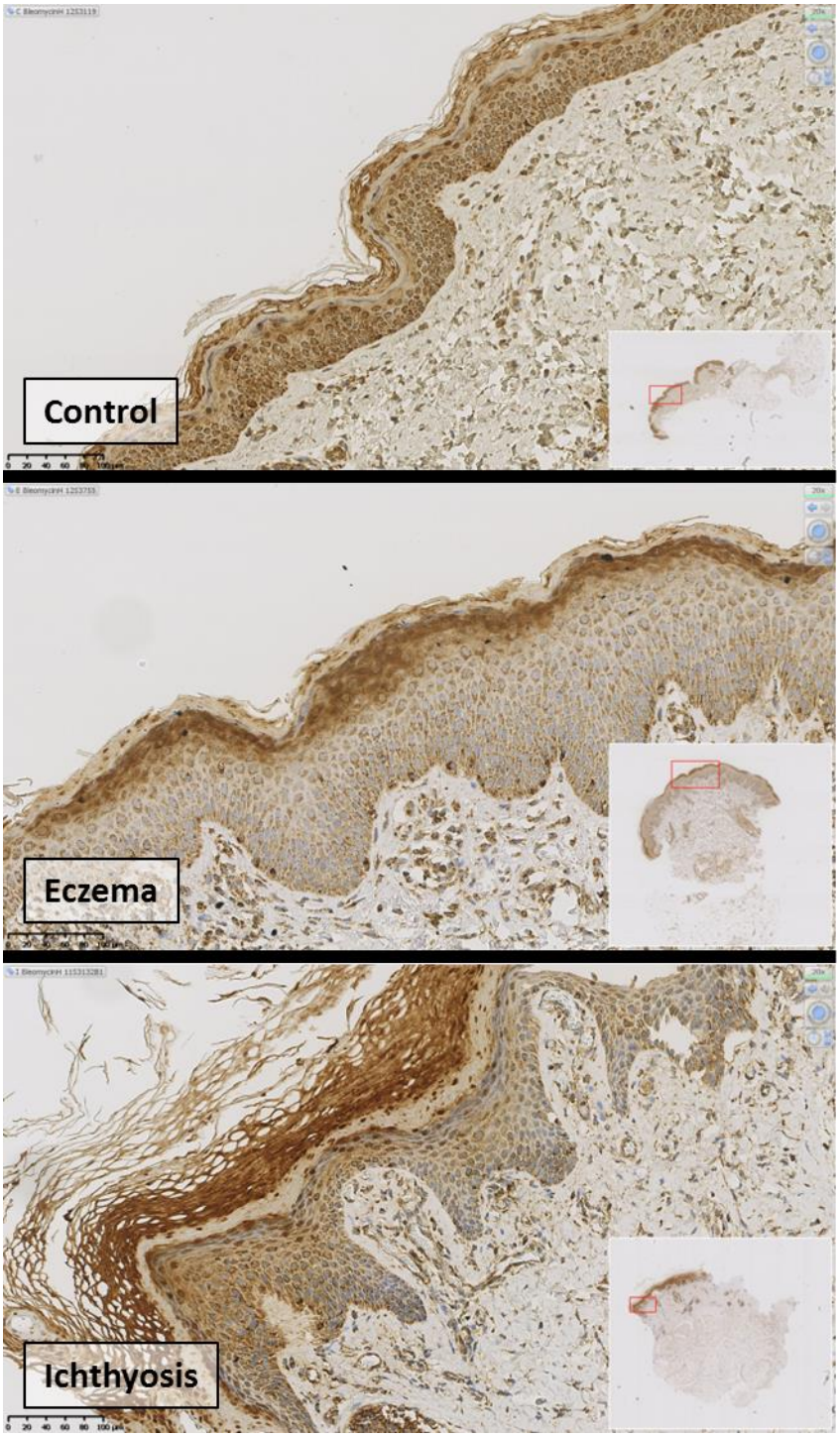

Figure 3.3. **Images showing the results of IHC staining for BH in control, eczema and ichthyosis patients.** BH protein is stained brown according to the IHC protocol (10.2.2), the nuclei have been counterstained blue with haematoxylin solution (Mayer's), the black bar represents 100 µm.

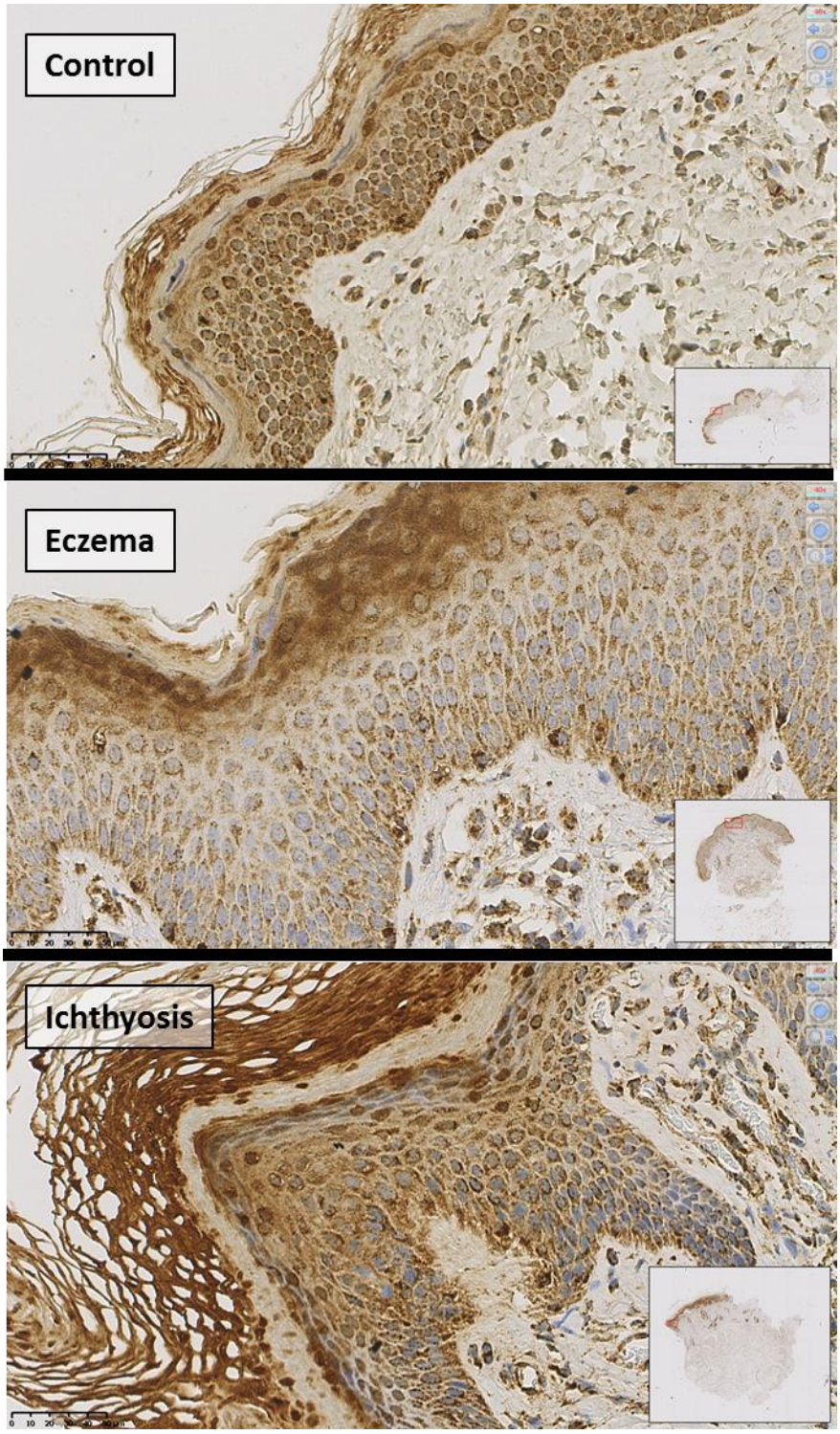

Figure 3.4. **Skin sections showing the images in Figure 3.3 in higher magnification.** This series of images is at higher magnification to illustrate some of the intracellular and more subtle differences in staining patterns. Bar represents 50 µm.

These images show generally consistent staining in controls throughout the whole epidermis, there is no nuclear staining apart from concentrates around the nucleus. The eczematous samples show staining around the nucleus in a nuclear envelope/peripheral chromatin distribution and particularly dark staining in the stratum granulosum. The ichthyosis samples

show staining around the nucleus in a nuclear envelope/peripheral chromatin distribution and very dark staining of the stratum corneum. There is even distribution of staining in controls which is not observed in eczema or ichthyosis samples. Skin proteases, such as BH are important to ensure correct desquamation which in turn maintains proper barrier function[74] (as discussed further in chapter 4). The IHC images show differential expression of BH in these samples due to its intrinsic role in skin maintenance. It is unsurprising that the protein expression is different in these two skin barrier diseases compared with controls. The Human Protein Atlas BH database (http://www.proteinatlas.org/) details BH staining as mostly limited to the cytoplasm, nucleus, but not nucleolus[75]. This correlates with our data. The images shown on the Human Protein Atlas database are of fibroblasts and do not show such dark staining around the nucleus, this could be attributed to the fact that we are looking at differentiating keratinocytes in tissue rather than fibroblasts in culture, the protein expression could be different. Of the BH roles, the most pertinent to the skin is its role in citrullination of filaggrin.

An immunofluorescence study investigating the roles of BH and filaggrin in AE showed different co-localisation of BH and filaggrin in controls compared with AE samples for AE affected skin regions and unaffected regions. They demonstrated that BH and filaggrin are co-localised in the superficial epidermis in controls, yet in AE lesional and non-lesional sites filaggrin expression is not as superficial resulting in reduced co-localisation in AE patients. They also described reduced BH expression in affected and unaffected skin regions of AE patients.[76] We have not investigated filaggrin distribution here, however, the distribution we observed of BH (Figure 3.3) does not agree with those published. The BH results described by Kamata et al. show varied BH expression in controls across the epidermis with more concentrated expression nearer the surface, whereas our results show a widespread, but diffuse staining across the whole epidermis. Kamata et al. show staining of both lesion and non-lesion sites which is difficult to see due to lack of staining. In contrast our observations show a distinct band of staining in the stratum granulosum (Figure 3.3).

Eczema patients have dry skin, it could be inferred that there is less citrullination of filaggrin. A reduction of BH could lead to reduced citrullination, but equally it could be a reduction of calpain I that is responsible for reducing the citrullination of filaggrin, or even genetic mutations in filaggrin resulting in it being less susceptible to citrullination. The MS data demonstrated no change between controls and eczema samples for BH and a 3.6-fold increase in ichthyosis patients. It is unsurprising that no significant changes were observed between controls and eczema patients.

3.5.3 Immunohistochemical staining of calmodulin-like protein 3

Calmodulin-like protein 3 (CLP3) is a 17 kDa, 149 amino acids long protein made up of helixes and beta strands described as having a role in myosin-X binding[77]. The calmodulin family of

proteins are responsible for regulating calcium transport and function in the skin[78], CLP3 itself is an epithelial-specific calcium ion (Ca^{2+}) binding protein and an *in vivo* study shows its importance during would healing in keratinocytes[79].

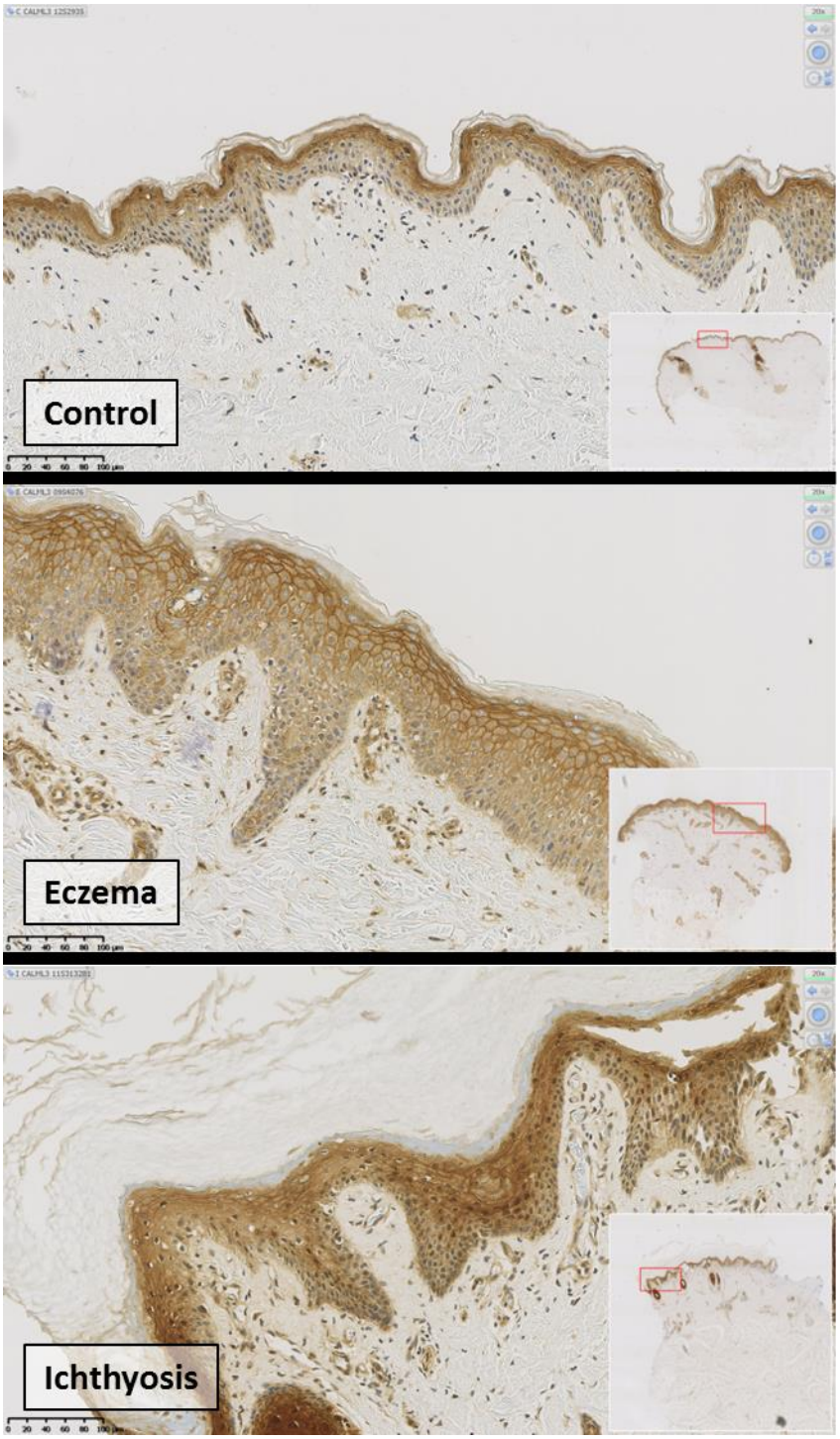

Figure 3.5. **Images showing the results of IHC staining for CLP3 in control, eczema and ichthyosis patients.** CLP3 protein is stained brown following the IHC protocol (10.2.2), the nuclei have been counterstained blue with haematoxylin solution (Mayer's), the black bar represents 100 µm.

For CLP3 controls show darkest staining in the stratum granulosum, with diffuse staining throughout the rest of the epidermis. The staining is specific to cell membranes. For eczema samples staining is largely similar to that of controls; cell membrane staining, predominantly in the stratum granulosum. Ichthyosis samples show specific staining to cell membranes in the stratum granulosum, but not as pronounced as the eczema samples.

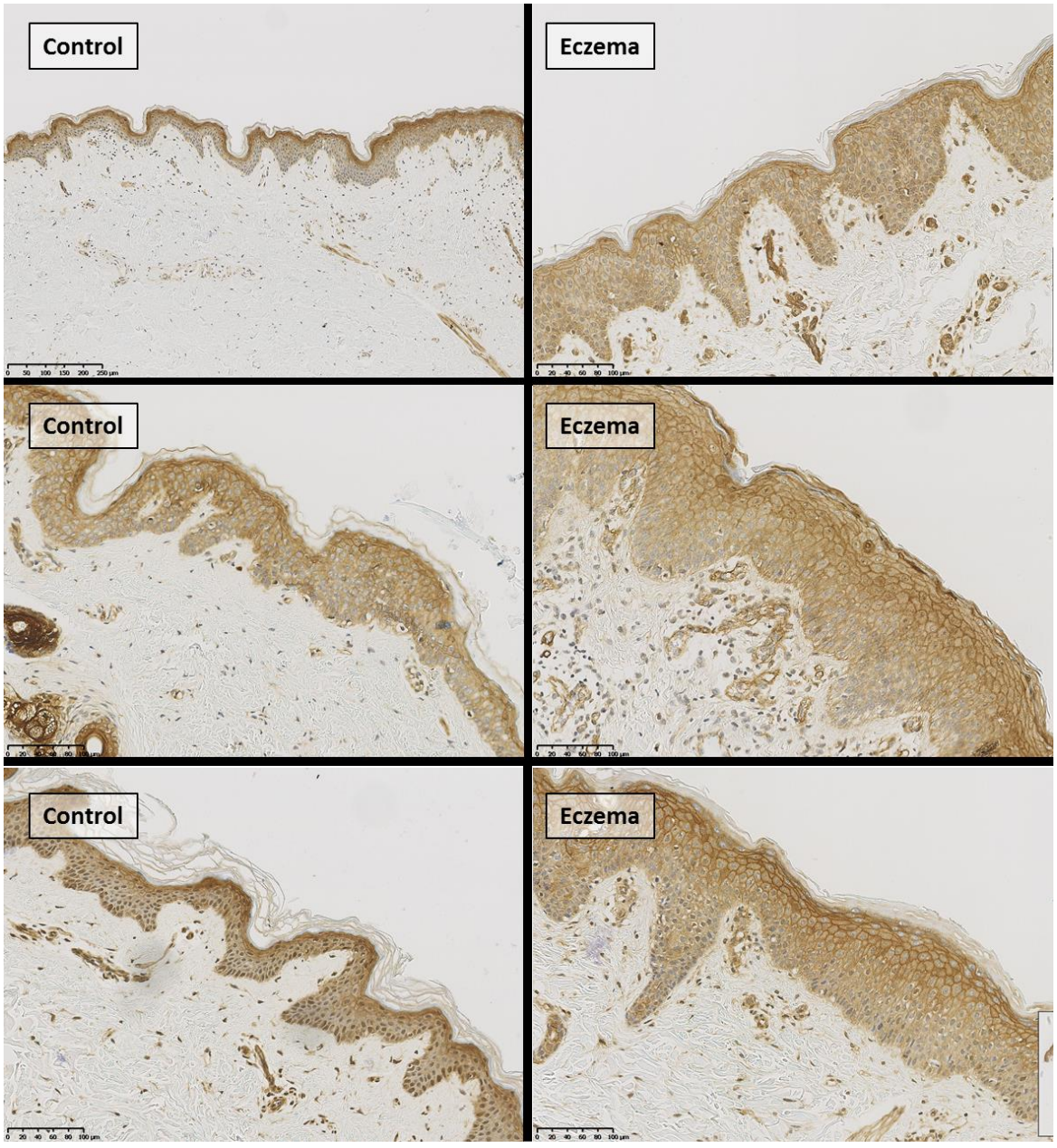

Figure 3.6. **Panel of IHC stained skin samples for CLP3 for three control samples and three eczema samples.** Panel shows the variation between three different control and three different eczema samples for the CLP3 staining. Bar represents 100 µm.

CLP3 is a light chain regulator of the unconventional myosin-X[79]. Myosin-X belongs to the family of myosins which are ATP-dependent motors largely made up of actin. Myosin-X is an unconventional myosins because it has a role in intracellular rather than extracellular

movements. Myosins are structurally made up of two light chains and two heavy chains, CLP3 regulates the light chain of myosin-X and has many roles in cell movement, growth and intracellular transport[80]. The pilot mass spectrometry data showed a 16-fold decrease in protein expression in eczema samples compared with controls and a 58.8-fold decrease in ichthyosis patients compared to controls. It is surprising that a more significant change was not observed here (Figure 3.5). However, the MS data was acquired from surface skin scraping whereas IHC analysis interrogates the full thickness of the epidermis which could account for this discrepancy. Controls have dark staining in the stratum granulosum with more diffuse staining in the stratum spinosum. Eczema samples do not have such intense staining in the stratum granulosum. CLP3 has not been associated previously with AE, which is surprising when the pilot MS data was so significant, there are some changes in the IHC results too. Bennett et al., describe CLP3 in keratinocytes[79], its role with Ca^{2+} in wound healing and concludes that CLP3 upregulation in keratinocytes stimulates myosin-X to re-epitheliate wounds *in vivo*. As CLP3 has an intrinsic role with myosin-X it is inconceivable that myosin-X may be involved in skin barrier function, which in turn could explain the reduced protein expression identified in the pilot MS data.

3.5.4 Immunohistochemical staining of calmodulin-like protein 5

Calmodulin-like protein 5 (CLP5) or calmodulin-like skin protein is a 16 kDa protein comprising helixes, beta strands and Ca^{2+} binding domains. It is secreted by keratinocytes and released into the circulation[81]. CLP5 is expressed exclusively in the stratum granulosum and lower layers of the stratum corneum. It has been described in neuronal cell death[81], breast cancer[82], psoriasis[83] and to have cation- and peptide-binding properties[84]. In psoriasis the Ca^{2+} gradient within the epidermis is disturbed[85], which would affect the family of calmodulins in the skin. If the Ca^{2+} gradient is disturbed in psoriasis it could be disturbed in other skin diseases such as eczema. If the Ca^{2+} gradient is disrupted in AE a change in calmodulin expression and other calcium-dependent or modulating proteins would be observed.

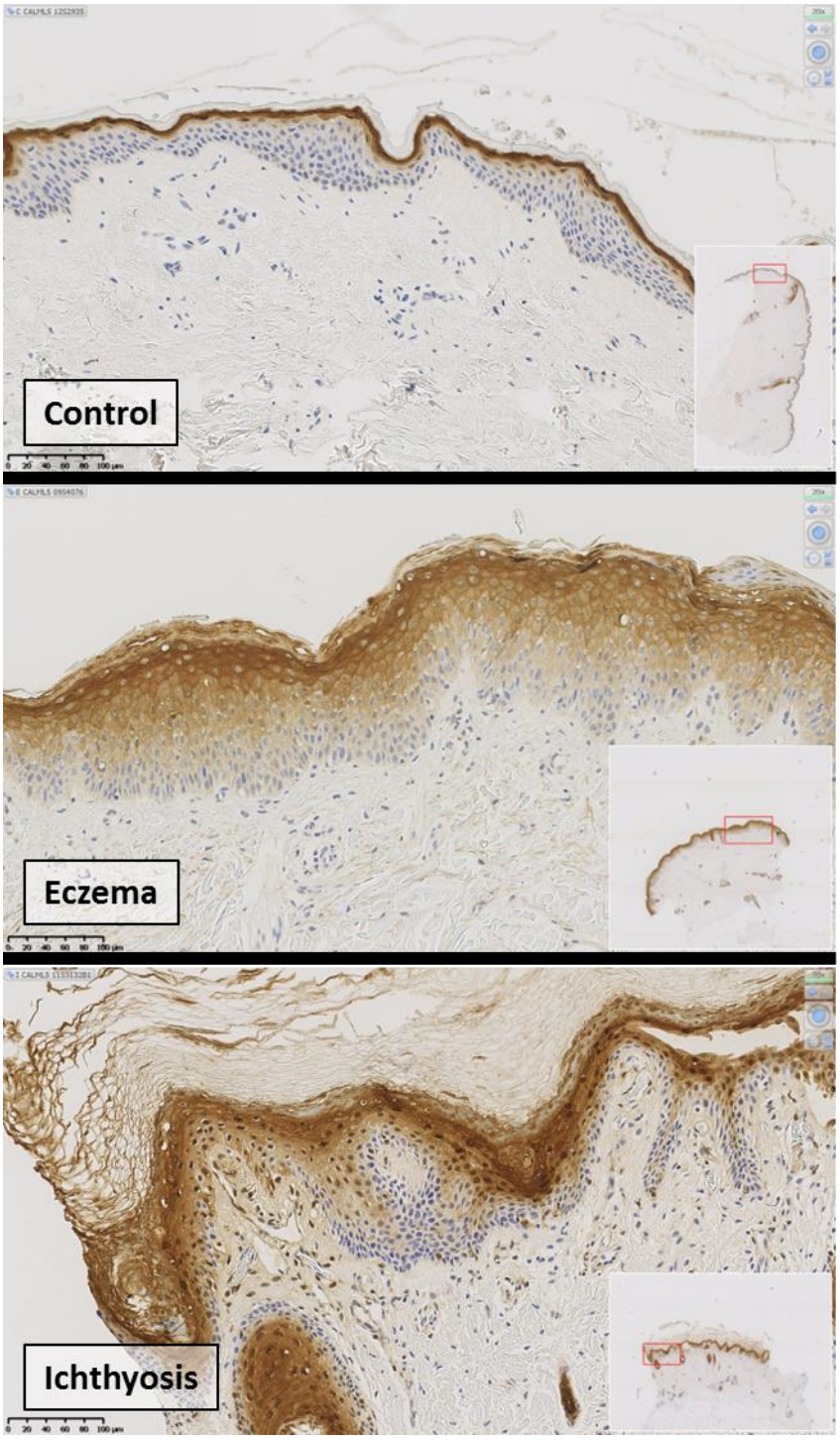

Figure 3.7. **Images showing the results of IHC staining for CLP5 in control, eczema and ichthyosis patients.** CLP5 is stained brown following the IHC protocol (10.2.2), the nuclei have been counterstained blue with haematoxylin solution (Mayer's), the black bar represents 100 µm.

The staining results show intense staining of the stratum granulosum in controls, with limited staining elsewhere. In the eczema samples there is distinct staining in the stratum granulosum, but there is further diffuse staining in the stratum spinosum. The ichthyosis samples show

stratum granulosum staining with some staining in the stratum spinosum and stratum corneum, but not to as diffuse as observed in the eczema samples.

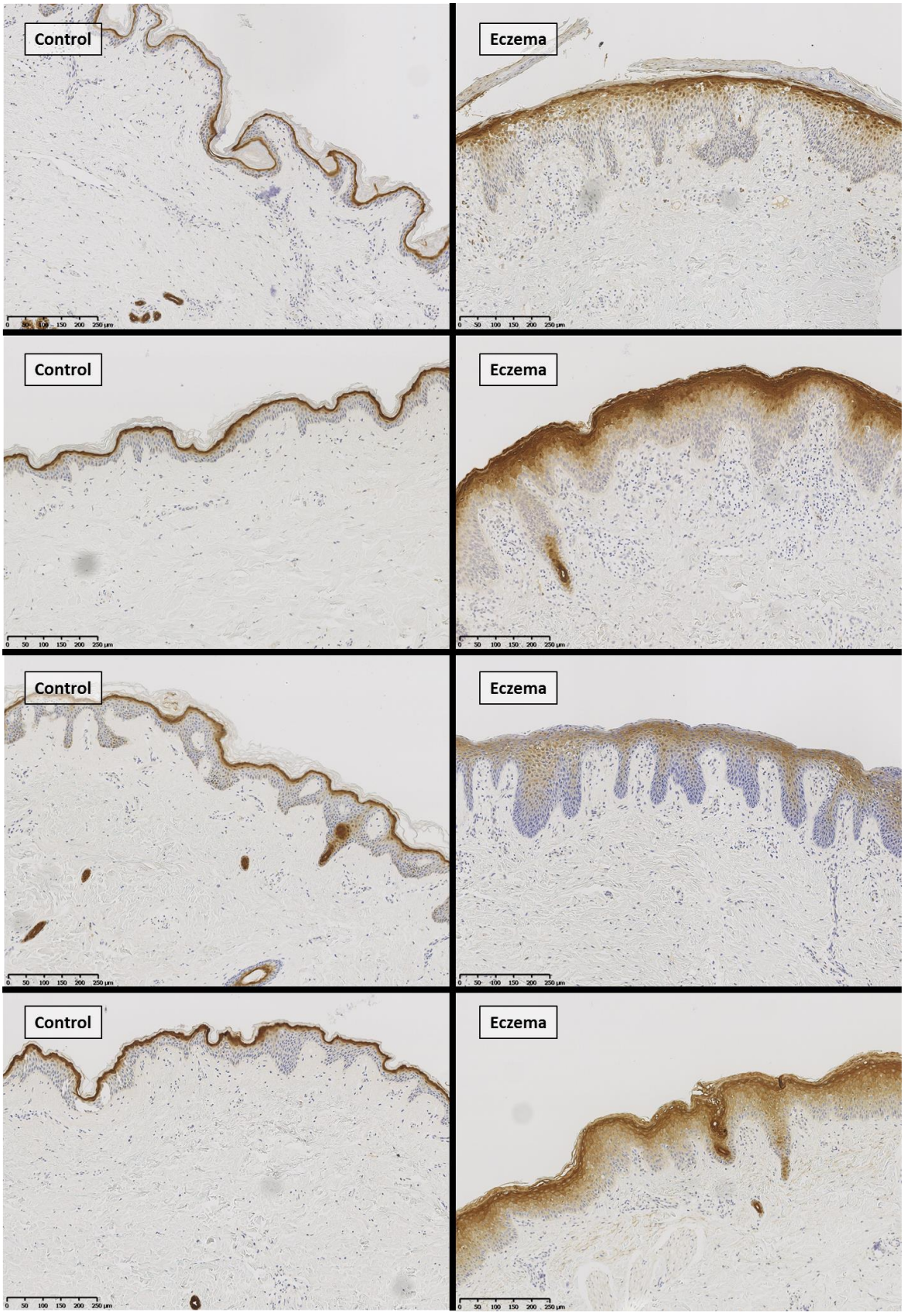

Figure 3.8. **Panel of IHC stained skin samples for CLP5 for four control samples and four eczema samples.** Panel shows the consistency of the CLP5 staining in controls and more variation between the eczema samples. Bar represents 100 µm.

Keratinocyte maturation is Ca^{2+} dependent[86], with a Ca^{2+} gradient across the epidermis, with highest Ca^{2+} concentrations at the surface of the skin. The low Ca^{2+} concentration in the stratum basale favours proliferation of keratinocytes, whereas higher concentrations in the stratum corneum favour terminal differentiation.[87] CLP5 is Ca^{2+} dependent and involved in keratinocyte differentiation[78] the same research group demonstrated immunofluorescence and IHC staining of CLP5 which correlated with keratinocyte differentiation[88]. This theory is supported by the control IHC images shown here illustrating CLP5 staining correlating with differentiated keratinocytes in the stratum granulosum.

A link between CLP5 and AE has already been described[89] through IHC, western blot and ELISA analyses demonstrating that CLP5 expression is increased in the upper epidermis of AE compared to controls. This contradicts our findings which demonstrate that there is a different expression profile rather than a difference in intensity of the stain and in fact that appears to be increased CLP5 staining in the upper epidermis of controls. It could be postulated that in eczema the skin barrier defects are initiated by poor keratinocyte differentiation. It is difficult to know the cause of a change based on IHC staining, whether a poor Ca^{2+} gradient causes CLP5 to be expressed in the stratum spinosum, or if another factor has interfered with keratinocyte differentiation, having a knock-on effect for the Ca^{2+} gradient and therefore CLP5. Irrespective of the cause and effect order, there is a difference in CLP5 expression in controls compared with eczema samples. Ichthyosis patients are expressing a similar pattern to eczema samples. The same conclusions could be drawn that there is disruption of keratinocyte differentiation that is affecting the Ca^{2+} gradient and therefore CLP5 expression.

The pilot MS data for this protein showed a 3-fold decrease in expression for eczema samples compared with controls and an 11.1-fold increase in ichthyosis samples (Table 3.1). Comparing the stratum corneum of controls and eczema samples it can be seen that the staining is less intense for the eczema patients than the controls which corroborates the skin scraping MS findings.

3.5.5 Immunohistochemical staining of caspase-14

Caspase-14 is a cysteine protease[90] involved in regulation of keratinocyte differentiation and is a non-apoptotic caspase[91]. It has roles in epidermal cornification[92; 93], filaggrin and prosaposin processing[94], DNA degradation in differentiated keratinocytes[95] and protects the skin from UV rays[96; 97]. Caspase-14 is a known cysteine protease that has been shown to be inhibited by LEKTI which is a serine protease inhibitor. Recessive mutations in the *SPINK5* gene which codes for the full length LEKTI protein gives rise to the chronic skin barrier disease called Netherton syndrome. Polymorphisms in the *SPINK5* gene have also been associated with susceptibility to AE[98; 99; 100], this could suggest that changes may be observed in LEKTI and associated proteases in AE.

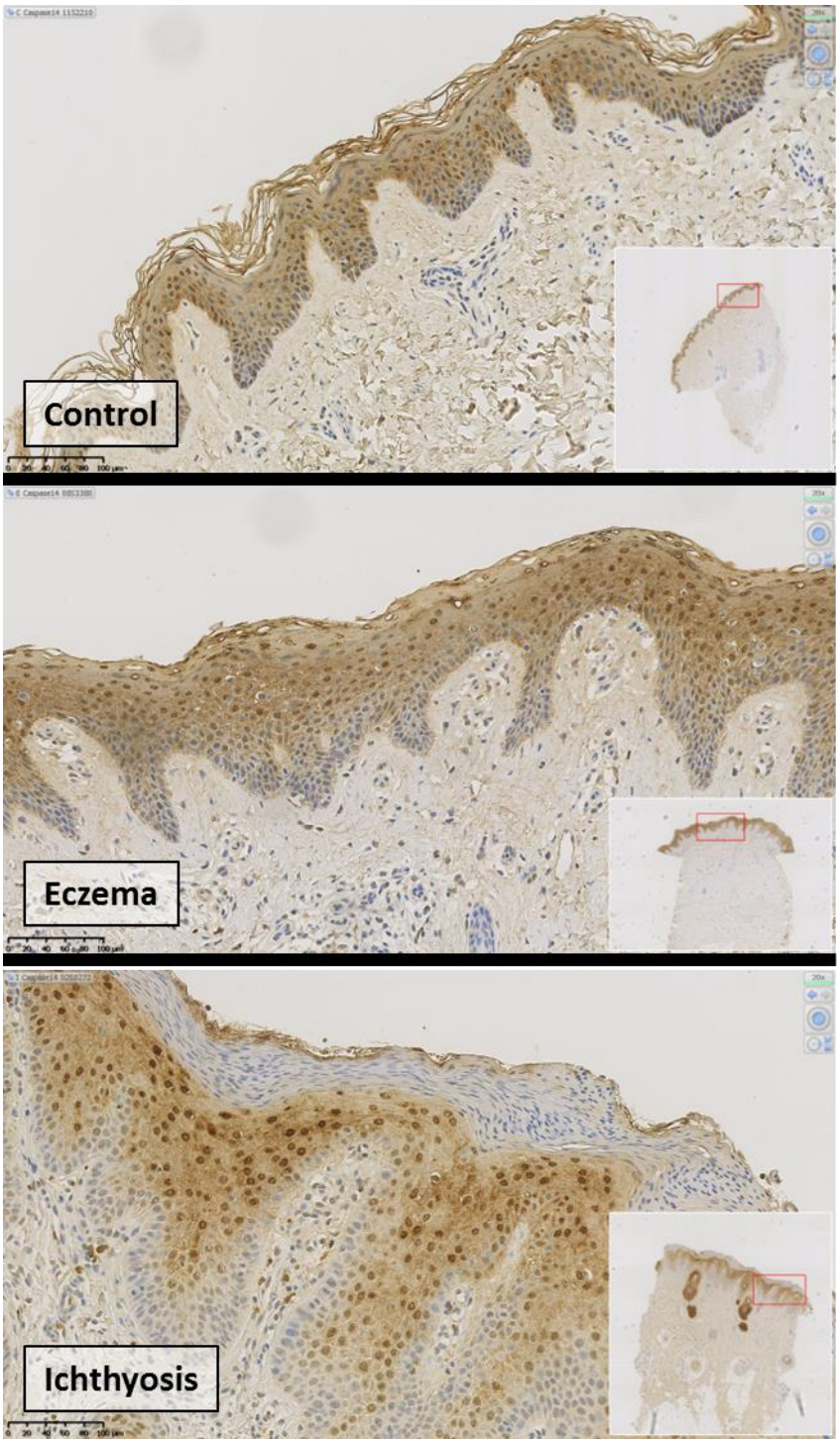

Figure 3.9. **Images showing the results of IHC staining for caspase-14 in control, eczema and ichthyosis patients.** Caspase-14 protein is stained brown following the IHC protocol (10.2.2), the nuclei have been counterstained blue with haematoxylin solution (Mayer's), the black bar represents 100 µm.

Staining of caspase-14 in controls shows cytoplasmic staining throughout the epidermis and darker nuclear staining in all layers of the epidermis apart from the stratum basale. Eczema samples show a similar distribution to controls; cytoplasmic staining throughout the epidermis and darker nuclear staining in all layers of the epidermis apart from the stratum basale.

Ichthyosis samples show the same distribution. There is no staining of the thickened stratum corneum, which is different to the control and eczema samples. No differences were observed in the location and distribution of caspase-14 in the skin of eczema and control samples, this finding demonstrates that not all proteins are affected equally by disease. For example CLP5 (section 3.5.4) demonstrated diffuse staining in eczema which potentially illustrates the disruption in correct trafficking in the uppermost layers of the skin, however the trafficking of caspase-14 illustrated here appears unchanged in health and disease.

Other studies show caspase-14 is down regulated in AE in affected and unaffected skin sites[101] and in other inflammatory skin diseases[91]. Secondary skin infections could be responsible for those changes as infection will affect cytokine secretion and thus the function of the skin barrier. In the pilot MS data we showed no change in caspase-14 for eczema samples compared with controls and a 2.3-fold decrease in ichthyosis samples compared with controls. This was supported by the IHC data presented here as there were no noticeable difference between the controls and eczema samples. However, a difference in the stratum corneum staining of ichthyosis patients compared with controls was observed.

3.5.6 Immunohistochemical staining of cathepsin D

Cathepsin D is a lysosomal acidic aspartic protease involved in intracellular breakdown of proteins. Its main role is to convert prosaposin to saposin A, B, C and D[102; 103]. These are natural detergent-like proteins and chaperones critical for degradation of glycosphingolipids in the lysosome.[104; 105] Deficiencies in these saposins can lead to lysosomal storage defects[102]. Cathepsin D has been associated with many diseases including preeclampsia[106], cancers[107] including malignant melanoma[108], breast carcinoma[109] and pancreatic ductal adenocarcinoma[110]. Cathepsin D also plays a role in skin from hair follicle morphogenesis to dermal and epidermal cell proliferation apoptosis[111].

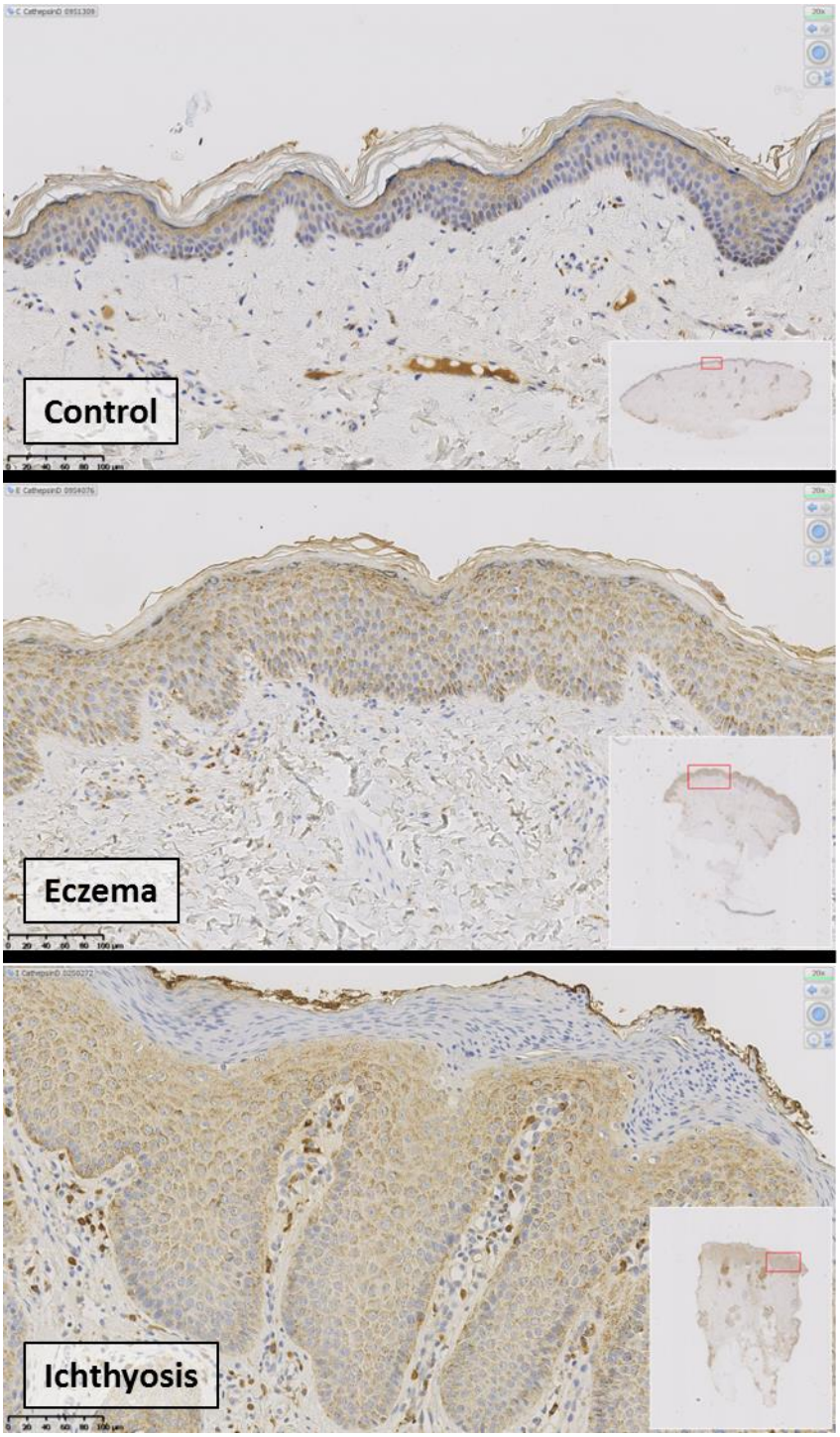

Figure 3.10. **Images showing the results of IHC staining for cathepsin D in control, eczema and ichthyosis patients.** Cathepsin D protein is stained brown following the IHC protocol (10.2.2), the nuclei have been counterstained blue with haematoxylin solution (Mayer's), the black bar represents 100 µm.

IHC staining of cathepsin D shows most staining in the cytoplasm of keratinocytes in the stratum granulosum and spinosum with no nuclear staining for controls. Eczema samples show more diffuse staining throughout cytoplasm of keratinocytes in the epidermis. Ichthyosis samples

show diffuse staining throughout the cytoplasm of the epidermis and little staining in the thickened superficial layer of skin.

There is sparse literature about research into cathepsin D in the skin, let alone in AE. Most research is focused on the involvement of cathepsin D in cancer. Cathepsins function best in slightly acidic conditions such as those found in solid tumours[112], its optimum pH is 3.7, yet it is still active at pH 6.8[107]. The epidermal pH in these samples could be causing the differential distribution. Skin pH varies across the body and with gender (men have lower skin pH) human skin pH ranges from pH 4.05-5.66[113]. Studies have investigated the role of pH in AE and have shown that skin pH is higher in AE and severity of AE correlates with skin pH[114]. Skin pH only pertains to the stratum corneum pH. A disruption of pH is enough to affect lipid synthesis, protease activity and the skin microflora, all of which are affected in AE.

The pilot MS data for cathepsin D showed no change in eczema samples compared with controls and a 100-fold increase in ichthyosis. The superficial layer of skin in the ichthyosis patients is quite darkly stained compared with the same layer in the controls (which would represent the skin scrapings taken from MS analysis). Changes in the ichthyosis and eczema samples could be attributed to pH changes, the pH change in eczema is thought to be caused by a deficiency of free amino acids, lactic acids and urocanic acids, making the skin environment more favourable to bacteria such as *S. aureus* which aggravate the condition[115].

3.5.7 Immunohistochemical staining of dermcidin

Dermcidin has antimicrobial properties and limits skin infections after bacterial colonisation. It expresses proteolytic activity against peptide and protein substrates[116]. Dermcidin is a binding partner of LEKTI in which mutations are the cause of the chronic skin barrier disease Netherton syndrome[58]. As described with caspase-14 (section 3.5.5) the relationship between dermcidin and LEKTI could have a knock-on effect for AE. Seeing as polymorphisms in the gene (*SPINK5*) that codes for LEKTI have been associated with AE susceptibility[98; 99; 100] proteins that interact with LEKTI could have altered expression in eczema.

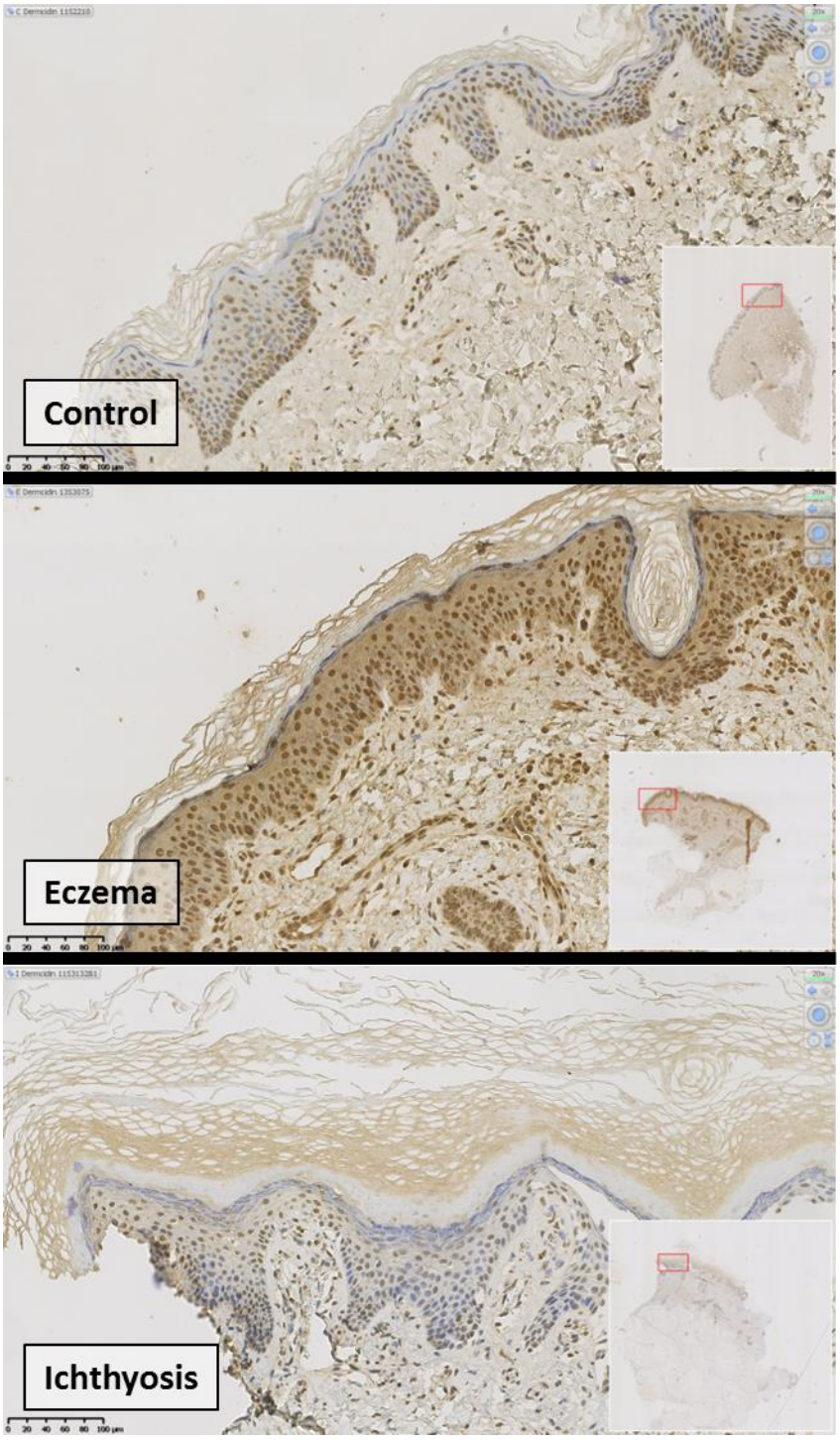

Figure 3.11. **Images showing the results of IHC staining for dermcidin in control, eczema and ichthyosis patients.** Dermcidin is stained brown according to the IHC protocol (10.2.2), the nuclei have been counterstained blue with haematoxylin solution (Mayer's), the black bar represents 100 µm.

Dermcidin IHC staining shows an irregular, largely nuclear staining pattern for controls limited to the lower layers of the epidermis. Eczema samples show nuclear staining throughout the epidermis. Ichthyosis samples show faint nuclear staining, but not of all cells in the epidermis.

Dermcidin is present mainly in eccrine sweat glands. Its precursor is excreted in sweat and processed into peptides that exhibit broad-spectrum antimicrobial functions at the surface of the skin.[117] Here however, dermcidin has been observed in the epidermis. The staining appears weak because skin dermcidin concentration is low, its presence in the epidermis may be due to leakage from eccrine sweat ducts, this may also explain why staining is not consistent within some of the groups.

Dermcidin is involved in other diseases such as Netherton syndrome where dermcidin is a binding partner for LEKTI. The same paper describes the same phenomenon that has been observed here; that dermcidin is expressed throughout the epidermis.[58] Perhaps dermcidin plays a role in other skin barrier diseases as it has been shown to do in Netherton syndrome. The pilot MS data did not show a change in expression for dermcidin in eczema samples compared with controls but a 5.8-fold increase was measured in ichthyosis (Table 3.1). This was not observed in the IHC staining, but may be due to small fold change.

3.6 Further investigations into calmodulin-like protein 5

3.6.1 Is the percentage coverage of calmodulin-like protein 5 stain different between controls and eczema?

To establish whether there was a quantifiable difference in “amount” of CLP5 stain within the epidermis between control and eczema samples we used ImageJ densitometry software to determine percentage epidermal staining. The images were converted to black and white (Figure 3.12) and coverage of black (i.e. stain) calculated as a percentage of the epidermis.

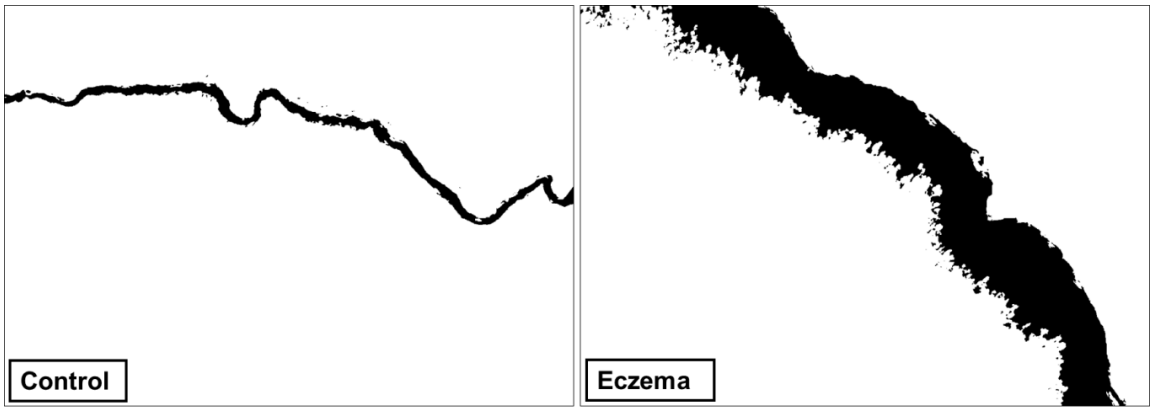

Figure 3.12. **Figure of sections of converted images from Figure 3.7 to black and white using ImageJ.** The whole images from Figure 3.7 of the control and eczema samples were converted into black and white images in order to calculate the percentage coverage of the stain within the epidermis a section of the epidermis is shown here.

Figure 3.13 shows significantly higher percentage coverage of the stain within the epidermis of eczema samples compared with the controls:

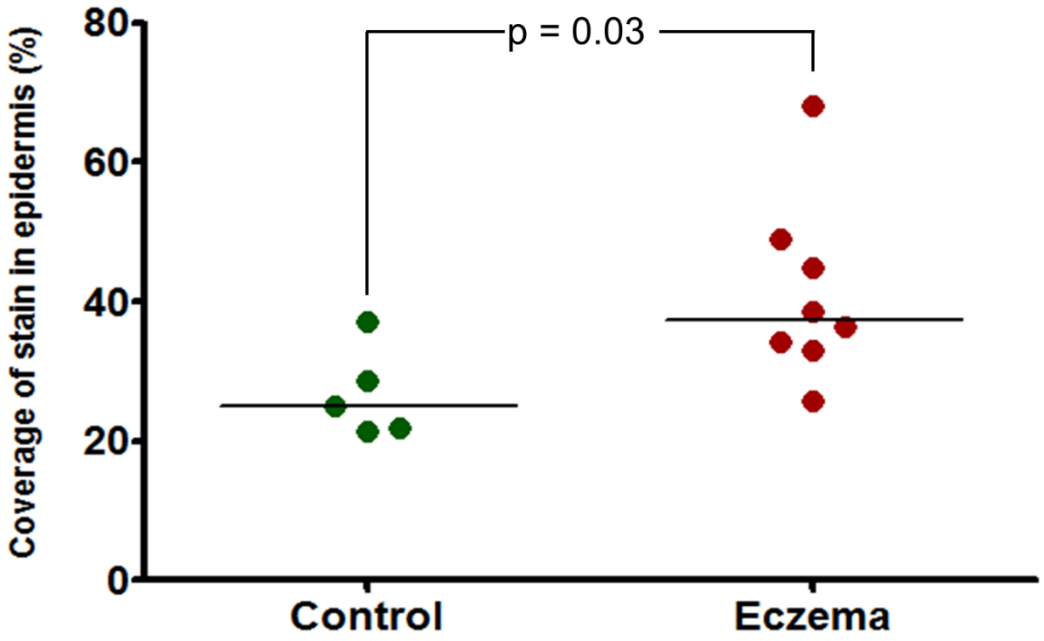

Figure 3.13. **Scatter plot of the percentage coverage of the IHC CLP5 stain.** This scatter plot shows the differing percentage coverages of the CLP5 IHC stain within the epidermis of the 5 controls and 8 eczema samples, a two-tailed, Mann Whitney t-test was used to determine the significance of these data.

ImageJ analysis demonstrated quantifiable changes in the staining pattern between controls and eczema samples (Figure 3.7) for CLP5 distribution in the epidermis. This secondary analysis demonstrates and confirms quantitative difference between the groups.

3.6.2 Could calmodulin-like protein 5 be a new marker of keratinocyte differentiation?

In order to investigate whether CLP5 could be a new marker of keratinocyte differentiation in the skin the staining pattern was compared to other established markers of keratinocyte differentiation: filaggrin and involucrin. Filaggrin and involucrin are markers of late keratinocyte differentiation.

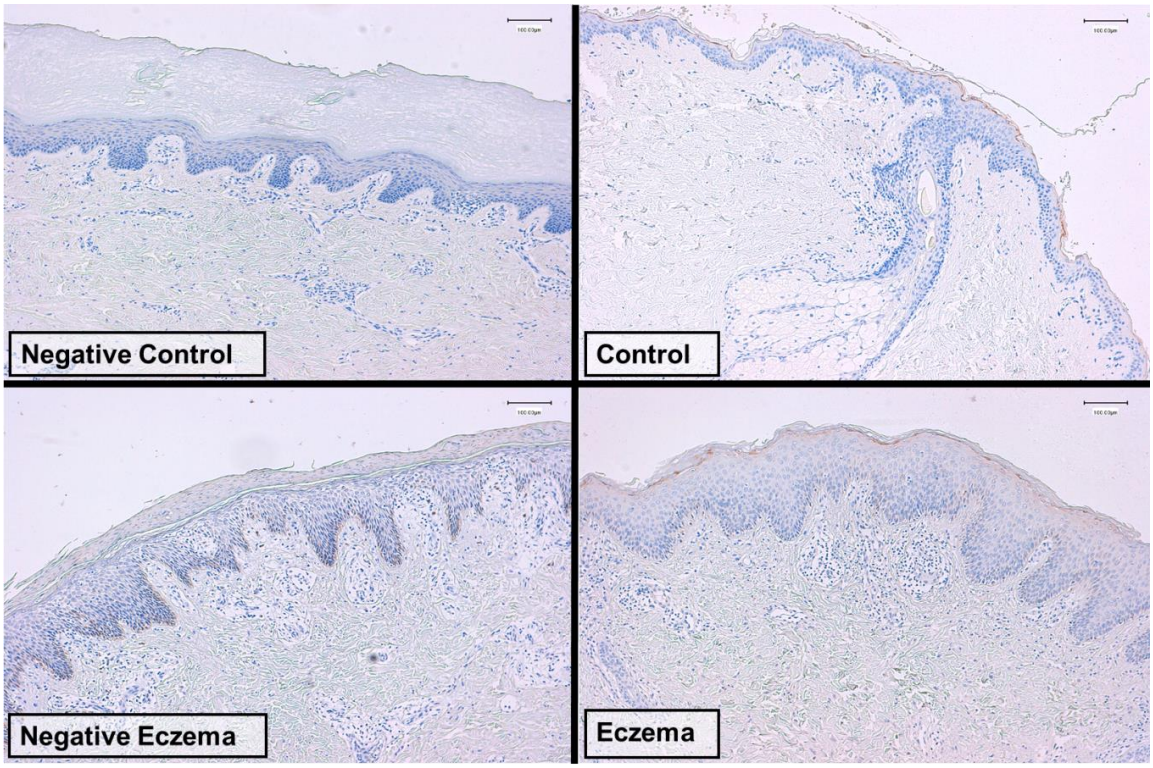

Figure 3.14. **Image showing filaggrin staining pattern.** Images showing filaggrin staining pattern for eczema and control samples with negative controls (omitting primary antibody), the bar represents 100µm.

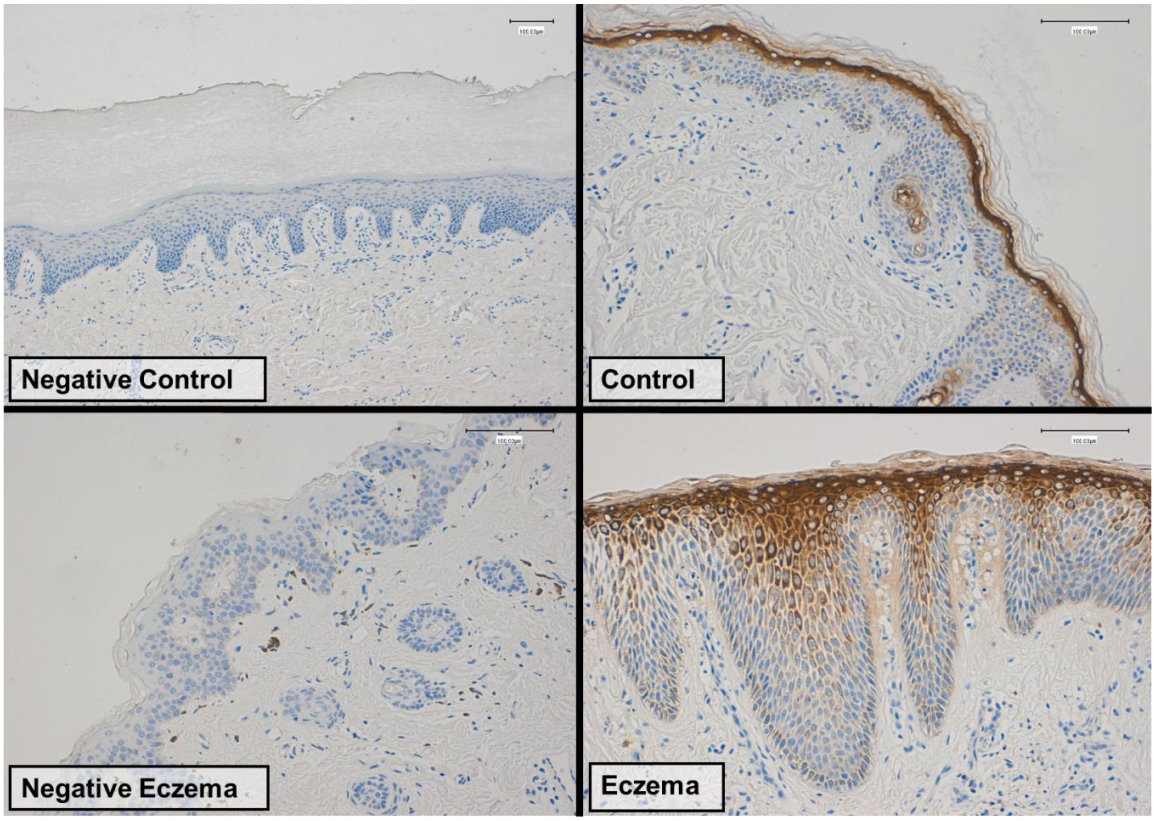

Figure 3.15. **Image showing involucrin staining pattern.** Images showing involucrin staining pattern for eczema and control samples with negative controls (omitting primary antibody), bar represents 100µm.

Filaggrin staining in these images is faint, however involucrin staining shows the same pattern as we showed for CLP5 (Figure 3.7). This is evidence to suggest that CLP5 could be a marker of late keratinocyte differentiation because it shares the same staining pattern in controls and eczema as current known markers.

3.6.3 Protein interaction study for calmodulin-like protein 5

CLP5 was the most altered protein in the IHC data set between controls and eczema samples. To investigate CLP5 in the skin further we identified its protein binding partners using magnetic beads. The protein interaction experiments (method 10.2.3) was carried out using a bead array to immobilise CLP5 and to identify the other proteins with which it interacts in skin homogenate. The magnetic beads used in this experiment contain a surface epoxy group that reacts with amine bonds within proteins to form a covalent complex, as shown in Figure 3.16:

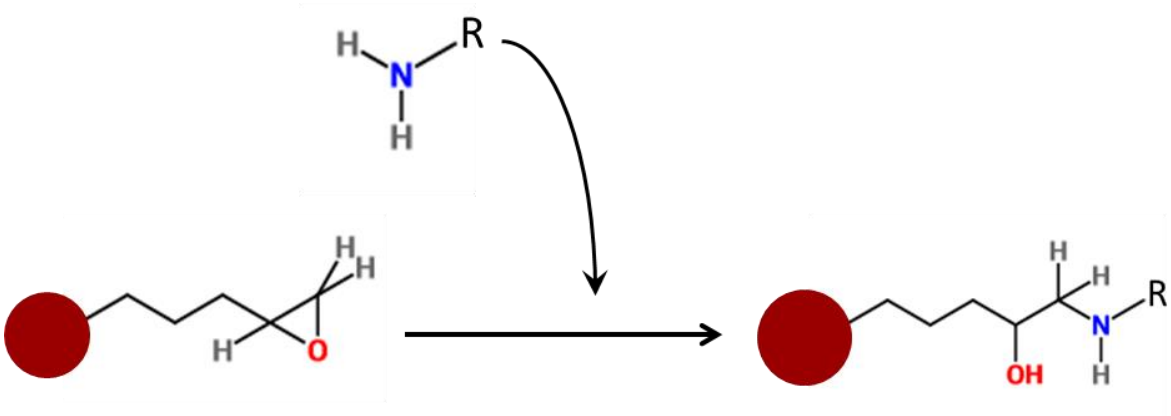

Figure 3.16. **Illustration showing how the epoxy group of the Dynabead® binds to proteins.** The proteins interact with the epoxy group which is bound to the magnetic bead and forms an amide covalent bond.

Due to the magnetic properties of the beads a magnet can be used to extract the "bead-CLP5-interacting proteins"-complex from the skin homogenate in order to isolate these proteins.

3.6.4 Proteins found to interact with calmodulin-like protein 5

A series of experiments were carried out to determine the best conditions as suggested in the manufacturer's protocol. Negative control samples were included where no CLP5 was bound to the beads and incubated in the same skin homogenate and prepared at the same time as the study samples. Proteins identified in the negative control sample were excluded as they were likely to be non-specific interactions. A yeast enolase peptide standard sample was included before the negative control sample for two purposes:

(i) to assess the chromatography quality such as peak shape, consistency of peptide retention times, signal intensity, lockmass accuracy

(ii) to identify human proteins that may be in the system and could be carried into subsequent study samples

Human proteins identified in the yeast enolase sample were also excluded. Finally, forty-two proteins were identified as interacting with CLP5, detailed in Table 3.2:

Protein Entry	Accession Number	Protein Full Name	Brief Description
1433E_HUMAN	P62258	14-3-3 protein epsilon	Mediates signal transduction by binding to phosphoserine-containing proteins
1433S_HUMAN	P31947	14-3-3 protein sigma	
1433Z_HUMAN	P63104	14-3-3 protein zeta/delta	
A1AT_HUMAN	P01009	Alpha-1-antitrypsin	Serine protease inhibitor
ACTB_HUMAN	P60709	Actin_ cytoplasmic 1	Involved in cell motility
ACTC_HUMAN	P68032	Actin_ alpha cardiac muscle 1	
ALBU_HUMAN	P02768	Serum albumin	Carrier protein
ANXA1_HUMAN	P04083	Annexin A1	Calcium-dependent phospholipid-binding proteins
ANXA2_HUMAN	P07355	Annexin A2	
ANXA5_HUMAN	P08758	Annexin A5	
ARGI1_HUMAN	P05089	Arginase-1	Catalyses: arginine -> orithine + urea
CALL3_HUMAN	P27482	Calmodulin-like protein 3	Calcium-ion binding
CASPE_HUMAN	P31944	Caspase-14	Cysteine-aspartic acid protease
CO1A1_HUMAN	P02452	Collagen alpha-1(I) chain	Major connective tissue component
CO1A2_HUMAN	P08123	Collagen alpha-2(I) chain	
CO6A3_HUMAN	P12111	Collagen alpha-3(VI) chain	
DCD_HUMAN	P81605	Dermcidin	Antimicrobial peptide
ENOA_HUMAN	P06733	Alpha-enolase	Glycolytic enzyme
FABP5_HUMAN	Q01469	Fatty acid-binding protein_ epidermal	Binds fatty acids + hydrophobic ligands
G3P_HUMAN	P04406	Glyceraldehyde-3-phosphate dehydrogenase	Antimicrobial + catalytic activity
GSTP1_HUMAN	P09211	Glutathione S-transferase P	Detoxifies reduced glutathion
H2A1A_HUMAN	Q96QV6	Histone H2A type 1-A	Responsible for nucleosome structure of chromosomal fibre
H2B1C_HUMAN	P62807	Histone H2B type 1-C/E/F/G/I	
H31T_HUMAN	Q16695	Histone H3.1t	
H4_HUMAN	P62805	Histone H4	
HBG2_HUMAN	P69892	Hemoglobin subunit gamma-2	Iron and oxygen binding
IGHG1_HUMAN	P01857	Ig gamma-1 chain C region	Antigen binding
K1H2_HUMAN	Q14532	Keratin_ type I cuticular Ha2	Forms hair and nails
KPYM_HUMAN	P14618	Pyruvate kinase PKM	Pyruvate kinase in glycolysis
LDHA_HUMAN	P00338	L-lactate dehydrogenase A chain	Catalyses step in anaerobic glycolysis
LEG3_HUMAN	P17931	Galectin-3	Carbohydrate-binding + antimicrobial
LUM_HUMAN	P51884	Lumican	Binds collagen fibres
PPIA_HUMAN	P62937	Peptidyl-prolyl cis-trans isomerase A	Accelerates the folding of proteins
PRDX1_HUMAN	Q06830	Peroxiredoxin-1	Antioxidant enzymes which reduce hydrogen peroxide
PRDX2_HUMAN	P32119	Peroxiredoxin-2	
PROF1_HUMAN	P07737	Profilin-1	Regulates actin polymerisation
S10A6_HUMAN	P06703	Protein S100-A6	Regulates cell cycle progression + differentiation
S10AA_HUMAN	P60903	Protein S100-A10	
SPB5_HUMAN	P36952	Serpin B5	Serine protease inhibitor
TRFE_HUMAN	P02787	Serotransferrin	Iron transport
VIME_HUMAN	P08670	Vimentin	Intermediate filament

Table 3.2. **Table listing the 42 proteins identified as interacting with CLP5.** Table contains the 42 proteins found to interact with CLP5 in a bead 'bait' binding study. For further information such as protein score, number of peptides and amount of protein detected please see appendix 12.1.

These proteins identified as interacting with CLP5 give an indication of CLP5's role within the skin and how it could be a marker of keratinocyte differentiation as demonstrated in Figure 3.7. PANTHER (http://www.pantherdb.org/) was used to classify the proteins in Table 3.2.

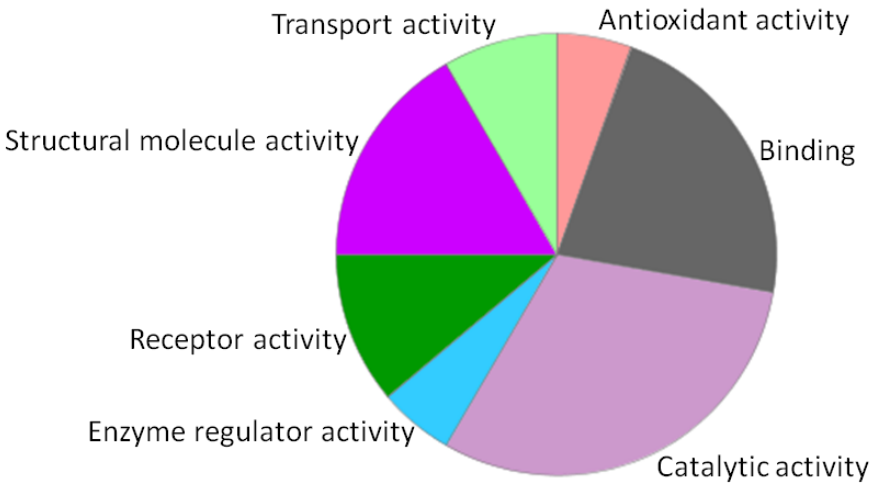

Figure 3.17. **Pie chart showing the molecular function distribution of the proteins in Table 3.2.** This pie chart shows the relative distribution of the proteins found to bind to CLP5 according to their molecular function.

This shows that the majority of the proteins shown to bind to CLP5 have catalytic activity, binding or structural molecular activity.

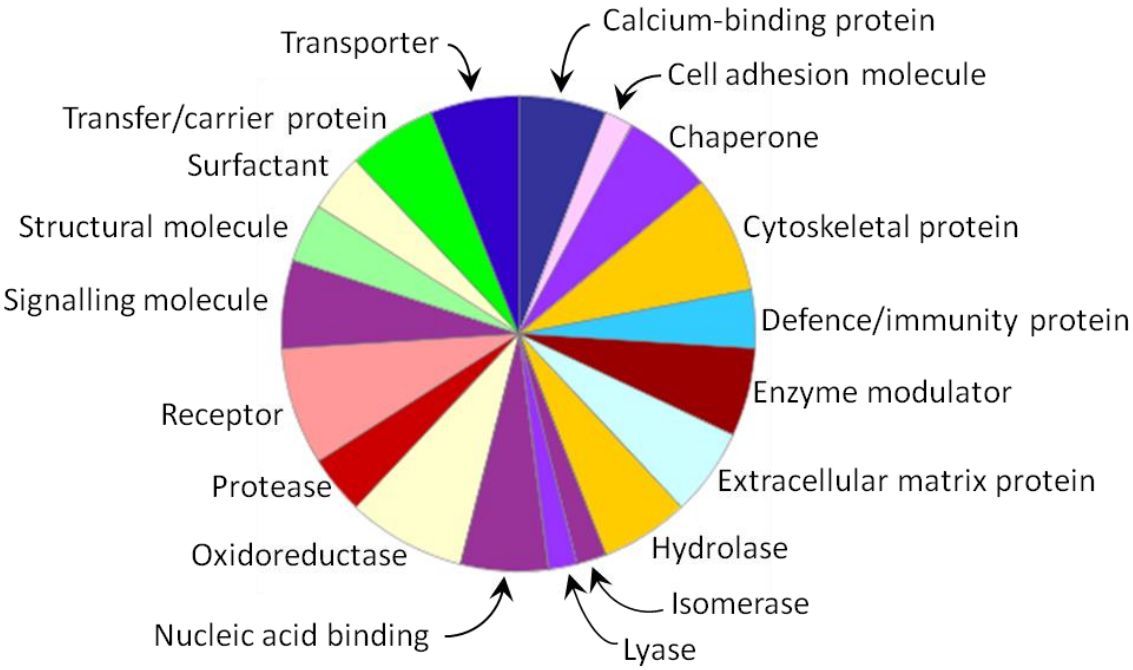

Figure 3.18. **Pie chart showing the protein class distribution of the proteins in Table 3.2.** This pie chart shows the relative distribution of the proteins found to bind to CLP5 according to protein class.

This figure illustrates that there is a diverse range of protein classes represented in the list of proteins found to bind to CLP5. Calcium-binding proteins, cytoskeletal, structural and defence/immunity components are all represented. Other calcium-dependant proteins such as

annexins and CLP3 have been identified as interacting with CLP5. CLP3 was stained for in section 3.5.3 showing a similar staining pattern to CLP5. This is not surprising as both proteins are from the same family. One protease and two protease inhibitors were identified: caspase-14, alpha-1-antitrypsin and serpin B5, respectively. This suggests that CLP5 could be involved in the mechanism that transports these proteins to the outer layers of the skin. This suggests that CLP5 is important in correct localisation of other proteins and the protease and protease inhibitor relationship in the skin. There is a critical balance within the skin between proteases and protease inhibitors, controlling the rate at which keratinocytes mature and in turn are shed. There are numerous skin diseases that arise from dysregulation in this balance. This indicates that the correct cellular trafficking of proteins may be disrupted in eczema and lead to defective barrier formation. This is important for barrier maintenance between host and the outside world.

Three proteins with antimicrobial properties were identified: dermcidin, glyceraldehyde-3-phosphate dehydrogenase and galectin-3. People who suffer from eczema are more susceptible to skin infections, the fact that antimicrobial proteins are associated with CLP5 and that CLP5 is found in the deeper layers of the epidermis in eczema compared with controls would support this. Maturation of keratinocytes is incomplete in eczema compared with controls, this allows microbes to penetrate deeper into the layers of the epidermis and therefore there is a greater need for antimicrobial proteins in those deeper layers in eczema. Or perhaps people with eczema are more prone to infection because anti-microbial proteins are not being trafficked to the outer layers of the skin where they are required for protection. Possibly CLP5 has a role in correct trafficking of proteins for skin barrier formation and defence, which is disrupted in eczema.

There are structural proteins found to interact with CLP5 such as actins, collagens, histones, keratin and vimentin as well as associated proteins such as lumican and profillin-1. Together these proteins are responsible for structural foundations of the skin, linking with the eczema hypothesis that there is a structural breakdown in the epidermis in eczema with CLP5 playing a role in this process.

3.7 Conclusions

From the seven selected proteins, CLP5 showed the most significant differences between controls, where the staining is limited to the layers of the stratum granulosum, and eczema samples, where staining also involved the stratum spinosum. The results reported previously in the literature describe increased CLP5 expression in AE compared with controls[89]. However, this was not observed in this chapter. Unlike mass spectrometry, the relative intensity of IHC staining cannot be measured reliably, but the differential expression pattern can be visualised. Our quantitative data supported the observation that there was a greater coverage of the CLP5 stain in the whole epidermis of the AE samples compared with controls. Further investigations

suggested that CLP5 could be a marker of keratinocyte differentiation due as it is comparable to the staining pattern of two other established markers of keratinocyte differentiation: filaggrin and involucrin. This correlation indicates the significance of CLP5 in differentiation and maintenance of the skin barrier in the epidermis. CLP3 shows less marked differences, but a similar distribution. They are both calmodulins and are linked with the skin's Ca^{2+} gradient. IHC staining of BH also showed changes in expression.

MS data results and IHC findings effectively provided different and complementary information. The MS data was obtained from skin scrapings of controls, eczema and lamellar ichthyosis patients. Skin scrapings will only obtain the uppermost layers of skin cells such as the stratum corneum. Whereas IHC was carried out on full thickness skin sections of which the stratum corneum only contributes a small percentage. IHC is less sensitive; MS analysis can detect changes of less than 2-fold whereas IHC detects changes of more than 10 orders of magnitude. Finally, the protein interaction study was designed to shed more light on the network of interactions involving CLP5 in the skin and proved to illustrate the complex network of relationships that CLP5 is involved with. CLP5 was shown to interact with structural proteins, proteases, proteases inhibitors and antimicrobial proteins.

Chapter 4

Proteases and protease inhibitors in the skin, their roles and interactions with other proteins in the skin

4 Proteases and protease inhibitors in the skin, their roles and interactions with other proteins in the skin

Contents

4.1 Proteases

Protease is a term that is used to describe a group of proteins or enzymes that act to cleave other proteins into peptides. An example is trypsin, an enzymatic protein that cleaves proteins at the carboxyl side of positively charged amino acids such as lysine or arginine provided that they are not followed by a proline residue. There are many proteases in the human body, some of which act similarly to trypsin, and others that act differently. Proteases can be split into six classes: serine proteases, cysteine proteases, aspartic proteases, metalloproteases[118], threonine proteases and glutamic acid proteases. The protease classes are dictated by mechanism of action. For serine, cysteine, aspartic acid, threonine and glutamic acid protease classes the amino acid in the name describes where the protease's active site is. For metalloproteases, this class contains proteases whose catalytic activity is dependent on a metal as a cofactor.

4.1.1 Proteases in the skin

Proteases and their regulation by inhibitors are extremely important for the correct formation and function of the skin barrier. In the skin proteases from the serine, metallo, aspartic and cysteine protease classes have been described previously. Protease classes can be further divided into families. A table of proteases present in the skin is shown overleaf (Table 4.1):

Type	Family	Specific Protease Name
Serine	S1	Human Kallikrein 1 (hK1)[119]
		Human Kallikrein 5 (hK5)
		Human Kallikrein 6 (hK6)[120]
		Human Kallikrein 7 (hK7)
		Human Kallikrein 8 (hK8)[121]
		Human Kallikrein 9 (hK9)
		Human Kallikrein 10 (hK10)
		Human Kallikrein 11 (hK11)
		Human Kallikrein 13 (hK13)[122]
		Human Kallikrein 14 (hK14)[123]
		chymotrypsin
		trypsin[124]
		elastase 2/neutrophil elastase[125]
		chymase
		Transmembrane protease serine 11E
		plasminogen[126]
		coagulation factor II/thrombin
Metallo	M10	matrix metallopeptidase-1[127]
		matrix metallopeptidase-2[128]
		matrix metallopeptidase-3[129]
		matrix metallopeptidase-8[130]
		matrix metallopeptidase-9
		matrix metallopeptidase-10
		matrix metallopeptidase-11[131]
		matrix metallopeptidase-12[132]
		matrix metallopeptidase-13[133]
		matrix metallopeptidase-19
		matrix metallopeptidase-28[134]
		membrane-type matrix metallopeptidase-1[135]
		membrane-type matrix metallopeptidase-2[136]
		membrane-type matrix metallopeptidase-3[137]
	M12	ADAM10
	M48	farnesylated-protein converting enzyme 1
Aspartic	A1	cathepsin D[138]
		cathepsin E[139]
	A2	retroviral-like aspartic protease 1[140]
	A22	presenilin 1[141]
Cysteine	C1	cathepsin B
		cathepsin C
		cathepsin F[142]
		cathepsin H[143]
		cathepsin K[144]
		cathepsin L
		cathepsin S
	C13	legumain[145]
	C14	caspase-1[146]
		caspase-3[147]
		caspase-4[148]
		caspase-5[149]
		caspase-6[150]
		caspase-7[151]
		caspase-8[152]
		caspase-9
		caspase-14[95]

Table 4.1. **Table listing the proteases described in skin.** This table shows the names and classes of proteases that have been described previously to be present in human skin.

In the skin proteases act to cleave proteins into smaller fragments. The purpose can be to degrade or modify a protein or to activate a cellular pathway. In the skin proteases are most active in the epidermis. The expression of proteases is different within each layers of the epidermis.[153] Proteases are synthesised as inactive precursor proteins, they have an additional

amino acid sequence at the N-terminus. Once this amino acid sequence or pro-peptide has been cleaved, the protease it becomes active, as illustrated in Figure 4.1:

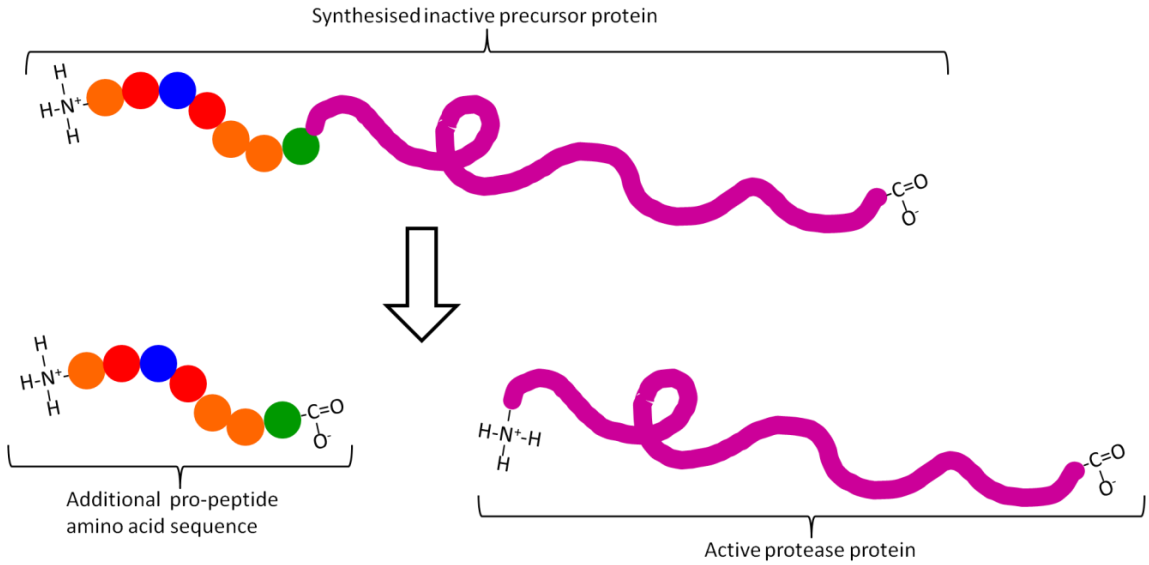

Figure 4.1. **Figure illustrating how a protease becomes activated after synthesis.** This figure represents the inactive precursor protein which is originally synthesised and then cleaved to release the active protease protein.

These proteases found in the skin have a role in the development of the epidermis. The activation cascades that these proteases are involved in dictates keratinocyte differentiation.[153] Experiments demonstrate that knocking out a single protease in mice can disturb the whole protease network and result in mice with a poorly developed skin phenotype[154]. Despite the fundamental role of proteases in the development and maintenance of the epidermis, their activity must be controlled and this is performed by protease inhibitors.

4.2 Protease inhibitors

Protease inhibitors inhibit and therefore regulate the activity of proteases. Similarly to proteases there are different classes of protease inhibitor depending on protease class affinity. The six classes of protease inhibitor are: serine protease inhibitors, cysteine protease inhibitors, aspartic protease inhibitors, metalloprotease inhibitors, threonine protease inhibitors and glutamic acid protease inhibitors. Not all protease inhibitors are proteins, some may be metal ions or lipid molecules for example zinc ions or cholesterol sulphate[155].

4.2.1 Protease inhibitors in the skin

In the skin, protease inhibitors control protease activity, particularly in the epidermis where proteases act to cleave proteins as part of the keratinocyte maturation process. A table of

protein protease inhibitors alongside the proteases they are known to inhibit in the skin is shown (Table 4.2):

Type	Specific Inhibitor Name	Inhibits
Serine	LEKTI	KLK5, KLK7, KLK14
	elafin/trappin 2	elastase
	SLPI	elastase, neutrophil elastase, cathepsin G, leucocyte elastase, trypsin, mast cell chymase
	SERPINB3	cathepsin L, cathepsin K, cathepsin S
	SERPINB4	
	SERPINB8	
	alpha-1-antitrypsin/SERPINA1	caspase-3
Cysteine	Cystatin A	IL-8, cathepsin B, cathepsin C, cathepsin H, cathepsin L, cathepsin S
	Cystatin C	
	Cystatin E/M	

Table 4.2. **Table listing the protease inhibitors described in the skin and the respective proteases they inhibit.** This table shows the protein protease inhibitors described in human skin alongside the proteases that they inhibit.

4.3 The role and function of proteases and protease inhibitors in the skin

Proteases and protease inhibitors work together in balance to control development and maturation of keratinocytes in the epidermis. Proteases trigger activation cascades responsible for desquamation[156], terminal differentiation[157] and cross-linkages within the extracellular matrix[138; 158]. However, these processes require controlling by protease inhibitors to prevent 'over'-desquamation, differentiation and/or cross-linking which leads to disease.

Undifferentiated pluripotent cells are found in the basal layer of the epidermis, here proteases associated with early stage differentiation are found: ADAMs (a disintegrin and metalloproteases), notably ADAM10. The activation cascade that ADAM10 induces modulates transcription[159] and expression of target genes within the nucleus of the basal cells[160; 161]. ADAM17 is activated at a later stage where it maintains the skin barrier[162] and regulates shedding of mature keratinocytes[163]. Caspases (cysteine proteases) are responsible for healthy maturation of skin in the central epidermal layers. A caspase-14 knock-out mouse presented a range of skin abnormalities such as parakeratosis, delayed cornification and incomplete filaggrin processing[92; 94]. Caspase-8 plays a role in regulation of keratinocyte differentiation, an absence of which leads to hyper-proliferation and a state of persistent inflammation[152]. Cathepsins span the cysteine and aspartic protease classes, cathepsins D and L are responsible for correct

cornification and hair follicle formation respectively, an insufficiency of either is associated with epidermal over-growth[138; 164].

During keratinocyte terminal differentiation the sequential shortening of filaggrin is initiated. Filaggrin is a large protein comprising mostly of repeating amino acid units, it is shortened by proteases as it moves up the layers of skin towards the surface of the epidermis. When filaggrin has been completely cleaved into single sub-units those units moisturise and protect the skin.[153] Finally, at the epithelial surface keratinocytes are fully differentiated desquamation occurs; corneocytes are shed from the surface of the skin. Proteases are responsible for cleaving and degrading the internal and external structural components to facilitate this. The main group of proteases involved are kallikreins (serine proteases). Desquamation by kallikreins is regulated by LEKTI (serine protease inhibitor) to avoid 'over'-desquamation[165]. Cytokine transforming growth factor beta (TGF-β) has roles in fibrosis and scarring of the skin. There are three subtypes: TGF-β1, TGF-β2 and TGF-β3, each have slightly different roles in maintenance of the epidermal skin barrier following injury.[166]

4.4 Under- or over-expression of key proteases, protease inhibitors and other proteins in the skin can lead to a range of skin disease phenotypes

When the balance between proteases and protease inhibitors in the skin becomes disturbed, normal development and maintenance does not continue and disease phenotypes develop.

4.4.1 Loss of function mutations in ADAM10

As mentioned in section 4.3 ADAM10 plays a role initiating differentiation in the basal layer of the epidermis. It has been shown that a loss of function mutation in the gene coding for the ADAM10 protease causes a disease called reticulate acropigmentation of Kitamura[167]. Reticulate acropigmentation of Kitamura (RAC) is a rare autosomal dominant disease with fewer than 200 cases reported, there are other associated diseases: Dowling Dego's disease, reticulate acropigmentation of Dohi, Haber's syndrome and Galli-Galli disease. This condition presents before the third decade of life when brown areas of skin appear, often on the backs of hands and feet. The lesions continue to grow for many decades.[168; 169] Histopathology shows the epidermis is thinner and the rete pegs are more elongated and thinner than in controls[167] demonstrating the changes that can result from the loss of function of a protease.

4.4.2 Loss of function mutations in ADAM17

Another ADAM protease mentioned in section 4.3 was ADAM17. It is activated at a later stage of differentiation and is responsible for maintaining the skin barrier. A loss of function deletion in the ADAM17 gene causes inflammatory skin and bowel disease[170]. There are many inflammatory diseases such as psoriasis, coeliac disease or eczema, that have been associated with disturbances in barrier function, be it of the skin or gut lining, as these two surfaces share common barrier properties. In a case report of two siblings, they both developed barrier symptoms within a few days of life, the symptoms were not confined to the skin, they also displayed gastrointestinal and cardiac pathologies. The skin lesions were rash-like, dry, blistering, red distributions around the mouth and anus. Both children were susceptible to frequent skin infections. The symptoms suggest a severe breakdown of barrier function, leading to increased risk of *Staphylococcus aureus* infection, which are otherwise uncommon. Both children had a homozygous deletion in *ADAM17*; the resulting ADAM17 protein was predicted to have no functioning properties.[170] This finding is supported by a mouse knock-out model of ADAM17 which presented with a systemic phenotype including impaired epithelial cell differentiation and maturation[171].

4.4.3 Loss of function mutations in cathepsin C

Papillon-Lefèvre syndrome (PLS) is an autosomal recessive disease arising from a loss of function mutation in the cathepsin C (cysteine protease) gene. PLS presents with dental growth abnormalities and skin complications: thickening of the stratum corneum on the backs of hands and feet.[172] Cathepsin C triggers enzyme cascades in epithelia throughout the body and degrade proteins[173]. Demonstrated in PLS, without cathepsin C the skin is unable to regulate growth of keratinocytes in the stratum corneum, because mature corneocytes are not being degraded at the same rate at which they are being produced. The underlying mechanism linking cathepsin C and desquamation in the skin is not fully known[45; 153].

4.4.4 Loss of function mutations in filaggrin

Filaggrin is not a protease like the three described previously (sections 4.4.1-4.4.3), but is a protein involved in the healthy development of the epidermis. Mutations in filaggrin have been associated with multiple skin diseases, notably AE. Despite the range and diversity of AE pathologies, a filaggrin mutation is the single greatest risk factor for the development of AE[174]. AE symptoms and the link to filaggrin mutations illustrate how fundamental filaggrin is in the skin.[153]

4.4.5 Loss of function mutations in cystatin A

Cystatin A (cysteine protease inhibitor) is found in the cornified envelope of the epidermis and inhibits cathepsin L, cathepsin V and the production of interleukin 8 by keratinocytes[175; 176]. Loss of function mutations in the cystatin A gene have shown to cause two diseases: exfoliating ichthyosis and acral peeling syndrome. Both of these diseases are characterised by excessive shedding or peeling of the skin predominantly affecting the hands and feet.[177; 178] These diseases differ from those described in sections 4.4.1-4.4.3, which were characterised by epidermal thickening due reduced protease cleaving, however, the reverse is true of exfoliating ichthyosis and acral peeling syndrome, there is too much epithelial degradation because of a lack of protease inhibitor to control the protease activity, leading to excessive skin cell shedding.

4.4.6 Loss of function mutation in LEKTI

LEKTI is a protease inhibitor that regulates desquamation it limits the proteolytic activity of kallikreins (serine proteases) which break down junctions linking adjacent. Netherton syndrome is a severe skin disease where there is excessive skin cell shedding, malformation of hair shafts and reddened skin. It is caused by a loss of function mutation in the LEKTI gene, there is no longer control of the rate at which kallikreins break apart corneocytes such that skin cells are constantly being shed.[153; 165]

4.5 When new roles for protease inhibitors are discovered

There are many unknowns associated with various cascades, pathways and interactions within the epidermis. Many of the protein roles discussed above were only determined when found to be mutated or deficient in disease (section 4.4). One such example is the case of LEKTI involvement in Netherton syndrome (section 4.4.6). Netherton syndrome was the first skin disease to be discovered as arising from mutations in a protease inhibitor in the skin. This discovery sparked new research in the field to uncover further roles of protease inhibitors in the skin and in disease.[45] Experiments were carried out on Netherton syndrome mouse models to investigate the causative mechanism of action in Netherton syndrome due to the LEKTI mutation. Mouse models demonstrated the link between Netherton syndrome and impaired desmosome function in the epidermis as well as LEKTI's crucial role in desquamation, hair formation, keratinisation and barrier formation.[179; 180] Further investigations into LEKTI and its relationship with other proteases in the skin led to the discovery that it may not be specific to serine proteases[45]. Proteomic investigations discovered that caspase-14 (cysteine protease), bound LEKTI fragments in *in vitro* experiments[57; 58].

The discovery that protease inhibitors, may not be strictly confined to their “class” as previously predicted, led to the postulation that other protease inhibitors may have binding sites for different proteases from different classes throughout their length. In this chapter we test the hypothesis that the protease:protease inhibitor balance is critical for correct maturation of the skin barrier. Using a series of immobilised ‘bait’ protease inhibitor arrays we identified potentially critical proteins/proteases in the skin responsible for the correct development of the skin barrier.

4.6 Selecting protease inhibitors in the skin for proteomic analysis

Table 4.2 lists the protease inhibitors known to be present in the skin, that list was interrogated to identify protease inhibitors commercially available, in full-length human sequence form and produced in a way compatible with the downstream processes. The resulting list of protease inhibitors is shown (Table 4.3):

Type	Specific Inhibitor Name	Inhibits
Serine	elafin/trappin 2	elastase
	alpha-1-antitrypsin/SERPINA1	caspase-3
Cysteine	Cystatin A	IL-8, cathepsin B, cathepsin C, cathepsin H, cathepsin L, cathepsin S
	Cystatin C	

Table 4.3. **Table showing the protease inhibitors selected for further proteomic analysis.** These protease inhibitors were selected from the list in Table 4.2 according to their commercial availability and suitability for subsequent experiments.

To test this hypothesis and to identify critical skin proteases a series of experiments were carried out to determine the best experimental conditions (method 10.2.3). These protein interaction experiments used bead arrays to immobilise the protease inhibitors and to investigate the proteins with which they interact in skin homogenate. We aimed to determine whether there were other protease inhibitors that have a role in correct desquamation of the skin in a similar way to LEKTI. The magnetic beads used in these experiments contain an activated surface epoxy group that reacts with amine bonds within proteins to form a covalent complex, as shown in Figure 3.16 and proteins were isolated. Negative control samples were included where no protease inhibitor was bound and incubated in the same skin homogenate used for the study samples and they were prepared at the same time. Proteins identified in the negative control sample were excluded from further results as they were likely to be non-specific interactions. A yeast enolase peptide standard sample was included before the negative control sample for two purposes:

(i) to assess the chromatography quality such as peak shape, consistency of peptide retention times, signal intensity, lockmass accuracy

(ii) to identify human proteins that may be contaminating the system and could be carried over into subsequent samples

Human proteins identified in the yeast enolase sample were excluded from further results.

4.6.1 Immobilising alpha-1-antitrypsin using magnetic beads to investigate its interactions with other proteins in the skin

Alpha-1-antitrypsin is a well-characterised serine protease inhibitor it was expected to interact with serine proteases in the skin such as neutrophil elastase as well as other members of the trypsin family such as chymotrypsin-like proteases[181]. However, the results from our protein interaction experiment using magnetic beads did not demonstrate this. From the experimental data 35 proteins were identified as shown in Table 4.4:

Protein Entry	Protein Accession Number	Protein Full Name	Protein Function
1433B_HUMAN	P31946	14-3-3 protein beta/alpha	
1433E_HUMAN	P62258	14-3-3 protein epsilon	
1433F_HUMAN	Q04917	14-3-3 protein eta	
1433G_HUMAN	P61981	14-3-3 protein gamma	Mediate signal transductions
1433S_HUMAN	P31947	14-3-3 protein sigma	
1433T_HUMAN	P27348	14-3-3 protein theta	
1433Z_HUMAN	P63104	14-3-3 protein zeta/delta	
ANXA2_HUMAN	P07355	Annexin A2	Calcium-dependent phospholipid-binding proteins
ANXA5_HUMAN	P08758	Annexin A5	
AXA2L_HUMAN	A6NMY6	Putative annexin A2-like protein	
CALL3_HUMAN	P27482	Calmodulin-like protein 3	
CALL5_HUMAN	Q9NZT1	Calmodulin-like protein 5	Calcium-binding proteins
CALM_HUMAN	P62158	Calmodulin	
ENOA_HUMAN	P06733	Alpha-enolase	Glycolytic enzyme
G3P_HUMAN	P04406	Glyceraldehyde-3-phosphate dehydrogenase	Carbohydrate metabolism
GRP78_HUMAN	P11021	78 kDa glucose-regulated protein	Protein folding and assembly
GSTP1_HUMAN	P09211	Glutathione S-transferase P	Detoxification
HBAZ_HUMAN	P02008	Hemoglobin subunit zeta	Oxygen transport
HS71L_HUMAN	P34931	Heat shock 70 kDa protein 1-like	Stabilise proteins against aggregation + mediate folding
HSP71_HUMAN	P08107	Heat shock 70 kDa protein 1A/1B	
HSP72_HUMAN	P54652	Heat shock-related 70 kDa protein 2	
HSP7C_HUMAN	P11142	Heat shock cognate 71 kDa protein	Chaperone protein
IGHG1_HUMAN	P01857	Ig gamma-1 chain C region	Antigen binding
MDHC_HUMAN	P40925	Malate dehydrogenase_ cytoplasmic	Citric acid cycle
PAL4A_HUMAN	Q9Y536	Peptidyl-prolyl cis-trans isomerase A-like 4A/B/C	Peptidyl-prolyl cis-transferase isomerase (PPIase)
PAL4D_HUMAN	F5H284	Peptidyl-prolyl cis-trans isomerase A-like 4D	
PAL4G_HUMAN	A2BFH1	Peptidyl-prolyl cis-trans isomerase A-like 4G	
PGK1_HUMAN	P00558	Phosphoglycerate kinase 1	Glycolytic enzyme
PGK2_HUMAN	P07205	Phosphoglycerate kinase 2	Kinase activity
PPIA_HUMAN	P62937	Peptidyl-prolyl cis-trans isomerase A	PPIase
PROF1_HUMAN	P07737	Profilin-1	Actin-binding protein
RAB44_HUMAN	Q7Z6P3	Ras-related protein Rab-44	Calcium-binding protein
SBSN_HUMAN	Q6UWP8	Suprabasin	Unknown primary function
SH3L3_HUMAN	Q9H299	SH3 domain-binding glutamic acid-rich-like protein 3	GTPase activity
TRFE_HUMAN	P02787	Serotransferrin	Iron transport

Table 4.4. **Table listing proteins identified from the protein interaction study of alpha-1-antitrypsin.** This table lists the 35 proteins identified as interacting with alpha-1-antitrypsin in this protein binding study. For further mass spectrometry information such as protein score, number of peptides and amount of protein detected please see appendix 12.2.

Although this does not show the results that we were expecting, it does demonstrate the role of alpha-1-antitrypsin in the processing of proteins. It is shown to interact with proteins covering a diverse set of roles from cellular responses to protein folding, phospholipid binding and proteins involved in monosaccharide catabolism. Suprabasin is the only protein with unknown function, there are only 5 publications on PubMed with suprabasin in the title[182] the oldest of which was published in 2002 and indicates it could be a substrate for transglutamase 2 and 3 and that it plays a role in epidermal differentiation as demonstrated in human and murine keratinocyte cell lines[183]. Perhaps suprabasin's role in binding here to alpha-1-antitrypsin in the skin expands on its role in the skin. Three papers outline suprabasin's role as a candidate oncogene marker in salivary gland adenoid cystic carcinoma[184], tumour endothelial cells[185] and oesophageal squamous cell carcinoma[186]. Finally it is also documented that suprabasin may have a role in vein graft failure[187]. However, it is possible that some of these interactions were non-specific.

4.6.2 Immobilisation of cystatin A and cystatin C using magnetic beads to investigate their interactions with other proteins in the skin

Cystatin A and cystatin C come from the same family of cysteine protease inhibitors and are predicted to interact with cysteine proteases such as cathepsins. Despite being closely related there is actually only 12.3% homology between their amino acid sequences[188]. The resulting proteins shown to interact with cystatin A and cystatin C are shown overleaf in Table 4.5 and Table 4.6, respectively:

Protein Entry	Protein Accession Number	Protein Full Name	Protein Function
1433B_HUMAN	P31946	14-3-3 protein beta/alpha	Mediate signal transductions
1433E_HUMAN	P62258	14-3-3 protein epsilon	
1433S_HUMAN	P31947	14-3-3 protein sigma	
1433Z_HUMAN	P63104	14-3-3 protein zeta/delta	
A1AT_HUMAN	P01009	Alpha-1-antitrypsin	Serine protease inhibitor
ACTB_HUMAN	P60709	Actin_ cytoplasmic 1	Cell motility + structure
AL1A1_HUMAN	P00352	Retinal dehydrogenase 1	Alcohol metabolism
ALBU_HUMAN	P02768	Serum albumin	Carrier protein
ALDOA_HUMAN	P04075	Fructose-bisphosphate aldolase A	Glycolytic enzyme
ANXA1_HUMAN	P04083	Annexin A1	Calcium-dependent phospholipid-binding proteins
ANXA2_HUMAN	P07355	Annexin A2	
ANXA4_HUMAN	P09525	Annexin A4	
ANXA5_HUMAN	P08758	Annexin A5	
ANXA6_HUMAN	P08133	Annexin A6	
ARGI1_HUMAN	P05089	Arginase-1	Urea cycle enzyme
ATPA_HUMAN	P25705	ATP synthase subunit alpha_ mitochondrial	Oxidative phosphorylation
CALL3_HUMAN	P27482	Calmodulin-like protein 3	Calcium-binding proteins
CALL5_HUMAN	Q9NZT1	Calmodulin-like protein 5	
CALM_HUMAN	P62158	Calmodulin	
CASPE_HUMAN	P31944	Caspase-14	Protease
CD44_HUMAN	P16070	CD44 antigen	Cell surface glycoprotein
CO1A1_HUMAN	P02452	Collagen alpha-1(I) chain	Integrate collagen bundles, bind extracellular matrix proteins, structural component of micro fibrils
CO1A2_HUMAN	P08123	Collagen alpha-2(I) chain	
CO6A1_HUMAN	P12109	Collagen alpha-1(VI) chain	
CO6A2_HUMAN	P12110	Collagen alpha-2(VI) chain	
CO6A3_HUMAN	P12111	Collagen alpha-3(VI) chain	
COEA1_HUMAN	Q05707	Collagen alpha-1(XIV) chain	
DCD_HUMAN	P81605	Dermcidin	Antimicrobial + antifungal
DHE3_HUMAN	P00367	Glutamate dehydrogenase 1_ mitochondrial	Mitochondrial matrix enzyme
ENOA_HUMAN	P06733	Alpha-enolase	Glycolytic enzyme
FABP5_HUMAN	Q01469	Fatty acid-binding protein_ epidermal	Bind long chain fatty acids
FIBB_HUMAN	P02675	Fibrinogen beta chain	Blood clotting
FIBG_HUMAN	P02679	Fibrinogen gamma chain	
GDIB_HUMAN	P50395	Rab GDP dissociation inhibitor beta	Vesicle trafficing
GELS_HUMAN	P06396	Gelsolin	Calcium-regulated protein
GRP78_HUMAN	P11021	78 kDa glucose-regulated protein	Protein folding + assembly
GSTP1_HUMAN	P09211	Glutathione S-transferase P	Detoxification
H12_HUMAN	P16403	Histone H1.2	Nucleosome structure
HNRPK_HUMAN	P61978	Heterogeneous nuclear ribonucleoprotein K	Nucleic acid binding
HPT_HUMAN	P00738	Haptoglobin	Haemoglobin binding
HS90A_HUMAN	P07900	Heat shock protein HSP 90-alpha	Stabilise proteins against aggregation + mediate folding
HSP71_HUMAN	P08107	Heat shock 70 kDa protein 1A/1B	
HSP7C_HUMAN	P11142	Heat shock cognate 71 kDa protein	
IGHG1_HUMAN	P01857	Ig gamma-1 chain C region	Antigen binding
KPYM_HUMAN	P14618	Pyruvate kinase PKM	Glycolysis
LDHA_HUMAN	P00338	L-lactate dehydrogenase A chain	Anaerobic glycolysis
LMNA_HUMAN	P02545	Prelamin-A/C	Nuclear stability
LRIQ3_HUMAN	A6PVS8	Leucine-rich repeat and IQ domain-containing protein 3	Protein-protein interactions
LUM_HUMAN	P51884	Lumican	Binds collagen
MDHC_HUMAN	P40925	Malate dehydrogenase_ cytoplasmic	Citric acid cycle enzyme
MDHM_HUMAN	P40926	Malate dehydrogenase_ mitochondrial	
PDIA1_HUMAN	P07237	Protein disulfide-isomerase	Preprocollagen hydroxylation
PDIA3_HUMAN	P30101	Protein disulfide-isomerase A3	Modulates protein folding
PGAM1_HUMAN	P18669	Phosphoglycerate mutase 1	Glycolytic enzymes
PGK1_HUMAN	P00558	Phosphoglycerate kinase 1	
PGS2_HUMAN	P07585	Decorin	Collagen binding
PLST_HUMAN	P13797	Plastin-3	Actin binding protein
PPIA_HUMAN	P62937	Peptidyl-prolyl cis-trans isomerase A	Protien folding

Continued overleaf

PRDX1_HUMAN	Q06830	Peroxiredoxin-1	Antioxidants, protective roles in cells
PRDX2_HUMAN	P32119	Peroxiredoxin-2	
PRDX6_HUMAN	P30041	Peroxiredoxin-6	
PROF1_HUMAN	P07737	Profilin-1	Acin binding protein
S10A6_HUMAN	P06703	Protein S100-A6	Regulates cellular processes
SBSN_HUMAN	Q6UWP8	Suprabasin	Unknown primary function
SPB5_HUMAN	P36952	Serpin B5	Serine protease inhibitor
TAGL2_HUMAN	P37802	Transgelin-2	Tumour suppressor
TALDO_HUMAN	P37837	Transaldolase	Lipid biocynthesis
TPM4_HUMAN	P67936	Tropomyosin alpha-4 chain	Actin binding protein
TRFE_HUMAN	P02787	Serotransferrin	Iron transport
VIME_HUMAN	P08670	Vimentin	Intermediate filament
VTDB_HUMAN	P02774	Vitamin D-binding protein	Transport protein

Table 4.5. **Table listing the proteins found to interact with cystatin A.** This table details the 71 proteins found to interact with cystatin A from this protein binding study. For further mass spectrometry information such as protein score, number of peptides and amount of protein detected please see appendix 12.3.

Protein Entry	Protein Accession Number	Protein Full Name	Protein Function
1433B_HUMAN	P31946	14-3-3 protein beta/alpha	
1433F_HUMAN	Q04917	14-3-3 protein eta	
1433G_HUMAN	P61981	14-3-3 protein gamma	Mediate signal transductions
1433S_HUMAN	P31947	14-3-3 protein sigma	
1433T_HUMAN	P27348	14-3-3 protein theta	
1433Z_HUMAN	P63104	14-3-3 protein zeta/delta	
ACTA_HUMAN	P62736	Actin_ aortic smooth muscle	
ACTB_HUMAN	P60709	Actin_ cytoplasmic 1	
ACTC_HUMAN	P68032	Actin_ alpha cardiac muscle 1	Cell motility + structure
ACTG_HUMAN	P63261	Actin_ cytoplasmic 2	
ACTH_HUMAN	P63267	Actin_ gamma-enteric smooth muscle	
ACTS_HUMAN	P68133	Actin_ alpha skeletal muscle	
ALBU_HUMAN	P02768	Serum albumin	Carrier protein
ANXA2_HUMAN	P07355	Annexin A2	Calcium-dependent protein
ARGI1_HUMAN	P05089	Arginase-1	Urea cycle enzyme
AXA2L_HUMAN	A6NMY6	Putative annexin A2-like protein	Calcium-dependent protein
CASPE_HUMAN	P31944	Caspase-14	Protease
CO1A1_HUMAN	P02452	Collagen alpha-1(I) chain	Binds extracellular matrix
ENOA_HUMAN	P06733	Alpha-enolase	Glycolytic enzyme
FIBG_HUMAN	P02679	Fibrinogen gamma chain	Blood clotting
G3P_HUMAN	P04406	Glyceraldehyde-3-phosphate dehydrogenase	Carbohydrate metabolism
H31_HUMAN	P68431	Histone H3.1	
H31T_HUMAN	Q16695	Histone H3.1t	Nucleosome structure
H32_HUMAN	Q71DI3	Histone H3.2	
H33_HUMAN	P84243	Histone H3.3	
HBAZ_HUMAN	P02008	Hemoglobin subunit zeta	Oxygen binding
NIT2_HUMAN	Q9NQR4	Omega-amidase NIT2	Detoxification
PPIA_HUMAN	P62937	Peptidyl-prolyl cis-trans isomerase A	Protein folding
PRDX2_HUMAN	P32119	Peroxiredoxin-2	Antioxidant
PROF1_HUMAN	P07737	Profilin-1	Actin binding protein

Table 4.6. **Table listing the proteins found to interact with cystatin C.** This table lists the 30 proteins found to interact with the protease inhibitor cystatin C in this protein binding study. For further mass spectrometry information such as protein score, number of peptides and amount of protein detected please see appendix 12.4.

The most noteworthy observation is that caspase-14 (cystatin protease) has been identified as interacting with both cystatin A and cystatin C protease inhibitors. Two other interesting proteins detected were the serine protease inhibitors alpha-1-antitrypsin and serpin B5, which were both detected as interacting with cystatin A and cystatin C. Cystatin C has already been described as interacting with serum albumin in a serum “interactome” study[189]. Overall proteins shown to interact with cystatin A show prominent roles in glucose processing, extracellular structural roles such as collagen and matrix organisation proteins as well as transport of proteins to and maintenance of the mitochondrial membranes. And overall the proteins identified as interacting with cystatin C show some similarities with cystatin A such as transport of proteins to and maintenance of the mitochondrial membranes as well as regulating mitochondrial membrane permeability and internal mitochondrial organisation. However, in common with alpha-1-

antitrypsin analysis it is possible that the long list of proteins identified may indicate some non-specific bindings; proteins that have a high affinity to bind to any proteins, or interacting with the bead surface and alternatively they could be interacting indirectly with the protease inhibitors. For example cystatin A and cystatin C have been shown to bind serum albumin, which itself is a transporter protein in the blood and therefore itself binds to several other types of protein.

4.6.3 Immobilising elafin using magnetic beads to investigate its interactions with other proteins in the skin

Elafin is a serine protease inhibitor, which was predicted to interact with serine proteases though it has not been extensively studied in the literature. Elafin plays a crucial role in the skin, particularly in the skin barrier, where it acts against the protease neutrophil elastase[190]. The results of our protein interaction study are shown for elafin in Table 4.7.

Protein Entry	Protein Accession Number	Protein Full Name	Protein Function
1433S_HUMAN	P31947	14-3-3 protein sigma	Mediates signal transduction
ACTA_HUMAN	P62736	Actin_ aortic smooth muscle	Cell motility + structure
ACTB_HUMAN	P60709	Actin_ cytoplasmic 1	
ACTC_HUMAN	P68032	Actin_ alpha cardiac muscle 1	
ACTG_HUMAN	P63261	Actin_ cytoplasmic 2	
ACTH_HUMAN	P63267	Actin_ gamma-enteric smooth muscle	
ACTS_HUMAN	P68133	Actin_ alpha skeletal muscle	
ALBU_HUMAN	P02768	Serum albumin	Carrier protein
ANXA2_HUMAN	P07355	Annexin A2	Calcium-dependent phospholipid-binding protein
AXA2L_HUMAN	A6NMY6	Putative annexin A2-like protein	
CO1A1_HUMAN	P02452	Collagen alpha-1(I) chain	Binds extracellular matrix
ENOA_HUMAN	P06733	Alpha-enolase	Glycolytic enzyme
FABP5_HUMAN	Q01469	Fatty acid-binding protein_ epidermal	Binds long chain fatty acids
GSTP1_HUMAN	P09211	Glutathione S-transferase P	Detoxification
H31_HUMAN	P68431	Histone H3.1	Nucleosome structure
H31T_HUMAN	Q16695	Histone H3.1t	
H32_HUMAN	Q71DI3	Histone H3.2	
H33_HUMAN	P84243	Histone H3.3	
MON1A_HUMAN	Q86VX9	Vacuolar fusion protein MON1 homolog A	Trafficking protein
PAL4A_HUMAN	Q9Y536	Peptidyl-prolyl cis-trans isomerase A-like 4A/B/C	Protein folding
PAL4D_HUMAN	F5H284	Peptidyl-prolyl cis-trans isomerase A-like 4D	
PAL4G_HUMAN	A2BFH1	Peptidyl-prolyl cis-trans isomerase A-like 4G	
PPIA_HUMAN	P62937	Peptidyl-prolyl cis-trans isomerase A	
PROF1_HUMAN	P07737	Profilin-1	Actin binding protein

Table 4.7. **Table listing the proteins found to interact with elafin.** This table lists the 24 proteins found to interact with the protease inhibitor elafin in this protein binding experiment. For further mass spectrometry information such as protein score, number of peptides and amount of protein detected please see appendix 12.5.

This experiment demonstrated that elafin interacts with have a predominant role in microfibrils, in particular actin and myosin structure and assembly.

4.7 What the proteins identified as interacting with the protease inhibitors of interest indicate

The aim of this chapter was to investigate the roles of different protease inhibitors in the skin similarly to Bennett et al., in 2010[57] with LEKTI. In order to do so we bound selected protease inhibitors to immobilised magnetic bead arrays individually and incubated them in skin homogenate before removing the bead-protease inhibitor-interacting protein complex. By doing so we hoped to understand more about the role of protease inhibitors and proteases in the skin. These findings can be applied to other skin diseases as potential drug therapy targets. Using this technique we were able to identify some undescribed interactions with protease inhibitors.

4.7.1 How the results from cystatin A and cystatin C binding experiments suggest new binding roles for these protease inhibitors

Cystatin C has been described previously as interacting with serum albumin[191] which corroborates with our results as we also identified serum albumin as an interactor. Both cystatin A and cystatin C protease inhibitors demonstrated an interaction with caspase-14, which is a cysteine protease. Caspase-14, unlike most of the other cysteine proteases is largely confined to the skin and more specifically the stratum corneum[192]. It is pivotal in the terminal differentiation of keratinocytes, correct maturation of the skin barrier, skin hydration and protection from UV radiation.[95] Caspase-14 is one of the main enzymes responsible for filaggrin break-down in the stratum granulosum and stratum corneum. In disease caspase-14 is absent in psoriatic lesions, but not in unaffected skin areas of the same patients[193]. However, caspase-14 deficient mice did not develop skin abnormalities[97]. Perhaps low levels of caspase-14 in psoriasis is a downstream effect of a signal triggering over-activity of cysteine protease inhibitors, such as cystatin A and cystatin C in the lesional area. Caspase-14 has also been described as interacting with LEKTI which revealed that LEKTI played a role in skin barrier development.[57]

Other proteins previously found to be associated with cystatin A include dermcidin, calcium-dependent proteins, structural proteins, protein S100-A6 and vitamin D3 binding protein, all of which have roles in the skin. Dermcidin is an antimicrobial peptide secreted from sweat glands and plays a role in protecting the skin barrier from infection. Calcium-dependent proteins include calmodulin and calmodulin-like proteins, their concentration in the skin increases with calcium ion concentration and thus proximity to the surface of the skin. As discussed in chapter 3 we propose that calmodulin-like protein 5 could be a marker of keratinocyte differentiation and demonstrates the lack of differentiation in AE. Protein S100-A6 belongs to a larger group of S100 proteins two of which (protein S100-A7 and protein S100-A15) have been linked to

psoriasis.[194] There were not as many interacting proteins identified for cystatin C, but similarly to cystatin A several structural proteins were detected, including actins and collagen as well as regulatory signalling molecules.

4.7.2 How the results of the alpha-1-antitrypsin binding experiment differ from our expectations

Alpha-1-antitrypsin is renowned for being particularly “sticky”, it binds to and interacts with many proteins. There are reports of alpha-1-antitrypsin interacting with kallikrein proteins[195]. This is of interest as kallikreins are serine proteases, we might expect to find them interacting with the serine protease inhibitor alpha-1-antitrypsin. However, kallikreins were not detected in this series of experiments, this was also true when another group were looking for kallikreins from human skin tissue[57]. Kallikreins play a key role in initiating a cascade to control desquamation of the skin. There are many potential reasons why we were unable to identify kallikreins. In the stratum granulosum, kallikreins are stored in lamellar bodies within the granular cell, these lamellar bodies contain lipids and are impermeable and highly hydrophobic. It would be unlikely that the mass spectrometry technique used here would identify proteins in highly lipophilic regions. In order to study those proteins a modified approach would be required.[196]

4.7.3 How the results from the elafin binding experiment differ from our expectations

Elafin showed a similar interacting profile to the previous protease inhibitors (sections 4.6.1 and 4.6.2) with a large number of structural/cytoskeletal proteins, protein modification enzymes, glucose processing and DNA packaging proteins. We were expecting to identify elastase (serine protease) (Table 4.2). Elastase is an enzyme responsible for breaking down elastin, one of the major connective tissue components. However, due to the low levels of elastase in healthy skin we were unable to detect it[197]. Elafin also controls the serine protease neutrophil elastase within the skin[198]. Neutrophil elastase destroys pathogens that have been phagocytosed as part of the inflammatory response and elafin acts to quench the inflammatory reaction[190; 199]. Elafin also has antimicrobial properties; antiviral[200; 201], antibacterial[202; 203] and antifungal[204]. To further interrogate the dataset generated in Table 4.7, blast searched against two bacterial proteomes: *Proprionbacteria* and *Staphylococcus*. These are the two most abundant bacteria found on the skin’s surface and within the uppermost layers of the epidermis. Only one bacterial protein was identified and that was a phosphocarrier protein of *Staphylococcus aureus*. This is a protein involved in the carbohydrate metabolism pathway.

4.8 Conclusions from the protein binding experiments discussed in this chapter

The work carried out in this chapter describes an isolation technique combined with mass spectrometry to identify proteins from skin homogenate interacting with protease inhibitors. Within that remit we hoped to identify new proteases within the skin that may be therapeutic targets or importance to skin barrier formation. We studied the protease inhibitors alpha-1-antitrypsin, cystatin A, cystatin C and elafin. This method designed to identify proteases and their interactions with isolated protease inhibitors in the skin successfully identified cystatin A and cystatin C as inhibitors or the serine protease caspase-14 (Table 4.5 and Table 4.6). Dermcidin, an antimicrobial peptide, was also found to bind to cystatin A (Table 4.5).

AE is a skin disease caused by a defective skin barrier. We thought that investigation into protease inhibitors and proteases in the skin would shed more light on their roles, and thus be of potential used as therapeutic targets in skin disease. Caspase-14 is a protein responsible for the breakdown and processing of filaggrin monomers into free amino acids[205]. A deficiency of caspase-14 in mice leads to accumulation of filaggrin monomers, unable to be processed to free amino acids[94]. Not only is caspase-14 a fundamental protease required for correct processing of filaggrin and therefore moisturising of the skin, it has also been found that there is reduced caspase-14 expression in patients with AE[91; 101].

Dermcidin is an antimicrobial peptide expressed in eccrine sweat glands protecting epithelial surfaces of the body. Unlike other antimicrobial proteins, dermcidin is not produced by keratinocytes.[206; 207] It does however, play a role in triggering keratinocytes to release cytokines and chemokines[208]. Patients with AE suffer more frequent skin microbial infections compared with controls and they have reduced amounts of dermcidin peptides in their sweat. Furthermore, patients with AE who have a long history of skin infections had an even lower amount of dermcidin peptides[209].

In this chapter cystatin A was found to interact with both caspase-14 and dermcidin. This has interesting implications for AE. Dermcidin and caspase-14 have both shown to be downregulated in AE, suggesting that there could be over-activity of cystatin A in patients with AE leading to over-suppression of dermcidin and caspase-14. There is only one publication linking both cystatin A and AE[210]. They found a significant association between polymorphisms in cystatin A and AE[211]. The results in this chapter appear compelling enough to suggest that cystatin A could be a key player in manifestations of AE in susceptible children alongside two of its binding partners: dermcidin and caspase-14.

Chapter 5

Optimisation of protocols for the proteomic analysis of full-thickness skin biopsies

5 Optimisation of protocols for the proteomic analysis of full-thickness skin biopsies

Contents

5.1 Introduction

The analysis of full thickness skin as a sample tissue type has never been studied before in the UCL Biological Mass Spectrometry Centre therefore extensive optimisation was required. Additionally, there is a paucity of research available for the analysis of full thickness skin using proteomics. This is probably due to the high complexity of skin; containing extensive cross-linkage bonds between proteins and protein-lipid complexes which make the skin insoluble and resistant to digestion with MS compatible proteases (particularly trypsin, which is the most commonly used in mass spectrometry, due to the use of lysine residues in cross-link bonds). Secondly, the high lipid content in skin contributes to its insolubility and consequently a high number of proteins are membrane bound and therefore largely hydrophobic.

The first step in the analysis of tissue for proteomics involves a homogenisation step, preliminary work for this thesis suggested that in order to get the solid mass of skin tissue into solution it would be first crushed under liquid nitrogen using a pestle and mortar. A homogenisation buffer was then added and the mixture homogenised by hand in a glass homogeniser. Skin is a complex sample containing lipids, salts as well as the proteins of interest, there are also salt and buffer contaminants introduced by the homogenisation step that need to be removed. Prior to analysis method development was required to optimise conditions for analysis. Optimisation was necessary because an analysis method for skin had not been optimised in our laboratory. In order to purify the skin samples two techniques were evaluated:

(i) Desalting and purification of proteins using ultra-centrifugal filtration 3 kDa units (method 10.2.6)

(ii) Protein precipitation using organic solvents (chloroform:methanol) (method 10.2.7)

Initial optimisation experiments were performed on the less sensitive QToF Premier in our laboratory. Once the optimised extraction methods were determined all further analyses were carried out on the more sensitive SYNAPT G2-Si QToF-MS.

5.2 Purification of proteins from skin using ultra-centrifugal filtration techniques

Size exclusion filters were used to evaluate removal of lower molecular weight compounds from the skin homogenate, illustrated in Figure 5.1, step 5:

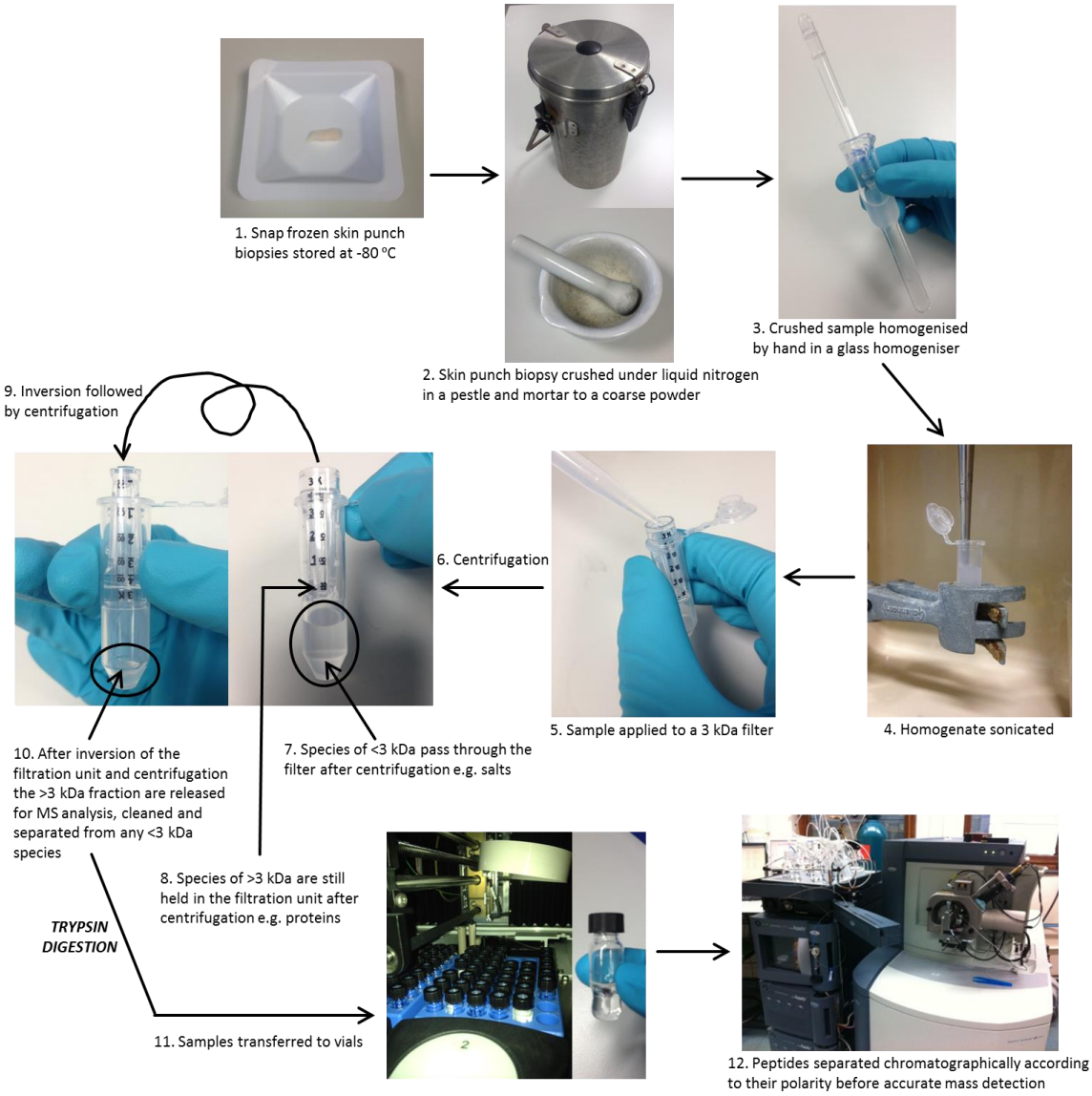

Figure 5.1. **Diagram showing the generic workflow for preparing skin punch biopsies for MS analysis, including a 3 kDa clean-up step.** Points 1-12 show the sample preparation procedure that was used at this stage of the project. The samples was initially snap frozen, crushed under liquid nitrogen with a pestle and mortar, further homogenised using a glass homogeniser, sonicated, low molecular (<3 kDa) weight species filtered, the samples trypsin digested and transferred to vials for MS analysis.

The principle of ultra-centrifugal filtration is a membrane which only allows molecules of a certain size to pass through it whilst being centrifuged at a specific speed. In this case, we chose 3 kDa filters as most salts, lipids, small molecules and peptides are less than 3 kDa. Proteins would be retained as their mass is greater than 3 kDa. The manufacturer's recommended protocol suggested that a series of wash steps may be required to increase purification and desalting capacity of the columns. We evaluated this by performing experiments that included 1, 2 and 3 wash steps. In each case the retained protein and eluent was analysed to determine the protein content. Both fractions were analysed on a Waters QToF Premier mass

spectrometer: the flow through containing the <3 kDa species (i.e. contaminants such as salts) and the concentrate containing the >3 kDa species.

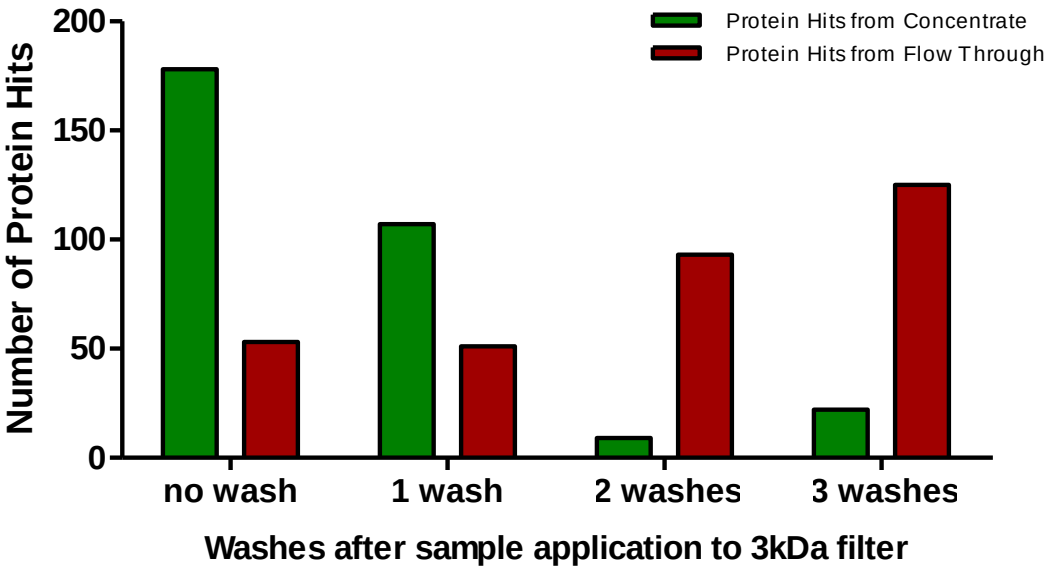

Figure 5.2. **Graph showing the number of proteins identified by MS analysis with a variable number of washes after filtration.** The bars in green show the proteins recovered from the concentrate (>3 kDa fraction) and in red show the proteins recovered from the flow through (<3 kDa fraction) for no wash after filtration up to 3 washes.

The results from this experiment were somewhat surprising as they show that with additional washes the protein content of the concentrated fraction (>3 kDa) decreases and the protein content of the flow through fraction (<3 kDa) increases. This indicates that the additional washes are damaging the 3 kDa filter therefore allowing proteins to be forced through the membrane. To recover as much protein as possible no wash steps were included for all further experiments using 3 kDa filtration.

5.3 The evaluation of organic solvent and protein precipitation as a method for the purification of proteins from skin

Precipitation, using chloroform and methanol in a 1:2 v/v extracts lipids from a sample without interfering with the proteins as described by Folch in 1957[212]. This is illustrated in, steps 5-7:

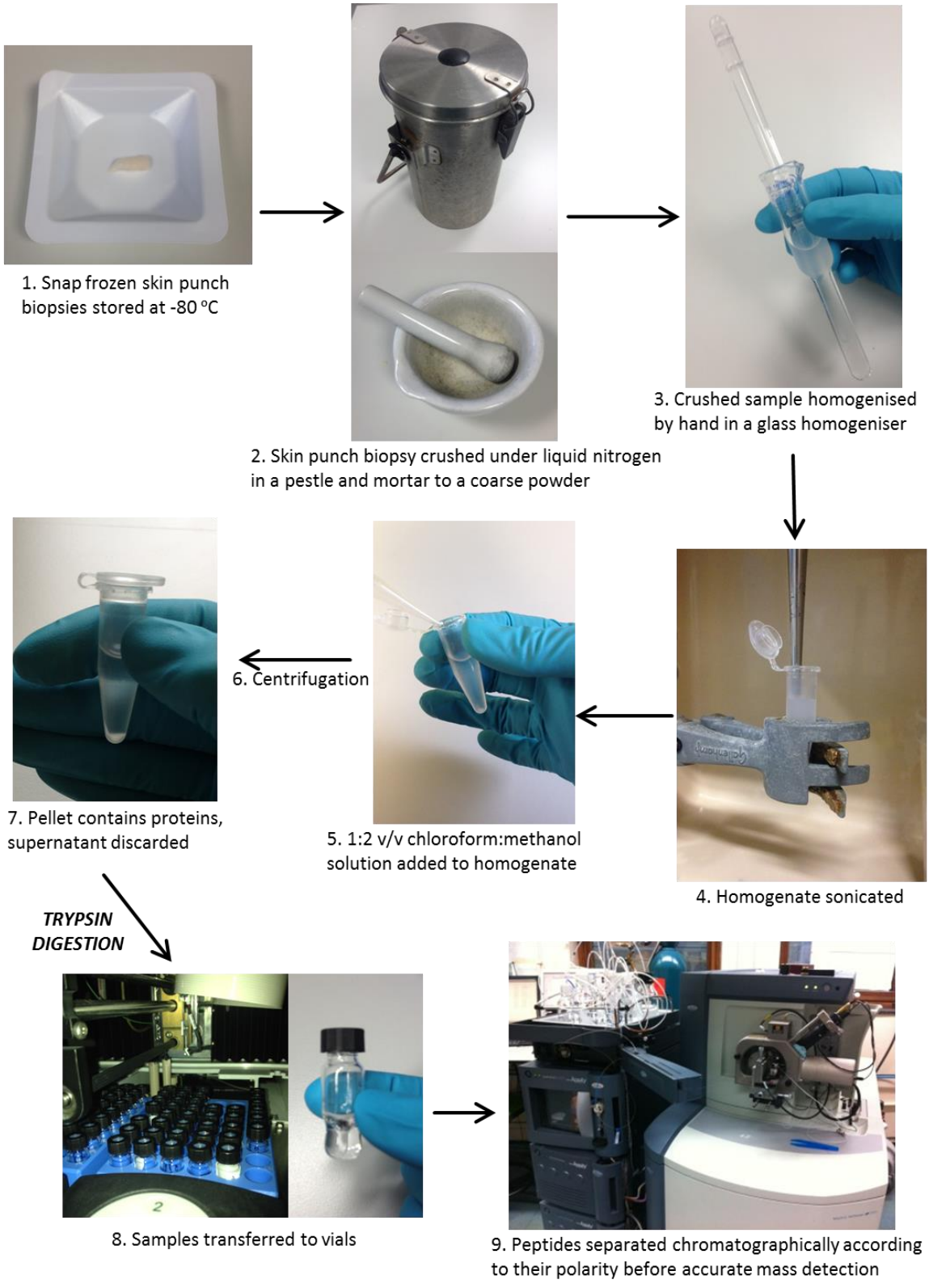

Figure 5.3. **Diagram showing the generic workflow for preparing skin punch biopsies for MS analysis, including an organic and protein precipitation step.** Points 1-9 show the sample preparation procedure that was used at this stage of the project. The sample was snap frozen and crushed under liquid nitrogen. Homogenised in a glass homogeniser, sonicated, lipids extracted in chloroform/methanol, proteins trypsin digested and transferred to vials for MS analysis.

To evaluate protein precipitation as a purification method the workflow in Figure 5.3 was used to evaluate whether precipitation after homogenisation would increase protein recovery.

Figure 5.4. **Graph showing the number of proteins identified by MS analysis when comparing 1:2 v/v $CHCl_3$:MeOH extraction and no extraction.** A slight decrease in proteins recovered after extraction with 1:2 v/v $CHCl_3$:MeOH solution was observed.

Figure 5.4 shows a slight loss of protein content (~10%) when this lipid extraction technique was used. It is most likely that this is loss of hydrophobic proteins or proteins that have interactions or are conjugated with lipids and therefore soluble in $CHCl_3$:MeOH. The rationale behind delipidating after homogenisation was to extract the lipids from the same sample as the proteins for lipidomic MS analysis. However, this data indicates that protein recovery is compromised post-delipidation (purple bar), compared with an untreated sample (blue bar). We concluded that delipidation at this stage was not favourable in light of the 10% protein loss.

5.4 Homogenisation buffer optimisation for frozen skin samples and MS analysis

The homogenisation buffer used at step 3 of Figure 5.1 and Figure 5.3 was optimised. It was based on solubilisation of skin proteins and compatibility with downstream MS analysis. Ten milligrams wet weight of the same skin tissue was homogenised in seven different buffers, the protein hits were assessed by MS analysis.

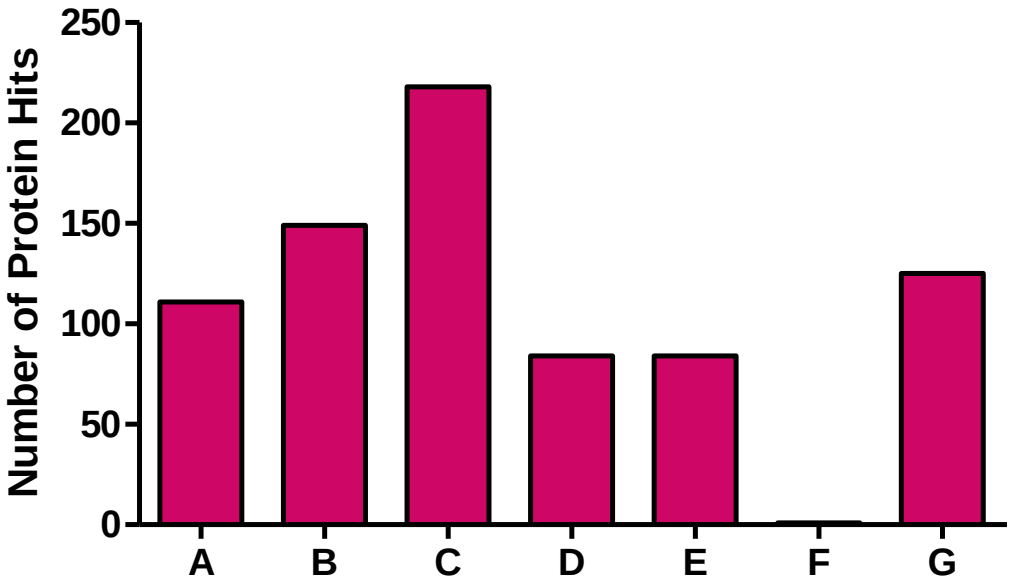

Figure 5.5. **Graph showing the number of proteins identified by LC-MS when comparing 7 different homogenisation buffers.** Seven different homogenisation buffers were used to determine which was most appropriate: A) 50 mM Tris, pH 8, containing 150 mM NaCl, 5 mM EDTA, 1% Triton X-100, B) 50 mM Tris-HCl, pH 7.4, containing 25 mM NaCl, 25 mM EDTA, C) 50 mM AmBic, pH 7.8, containing 2% ASB-14, D) 8 M urea, 2% CHAPS, 65 mM DTE, E) 6 M urea, 2 M thiourea, 65 mM DTE, F) 4 M guanidine HCl, 65 mM DTE, 10 mM EDTA, 50 mM sodium acetate, pH 5.8 and G) 150 mM PBS.

This experiment showed that homogenisation buffer C (50 mM AmBic, pH7.4, containing 2% ASB-14) yielded the most proteins (~50% greater than buffer B). In addition, the protein in this sample showed greatest diversity of cellular components than the other buffers.

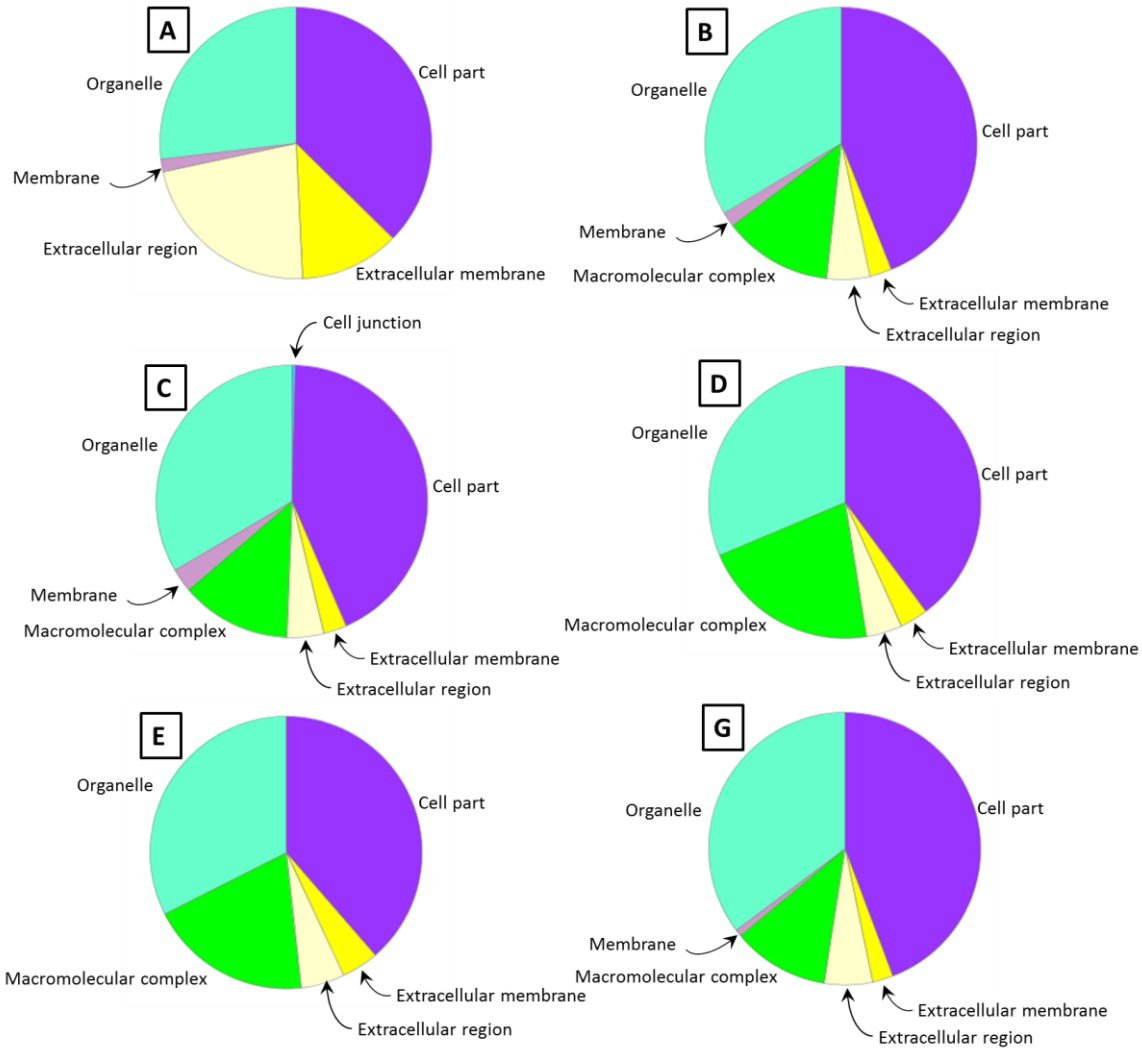

Figure 5.6. **Pie charts showing the cellular components represented by the proteins identified for six of the homogenisation buffers.** Using PANTHER Classification System (www.pantherdb.org), the proteins identified in Figure 5.5 are represented by cellular compartment. A-E and G represents the different homogenisation buffers: A) 50 mM Tris, pH 8, containing 150 mM NaCl, 5 mM EDTA, 1% Triton X-100, B) 50 mM Tris-HCl, pH 7.4, containing 25 mM NaCl, 25 mM EDTA, C) 50 mM AmBic, pH 7.8, containing 2% ASB-14, D) 8 M urea, 2% CHAPS, 65 mM DTE, E) 6 M urea, 2 M thiourea, 65 mM DTE and G) 150 mM PBS.

The PANTHER cellular component analysis indicated that buffer C (50 mM AmBic, pH 7.8, containing 2% ASB-14) covered proteins from seven different cellular components: cell junction, cell part, extracellular membrane, extracellular region, macromolecular complex, membrane and organelle, with at least 5% of proteins represented in each section.

5.5 LC-MS/MS parameter optimisation to optimise chromatography parameters for increased protein coverage

The MS analyses described previously in this chapter involve samples being analysed by LC-MS/MS using a single chromatographic separation column, separating peptides over 1 h. To increase proteomic coverage in mass spectrometry, offline two-dimensional chromatographic separation or fractionation may be used. Fractionation is when a single sample is separated into multiple fractions according to molecular weight or pKa, for example, in this case we used a high pH acetonitrile gradient. When a sample has been fractionated into 10 fractions in theory, there is ~1/10th of the complexity in each fraction. Each fraction is separated by the same 1 h LC gradient and analysed by MS individually, totalling 10 h of LC time. This will increase the proteome coverage (for combined fractions) due to decreased complexity of individual fractions and increased MS acquisition time.

Using buffer C (50 mM AmBic, pH 7.8, containing 2% ASB-14), two fractionation experiments were compared. Separation based on protein molecular weight (MW) using 1D SDS-PAGE, fractionating the gel column into 10 bands (method 10.2.9), and fractionation using high pH C18 chromatography (method 10.2.11).

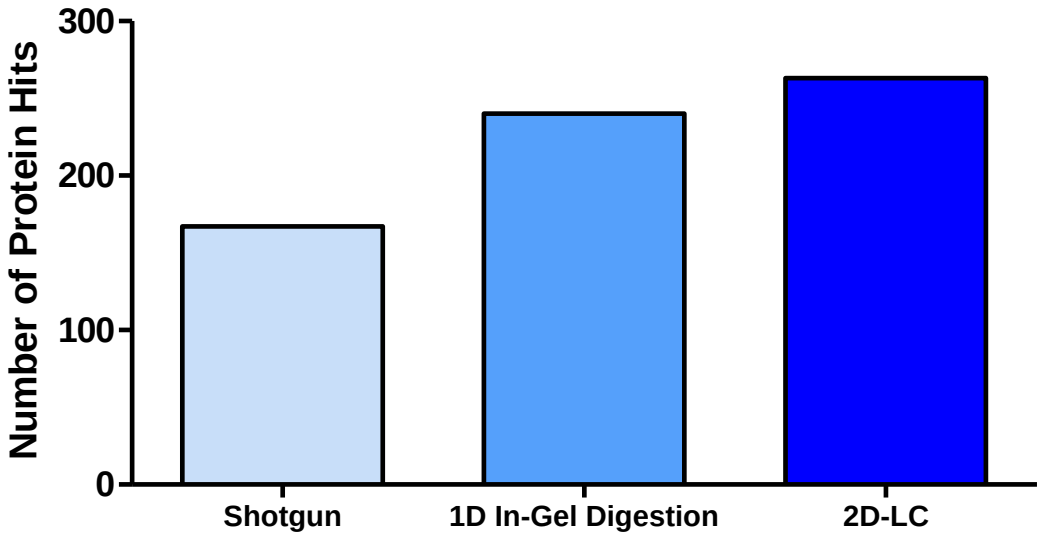

Figure 5.7. **Graph showing the number of proteins identified for shotgun analysis compared with two different fractionation techniques.** Shotgun refers to analysis of the whole sample in one single acquisition, 1D in-gel digestion is the fractionation by separating proteins by MW (10 bands) and 2D-LC fractionating by hydrophobicity using a high pH ACN gradient (10 fractions).

Figure 5.7 illustrates how fractionating increases the number of proteins identified compared with shotgun analysis. This is unsurprising due to reasons discussed previously that decreased

complexity of individual fractions and increased MS acquisition time for all fractions combined will increase proteomic coverage. The 2D-LC method detected in excess of 250 proteins, an improvement on the initial experiments.

5.5.1 Distribution of proteins detected according to protein class depending on the LC-MS/MS parameters applied

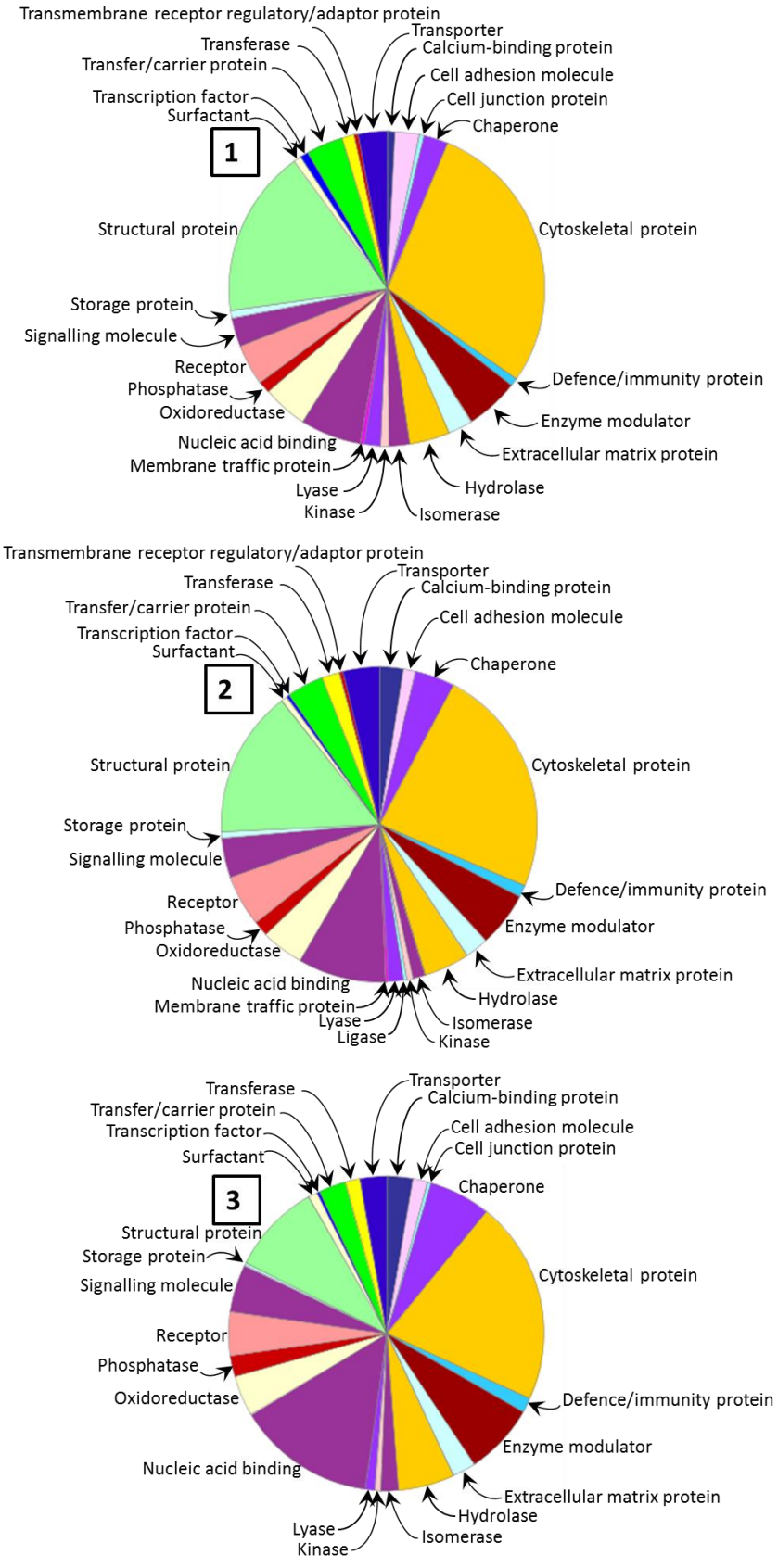

Figure 5.8. **Pie charts showing protein class representation by the fractionation methods.** Using PANTHER Classification System (www.pantherdb.org) the proteins represented in Figure 5.5 were analysed to identify their protein class. 1) shotgun analysis, 2) 1D in-gel digestion and 3) 2D-LC.

These pie charts show a range of protein classes, it is interesting to note that 2D-LC shows the most even distribution between all the classes compared with the other two methods. Irrespective of the LC-MS/MS method used, structural and cytoskeletal proteins are abundant in Figure 5.8. We want to apply these LC-MS/MS methods to skin samples in health and disease. The structural infrastructure of the skin is a key part of the skin's role in protecting the body from the external environment. In order to study changes in the skin, it is important that our method is able to identify proteins from the key protein classes, such as structural and cytoskeletal. Other key protein classes in the skin are cell adhesion and cell junction molecules, they are responsible for tight junctions between keratinocytes of the epidermis and in turn prevent excessive water loss from between cells which is a key role of the skin barrier.

As detailed in chapter 3 calcium-dependent proteins have a role in correct maturation and progression of keratinocytes in the epidermis. It is important therefore, that the LC-MS/MS method selected in this chapter would be able to detect these proteins. In chapter 3 we also suggested that proteins responsible for initiating keratinocyte differentiation in the epidermis were not being transported to the correct location in order to fulfil their function. It is also therefore important that in Figure 5.8 we were able to identify proteins from the classes: membrane traffic, transfer/carrier and transporter proteins as these proteins could indicate whether there are trafficking defects in disease.

5.6 Further optimisation of sample preparation to improve speed and reproducibility

An automated homogeniser (Minilys, Bertin technologies) was made available to the Biological Mass Spectrometry Centre, which meant that the pestle and mortar and hand homogenisation steps (steps 2 and 3 of Figure 5.1 and Figure 5.3) could be substitute for an automated method. This reduced the preparation time for each sample. Despite the use of an automated homogeniser it remained a challenge to solubilise all of the protein in a skin sample. To increase the surface area of the skin pieces pre-homogenisation, the tissue was cut into 20 µm sections using a cryostat.

The original method was changed to accommodate C18 column chemistry instead of 3 kDa filtration. Unlike the 3 kDa filters, C18 cartridges are available in a 96-well plate format which is amenable to up-scaling for higher-throughput. This optimised the protocol to reduce sample preparation time and to conform to requirements of the more sensitive SYNAPT G2-Si MS. The modified sample preparation procedure is shown:

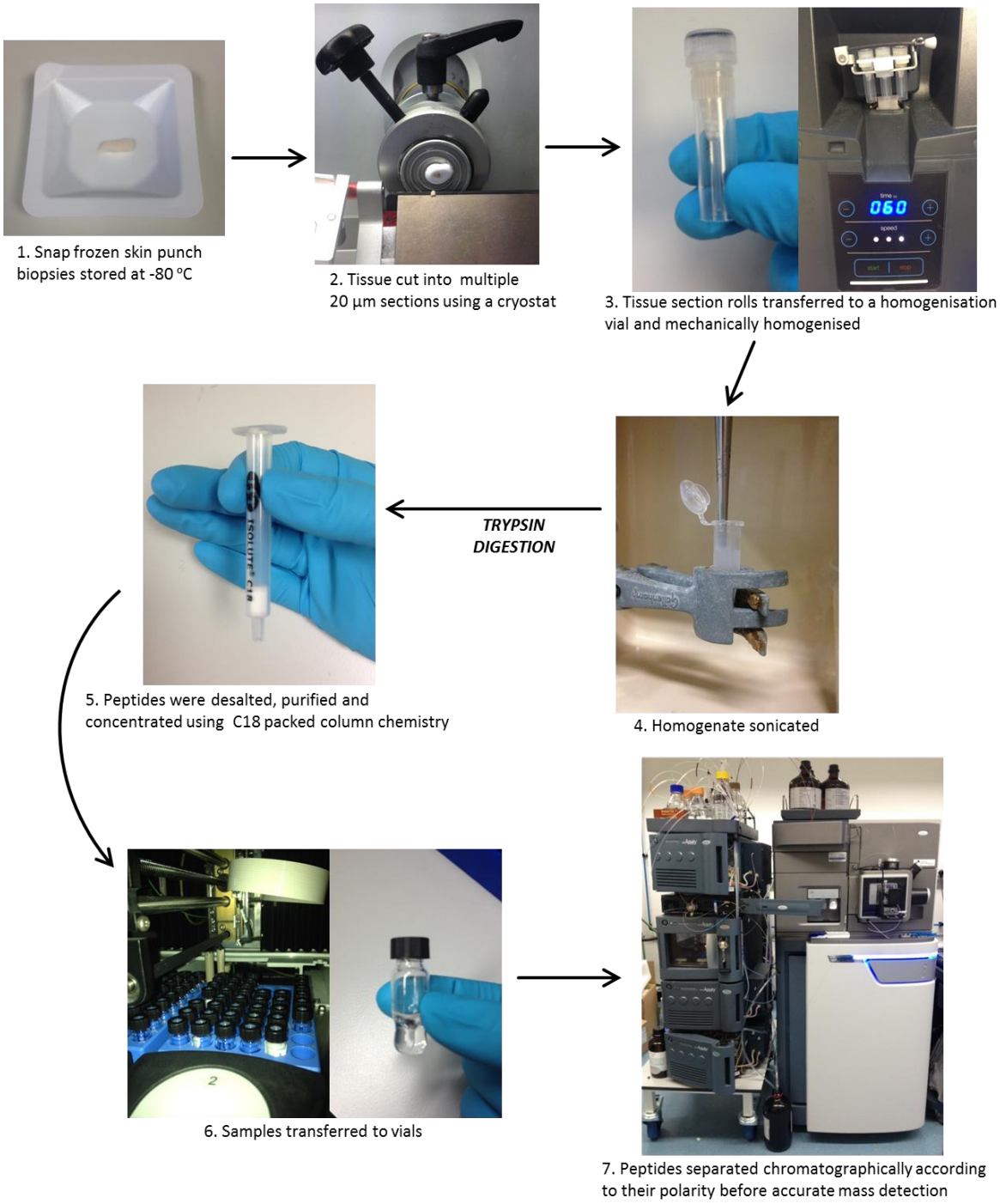

Figure 5.9. **Diagram showing the modified workflow for preparing skin punch biopsies for MS analysis.** Points 1-7 show the modified sample preparation procedure, this reduced sample preparation time, compared with the previous workflow (Figure 5.1). The sample was snap frozen, sectioned using a cryostat, homogenised in a mechanical homogeniser, sonicated, purified using C18 cartridges, transferred to vials and MS analysed.

5.7 Assessment of the LC-MS/MS method using a higher resolution mass spectrometer

The high resolution Waters SYNAPT G2-Si mass spectrometer is a high resolution/mass accuracy capable mass spectrometer. The main difference between the Waters QToF Premier and the Waters SYNAPT G2-Si is that the SYNAPT G2-Si has an additional degree of ion separation technology: ion mobility separation (IMS) (explained in the introduction section 1.1.7.1), alongside higher resolution and ten-fold increase in sensitivity. We used IMS here to separate co-eluting ions before fragmentation. This is of value to the proteomic work in this chapter as high complexity samples and relatively short acquisition times increases the likelihood that similar peptides will elute from the LC at the same moment in time. It is then a challenging to isolate the fragment ions from these co-eluting precursor ions. With IMS these co-eluting precursor ions will be separated by drift time before fragmentation. To assess the capacities of this method it was transferred to the higher resolution Waters SYNAPT G2-Si MS.

5.7.1 Optimisation of peptide loading amount

In order to determine how much sample was required, a sample loading experiment was carried out. Skin samples were prepared as detailed in Figure 5.9 and varying amounts of protein between 50 and 400 ng was loaded onto the LC system to identify which amount yielded most protein hits. The results are displayed below:

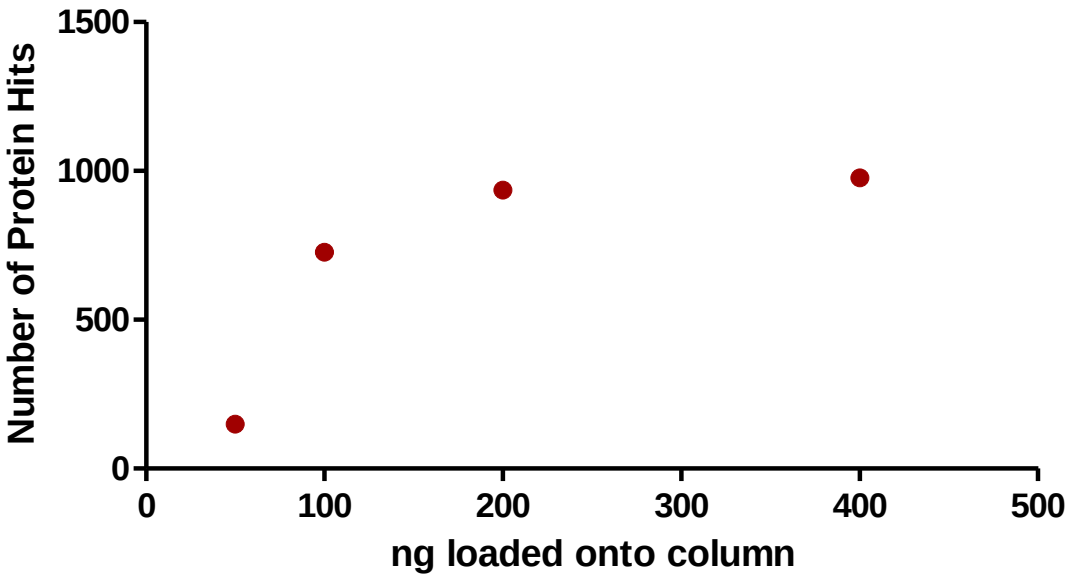

Figure 5.10. **Graph showing the number of proteins identified from varying protein loading amounts onto the LC system.** This graph shows that increasing the protein loaded onto the LC increases the number of proteins identified.

We decided that 300 ng of protein was appropriate; enough to ensure sufficient protein whilst avoiding the risk of overloading the system.

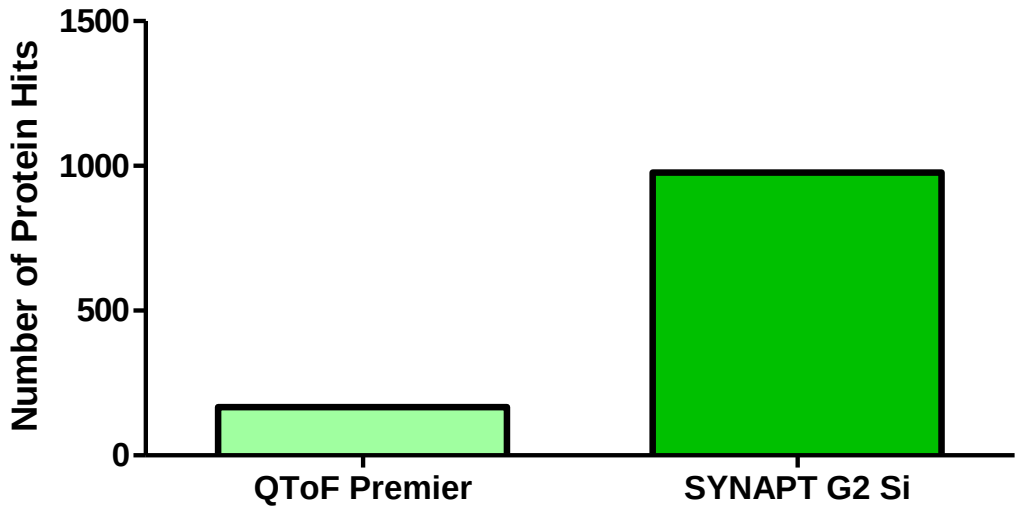

Figure 5.11. **Graph showing the comparison in number of proteins between the Waters QToF Premier and the SYNAPT G2-Si.** This figure shows how the SYNAPT has increased the protein coverage by ~5 fold from a sample of full-thickness skin.

There is a greater than 5-fold increase in protein coverage when using the Waters SYNAPT G2-Si compared with the Waters QToF premier. This will likely be due to the IMS separating out co-eluting compounds.

5.7.2 Upgrading the nanoAcquity liquid chromatography system to include “in-line” fractionation capabilities

The Waters nanoAcquity liquid chromatography system was upgraded to include an additional module capable of “in-line” fractionating (method 10.2.12). Instead of “off-line” fractionating (method 10.2.11) as described in section 5.5, this additional module and additional column enabled fractionation and application each fraction onto the analytical column to happen in one process.

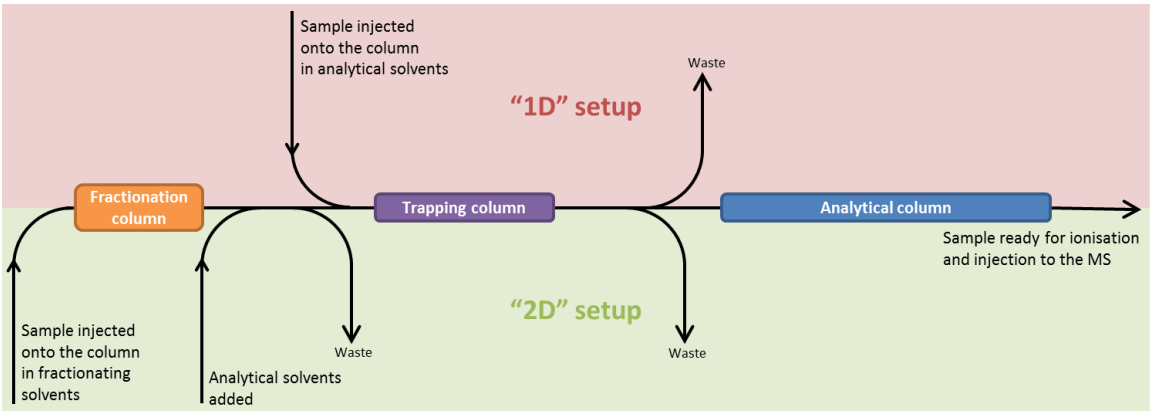

Figure 5.12. **Figure detailing the original "1D" setup of the nanoAcquity and the upgraded "2D" setup including an additional column and capacity for "in-line" fractionating.** This figure shows how the original nanoAcquity LC "1D" setup involved the sample being injected into the sampling loop, desalted on the trapping column and chromatographically separated on the analytical column. In the upgraded "2D" setup an additional column after the sampling loop is where the sample is first fractionated.

As detailed in Figure 5.12 the difference between the original "1D" setup of the Waters nanoAcquity and the "2D" version is an additional column which the peptides are sequentially eluted off in fractions of increasing high pH ACN concentrations. Post-fractionation desalting, concentrating and chromatographic separation of the peptides occurs in the same way as "1D". This method of "in-line" fractionating increases the overall analysis time compared with "off-line" fractionation (for the sample number of fractions), followed by the "1D" setup by ~20 min per fraction. However, it does reduce sample preparation time and lab consumables.

To test whether "in-line" fractionation increases the number of proteins identified, skin samples were prepared as illustrated in Figure 5.9, using 300 ng of protein per fraction, 4, 6 and 8 fractions were studied:

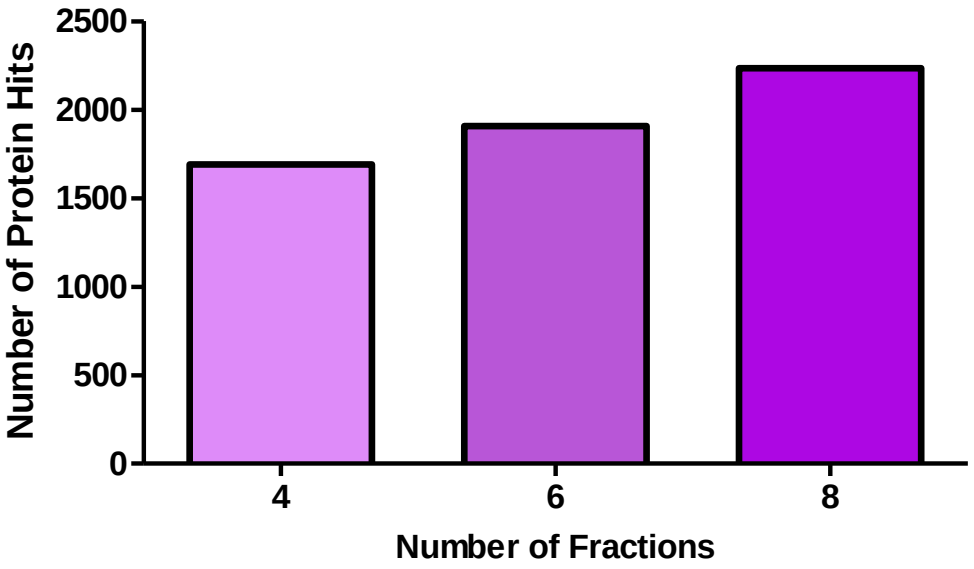

Figure 5.13. **Graph showing proteins detected from "in-line" fractionation of a skin sample into 4, 6 and 8 fractions.** This graph shows that with increasing number of fractions, the proteins identified also increase.

It would have been a compromise between protein hits and running time to investigate the number of fractions further, for examples 10, 15, 20 fractions as inevitably the number of protein hits would have continued to increase. Increasing the number of fractions requires greater processing power to successfully analyse and merge the data files which was unavailable at the time (each file is ~3 GB). Eight fractions was the limit of processing capabilities, it was considered prudent not to attempt fractions beyond that. Figure 5.13 illustrates the increase in proteins detected as the number of fractions increases.

5.8 Discussion of method development for mass spectral analysis of skin for proteomic coverage

These results show that by adapting the sample preparation method, modifying the LC system and upgrading the MS that the number of proteins identified has increased to an excess of 2000 proteins. In section 5.4, 50 mM AmBic and 2% w/v ASB-14 was selected as the most efficient homogenisation buffer. Many homogenising buffers are being used in the literature to solubilise various tissues for proteomic analysis. However, there is little agreement between research groups nor tissue types on which buffer to use, guanidine hydrochloride has been used to extract proteins from colorectal biopsies, PBS for extraction from rat liver and brain[213] and a mix of acetonitrile and PBS for protein extraction from porcine muscle, liver, kidney and fat tissues[214]. The array of published homogenisation buffers illustrates the need to optimise for tissue type and downstream workflow.

It was expected that upgrading the LC and MS technologies that the number of proteins detected would increase. Shliaha et al. report up to a 60% increase in proteome coverage comparing with and without IMS[215]. In this thesis we see a greater increase in the proteome coverage when using IMS (Figure 5.11), because we are comparing two different generations of time-of-flight MS as well as a slightly modified sample preparation method. The same paper describes how less sample is required for the same result when using IMS, this was also observed in this project (section 5.7.1). Again loading amounts in this project differed between different machines; one with IMS and one without.

In the introduction we discussed the challenges associated with analysing an insoluble and highly cross-linked tissue, this continued throughout the optimisation process and despite best efforts it was not possible to solubilise all the skin tissue. We attributed this to the heterogeneity of protein properties present in skin. For example, there are water insoluble proteins in the lipid bilayer and soluble proteins within the cytoplasm. It is challenging to create a homogenisation buffer that is capable of solubilising all extremes of solubility. A group in Maryland, targeted the solubilisation of membrane proteins in the epidermis using a 60% methanol solution[216; 217], this would not be so amenable to the solubilisation of hydrophilic proteins.

This method demonstrates an improvement on the original method and is able to cover the aim of this chapter in anticipation of clinical samples to investigate. This final optimised method has been published in Biological Procedures Online[218].

5.9 Conclusion and future research for the method development for mass spectral analysis of full thickness skin for proteome coverage chapter

This method development chapter has enabled the optimisation and adaptation of a robust and much improved LC-MS/MS method for the analysis of full-thickness skin tissue, as shown in Figure 5.9. If the method were to be developed further the main area of focus should be tissue solubilisation. For skin, this would have to be split into multiple phases, for example one buffer to extract hydrophobic proteins and another for hydrophilic proteins. Whether these phases would be compatible with recombining to one sample at a later step or not would have to be determined, otherwise this would increase sample numbers two-fold.

Chapter 6

Proteomic investigation of full-thickness skin biopsies from patients undergoing reconstructive surgery who develop hypertrophic scar tissue

6 Proteomic investigation of full-thickness skin biopsies from patients undergoing reconstructive surgery who develop hypertrophic scar tissue

Contents

Scarring is when fibrous collagen tissue replaces damaged tissue in wound repair. It is a common and healthy process in humans. Although not usually a medical problem, it can become a psychosocial problem especially if scars are exposed. As detailed in the introduction (chapter 1) the skin provides a vital barrier, protecting us from the external environment. The skin and the skin barrier can be damaged by trauma. If skin barrier function is impaired for prolonged periods of time microorganisms can colonise inside the body causing widespread infection. Consequently, the body has developed a process to manage and repair damage to the skin barrier as quickly as possible. A balance needs to be found between a “quick fix” barrier to seal off the exposed area, i.e. the initial scab and a “long-term” durable seal and the final, process of healing the defect is the scar tissue. Often superficial wounds will heal rapidly and will not require scar tissue formation to fully repair. More severe injuries require scar tissue formation in order to heal.

6.1 Wound healing affecting the full thickness of skin

If the wound penetrates the full thickness of the skin it will trigger epidermal and dermal repair. This is split into four phases: haemostasis, inflammation, proliferation and remodelling[219]. The haemostasis phase is when blood cells coagulate and blood vessels contract to reduce blood loss, at the same time from blood cells a matrix forms to recruit other cells to the wound site. This forms a fibrin plug is what is commonly called a scab. A complex cascade of signalling and recruitment of cells ensues. In the inflammatory phase an immune barrier is formed to prevent microorganisms that will have penetrated the wound from propagating. Neutrophils migrate towards the lesion to phagocytose foreign material[220]. In a second phase of migration macrophages move into the lesion site to continue phagocytosis and in the latter inflammatory phase lymphocytes are recruited to the wound[221]. The proliferative phase is when tissue repair starts. Re-epithelialisation, formation of new blood vessels, wound contraction and formation of a fibrous scar are triggered.[222] Fibroblasts migrate to the wound site and synthesise extracellular matrix and collagen proteins[223]. Blood vessel growth promoting factors are released to re-vascularise the damaged tissue. Endothelial cells attach to extracellular matrix structures in order to initiate re-epithelialisation.[224] Finally, the remodelling phase can take months or years during which time the dermis returns to its pre-injury state as final layers of scar tissue are laid down.[222; 225]

6.2 Abnormal wound healing

Usually scarring proceeds, however, sometimes wounds heal abnormally. This abnormal healing can have known causes for example smoking or diabetes, which alters the vasculature having a negative effect on wound healing due to compromised blood supply. Other causes of may be nutritional deficiency, metabolic disease, pre-existing medical conditions and

infection.[226] There are other examples where excess collagen is produced during the scarring process and the scar tissue becomes larger and more pronounced. The main two types of this are hypertrophic scarring and keloid scarring.

6.2.1 Hypertrophic scarring

In healthy wound healing there is a stop signal at the end of the remodelling phase preventing further collagen deposition. In hypertrophic scars that stop signal is not effective. There are genetic and environmental factors that can affect this stop signal as well as unknown causes. Hypertrophic scars are visually distinct to healthy scars, the scar tissue is noticeably raised, yet remains within the original margins of the scar tissue.[227]

6.3 Hypertrophic scars: a review of the literature, causes, associations and treatment

This chapter focuses on hypertrophic scarring. In the final stage of wound healing macroscopic hypertrophic changes can be seen. It is during the remodelling phase that collagen tissue does not stop proliferating to form the hypertrophic scar, but it is thought that earlier stages of the wound healing process could be altered by the disease too. In the haemostasis stage a fibrin plug is formed to seal the wound, the fibrin proteins are bound together by fibronectin, a glycoprotein. Fibronectin is only expressed for a few days after injury, whereas in hypertrophic cell lines its expression remains high for up to a year after the trauma[228]. In the inflammatory phase macrophages are recruited to phagocytose foreign components and cell debris. It is hypothesised that macrophages could be responsible for secreting cytokines that promote fibroblasts to over-produce collagen in a hypertrophic mouse model[229]. The three TGF-β isoforms (section 4.3) are able to stimulate fibroblast proliferation, inflammatory cell and fibroblast cell migration, angiogenesis and extracellular matrix synthesis.[230] TGF-β1 and TGF-β2 promote hypertrophic scar formation and TGF-β3 has anti-fibrotic properties[231; 232]. Experiments in non-scarring foetal skin show that endogenous levels of TGF-β are lower than in adults and that when non-scarring foetal wounds are treated with TGF-β1 and TGF-β2 it leads to scarring[233; 234; 235]. Re-epithelialisation changes have been observed too, in health keratinocytes are activated for re-epithelialisation and deactivated once the wound has healed, however, in hypertrophic scar tissue the keratinocytes are not deactivated and continue to proliferate in an uncontrolled manner[236; 237; 238]. There are also other known associations with predisposition to hypertrophic scar formation for example hypertension, reduced collagenase gene expression and free radical damage[239; 240; 241].

A separate area of hypertrophic scarring is treatment and management. The most widely used treatment is silicone gel. These come in the form of gels or sheets applied to the wound site

after a surgical intervention or more commonly after a burns injury. Their mechanism of action is not yet established, research would suggest that hydration is a key factor[242; 243]. There are difficulties with patient compliance and wound management can be complicated outside of the hospital environment[244; 245; 246]. In hypertrophic scars, corticosteroid injections have been shown to be effective for reducing hypertrophic scar appearance[247]. Steroids are anti-inflammatory agents and through this mechanism they are thought to improve hypertrophic scar appearance. By supressing the inflammatory response steroids decrease fibroblast proliferation and in turn decrease collagen synthesis[248]. Treating hypertrophic scars with corticosteroid injections has been shown to be effective, however, it is not without side effects[247], such as tissue wasting, loss of skin pigmentation and the appearance of dilated capillaries under the skin surface[249].

6.4 Significance of hypertrophic scarring

Hypertrophic scars can be disfiguring other symptoms not shown in that image include discomfort, pain, itchiness and functional difficulties[250]. Despite research there are few results indicating causality or effective, quick and safe treatment. In this chapter we investigate disease mechanism or characteristic differences in pre-operative unscarred skin of children, this could be used as a predictive measure of pathological scar outcome. We aim to use the proteomics method developed in chapter 5 to profile endogenous differences in unscarred skin of children who will and will not, develop a hypertrophic scar.

6.5 Investigating the biochemical skin differences in patients who will and will not develop hypertrophic scars

This chapter is part of a collaboration with colleagues from the Dermatology Research Group at the UCL Great Ormond Street Institute of Child Health (Drs Benjamin Way and Ryan O'Shaughnessy). The study design, recruitment of patients and collection of samples was arranged by Dr Way who used transcriptomic techniques to try to find potential disease mechanisms in hypertrophic scarring. Our role was a complementary analysis to study changes in protein expression of the same tissues using mass spectrometry-based techniques.

6.5.1 The study design

Children who were undergoing surgical ear reconstructions for microtia were recruited into the study. Microtia is a birth defect whereby children are born with one or two of their external ears not fully formed. There is no single cause of this malformation and there have been several documented ranging from environmental factors, genetic mutations and causes associated with other systemic diseases[251; 252]. Surgical treatment is available and involves two operations approximately six months apart to reconstruct the external ear, both operations involve excision

of rib cartilage via the same thoracic incision[253]. In this study skin samples were taken from the thoracic surgical incision site and the scar tissue was excised at the second microtia operation. These tissues were used to collect paired samples of healthy and scar tissue. The quality of scar at the second operation was graded in order to determine whether individuals had a healthy or hypertrophic scar. Figure 6.1 illustrates the workflow for this study and Figure 6.2 shows images of the scar of two patients included in this analysis.

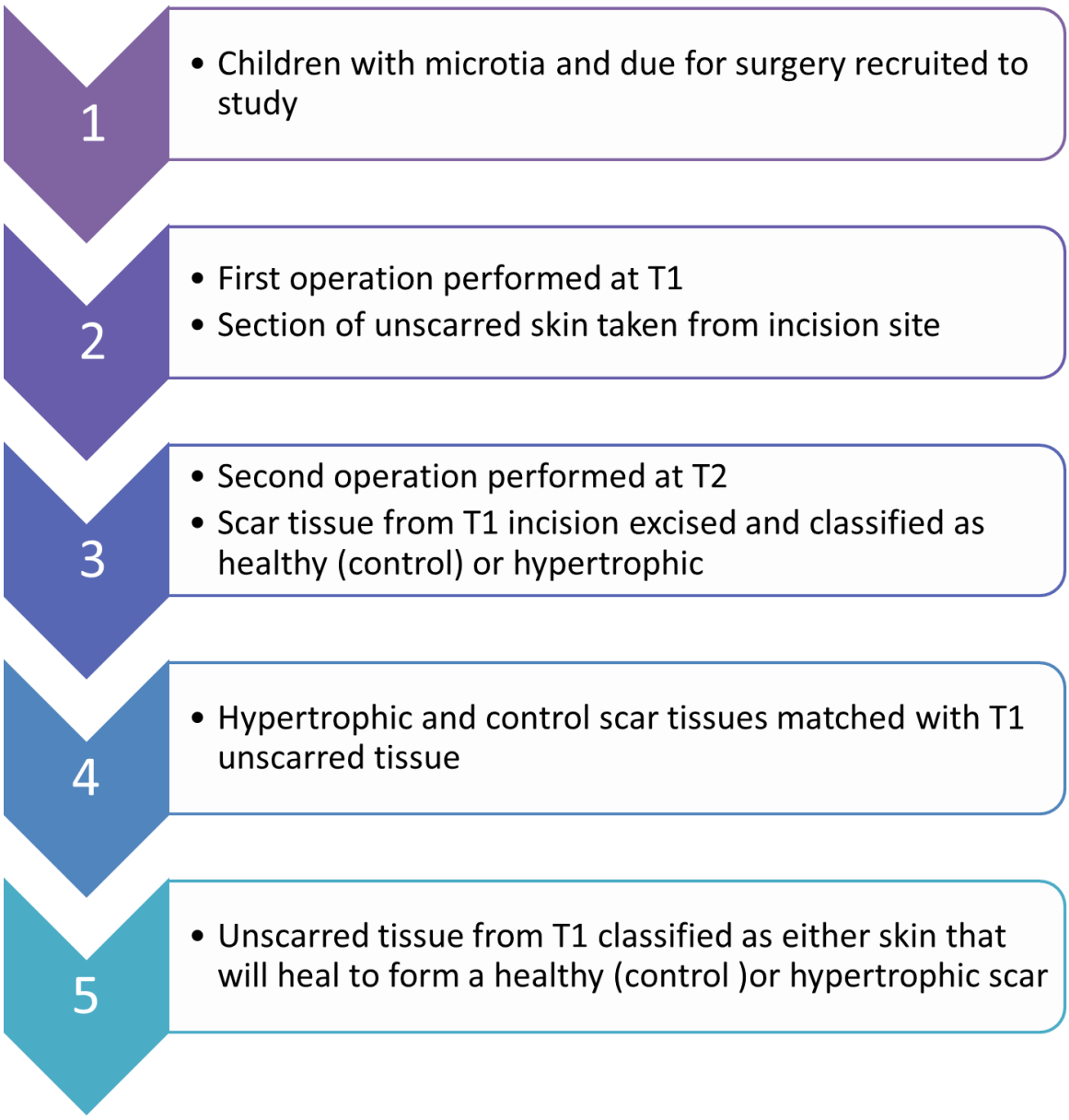

Figure 6.1. **Figure illustrating the tissue acquisition and classification of samples in this study.** This flowchart outlines the time line and points of tissue acquisition for the study. It also outlines how the healthy unscarred tissue is identified as skin that will heal to form a healthy of hypertrophic scar. T2 was approximately 6 months after T1.

Figure 6.2. **Images illustrating scarred control (left) and scarred hypertrophic (right) of patients in this study.** These images were taken of two patients recruited into this study and illustrate the difference in a control scar (left) and a hypertrophic scar (right) where the scar tissue is visibly raised compared with the control.

This study design is unique in many ways, the most significant being that other hypertrophic scar studies focus on the scar tissue itself or individuals who are known to have scarred hypertrophically previously. In this study we have access to healthy skin of individuals with no history of hypertrophic scarring or other skin condition before a hypertrophic scar is observed. The terms used to refer to these samples in this thesis are “unscarred control”, “scarred control”, “unscarred hypertrophic” and “scarred hypertrophic” as illustrated below:

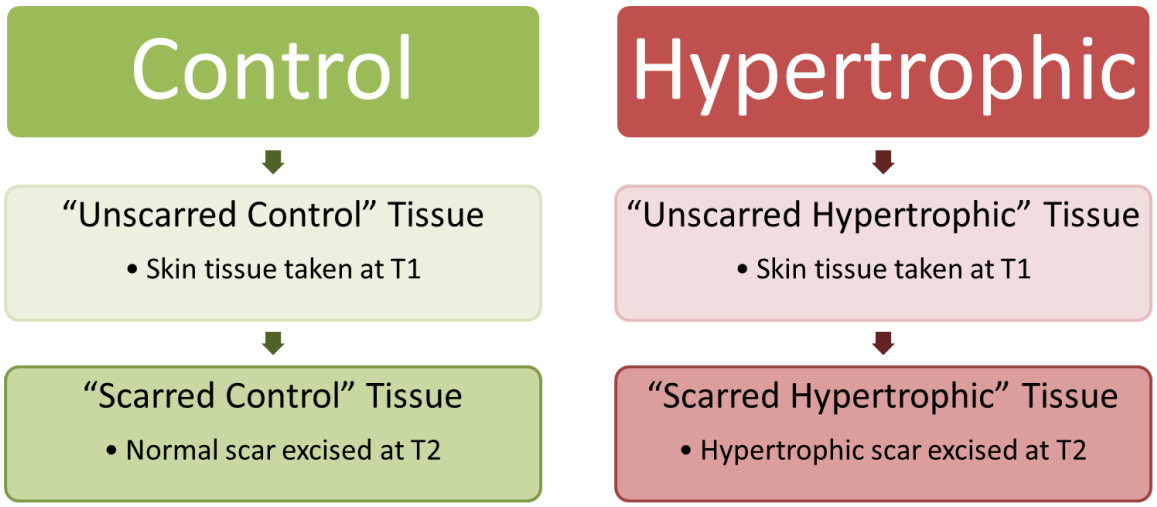

Figure 6.3. **Figure illustrating the sample groupings.** “Unscarred control” and “unscarred hypertrophic” describe skin samples taken at T1 when the skin is macroscopically healthy and shows no differences between the groups. “Scarred control” and “scarred hypertrophic” describe the scar tissue excised at T2 that has been classified as either a normal scar or a hypertrophic scar, respectively.

6.6 Proteomic analysis of pre-scar tissue

The most interesting and clinically significant perspective of this study was whether there were changes in the endogenous profile of healthy skin that could predict whether a healthy scar or a hypertrophic scar would form after surgical injury. Five samples from each group were prepared for analysis using the method developed in chapter 5 and analysed anonymously. These samples were “unscarred control” and “unscarred hypertrophic” (Figure 6.3).

6.6.1 Quality control of samples prior to analysis

Samples were prepared according to the method developed in chapter 5 : samples were snap frozen after collection, stored at -80 °C before being sectioned, homogenised, sonicated, digested, purified, fractionated and the MS data acquired. The size of the tissue sample varied, therefore protein content was standardised using a bicinchoninic acid protein assay (method 10.2.8) after homogenisation. Twenty-five micrograms of protein solution was taken for tryptic digestion. Quality control samples (yeast enolase peptides) were analysed within the batches to ensure quality of data such as spray stability, chromatography performance and consistent protein identifications.

6.6.2 Proteomic analysis of skin biopsies from patients who heal healthily compared with those who developed hypertrophic scars

Five children who scarred normally and 5 who developed hypertrophic scars were included in this analysis. Their ages, skin tone as described according to the Fitzpatrick skin type scale and sex are summarised in Table 6.1.

	Age (years) at T1	Age (years) at T2	Time (months) between operations (T2-T1)	Fitzpatrick Skin Type	Sex
Control					
1	10.9	11.5	6	2	M
2	10.5	11.2	7	2	M
3	9.1	9.6	5	2	M
4	14.5	15.0	5	5	M
5	9.9	10.3	5	2	M
Hypertrophic					
6	9.1	9.6	5	6	F
7	13.7	14.2	5	5	M
8	16.8	17.4	7	4	M
9	10.8	11.3	5	4	F
10	11.5	12.1	6	5	M

Table 6.1. **Table detailing clinical information of the samples in this study.** This table shows the samples used in this analysis their age, sex and Fitzpatrick skin type. T1 refers to the first operation when the unscarred samples were taken and T2, the second operation approximately six months after T1 when the scar tissue was excised.

The main difference between the control group and the group that had hypertrophic scars is illustrated in the 'Fitzpatrick Skin Type' column. Those individuals that scarred hypertrophically had on average a darker skin tone than those in the control group. It is documented that people from different ethnic groups have different tendencies to scar hypertrophically[254]. This may affect my results as there are different proteins (e.g. melanins) expressed in different skin tones. However, this is not of detriment to the study, the fact that people of darker skin tone are more susceptible to hypertrophic scarring may suggest that the cause of hypertrophic scarring is related to ethnicity. Both the scarred and unscarred tissues for children in both groups were prepared as described in chapter 5 . Over 5000 different skin proteins were detected. Figure 6.4 shows a principle components analysis (PCA) plot of the four different groups in this analysis:

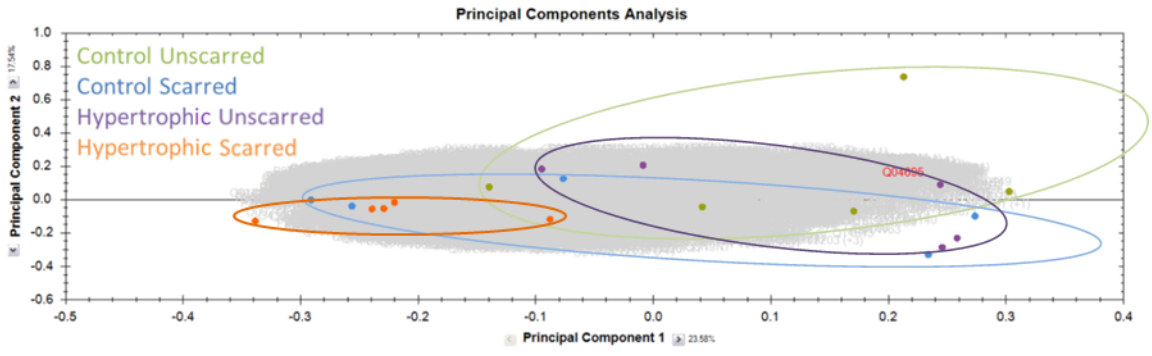

Figure 6.4. **A PCA plot detailing the proteins identified for the four different groups in this experiment.** This PCA plot shows the distribution of the four groups with respect to proteins identified: unscarred control (green), scarred control (blue), unscarred hypertrophic (purple) and scarred hypertrophic (orange) tissue.

This PCA plot shows no significant or major proteomic differences between the 4 groups. However, a separation between the scarred and unscarred hypertrophic groups (orange and purple, respectively) and between unscarred control and scarred hypertrophic groups (green and orange, respectively) was observed. This is not surprising because scar and unscarred tissue are known to have slightly different protein compositions (more collagen in scar tissue).

6.6.3 Significantly differentially expressed proteins between patients who heal healthily compared with those who developed hypertrophic scars

In excess of 5000 proteins were identified in this experiment, 89 were differentially expressed with a minimum fold change of 2 and an ANOVA p-value of less than 0.05 between the unscarred skin of patients that went on to scar healthily compared with those who scarred hypertrophically. Of those proteins 30 were selected, shown in Table 6.2, these proteins were selected based on unique peptide count, Progenesis score and sequence coverage.

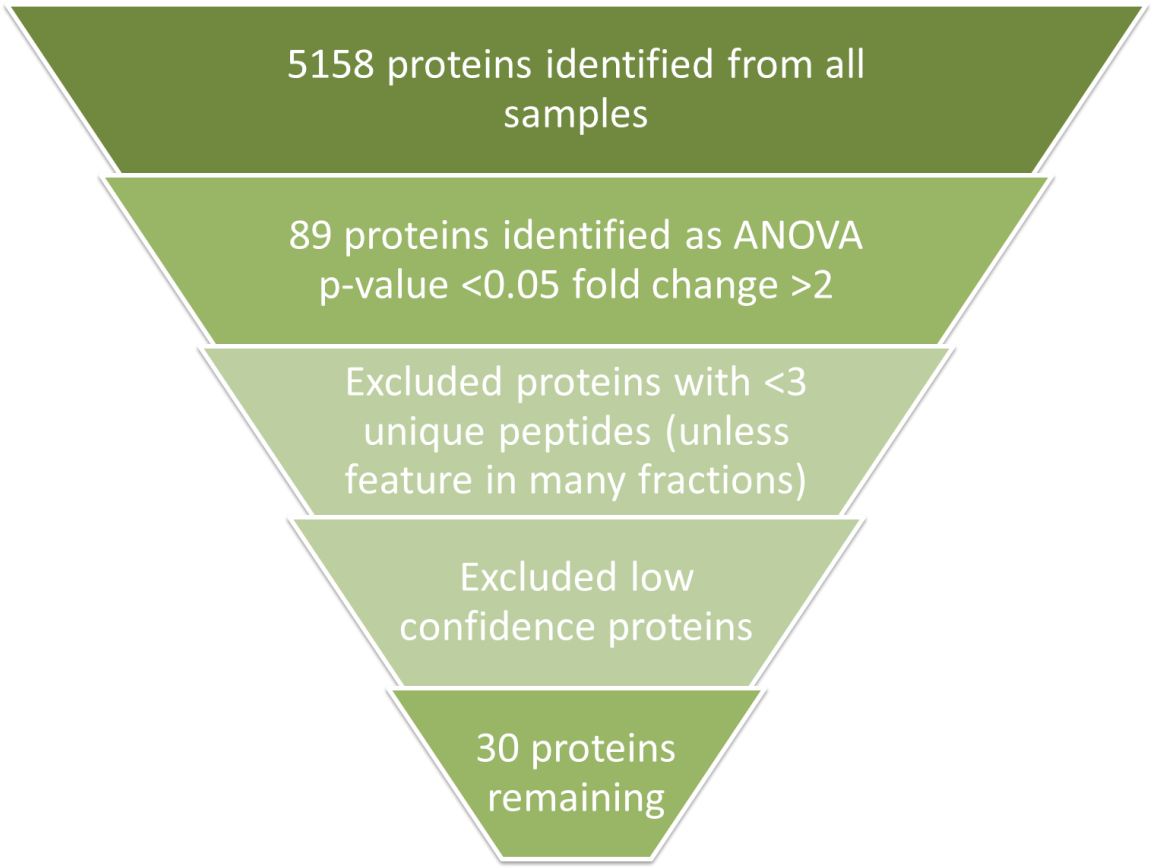

Figure 6.5. **Figure illustrating selection of the 30 proteins listed in Table 6.2.** Of the 5158 proteins identified, 89 were significantly differentially expressed between the unscarred control and the unscarred hypertrophic samples, this was reduced to 30 when accounting for quality of the data. Although ANOVA p-value <0.05 is not a suitable measure to identify significance here because of multiple testing and the fact that we identified ~5000 proteins, it was just used as an aid to identify the strongest protein candidates.

Accession Number	Description	Peptide Count	ANOVA (p-value)	Maximum Fold Change	Protein Function
Q9NX46	Poly(ADP-ribose) glycohydrolase ARH3	10	0.0129	33.7	Synthesised after DNA damage
P02545	Lamin A.	34	0.0384	8.7	Nuclear stability + structure
P19012	Keratin, type I cytoskeletal 15	121	0.0027	4.1	Cell structural integrity in epithelia
P13646	Keratin, type I cytoskeletal 13	75	0.0002	3.1	Cell structural integrity in epithelia
P36969	Phospholipid hydroperoxide glutathione peroxidase, mitochondrial	11	0.0019	3.0	Reduction of hydrogen peroxide
Q15366	Poly(rC)-binding protein 2	19	0.0019	2.9	RNA binding
Q08380	Galectin-3-binding protein	11	0.0114	2.7	Cell-cell + cell-matrix interaction
P02533	Keratin, type I cytoskeletal 14	167	0.0342	2.5	Cytoskeleton of epithelial cells
Q04695	Keratin, type I cytoskeletal 17	105	0.0007	2.3	Expressed in epidermal appendages
P62136	Serine/threonine-protein phosphatase PP1-alpha catalytic subunit	16	0.024	2.3	Regulation of cellular processes
Q14203	Dynactin subunit 1	56	0.0472	2.1	Transport + intracellular movement
P62158	Calmodulin	16	0.0323	2.1	Calcium-binding protein
P01859	Ig gamma-2 chain C region	108	0.0437	2.1	Antigen binding
Q53GQ0	Estradiol 17-beta-dehydrogenase 12	13	0.0212	2.2	Fatty acid elongation
P27348	14-3-3 protein theta	36	0.0419	2.2	Mediates signal transduction
Q15363	Transmembrane emp24 domain-containing protein 2	7	0.0412	2.3	Vesicle trafficing
O14980	Exportin-1	24	0.0443	2.3	Mediates nuclear protein export
P39023	60S ribosomal protein L3	12	0.0371	2.5	Catalyses protein synthesis
P55084	Trifunctional enzyme subunit beta, mitochondrial	46	0.0201	2.6	Catalyses oxidation of fatty acids
Q9UJ71	C-type lectin domain family 4 member K	9	0.0051	2.7	Antigen processing
P16083	Ribosyldihydronicotinamide dehydrogenase	9	0.0379	2.9	Quinone reductase
P09486	SPARC	11	0.0033	2.9	Bone collagen calcification
Q99538	Legumain	16	0.0357	3.0	Cysteine protease
P04196	Histidine-rich glycoprotein	35	0.0365	3.4	Antimicrobial and binding protein
Q13838	Spliceosome RNA helicase DDX39B	31	0.0328	3.6	Nuclear export of mRNA
P06744	Glucose-6-phosphate isomerase	15	0.0218	4.2	Glycolytic enzyme
A2RUR9	Coiled-coil domain-containing protein 144A	16	0.0223	6.7	Unknown biological function
O94973	AP-2 complex subunit alpha-2	30	0.0498	10.5	Transport + endocytosis
Q31612	HLA class I histocompatibility antigen, B-73 alpha chain	10	0.036	12.6	Peptide presentation
P16403	Histone H1.2	28	0.0183	118.9	DNA binding

Table 6.2. **Table detailing the 30 proteins selected from the Progenesis analysis.** These 30 proteins have a fold change of at least 2 (5th column) and an ANOVA p-value of less than 0.05 (4th column), from the Progeneis QI for proteomics analysis of the unscarred skin. The proteins in green were over-expressed in unscarred control samples and the proteins in red were over-expressed in unscarred hypertrophic samples. The list of 89 proteins and further mass spectrometry data for these 30 proteins can be found in appendices 12.6 and 12.7 respectively.

Poly (ADP-ribose) glycohydrolase ARH3 was the protein of greatest increase in the control group compared with the hypertrophic group. It has not been described as playing a role in correct scar formation previously, however its inhibition has been linked to improved treatment of malignant melanoma of the skin[255]. It is an enzyme that hydrolyses poly (ADP) ribose, it is involved in cell cycle regeneration, mitotic spindle assembly, DNA repair, cell death, development and differentiation[256; 257; 258].

6.6.4 Bioinformatics: gene ontology analysis

Gene Ontology is a tool for classification of genes and proteins, to construct pan-species gene and protein representations and vocabularies. The demand for these tools has increased with the surge in genome-wide studies and subsequent need to classify unrelated lists of genes. It is laborious to establish relationships between genes individually with regards to a specific biological question. These tools establish categories for genes and proteins such as protein function, cellular component and molecular function, they are increasingly accessible to classify

lists of genes or proteins from biomarker discovery experiments. Pathway analysis tools find biological pathway links between lists of genes or proteins. There are several freely available resources and programs providing this type of analysis. The main tools that were selected for use in this chapter were: PANTHER (http://pantherdb.org/), Webgestalt (http://bioinfo.vanderbilt.edu/webgestalt/) and GeneMANIA (http://www.genemania.org/).

PANTHER gives an overall representation of the data set as far as molecular function, biological processes, cellular components, protein class and pathway components are concerned. This information can be represented in a pie chart format and was used initially to get an overview from which parts of the tissue matrix the proteins of interest originated. Figure 6.6 shows this overview for the proteins in Table 6.2.

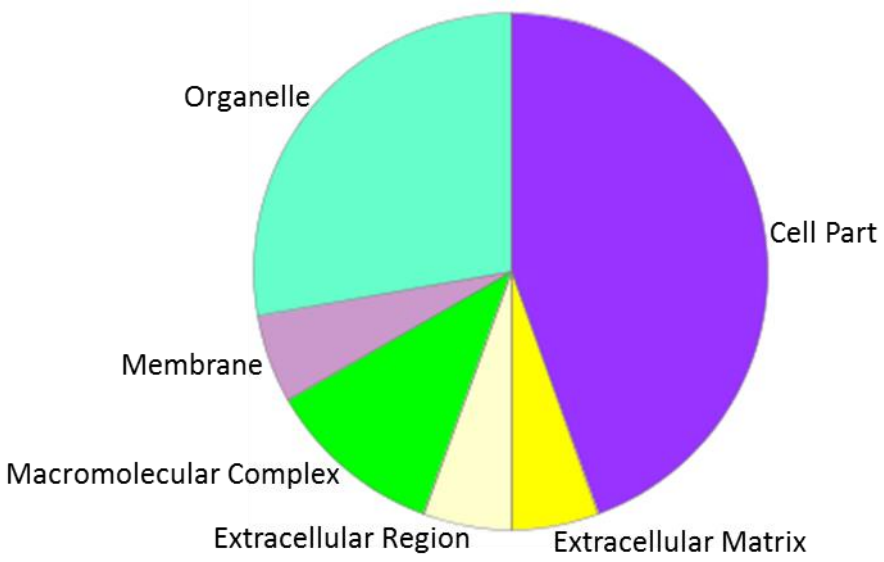

Figure 6.6. **Pie chart showing the cellular components of the protein in Table 6.2.** This pie chart shows the proteins in Table 6.2 according to sub-cellular location.

Figure 6.6 shows that most proteins in Table 6.2 belong to the cell part of the tissue. Together cell part, organelle and membrane proteins make up approximately 75% of all cellular components represented. Figure 6.7 and Figure 6.8 show pie charts for the 30 proteins in Table 6.2 for molecular function and biological processes, respectively.

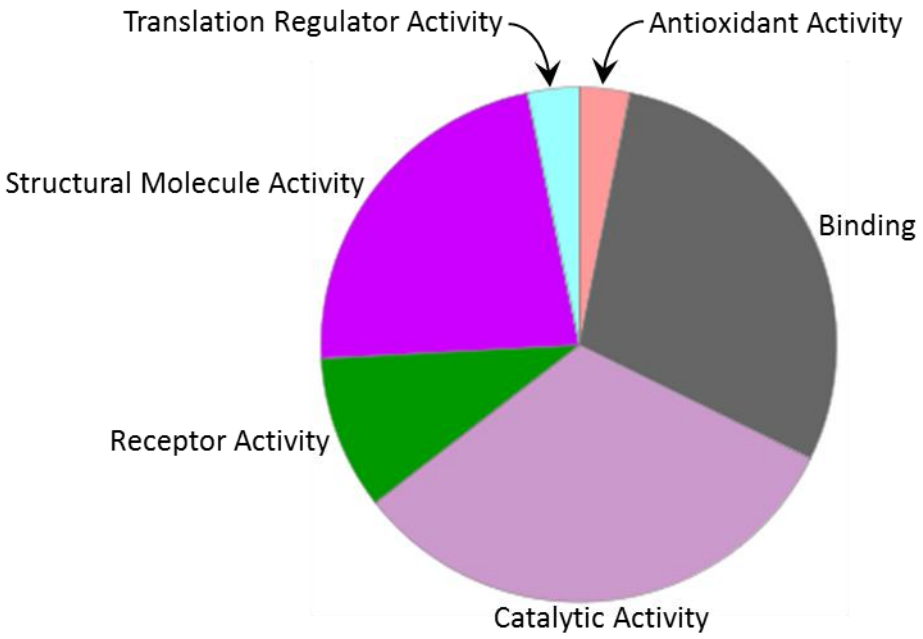

Figure 6.7. **Pie chart showing molecular function for proteins in Table 6.2.** This pie chart separates the proteins listed in Table 6.2 according to their molecular function.

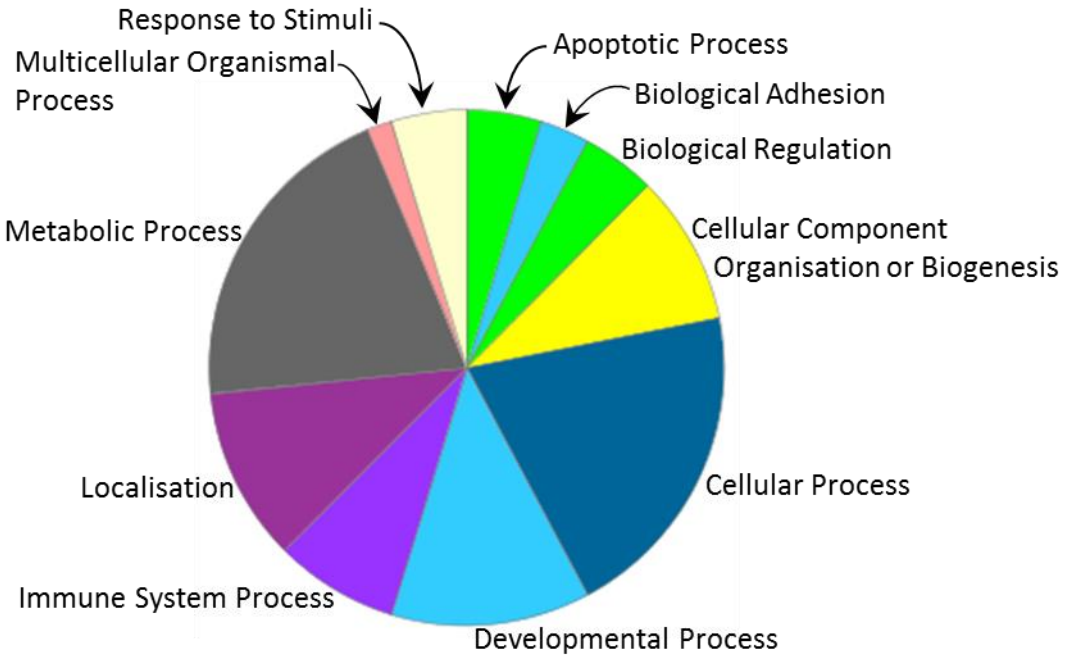

Figure 6.8. **Pie chart showing biological processes for the proteins in Table 6.2.** This pie chart separates proteins in Table 6.2 into their respective biological processes.

Molecular function data shows that structural, binding and receptor components are key aspects for the recovery and repair of skin tissue post-surgery. The categories identified in the biological processes analysis alone are not that informative. It would be useful to know more specifically

what immune system processes or multicellular organismal processes are represented. Webgestalt is a tool for further mining the data set, it can identify more specific roles, as illustrated in Figure 6.9, Figure 6.10 and Figure 6.11:

.

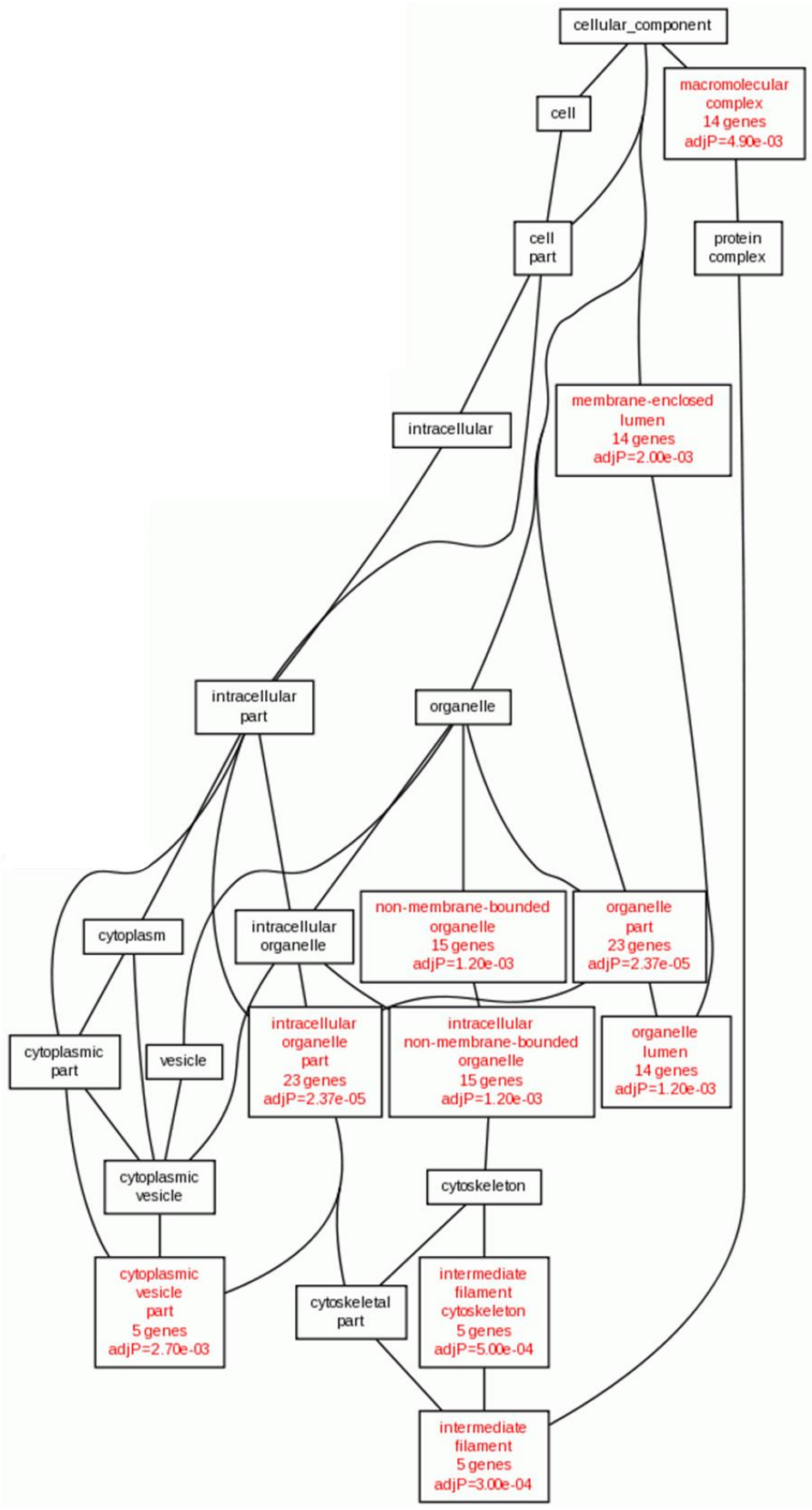

Figure 6.9. **Flow chart showing the cellular processes for the proteins in Table 6.2.** Flow chart generated by Webgestalt (http://bioinfo.vanderbilt.edu/webgestalt/).

Figure 6.9 highlights cellular components represented by the proteins identified as being significantly differentially expressed between the unscarred tissue of the children that went on to scar healthily compared with those that scarred hypertrophically. Cytoplasmic vesicles and cytoskeletal functions stand out as key components for healthy healing function. Vesicles are key for transport within the cytoplasm as well as expelling compounds from within the cell. Secondly, underlying skin structure is important for barrier formation and maintenance of structural integrity which is key for the skin to fulfil its function as a protective barrier.

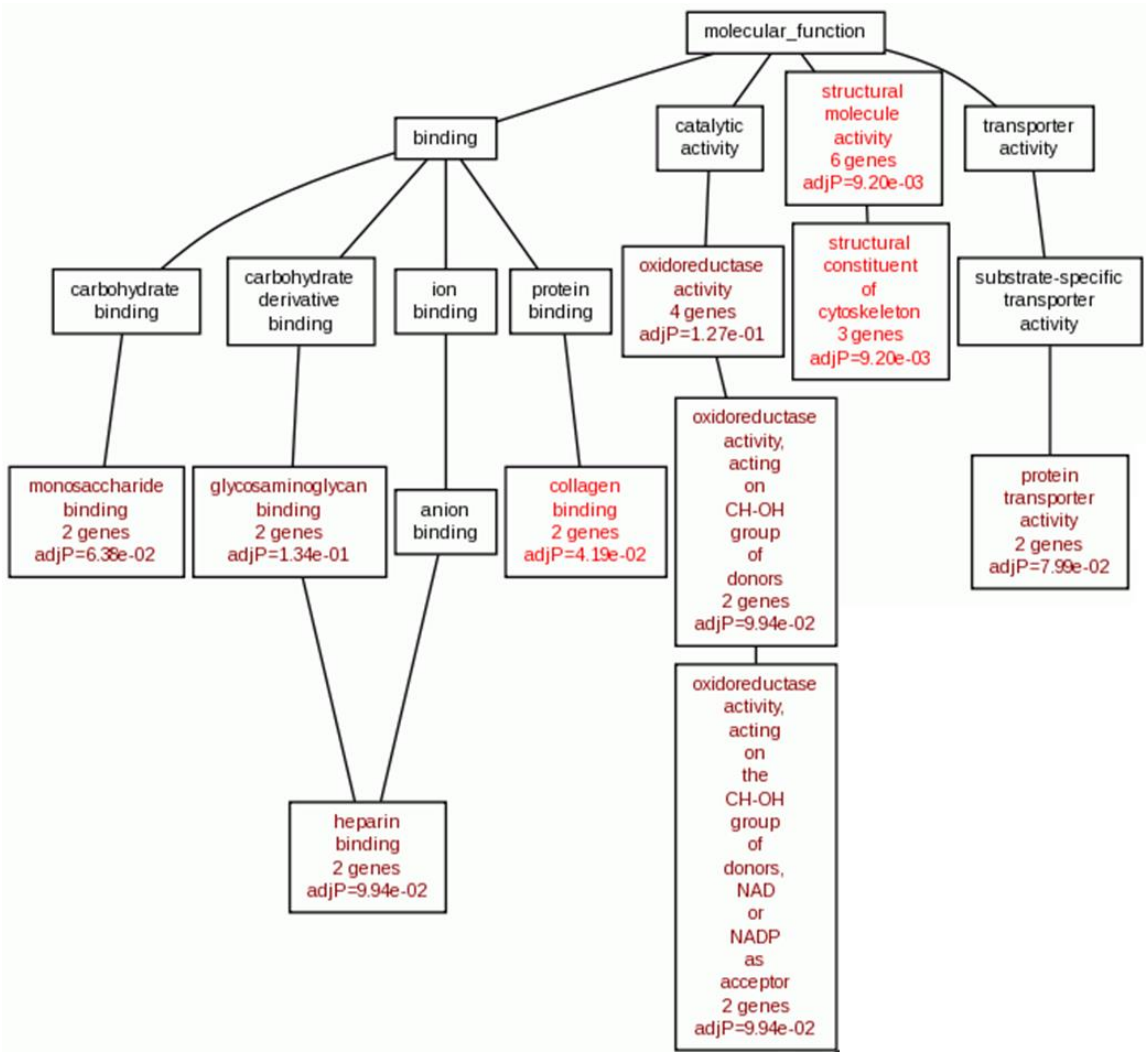

Figure 6.10. **Flow chart showing the molecular function for the proteins in Table 6.2.** Flow chart generated by Webgestalt (http://bioinfo.vanderbilt.edu/webgestalt/).

Figure 6.10 illustrates the molecular functions represented by the proteins in Table 6.2. Protein transport activity is associated with two of the proteins. As described in chapters 3 and 4 , protein transport is crucial for correct barrier function and skin integrity. Binding represents a significant branch of this flow chart (Figure 6.10). The binding branch links to heparin binding. Heparin is a glycosaminoglycan, consisting of repeating sulphated disaccharide units. In medicine it is administered to reduce the formation of clots. It is also endogenously released

from mast cells in the body. Its role within the body could be as a defence molecule[259]. Perhaps heparin has a role in wound healing and is dysregulated in individuals who develop hypertrophic scars. Finally, a group of oxidoreductase proteins have been identified. Oxidoreductases are a group of enzymes responsible for electron transfer between compounds. These reactive oxygen species (ROS) contribute to oxidative stress which in turn modifies DNA, lipids, proteins and carbohydrates within the body.[260] This links to the antioxidant activity shown in Figure 6.7 and could suggest that underlying oxidative stress within the body influences predisposition to develop a hypertrophic scar.

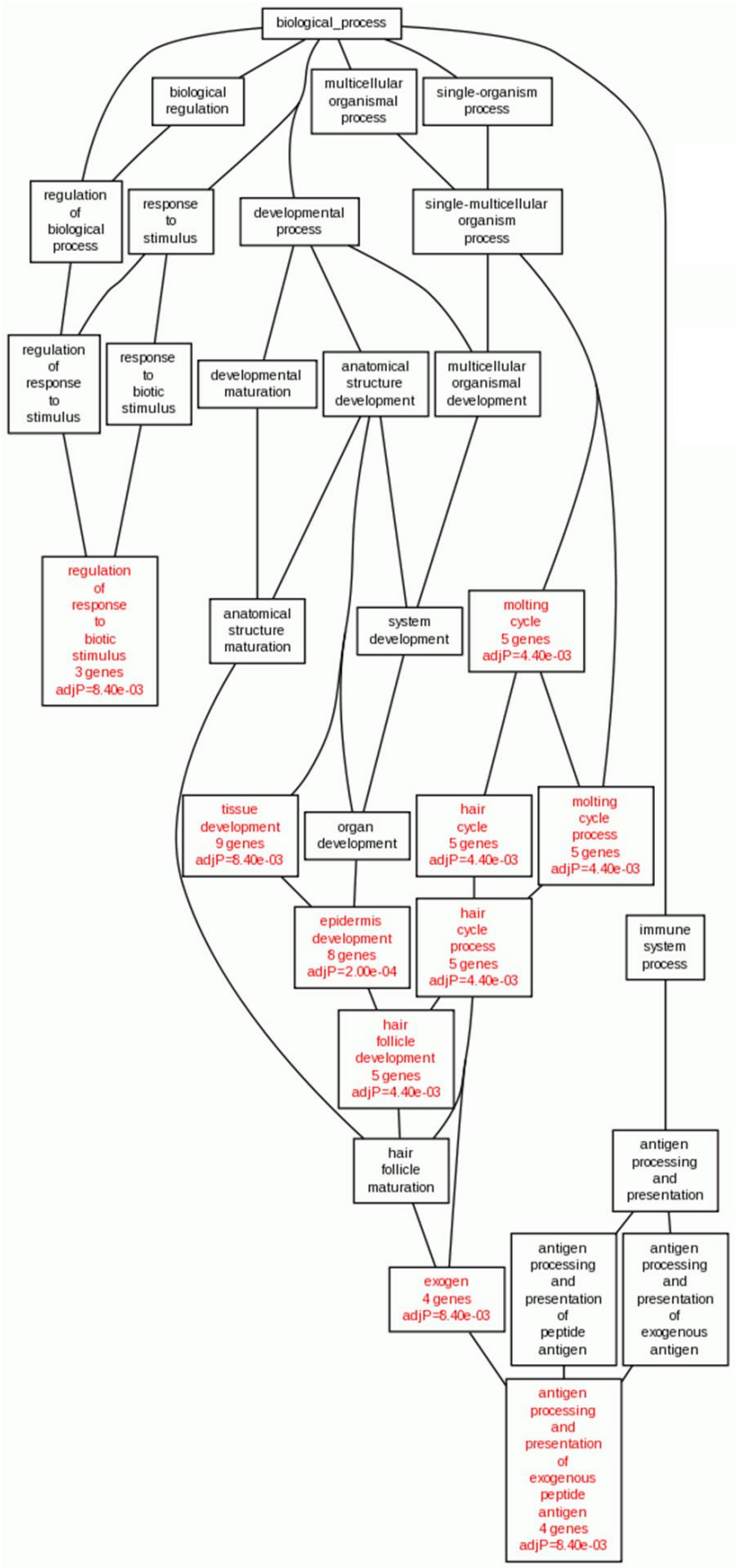

Figure 6.11. **Flow chart representing biological processes for the proteins in Table 6.2.** Chart generated by Webgestalt (http://bioinfo.vanderbilt.edu/webgestalt/).

Figure 6.11 shows the biological processes associated with the proteins significantly differentially expressed in patients that developed hypertrophic scars and those that did not. From those proteins (Table 6.2) eight genes are associated with epidermis development, this is unsurprising since the original tissue was skin. However, of the thousands of proteins present in skin for 8 of 30 to be involved in epidermal development is perhaps not just a result of proportional representation. This could suggest that there is a different composition of epidermal development proteins in those that have a predisposition to develop a hypertrophic scar. Secondly, Figure 6.11 shows differences in the immunological component between the two groups and more specifically antigen processing.

Webgestalt also links the proteins to related diseases. Table 6.3 lists the associated diseases linked with proteins in Table 6.2.

Disease	#Gene	EntrezGene	Statistics
Parakeratosis	2	3860 3861	C=14;O=2;E=0.02;R=107.32;rawP=0.0002;adjP=0.0094
Keratoderma, Palmoplantar	2	3872 3861	C=34;O=2;E=0.05;R=44.19;rawP=0.0009;adjP=0.0106
Skin Abnormalities	3	3872 3861 4000	C=145;O=3;E=0.19;R=15.54;rawP=0.0009;adjP=0.0106
Diphtheria	2	50489 54936	C=32;O=2;E=0.04;R=46.95;rawP=0.0008;adjP=0.0106
Hemolysis	2	2821 3032	C=56;O=2;E=0.07;R=26.83;rawP=0.0025;adjP=0.0127
Skin Diseases	4	3872 3866 3861 4000	C=388;O=4;E=0.52;R=7.74;rawP=0.0016;adjP=0.0127
Alopecia	2	3866 4000	C=50;O=2;E=0.07;R=30.05;rawP=0.0020;adjP=0.0127
Newcastle Disease	2	4835 2879	C=51;O=2;E=0.07;R=29.46;rawP=0.0021;adjP=0.0127
Ectodermal Dysplasia	2	3872 3861	C=52;O=2;E=0.07;R=28.89;rawP=0.0022;adjP=0.0127
Skin and Connective Tissue Diseases	4	3872 3866 3861 4000	C=444;O=4;E=0.59;R=6.77;rawP=0.0027;adjP=0.0127

Table 6.3. **A table listing the diseases associated with the proteins in Table 6.2.** This table (generated by Webgestalt) lists the diseases known to be linked to the proteins from Table 6.2. C = the number of reference genes in the category, O = the number of genes in the gene set and also in the category, E = the expected number in the category, R = the ratio of enrichment, rawP = p-value from hypergeometric test, adjP = p-value adjusted by the multiple test adjustment.

Most of the associated diseases in Table 6.3 are skin diseases, it is interesting to note that keratin 14 (EntrezGene 3861) has been associated with 6 of the 10 listed diseases, particularly with diseases of overgrowth such as parakeratosis and keratoderma where the epidermis continues to grow at a rate exceeding the rate at which skin cells are being shed. This is similar to the overgrowth of scar tissue described in hypertrophic scarring.

Finally GeneMANIA was used to visualise and map the links between those selected proteins and to highlight pathways with specific functions as shown in Figure 6.12.

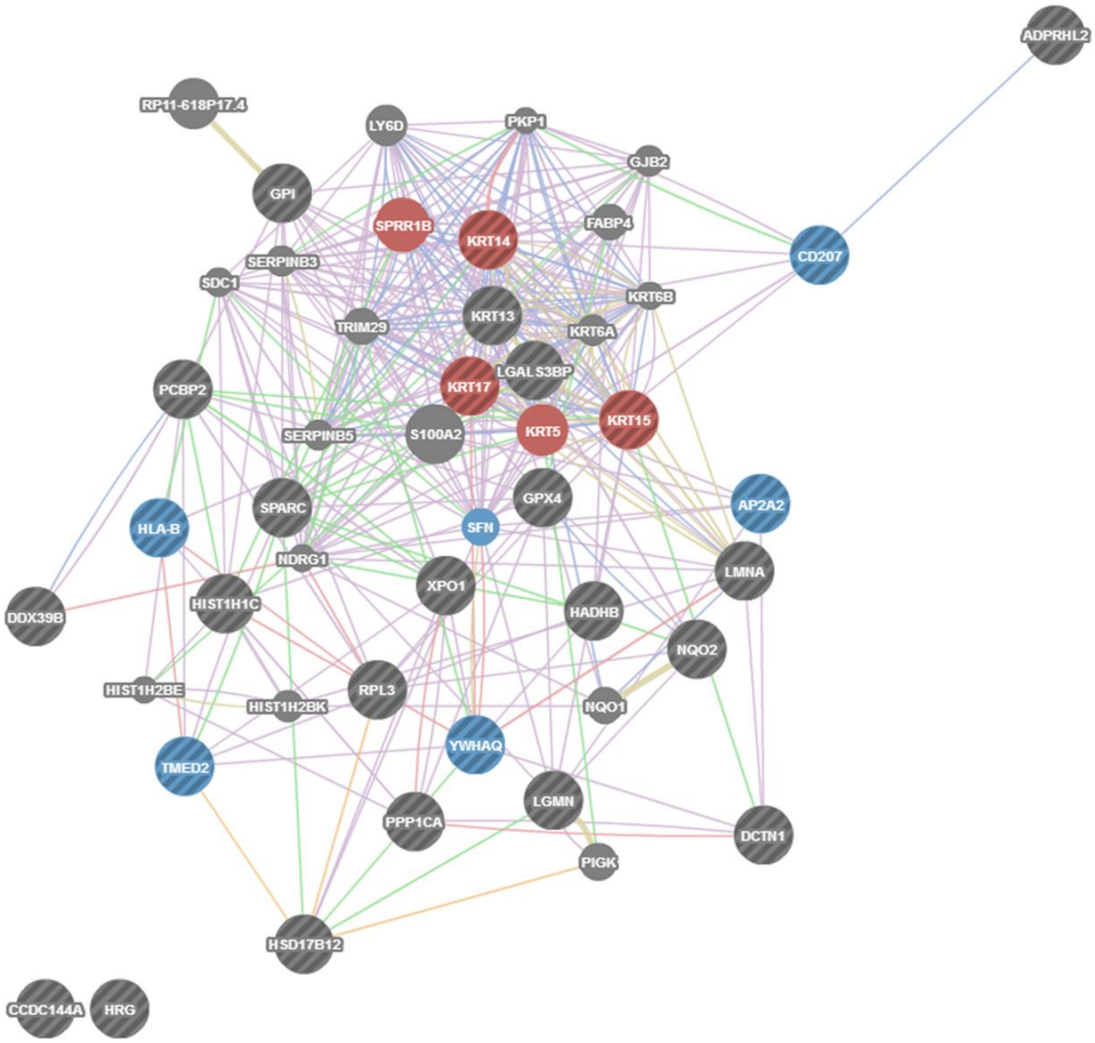

Figure 6.12. **Figure illustrating protein interactions from Table 6.2.** This figure illustrates the interactive network between the proteins of Table 6.2. Purple links = co-expression, blue = co-localisation, pink = physical interaction, yellow = shared protein domains, green = genetic interactions. The protein nodes highlighted in red are involved with epidermal development and those in blue are associated with vesical membranes.

This way of visualising the data helps to identify new links between proteins and. For example, it is interesting that keratins have a very central role, with more connections to other proteins than any other class. One protein of interest was HLA class I histocompatibility antigen, B-73 alpha chain, this figure identifies four other proteins from that list that associated with it: dynactin subunit 1, c-type lectin domain family 4 member k, legumain and AP-2 complex subunit alpha-2. C-type lectin domain family 4 member k helps to facilitate antigen uptake to lysosomes and transport vesicles, legumain acts to process proteins for antigen presentation and dynactin subunit 1 and AP-2 complex are involved in vesicle, early endosome and lysosome transport.[261]

6.6.5 Modified protein validation in the sample analysis

After acquisition MS raw files contain all the mass ion information for that sample. These raw files can be re-analysed to interrogate different aspects of the data, for example possible changes in post-translational modifications (PTMs) of proteins. Most proteins in the body have some degree of post translational modification, proteins in the skin are no exception. Common skin PTMs include: deamidation, oxidation, hydroxylation, methylation, sulphation, carbonylation and citrullination. Deamidation is the removal of the amide functional group from asparagine or glutamine and is part of the protein degradation. Methionine oxidation is a reversible enzymatic electron releasing reaction that occurs as proteins age *in vivo*. Hydroxylation most commonly involves proline, but also affects aspartic acid, lysine and asparagine residues. During hydroxylation a hydrogen atom is enzymatically modified to a hydroxyl group and is commonly found in collagen. Methylation, the addition of a methyl group to an amino acid ($-CH_3$) of aspartic acid, leucine, lysine, glycine and asparagine residues occurs frequently on histones. Sulphation, the addition of a sulpho group ($-SO_3H$) to an amino acid is involved in a range of biological processes. Carbonylation occurs when carbon monoxide modifies or oxidises amino acids. Finally, citrullination is the conversion of arginine to a citrulline residue. Citrulline is an amino acid, but not coded for in DNA and only occurs as a result of this PTM. Citrullination occurs in inflammation and cell death.

Macros were developed for the analysis of the PTMs described above and Progenesis QI for proteomics (Nonlinear Dynamics) was used to analyse data from all the patient samples in chromatographic fraction 5 of the experiment. Fraction 5 was selected because this was the fraction containing the greatest number of proteins. The quality of spectra data for modified peptides tends not to be as high as the respective unmodified peptide. Figure 6.13 and Figure 6.14 illustrate this, they are both spectra for the peptide with sequence NMQDLVEDFK, however, Figure 6.13 shows the spectrum for the unmodified peptide and Figure 6.14 shows the spectrum for the same peptide, yet with a hydroxylasparagine (N) at the beginning of the sequence instead of a 'standard' asparagine (N).

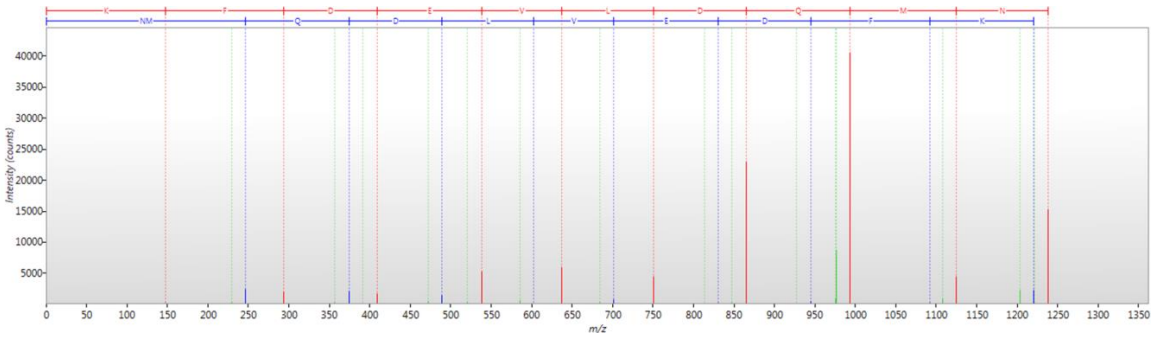

Figure 6.13. **Figure showing the spectrum of an unmodified peptide NMQDLVEDFK.** This spectrum shows the b and y ions for the unmodified peptide NMQDLVEDFK from keratin type II cytoskeletal 5.

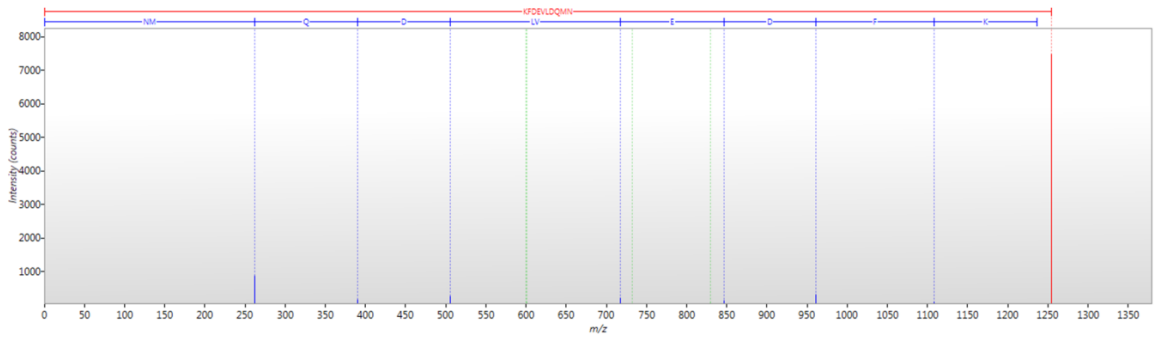

Figure 6.14 **Figure showing the spectrum of a modified peptide NMQDLVEDFK.** This spectrum shows the b and y ions for the modified peptide **N**MQDLVEDFK from keratin type II cytoskeletal 5, where the N-terminal asparagine residue is hydroxylated.

The unmodified spectrum (Figure 6.13) is of a higher quality than the modified one (Figure 6.14); there are several y ions (red) at greater that 10% signal intensity and although not as intense there are also corresponding b ions (blue). The unmodified peptide (Figure 6.14) shows a high intensity y ion (red) peak for the unfragmented peptide (~1250 m/z) and low intensity b ion (blue) fragments. This is the nature of fragmented peptides that they tend to act slightly different to their unmodified counterparts and thus have poorer fragmentation and therefore less accurate identification.

Of the selected PTMs, nitrosylation of cysteine (whereby nitric oxide is incorporated into the cysteine residue) showed the greatest difference in between the unscarred control and hypertrophic tissues as illustrated in Figure 6.15:

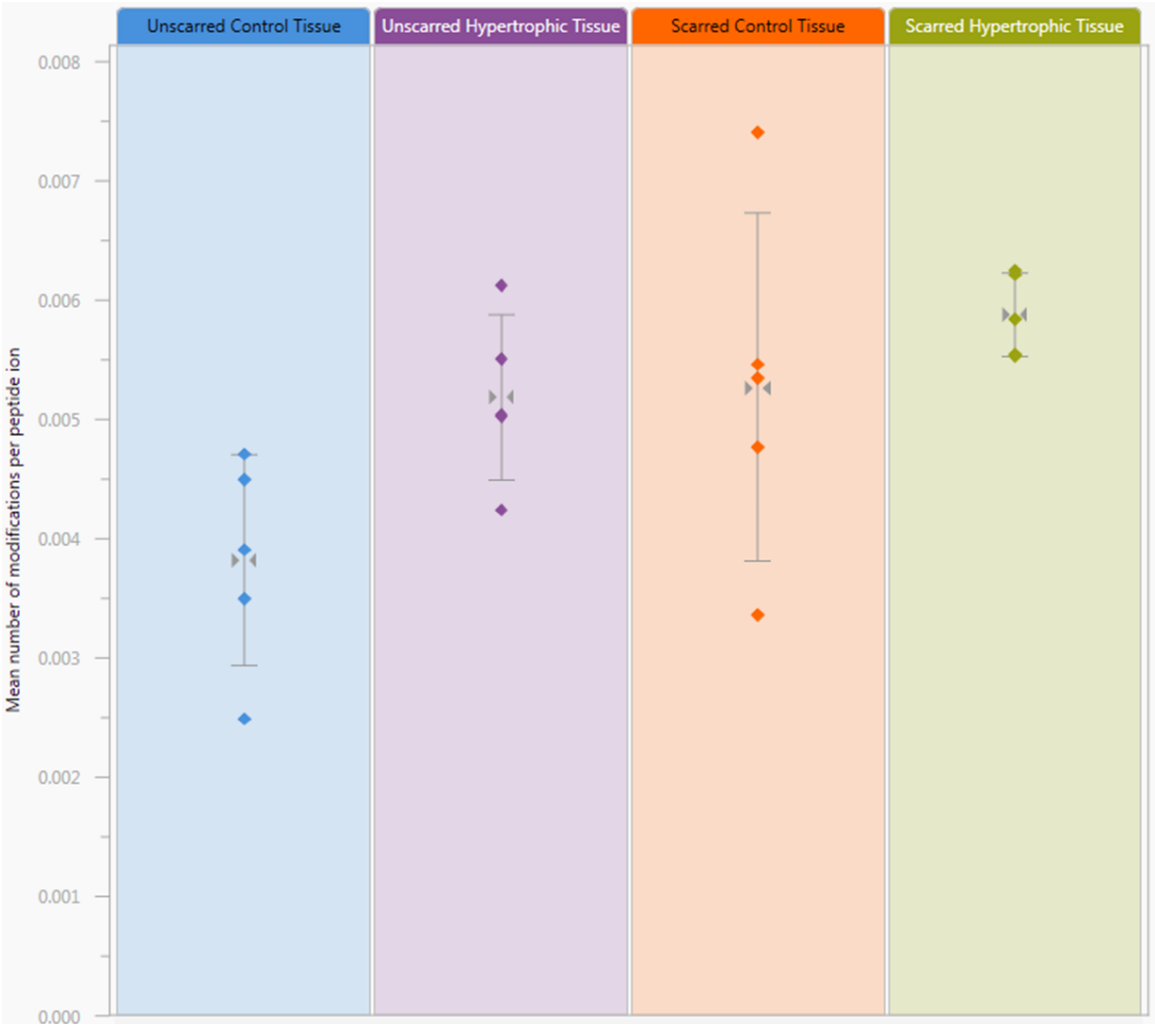

Figure 6.15. **Scatter plot illustrating the mean number of nitrosylated cysteine per peptide.** Scatter plot showing a higher number of modifications per peptide ion for the proteins in the unscarred hypertrophic tissue (purple) compared with the unscarred control tissue (blue). This type of analysis does not give statistical significance.

Cysteine nitrosylation facilitates redox-dependent signalling and protein function regulation[262]. Figure 6.15 shows the lowest mean in the unscarred controls, the highest mean in the scarred hypertrophic tissue. Nitrosylation of cysteine residues occurs as a response to oxidative stress and ROS damage in cells[262].

Figure 6.16 **Scatter plot illustrating the mean number of trimethylated lysine per peptide.** Scatter plot showing a higher number of modifications per peptide ion for the proteins in the unscarred hypertrophic tissue (purple) compared with the unscarred control tissue (blue). This type of analysis does not give statistical significance.

Figure 6.16 shows lowest levels of trimethyllysines (whereby three methyl groups are added sequentially to a lysine residue) in unscarred hypertrophic tissue. There is a difference in the means of unscarred and scarred hypertrophic tissues. Lysines can be single, doubly or triply methylated, most often histones contain methyllysines[263]. Methylation is controlled by methyl transferases and demethyltransferases and regulates gene expression[264]. The small difference in methylation state between unscarred control and unscarred hypertrophic samples appears to have consequences for gene expression. Table 6.2 lists histone as a protein upregulated in unscarred hypertrophic tissue compared with controls from our proteomic analysis. This is not the same as the pattern shown by trimethyllysine in Figure 6.16.

Figure 6.17. **Scatter plot illustrating the mean number of deamidated glutamines per peptide.** Scatter plot showing a higher number of modifications per peptide ion for proteins in unscarred hypertrophic tissue (purple) compared with unscarred control tissue (blue). This type of analysis does not give statistical significance.

Protein deamidation is a PTM found in ageing and age-related diseases[265; 266]. Glutamine deamidation describes the removal of an amide functional group from a glutamine amino acid[267]. Protein deamidation rate is influenced by factors such as protein shape[268], exposed surface of the protein[269] and surrounding environment[270; 271]. Figure 6.17 shows a greater amount of glutamine deamidation in hypertrophic samples compared with controls for both scarred and unscarred tissues. This suggests there a higher level of protein turnover in the children that develop hypertrophic scars.

6.7 Targeted lipidomic analysis of glycosphingolipid isoforms in the skin of children in this study of hypertrophic scar outcomes

Our results in Table 6.2 indicated differences in oxidative stress and free radical damage between the two groups. This was also indicated in Figure 6.7 showing antioxidant activity,

Figure 6.10 identified oxidoreductase activity and Figure 6.15 indicated free radical damage. Antioxidant and oxidoreductase activity suggests free oxygen within the skin is being converted by oxidoreductase to ROS. Antioxidants maintain ROS at a healthy level in the body and have can quench ROS reactions if their levels become too high. ROS includes hydroxyl radicals, hydrogen peroxide and superoxide anions[272] these highly reactive species have a healthy role in the body as signalling molecules for regulatory processes within the body[273] however, they also act to damage DNA, proteins and lipids[274]. When ROS species such as hydroxyl radicals interact with lipids they can initiate lipid peroxidation resulting in hydroxylated and peroxide lipids as intermediate species. Lipids are important in the skin, making up a large part of the skin barrier and protecting against excessive water loss[276]. The major lipid classes in the skin are cholesterols, free fatty acids and ceramides[277]. All these lipids are susceptible to peroxidation if the level of free radical species is high enough. We hypothesised that if proteomic and PTM data showed antioxidant and oxidoreductase activity there may be changes in lipid peroxidation in the skin. To test this, a glycosphingolipid (more specifically globotriaosylceramide) was characterised.

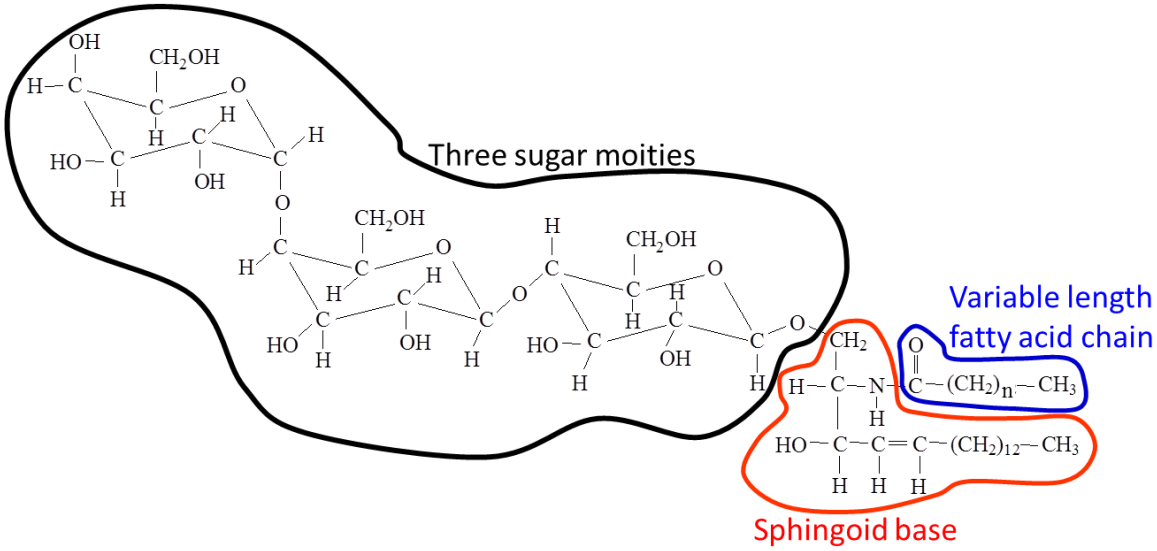

Figure 6.18. **The chemical structure of globotriaosylceramide (GB3).** GB3 consists of a sphingoid base with a fatty acid chain of varying length and three sugar moieties.

The length of the fatty acid component is variable in health, as illustrated in Figure 6.19:

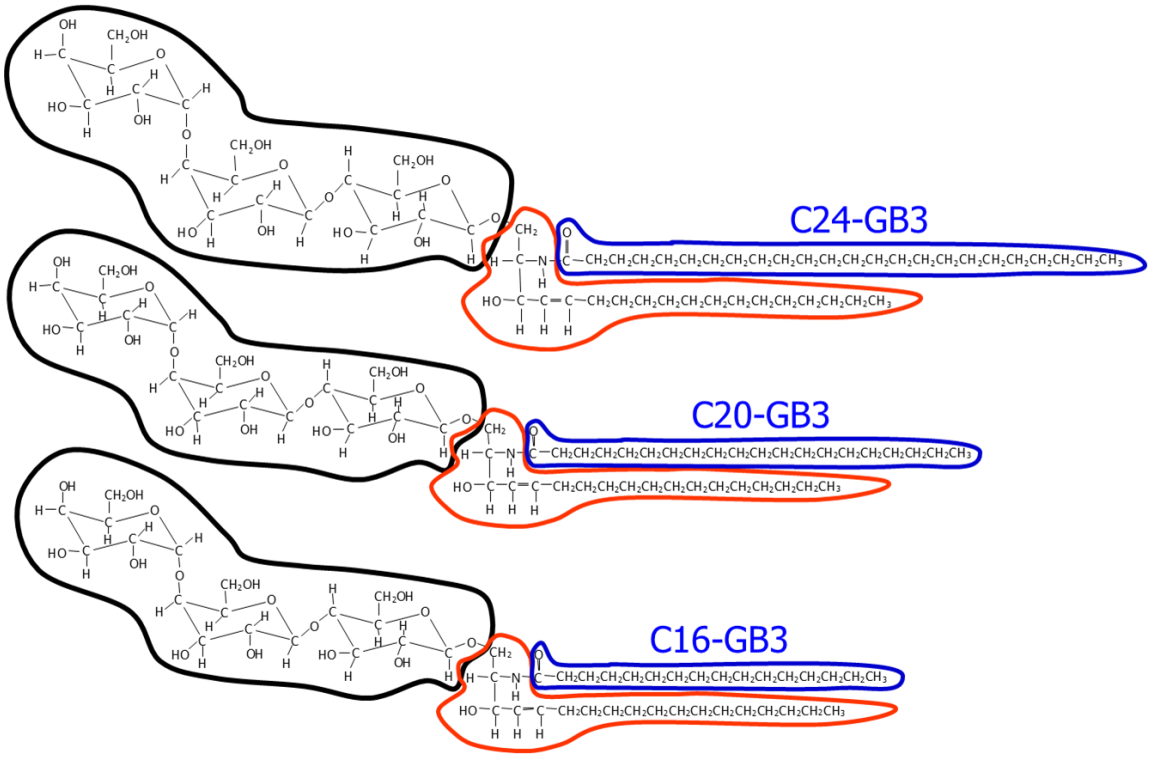

Figure 6.19 **The chemical structure of three globotriacylceramide isoforms: C24-GB3, C20-GB3 and C16-GB3.** These three GB3 isoforms differ only in fatty acid chain length, the sphingoid base and sugar moieties remain unchanged.

Figure 6.19 shows three isoforms of GB3 in which the fatty acid chain is saturated (there are no C=C double bonds in the chain). GB3 is a precursor of ceramide, which is the most abundant intracellular lipid in the skin and plays a role in barrier function[278]. An 11 minute LC-MS/MS assay (method 10.2.17) was developed to quantitate GB3 and GB3 isoforms in skin tissue, to investigate evidence of lipid peroxidation and signs of oxidative stress damage in these samples. The assay included 14 GB3 isoforms: C16:0, C18:0, C20:0, C22:0, C24:0, C26:0, C22:1, C24:1, C24:2, C22:0-OH, C24:0-OH, C24:0-OH-OH, C24:2-OH and C24:2-OOH as illustrated in Figure 6.20 with their respective retention times:

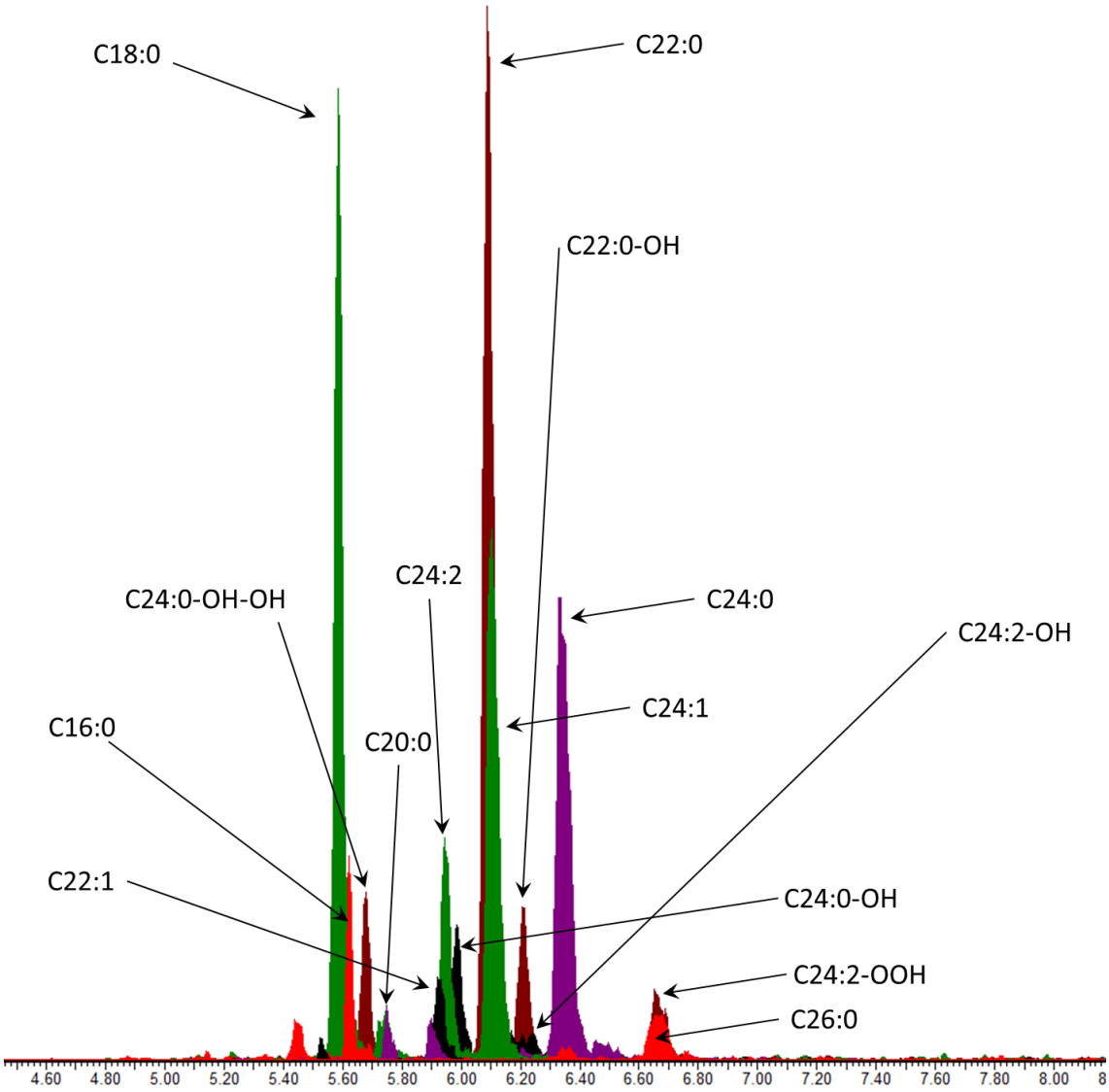

Figure 6.20. **Figure illustrating the GB3 isoforms quantified in this assay.** This figure shows the combined chromatograms of the GB3 isoforms in this assay. The x-axis represents retention time and the y-axis shows relative abundance.

Lipids were extracted from the same tissue homogenate that the proteomic analysis was carried out on in section 6.6. Lipids were extracted from 0.3mg of protein homogenate to standardise lipid content. The overall GB3 levels were slightly elevated in the hypertrophic samples, data shown in Figure 6.21:

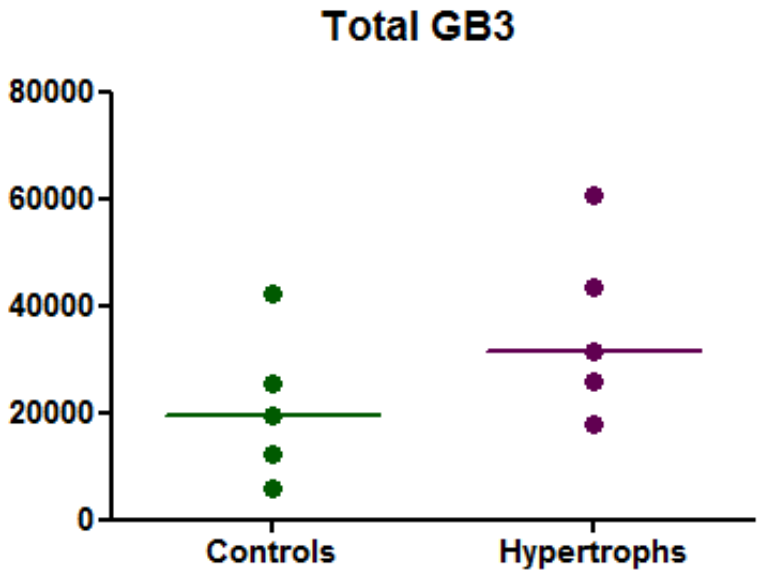

Figure 6.21. **Scatter plot for total GB3 levels, in the unscarred control and unscarred hypertrophic samples.** This scatter plot shows the relative amounts of globotriacylceramide (GB3). 'Controls' (median = 19459) refers to the healthy pre-surgery skin tissue from the children who post-surgery went on to develop a healthy scar. 'Hypertrophs' (median = 31478) refers to the healthy pre-surgery skin tissue from the children who post-surgery went on to develop a hypertrophic scar.

The individual isoforms of GB3 showing most noticeable differences were C24:2, C24:2-OH and C24:0-OH-OH. The scatter graphs for these isoforms are shown in Figure 6.22, Figure 6.23 and Figure 6.24:

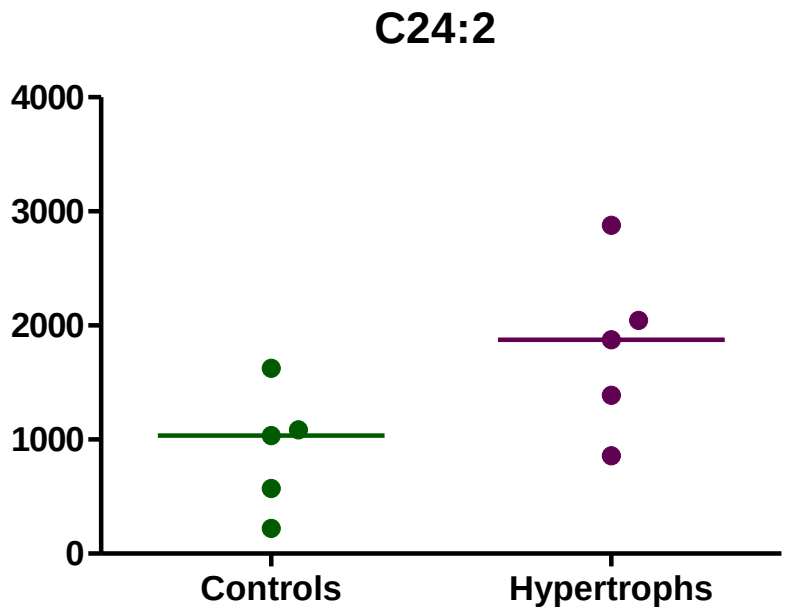

Figure 6.22. **This scatter plot shows the relative abundance of the C24:2 GB3 isoform.** This scatter plot shows the relative abundance and median of the C24:2 GB3 isoform in the control (median = 1036) and hypertrophic (median = 1873) groups.

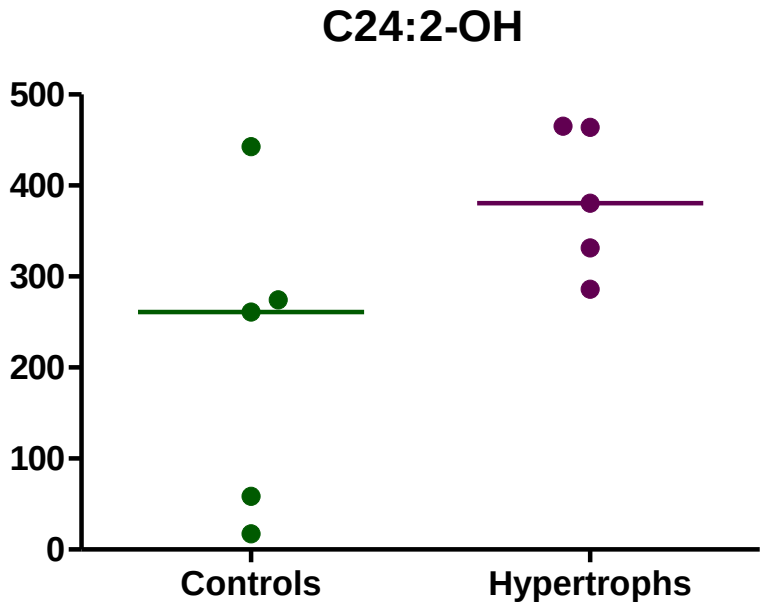

Figure 6.23. **This scatter plot shows the relative abundance of the C24:2-OH GB3 isoform.** This scatter plot shows the relative abundance and median of the C24:2-OH GB3 isoform in the control (median = 261.1) and hypertrophic (median = 380.8) groups.

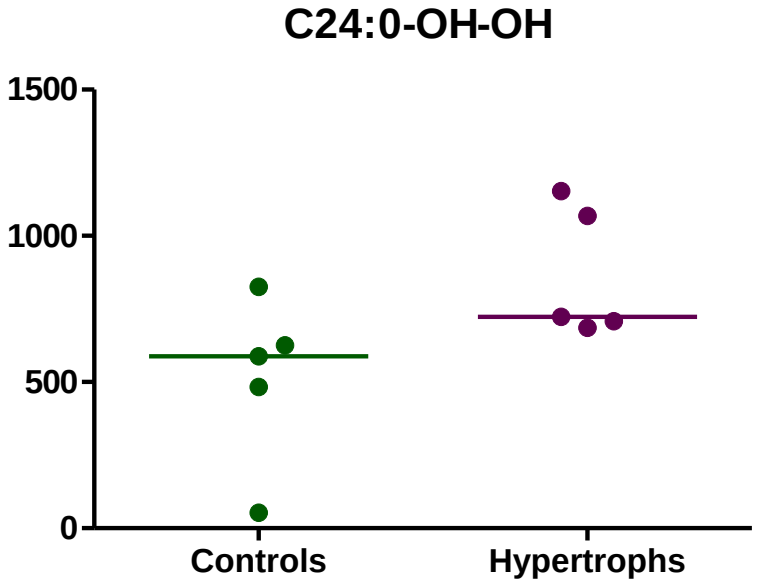

Figure 6.24. **This scatter plot shows the relative abundance of the C24:0-OH-OH GB3 isoform.** This scatter plot shows the relative abundance and median of the C24:0-OH-OH GB3 isoform in the control (median = 588.1) and hypertrophic (median = 723.1) groups.

Figure 6.22, Figure 6.23 and Figure 6.24 support the trend illustrated in Figure 6.21 indicating higher levels of GB3 in hypertrophic samples compared with controls, standardised for protein

content. To investigate lipid peroxidation the ratios of saturated to unsaturated and oxygenated to saturated of fatty acid chains were compared in Figure 6.25 and Figure 6.26, respectively:

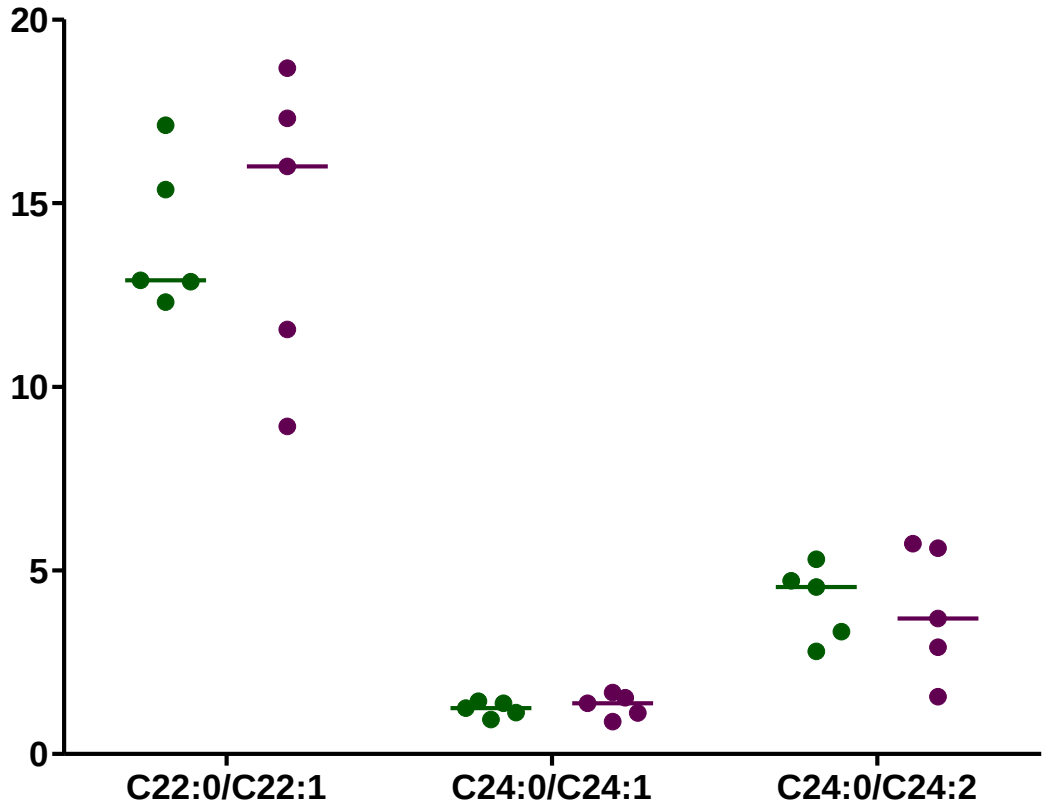

Figure 6.25. **Scatter plot illustrating the ratio of saturated to unsaturated fatty acid chains.** This scatter plot shows the relative abundances for saturated and unsaturated fatty acid chains of GB3 for C22 and C24 GB3 isoforms. C22:0/C22:1 medians: controls = 12.9 and hypertrophs = 16.0, C24:0/C24:1 medians: controls = 1.3 and hypertrophs = 1.4 and C24:0/C24:2 medians: controls = 4.5 and hypertrophs = 3.7.

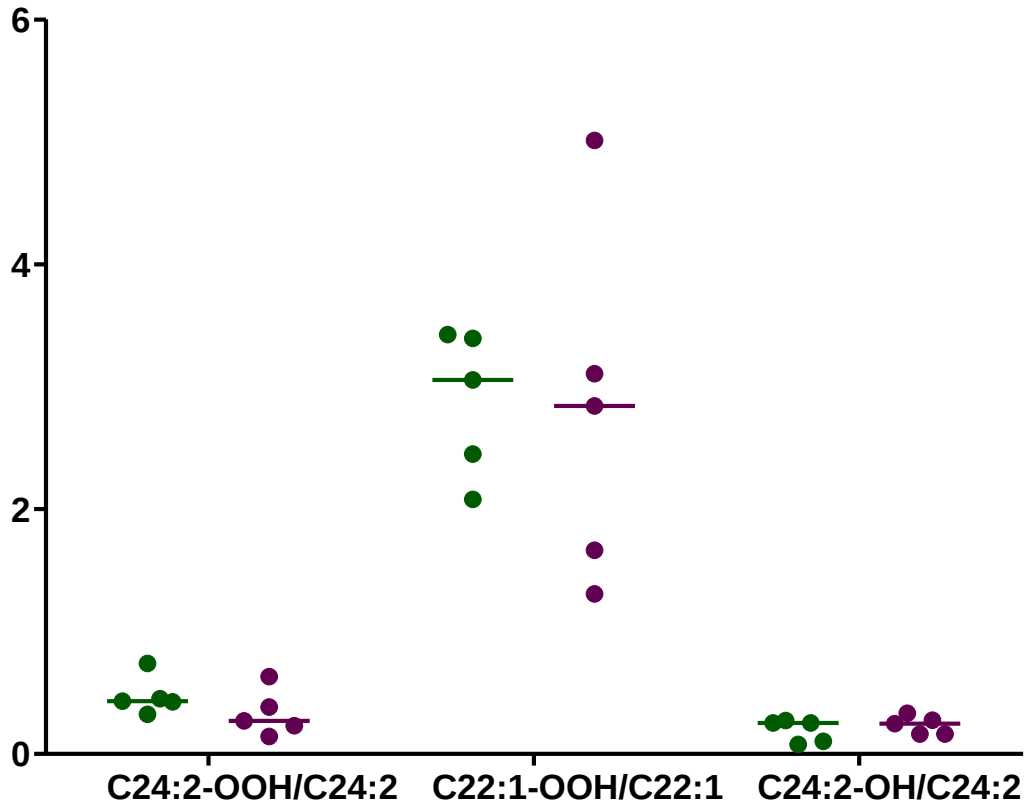

Figure 6.26. **Scatter plot illustrating the ratio of oxygenated to unsaturated fatty acid chains.** This scatter plot shows the relative abundances for oxygen-containing species and unsaturated fatty acid chains of GB3 for C22 and C24 GB3 isoforms. C24:2-OOH/C24:2 medians: controls = 0.43 and hypertrophs = 0.32, C22:1-OOH/C22:1 medians: controls = 3.06 and hypertrophs = 2.84 and C24:0-OH-OH/C24:2 medians: controls = 0.25 and hypertrophs = 0.25.

These graphs suggests that despite there being slightly higher GB3 levels in the patients who scar hypertrophically the ratio between oxidised lipids and un-oxidised lipids is not significantly different, suggesting little difference in lipid oxidative stress damage between the two cohorts.

6.8 Predisposing factors for the development of hypertrophic scars

The aim of this chapter was to analyse these samples and to identify predisposing factors that could indicate pre-surgically whether someone would develop a hypertrophic scar. Two different techniques: proteomics and a targeted lipidomic assay were used. Each technique is able to highlight different changes in their respective aspect of the data. This study was a unique opportunity to understand the biochemical pathways involved in scarring (section 6.5.1). The concept of having healthy skin samples from patients before they develop a hypertrophic scar is novel. Instead of studying hypertrophic or healthy scar tissue itself, we studied pre-scar tissue. The aim was to investigate predisposing indicators for the development of hypertrophic scars.

6.8.1 Summary of the findings of the proteomic analyses

Our proteomic profiling analysis took over fifteen hours per sample allowing identification of in excess of 5000 proteins. Thirty proteins were identified from the UDMS^{E} experiment (Table 6.2) and gene ontology and pathway analysis tools used to scrutinise these data, key themes and networks were identified and highlighted. Particularly Figure 6.6 showed over 75% of the proteins identified belonged to intracellular components rather than extracellular components. This could be due to the homogeneity of the extracellular matrix compared with the relative complexity of intracellular proteins, or perhaps due to intracellular protein solubility. Another element highlighted in Figure 6.7, Figure 6.9 and Figure 6.11 was the structural and developmental components of the proteins identified. This is important in the fundamental healing process, if there are irregularities in the structure of the pre-scar healthy tissue that could be the cause of impaired skin healing. The immunological component highlighted by a ten-fold upregulation or HLA class I histocompatibility antigen B-73 alpha chain in the children that went on to develop hypertrophic scars, suggests an underlying immune hyperactivity. The immune system plays a crucial role in healing and scar formation, an underlying upregulation of immune activity could conceivably affect the healing process. The was also evidence of free-radical damage, such as the presence of anti-oxidants (Figure 6.7) in our proteomics data.

6.8.2 Summary of findings from PTM investigations

Our MS dataset was further interrogated to investigate roles of modified proteins. PTMs are critical for proper cell function as well as a role in cell signalling.[279] Modified peptide analysis using mass spectrometry is challenging, they do not respond in the same was as their unmodified counterparts. The modification can not only changes the mass, but also the charge, polarity and/or three-dimensional shape. As demonstrated in Figure 6.13 and Figure 6.14 the quality of the spectrum was far superior for the unmodified peptide than the modified version. Modifications near trypsin cleavage sites may affect the ability of trypsin to cleave.

We were able to identify subtle changes in the modification of amino acid residues between the patient groups for three modifications: cysteine nitrosylation, trimethyllysine and glutamine deamidation. These changes indicated ROS activity, changes in gene expression and protein ageing. A different type of MS fragmentation technique called electron transfer dissociation (ETD) as opposed to collision induced dissociation (CID) fragments peptides to form “c” and “z” ions. It is a less aggressive fragmentation type allowing for greater preservation of potentially labile modifications.[280] With ETD scan time is increased and it identifies fewer proteins than CID[7] , however for specific peptide modification analysis ETD may be preferential.

A more targeted analysis of modified peptides may be more suited, such as MRM. The precursor and product ion mass would be specifically selected, this is more suited to lower abundancy species within a mix of other more abundant species.

6.8.3 Summary of findings from investigating lipid peroxidation in the skin samples using GB3

The aim of the targeted lipid analyses was to investigate the degree of lipid peroxidation in fatty acid side chains of GB3 in skin (the proteomics data indicated that there may be differences in ROS between groups). In particular hydroxyl radical damage, forming hydroxylated fatty acids from unsaturated fatty acids. We chose to develop a method to study GB3, a precursor of ceramide in the skin and the degree of saturation and hydroxylation of its fatty acid chain.

The most prominent observation was elevated levels of GB3 in the skin of children that developed a hypertrophic scar. This class of lipid was elevated in the hypertrophic samples however, that does not necessarily mean that all classes of lipid would be. GB3 is part of a network of glycosphingolipids, it is plausible that elevation of one class may be indicative of a reduction in a downstream component. There is a rare genetic lysosomal storage disorder, called Fabry disease caused by a deficiency in the enzyme that processes GB3 leading to an accumulation of GB3. There is no literature suggestive of abnormal scarring in Fabry disease, however patients with Fabry disease develop hypertrophic cardiomyopathy. Cardiomyopathy is a completely separate disease however, there are underlying similarities such as tissue overgrowth[281]. There are also skin abnormalities associated with Fabry disease such as angiokeratoma[282], a cutaneous blood capillary abnormality. No Fabry disease findings correlate directly with hypertrophic scarring, they do suggest that high levels of GB3 can manifest in physiological changes such as hypertrophic growth and skin abnormalities.

6.9 Conclusions

This chapter demonstrates the biochemical differences in the skin of children who scar healthily and those that scar hypertrophically. These differences can be detected prior to injury. Our proteomic study identified potential disease mechanisms leading to the development of hypertrophic scars. A validatory secondary method was developed to analyse peroxidation of lipids to confirm these findings. With further work, this avenue could be probed further to create a predictive test for hypertrophic scar, also allowing for development of pre-surgical interventions and/or treatments to prevent post-operative negative scar outcomes.

6.10 Further work

To continue this work it the protein biomarkers identified in Table 6.2 would be worth pursuing potentially using them to establish a targeted MRM-based assay. That assay would be used to analyse a larger cohort of samples identifying which markers are most sensitive and specific. Skin punch biopsies are invasive, the MRM method could be optimised to detect markers from skin scrapings which are less invasive or skin tapings. The final assay could be used as a predictive pre-operative test to identify individuals who are likely to develop a hypertrophic scar.

It would also be interesting to investigate the lipid aspect, to study other classes of lipids in the skin to see if they follow the same trends as GB3. Not only that, but lipids could act as drug or treatment target for interventional therapy aimed at reducing hypertrophic scar outcomes.

Chapter 7

Investigating how protein compositions within the skin change after major surgical operations

7 Investigating how protein compositions within the skin change after major surgical operations

Contents

Every year millions of operations or procedures are performed by the NHS, in the year March 2015 to February 2016 there were 11.6 million finished consultant episodes (a continuous period during which a patient is under the care a single consultant within a single NHS trust) which included at least one procedure or operation[283]. These will range from minor elective procedures such as the removal of a benign mole to highly complex life-saving operations such organ transplantations. With any surgery or intervention there is an element of risk and that risk changes depending on the nature of the surgery.

7.1 The risks associated with general anaesthetic

Anaesthetic is required in most surgical cases to reduce discomfort. This may be local anaesthetic (LA) where the patient is still conscious and awake and the area involved in the surgery has been numbed or general anaesthetic (GA) when a patient is in a controlled unconscious state. There are more risks associated with GA compared with LA. With GA the body loses control of physiological functions so it is more complex for the body to recover [284]. LA is not always a viable option because choice of anaesthetic is dictated by the length, complexity and nature of the surgery. Side-effects of GA can range from nausea and a sore throat to nerve damage and death, although sometimes it is difficult to separate the risks associated with GA and the risks associated with the procedure itself.

7.2 The importance of peri-operative oxygen delivery

7.2.1 The prevalence of post-operative morbidity

Morbidity after major surgery involving GA is of increasing concern. An ageing population means that major operations are being performed on patients of increasing age. Prevalence of post-operative morbidity in the elderly is becoming a major healthcare challenge.[285] Post-operative morbidity presents in 15% of surgical inpatients and 50% of complications are classed as “serious”[286]. These figures are not restricted to one study, there are multiple studies worldwide investigating the risk of peri-operative morbidity with age and disease status[285]. A nine fold increase in relative risk for prolonged hospital stay and mortality was reported for patients undergoing hepatectomy and oesophagectomy (both high risk procedures) in Maryland[287]. Post-operative morbidity three days after surgery was identified in 74% of patients undergoing major elective surgery in a UK prospective cohort study, that figure reduced to 16% 12 days later[288]. Another UK prospective cohort study identified post-operative complications in 27% of patients undergoing routine, moderate-risk surgery[289]. These figures illustrate risk associated with operations requiring GA.

7.2.2 Maintaining peri-operative oxygen delivery using haemodynamic therapy

Low oxygen delivery is associated with increased risk of post-operative morbidity, although, the exact physiological mechanism remains unknown[44]. A technique to control oxygen delivery during and around surgery is called peri-operative haemodynamic therapy, initially optimised by Shoemaker in 1982[290]. It was observed that patients who died after surgery had lower oxygen delivery and consumption than the post-surgery survivors[291]. Those who received and consumed less oxygen did not have the required physiological reserves to cope with the metabolic demand of GA and surgery. By controlling oxygen delivery and oxygen consumption patient morbidity was reduced[292; 293; 294]. Increasing oxygen delivery to reduce patient morbidity continues to be supported in systematic reviews[44; 295, 296].

The current understanding is that controlling oxygen delivery and consumption of a patient, before, during and after an operation, will reduce the oxygen debt and tissue injury so, the body will be better equipped to deal with the physiological challenges of operations thus reducing morbidity[297; 298]. Despite, positive results from some studies suggest that controlling oxygen delivery can reduce morbidity, this concept is still contended. An in depth systematic review suggested that reduction in renal impairment, respiratory failure and post-operative wound infection can be expected with haemodynamic therapy, however, reduction in mortality related to morbidities such as: arrhythmia, myocardial infarction, pulmonary oedema, congestive heart failure, generalised infection and venous thrombosis was not observed. Despite this the review highlighted a lack of recent studies with clear outcomes and a lack of stringent patient recruitemnt.[299]

The underlying mechanism of haemodynamic therapy is still unknown and there is controversy pertaining to its effectiveness in reducing all types of post-operative morbidity.

7.3 How can mass spectrometry be used to investigate the effects of major surgery and peri-operative oxygen delivery

This chapter uses mass spectrometry as applied to proteomics and lipidomics to investigate biochemical changes in the skin as a result of major surgery and haemodynamic therapy. It is predicted that systemic changes occurring as a result of the surgery and related interventions could be expressed in the skin in a similar manner as would be the case in other systems, particularly with regards to oxygen perfusion. If more could be understood about the underlying biochemical changes during major surgery, treatment and management of post-operative complication could be specifically adapted to those changes. Pre-operative strategies may also be modified to better prepare the body physiologically for surgery to reduce morbidity.

7.4 Investigating the differences in biochemical composition of skin tissue after major surgery

The work in this chapter was carried out in collaboration with Dr Gareth Ackland from the UCL Centre for Anaesthesia, Critical Care and Pain Management. As part of a controlled trial in 2014 Ackland et al. investigated clinical outcomes of patients randomly assigned to the standardised post-operative regime compared with a personalised protocol[44]. As part of the investigations skin biopsies were taken before surgery and two days post-surgery. We used paired skin biopsies from 18 patients undergoing oesophagectomies. An oesophagectomy is a procedure whereby part of, or the entire oesophagus is removed, usually due to oesophageal cancer and part of the stomach must be used to bridge the gap created by the excised oesophageal section. Skin biopsies were taken from sites adjacent to the surgical wound. They were taken before and after surgery. Samples were prepared as described in chapter 5 and separated into four chromatographic fractions as detailed in method 10.2.12. This method identified in excess of 4000 proteins.

7.5 Proteomic investigations into post-operative oxygen saturation levels

In order to investigate the hypothesis discussed in the introduction (section 7.2) that achievement of pre-operative oxygen saturation levels after surgery would correlate with post-operative morbidity, we used proteomics to investigate the skin tissue of patients undergoing oesophagectomy. Skin samples were taken before surgery to identify predictive markers for achievement of oxygen saturation. We identified 17 proteins as significantly differentially expressed between the two groups: achievers and non-achievers of pre-surgery oxygen saturation levels.

Protein Accession	ANOVA (p-value)	Maximum Fold Change	Protein Full Name	Protein Description
Q2TBE0	0.0236	13.6	CWF19-like protein 2	Catalytic activity
Q7Z2Z2	0.0478	3.2	Elongation factor Tu GTP-binding domain-containing protein 1	Ribosome biogenesis + activation
Q6ZMU5	0.0339	3.0	Tripartite motif-containing protein 72	Cell membrane repair
Q9BRX8	0.0353	2.7	Redox-regulatory protein FAM213A	Redox regulation, antioxidant
Q9BUH8	0.0380	2.3	Brain-enriched guanylate kinase-associated protein	Kinase activity
Q14141	0.0286	2.1	Septin-6	GTPase, cytokinesis
P51451	0.0376	2.2	Tyrosine-protein kinase Blk	Cell proliferation + differentiation
P27448	0.0259	2.3	MAP/microtubule affinity-regulating kinase 3	Phosphorylation of tau proteins
P04259	0.0289	2.4	Keratin, type II cytoskeletal 6B	Cytoskeletal signalling
Q6P3W2	0.0364	2.5	DnaJ homolog subfamily C member 24	Stimulates ATPase activity
Q96AC1	0.0167	2.6	Fermitin family homolog 2	Membrane scaffolding protein
Q03135	0.0277	3.2	Caveolin-1	Caveolar membrane scaffold protein
P35968	0.0356	3.4	Vascular endothelial growth factor receptor 2	Endothelial cell growth factor
P18859	0.0330	3.7	ATP synthase-coupling factor 6, mitochondrial	Catalyses ATP synthesis
Q9H3G5	0.0435	6.6	Probable serine carboxypeptidase CPVL	Serine protease
Q5SQN1	0.0241	45.4	Synaptosomal-associated protein 47	Intracellular membrane fusion
P60033	0.0234	55.8	CD81 antigen	Mediates signal transduction

Table 7.1. **Table listing the 17 proteins significantly differentially expressed between the achievers and non-achievers of pre-surgery oxygen saturation levels.** These 17 proteins were identified due to a fold change greater than 2 and an ANOVA p-value of less than 0.05 between the two groups. Proteins that were elevated in the group that achieved pre-surgery oxygen saturation levels are in blue and the protein elevated in the group that did not achieve pre-surgery oxygen saturation levels are displayed in red. Although ANOVA p-value <0.05 is not a suitable measure to identify significance here because of multiple testing and the fact that we identified ~5000 proteins, it was just used as an aid to identify the strongest protein candidates. Further mass spectrometry data can be found in appendix 12.8.

There is little literature detailing the roles of CWF19-like protein 2, brain-enriched guanylate kinase-associated protein and synaptosomal-associated protein 47 apart from association with catalytic activity, kinase activity and intracellular membrane fusion, respectively as detailed in Table 7.1. Elongation factor Tu GTP-binding domain-containing protein 1 is involved in cytoplasmic maturation of ribosomes and is mutated in Shwachman-Diamond syndrome[301], an autosomal recessive condition presenting in childhood with symptoms of bone marrow dysfunction, pancreatic insufficiency and growth abnormalities[302]. Tripartate motif-containing protein 72 binds phosphatidylserine and is a muscle-specific membrane repair protein. It is activated by intracellular ROS that penetrates damaged membranes from the extracellular environment[303]. Redox-regulatory protein FAM213A is an antioxidant that may be involved with bone maintenance, it is of relevance to this project because it has been described as enhanced in populations adapted to living at high altitude[304], our results concur with the study that a greater amount of this proteins is present in those who were able to achieve their post-operative oxygen saturation levels compared with those who did not. Septin-6 is a member of the family of guanosine triphosphatases which are required for cytokinesis and organisation of the cell cytoskeleton. Tyrosine-protein kinase Blk is involved in cell proliferation and differentiation particularly in B-cells, it is also associated with insulin synthesis and secretion. MAP/microtubule affinity-regulating kinase 3 is activated by phosphorylation and acts to phosphorylate microtubule-associated proteins (MAPs) and is involved in signalling and immune regulation. Type II cytoskeletal keratins are arranged in chains and expressed during epithelial

differentiation, there is high homology between the sub-proteins of this group. DnaJ homolog subfamily C member 24 is a histone protein which stimulates adenosine triphosphatase activity of chaperone proteins and in turn enhances iron binding which acts as an electron carrier. Fermintin family homolog 2 is a scaffolding protein that binds to phospholipid membranes. Caveolin-1 is another scaffolding protein, the main component of the caveolae plasma membrane (a lipid raft invagination of the cell membrane) and promotes cell cycle progression[305]. Vascular endothelial growth factor receptor 2 is a growth factor for endothelial cells that regulates angiogenesis and vascular proliferation, it is associated with a range of diseases such as rheumatoid arthritis[306], wound healing[307] and erythroderma[308]. It plays a role in restoring oxygen flow to tissues during hypoxia so it is surprising to note that it is upregulated in the patients that did not achieve their post-operative oxygen saturation levels. Mitochondrial ATP synthase-coupling factor 6, is involved in the process of generating adenosine triphosphate (ATP) from adenosine diphosphate via the transfer of protons across the inner membrane of the mitochondria. Probable serine carboxypeptidase CPVL is a protease that acts to cleave amino acid residues from the carboxyl-terminus of proteins. Finally CD81 antigen is a transmembrane, cell surface protein of B- and T-cells that mediates signal transduction, it has also been associated with diseases such as cancer[309], sclerosis[309] and hepatitis C virus[310]. The largest group of proteins in Table 7.1 are associated with enzyme activity and secondly proteins associated with signalling pathways. Using online tools this dataset was further interrogated to identify relationships and similarities between the proteins identified.

7.5.1 Using pathway analysis tools to understand the relationships between these proteins

Webgestalt (http://bioinfo.vanderbilt.edu/webgestalt/) was used to identify specific roles and interactions between the proteins in Table 7.1.

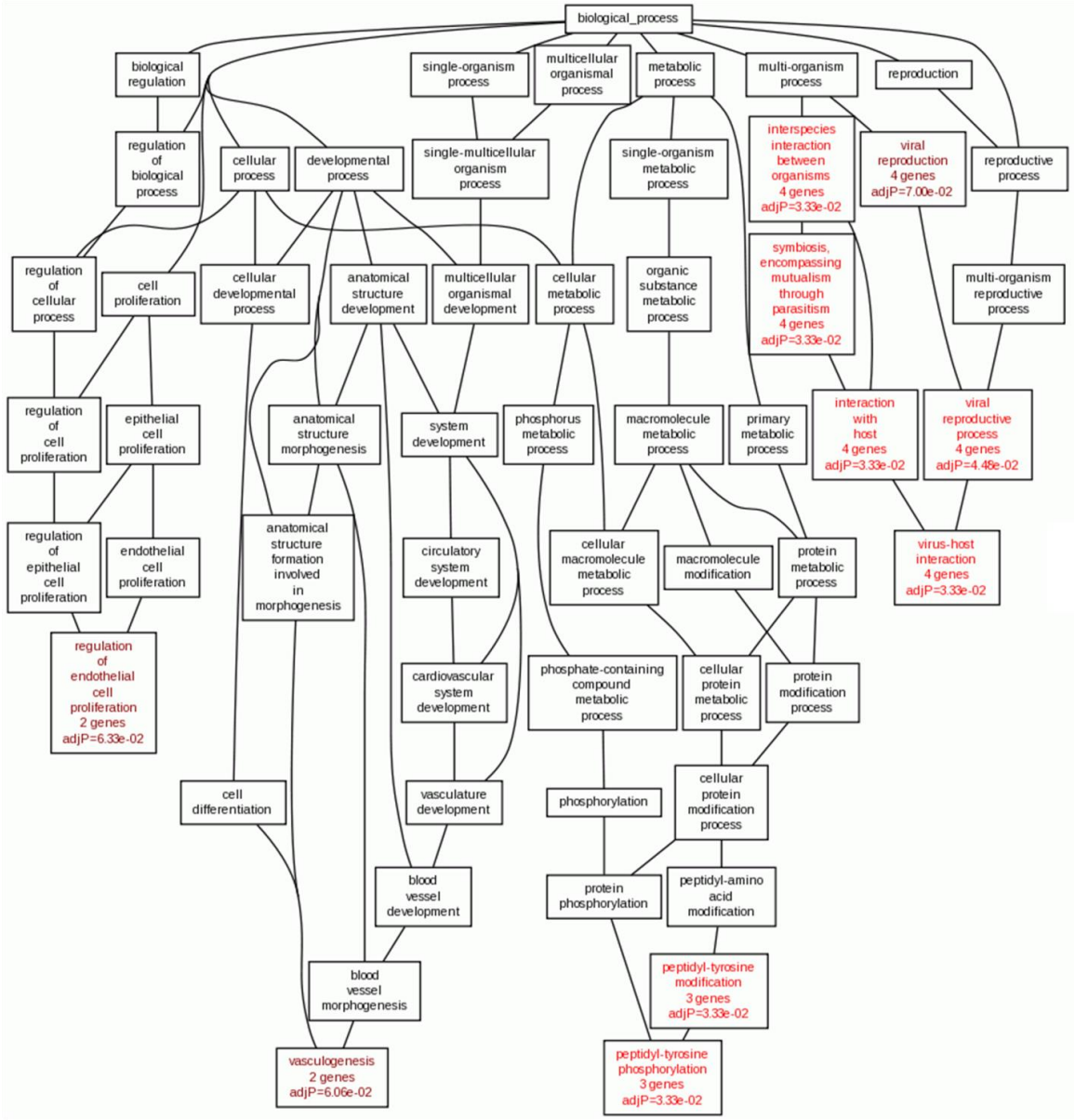

Figure 7.1. **Flow chart showing the biological processes for the proteins in Table 7.1.** Flow chart generated using Webgestalt (http://bioinfo.vanderbilt.edu/webgestalt/).

Figure 7.1 highlights the biological processes represented by the proteins which were significantly differentially expressed in the pre-operative skin biopsy samples of patients that achieved and did not achieve their target oxygen saturation levels post-surgery. On the left of Figure 7.1 there are links to regulatory processes, this is unsurprising as oxygen is key for respiration and in turn providing energy for biological processes. When patients are not achieving their post-operative oxygen saturation target levels it would be understandable that oxygen-related regulatory processes would be affected. Similarly, developmental processes, such as epidermal cell proliferation and differentiation. There is also a circulatory and blood vessel development section, this could be due to a reduced ability to form vascular networks. There is an inflammatory component to Figure 7.1, it could be that patients who do not achieve their oxygen saturation target levels are more susceptible to infection or the reverse could be

true and patients who have an underlying inflammatory response are less likely to achieve their oxygen saturation target levels. Finally, evidence of differences in protein modification has been identified.

IMPaLA (http://impala.molgen.mpg.de/) is an on line pathway-based tool designed to analyse sets of genes/proteins using information compiled from a range of other databases[311]. From the list of proteins in Table 7.1 IMPaLA generated a list of pathways which have been described previously as being associated with the listed proteins:

pathway name	pathway source	overlapping genes	all genes	P_{genes}	Q_{genes}
vegf hypoxia and angiogenesis	BioCarta	2	30 (31)	0.000275	0.673
Focal Adhesion	Wikipathways	3	184 (184)	0.000398	0.673
actions of nitric oxide in the heart	BioCarta	2	42 (43)	0.000541	0.673
Vatalanib Action Pathway	SMPDB	1	1 (1)	0.000848	0.673
Signaling events mediated by PTP1B	PID	2	53 (55)	0.000861	0.673
Signaling events mediated by VEGFR1 and VEGFR2	PID	2	68 (75)	0.00141	0.92
Bacterial invasion of epithelial cells - Homo sapiens (human)	KEGG	2	76 (76)	0.00176	0.984

Table 7.2. **Table showing the top 7 pathways associated with the proteins in Table 7.1.** This table lists pathways associated with the proteins in Table 7.1 which were significantly differentially expressed between the two groups of patients: those that achieved and those that did not achieve their oxygen saturation target levels.

The most significant of these pathways is 'vegf hypoxia and angiogenesis', vascular endothelial growth factor (VEGF) is a growth factor that is involved in restoring oxygen supply to tissues during hypoxia by promoting growth of blood vessels. There are two proteins from Table 7.1 that indicate involvement in this pathway they are caveolin-1 and VEGF receptor 2. Both were overexpressed in patients that did not achieve their oxygen saturation target levels. This suggests that those patients may actually already be in a slight state of hypoxia rendering them less able to reach their pre-surgery oxygen saturation levels.

7.5.2 Modified protein validation in the sample analysis

Figure 7.1 indicated evidence of differences in protein modification between the two experimental groups. As explained in section 6.6.5, this type of MS data can be interrogated to give information about PTMs. Similarly to chapter 6 , the experimental fraction with most proteins was selected to assess changes in PTMs, in this case it was the second fraction (section 6.6.5).

Figure 7.2. **Scatter plot illustrating the mean number of carbonylated threonine per peptide.** Scatter plot showing a higher number of carbonylated threonine modifications per peptide ion for the proteins in the pre-surgery sample of patients that achieved their oxygen saturation target levels (blue) compared with the pre-surgery sample for patients that did not achieve their oxygen saturation target levels (purple). This type of analysis does not give statistical significance.

Carbonylation is a form of PTM where amino acid are oxidised by ROS[312] and carbon monoxide is introduced to a threonine residue. As discussed previously, oxidative stress and reactions associated with ROS are not always detrimental as they also play a role in cell signalling[313; 314].

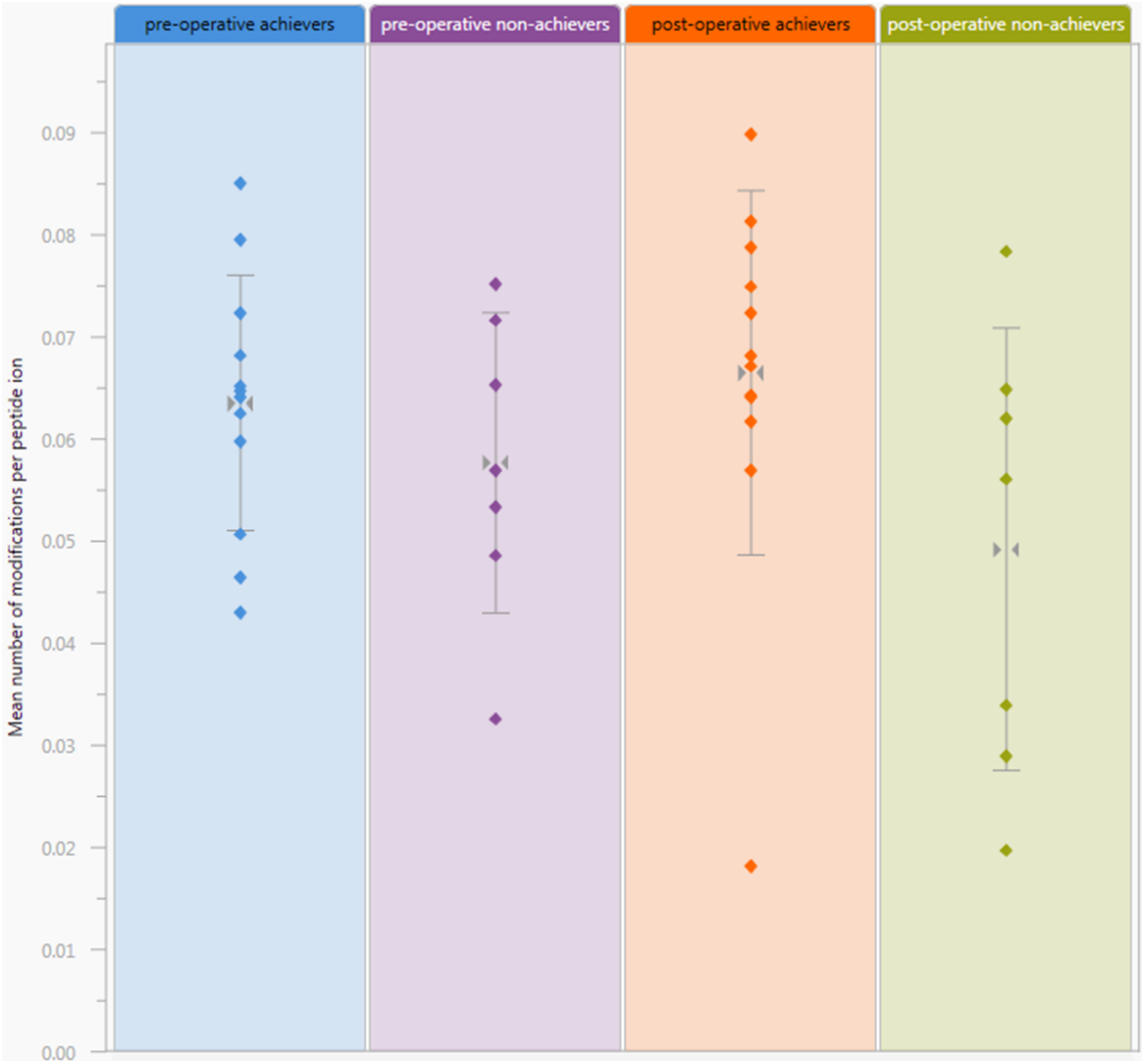

Figure 7.3. **Scatter plot illustrating the mean number of hydroxylated aspartic acid, lysine, asparagine and proline amino acids per peptide.** Scatter plot showing a higher number of hydroxyl modifications per peptide ion for the proteins in the pre-surgery sample of patients who achieved their oxygen saturation target levels (blue) compared with pre-surgery samples of patients that did not achieve their oxygen saturation target levels (purple). This type of analysis does not give statistical significance.

Hydroxylation is when a hydroxyl group (-OH) is introduced to an amino acid residue, to regulate gene expression[315]. Protein hydroxylation has been associated with cancer and poor prognosis[316]. However, the results here suggest the opposite – increased hydroxylation is indicated in the patients that achieved their target oxygenation levels compared with the group that did not.

Figure 7.4. **Scatter plot illustrating the mean number of methylated amino acid residues per peptide.** Scatter plot showing a higher number of methyl modifications per peptide ion for the proteins in the pre-surgery sample of patients that achieved their target oxygen saturation levels (blue) compared with the pre-surgery sample of patients that did not (purple). This type of analysis does not give statistical significance.

As explained in section 6.6.5 methylation of proteins is controlled by methyl transferases and demethyltransferases. Similarly to hydroxylation, methylation is a signalling state used for gene expression regulation within tissues.[264] Figure 7.4 shows a similar pattern to Figure 7.3; higher levels of protein methylation in the patients who achieved their target oxygenation levels compared with the patients that did not.

7.5.3 Summary of investigating the effects of post-operative oxygen saturation levels

In summary the results in section 7.5 show that the proteins differentially expressed between the patients who achieved their target oxygen saturation levels and those that did not are

predominantly enzymatic and signalling proteins, specifically, regulation of cell proliferation, circulatory development and viral interactions, illustrated in Figure 7.1. The PTM study indicated an increase in modified peptides in the group of patients who achieved their target oxygenation levels compared with those that did not. This was true specifically for threonine carbonylation, methylation and hydroxylation, suggesting changes in cell signalling and gene expression in the group of patients that did not go on to achieve their target oxygen saturation levels.

7.6 Proteomic investigations to assess post-operative patient clinical outcomes

Post-surgery patients were monitored and assessed for post-operative morbidity. The Clavien-Dindo (CD) classification system is designed to assess the extent of intervention required post-operatively for surgical complications. It is a scale that runs from grade I to grade V, where grade I represents minor complications and grade V is patient mortality as a result of post-operative complications. This cohort of patients were assessed on post-operative day 2 and classified into two groups: CD grade <2 and CD grade ≥2. A summary of the clinical information for these samples is shown in Table 7.3

	CD<2	CD≥2
Pre-operative		
Age (years)	66±6	69±5
Male (n, %)	7 (78%)	6 (55%)
Body mass index ($kg.m^{-2}$)	30.0±3.9	27.2±2.8
Haemoglobin ($g.L^{-1}$)	135±17	129±19
Diabetes mellitus (n, %)	2 (21%)	1 (27%)
Cardiovascular disease (n, %)	9 (20%)	7 (29%)
Intra-operative		
Duration (mins)	269±114	290±70
Lactate at end of op ($mmol.L^{-1}$)	1.9±1.3	2.3±1.0
Postoperative		
Oxygen delivery achieved (n, %)	8 (89%)	5 (45%)
Surgical wound infection (n, %)	2 (89%)	3 (45%)
Sepsis (n, %)	5 (56%)	9 (80%)

Table 7.3. **Baseline patient characteristics for CD<2 and CD≥2.** Data presented as mean (SD), or n (%). % patients/group provided within each complication category.

Pre-surgery biopsies were analysed using Progenesis QI for proteomics (Nonlinear Dynamics) to assess for pre-operative biochemical indications that a patient may require post-operative interventions as a result of surgical complications. The analysis revealed 47 proteins were significantly differentially expressed between the CD <2 and the CD ≤2 groups with a fold change of greater than two and are listed in Table 7.4:

Protein Accession	ANOVA (p-value)	Maximum Fold Change	Protein Full Name	Protein Description
Q29960	0.00502	205.5	HLA class I histocompatibility antigen, Cw-16 alpha chain	Peptide presentation to immune system
Q15019	0.00763	45.4	Septin-2	GTPase
A6NNZ2	0.00721	38.1	Tubulin beta-8 chain-like protein LOC260334	Constituent of microtubules
Q9NR30	0.03653	24.6	Nucleolar RNA helicase 2	RNA helicase
Q13561	0.03865	15.7	Dynactin subunit 2	Binds to microtubules and dynein
Q96MM6	0.02799	15.5	Heat shock 70 kDa protein 12B	Response to heat shock
P60903	0.00333	12.4	Protein S100-A10	Regulation of cellular processes
P11413	0.02505	11.5	Glucose-6-phosphate 1-dehydrogenase	Enzyme producing NADPH
O75083	0.04586	6.4	WD repeat-containing protein 1	Disassembly of actin filaments
Q9NZN3	0.00207	5.8	EH domain-containing protein 3	Controls membrane reorganisation
P61604	0.02986	5.7	10 kDa heat shock protein, mitochondrial	Chaperonin
P10721	0.03171	5.1	Mast/stem cell growth factor receptor Kit	Tyrosine-protein kinase
Q15751	0.02800	5.0	Probable E3 ubiquitin-protein ligase HERC1	Membrane transport processes
Q96AX2	0.04342	4.7	Ras-related protein Rab-37	GTPase
Q9NVA2	0.02440	4.3	Septin-11	Filament-forming GTPase
H7BZ55	0.00525	4.2	Putative ciliary rootlet coiled-coil protein-like 3 protein	Involved in mitosis
P49419	0.01810	4.0	Alpha-aminoadipic semialdehyde dehydrogenase	Detoxification of aldehydes
P68871	0.03064	3.6	Hemoglobin subunit beta	Oxygen and iron binding
O60240	0.02075	3.5	Perilipin-1	Coats lipid storage droplets
P07476	0.00327	3.4	Involucrin	Part of keratinocyte envelope
Q9P2J3	0.02985	3.4	Kelch-like protein 9	Mitotic progression and cytokinesis
P25311	0.04823	3.3	Zinc-alpha-2-glycoprotein	Transport and binding
Q5VTR2	0.02421	2.8	E3 ubiquitin-protein ligase BRE1A	Regulates chromosome structure
Q13228	0.03472	2.7	Selenium-binding protein 1	Ubiquitination/deubiquitination
P00915	0.04038	2.6	Carbonic anhydrase 1	Catalyse hydration of carbon dioxide
P69891	0.00816	2.6	Hemoglobin subunit gamma-1	Oxygen and iron binding
P31948	0.01867	2.4	Stress-induced-phosphoprotein 1	Adaptor protein
P39019	0.00622	2.4	40S ribosomal protein S19	RNA processing
Q00610	0.04951	2.4	Clathrin heavy chain 1	Intracellular trafficking
P32119	0.03136	2.3	Peroxiredoxin-2	Antioxidant enzyme
P04040	0.01111	2.2	Catalase	Antioxidant enzyme
Q8NCM8	0.01132	2.1	Cytoplasmic dynein 2 heavy chain 1	Transport in cilium
P32926	0.03068	2.3	Desmoglein-3	Calcium-binding cell-cell junction
P16070	0.01762	2.5	CD44 antigen	Cell surface glycoprotein
Q03135	0.03293	2.5	Caveolin-1	Scafold protein in caveolar membranes
Q13418	0.00689	2.5	Integrin-linked protein kinase	Regulates signal transduction
P78527	0.00561	2.7	DNA-dependent protein kinase catalytic subunit	Serine/threonine protein kinase
Q8IZD2	0.00827	2.7	Histone-lysine N-methyltransferase 2E	Methylation of histone proteins
P00352	0.00021	2.7	Retinal dehydrogenase 1	Aldehyde dehydrogenase
Q14141	0.00551	2.8	Septin-6	GTPase
Q6ZQQ6	0.00563	3.0	WD repeat-containing protein 87	Binding activity
Q96M02	0.00110	3.2	Centrosomal protein C10orf90	Histone deacetylase binding
Q9NZM1	0.04435	3.8	Myoferlin	Plasma membrane protein
P35968	0.00024	5.0	Vascular endothelial growth factor receptor 2	Endothelial cell growth factor
P14868	0.03443	5.5	Aspartate--tRNA ligase, cytoplasmic	Part of multienzyme complex
P58107	0.00067	5.6	Epiplakin	Cytoskeletal organisation
Q7L576	0.00708	11.3	Cytoplasmic FMR1-interacting protein 1	Protein complex binding

Table 7.4. **Table listing the 47 proteins that were differentially expressed between the CD <2 and the CD ≥2 groups.** Proteins in blue were significantly (ANOVA <0.05) overexpressed (fold change >2) in the CD <2 group of patients. Proteins in red were significantly (ANOVA <0.05) overexpressed (fold change >2) in CD ≥2 group of patients. Further mass spectrometry data can be found in appendices 12.9.

There are a large number of enzymatic proteins represented in this list as well as structural proteins. There is a greater than 200 fold increase in the human leucocyte antigen (HLA) class I histocompatibility antigen, Cw-16 alpha chain protein in the CD <2 group, these patients are

“healthier” in so far as they are not suffering serious post-operative complications as those in the CD ≥2. HLA class I is a heterodimer and the protein component detected here is the alpha chain, this chain is anchored to the membrane whilst presenting peptides to the immune system.

PANTHER (http://pantherdb.org/) was used to generate the pie chart below detailing the classification of the proteins in Table 7.4 according to their molecular function:

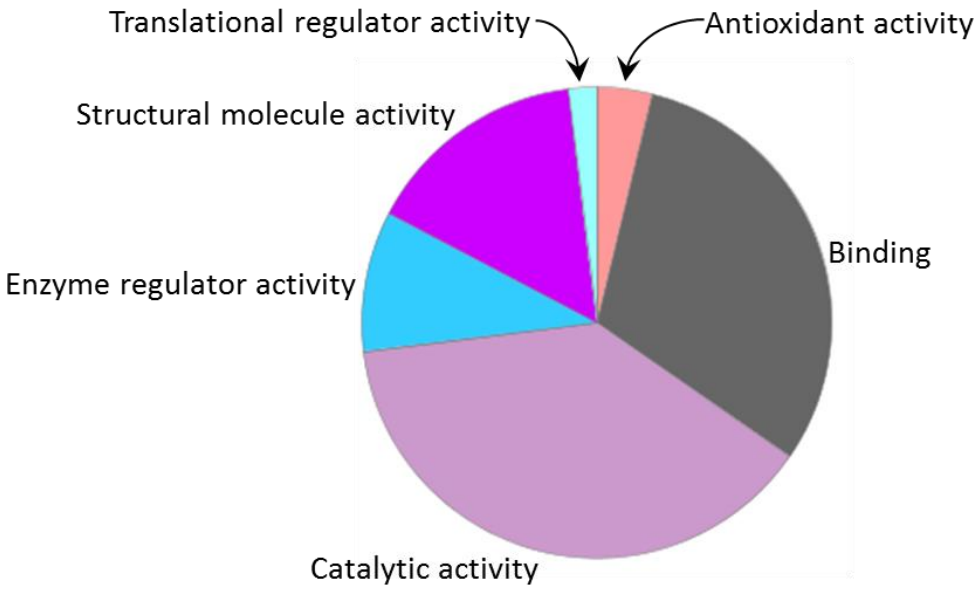

Figure 7.5. **This pie chart illustrates the molecular function of the significantly differentially expressed proteins between the CD <2 and CD ≥2 patients.** This pie chart shows the relative distribution of protein molecular function for the proteins identified as significantly different between CD <2 and CD ≥2 patients.

This pie chart shows most of the proteins in Table 7.4 have either catalytic activity or binding functions. The other four functions represented are enzyme regulator activity, structural molecule activity, translational regulator activity and antioxidant activity. Another way of assessing the data is to determine how protein classes are represented:

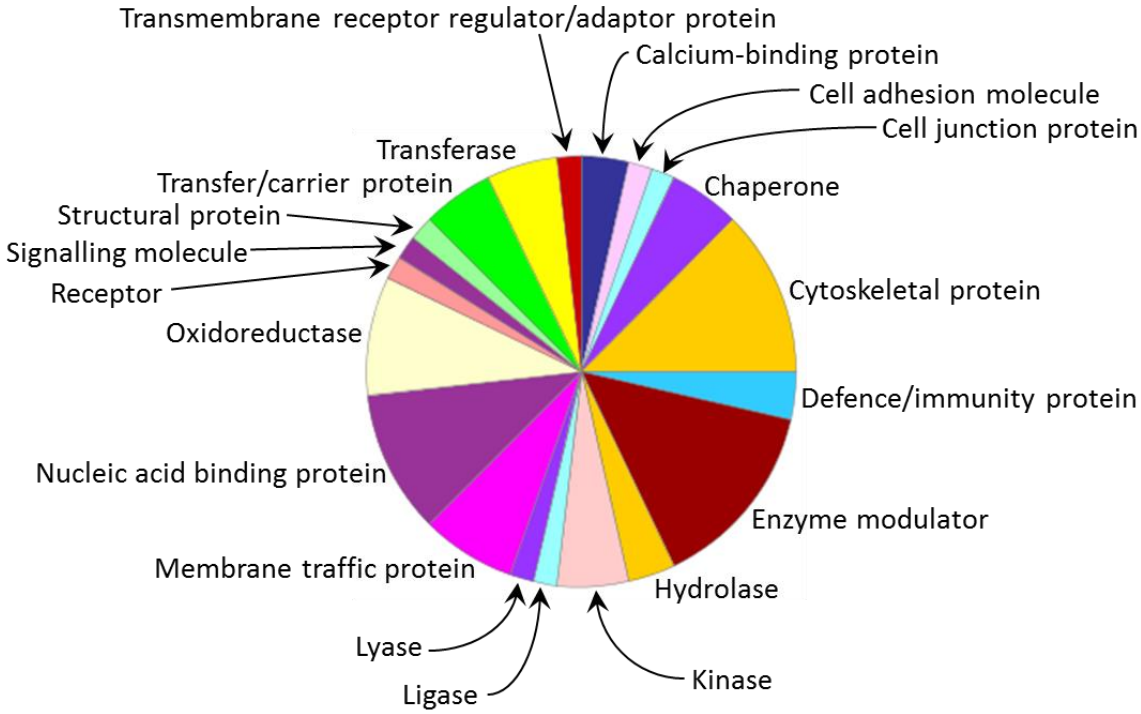

Figure 7.6. **Pie chart illustrating the protein classes represented by the proteins in Table 7.4.** This pie chart shows 20 protein classes that are represented by the proteins in Table 7.4, which were significantly differentially expressed between CD <2 and CD ≥2 patients.

The four most abundant classes from these proteins are enzyme modulators, cytoskeletal proteins, nucleic acid binding proteins and oxidoreductases.

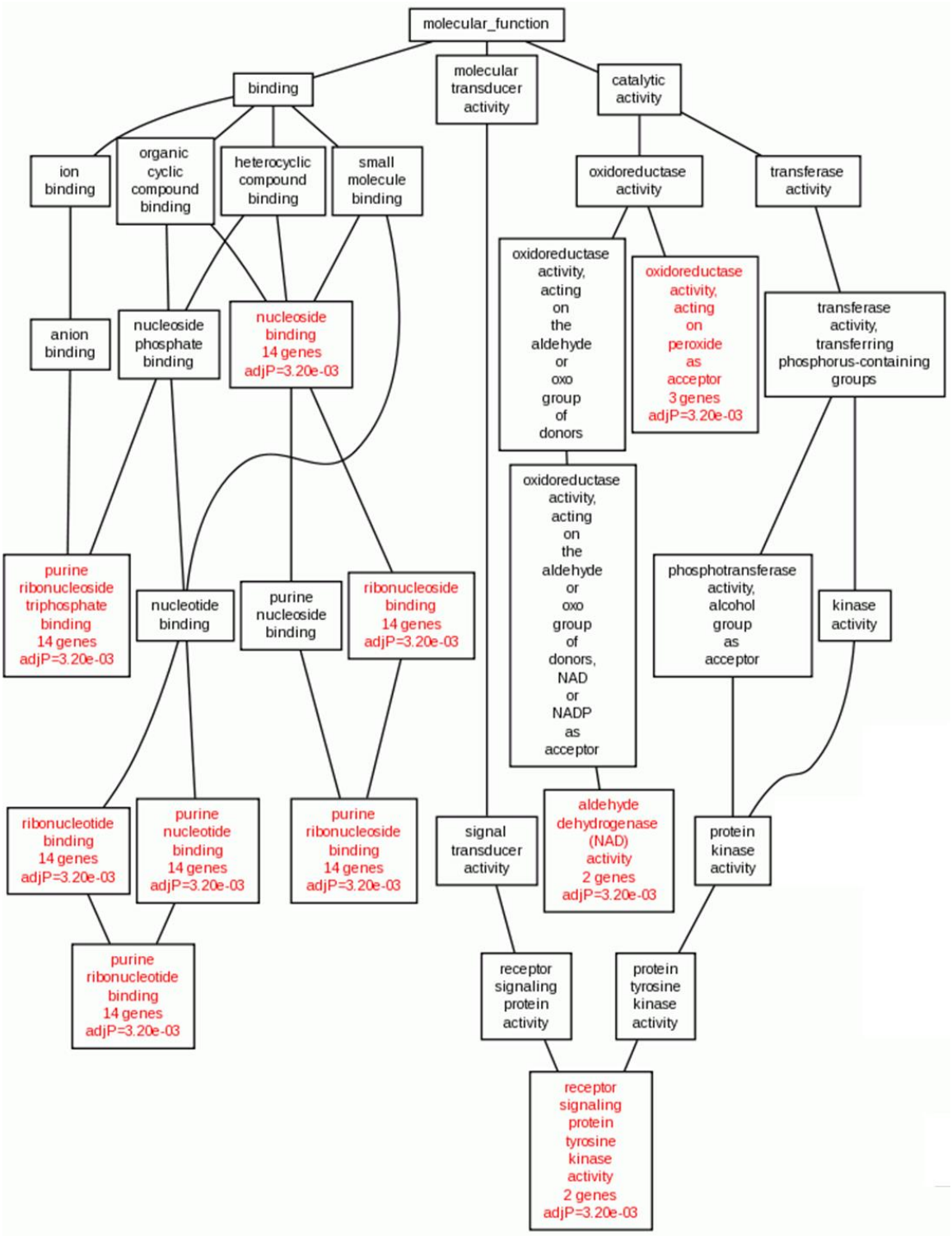

Figure 7.7. **Flow chart representing the molecular function for the proteins in Table 7.4.** Chart generated by Webgestalt (http://bioinfo.vanderbilt.edu/webgestalt/).

Figure 7.7 shows that there is a significant presence of binding proteins in Table 7.4 and oxidoreductase activity. Oxidoreductases as discusses in section 6.6.4 describes a group of enzymes which convert oxygen to ROS, this usually occurs under conditions of oxidative stress.

Reactome (http://www.reactome.org/) gives a visual representation of represented biochemical pathways:

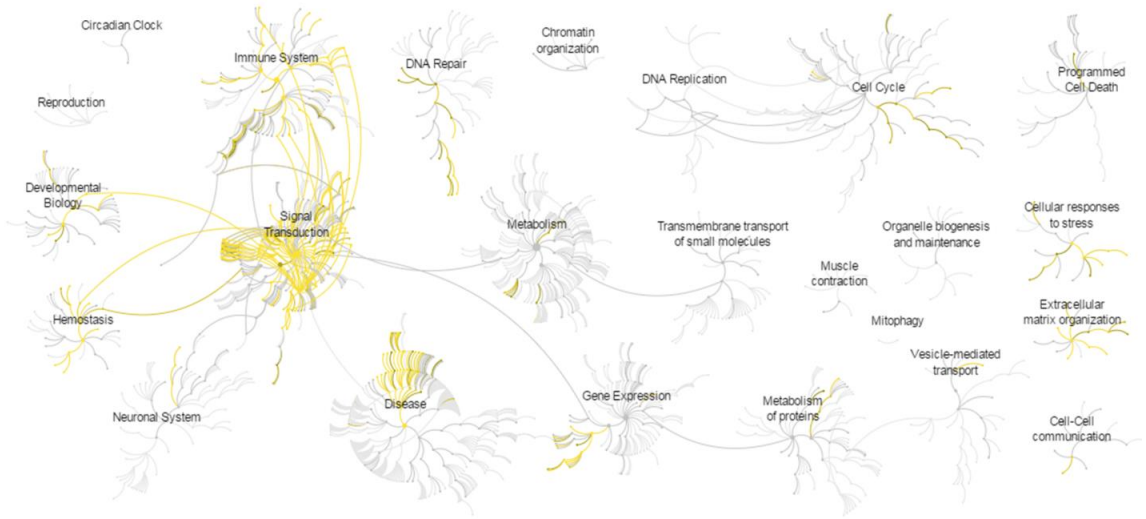

Figure 7.8. **Figure illustrating which pathways are represented by the proteins in Table 7.4.** Figure generated using Reactome highlighting in yellow pathways that are represented by the proteins in Table 7.4.

This figure illustrates the diversity of the pathways covered by the 47 proteins in Table 7.4 and highlights the different extent to which they are represented. Signalling pathways are highlighted as well as immune system, cellular responses to stress and extracellular matrix organisation.

Using the proteins in Table 7.4 and IMPaLA (http://impala.molgen.mpg.de/) the key pathways represented by these proteins were identified as follows:

pathway name	pathway source	overlapping genes	all genes	P_{genes}	Q_{genes}
Bacterial invasion of epithelial cells - Homo sapiens (human)	KEGG	6	76 (76)	2.15e-07	0.000839
Oxidative Stress Regulatory Pathway (Erythrocyte)	PharmGKB	2	7 (7)	0.000246	0.327
Erythrocytes take up carbon dioxide and release oxygen	Reactome	2	9 (9)	0.000419	0.327
O2/CO2 exchange in erythrocytes	Reactome	2	9 (9)	0.000419	0.327
Erythrocytes take up oxygen and release carbon dioxide	Reactome	2	9 (9)	0.000419	0.327
Hormone-sensitive lipase (HSL)-mediated triacylglycerol hydrolysis	Reactome	2	12 (12)	0.000763	0.422
Endocytosis - Homo sapiens (human)	KEGG	5	213 (213)	0.000802	0.422
EGFR1	NetPath	7	456 (471)	0.000865	0.422
Signaling events mediated by VEGFR1 and VEGFR2	PID	3	68 (75)	0.00167	0.682
Pathway_PA165959425	PharmGKB	2	18 (18)	0.00175	0.682

Table 7.5. **The top 10 pathways represented by the proteins in Table 7.4.** Pathways generated by IMPaLA (http://impala.molgen.mpg.de/) and ranked by significance.

Table 7.5 identifies bacterial invasion of epithelial cells as the single most significantly represented pathway by the proteins in Table 7.4, the following four pathways are all related to oxygen either exchange or ROS and oxidative stress. This could suggest that these patients are more susceptible to infection, perhaps they have a slightly weaker immune system.

7.6.1 PTM validation in sample analysis

As discussed in chapter 6 and section 7.5.2 the MS data can be used to interrogate the PTMs. The modification studies here included: Carbonylation of lysine, proline, arginine and threonine, citrullination, deamidation of asparagine and glutamine, methylation, demethylation and trimethylation, nitrosylation of cysteine and tryptophan and finally sulphenylation of cysteine.

Figure 7.9. **Scatter plot illustrating the mean number of citrullinated amino acid residues per peptide.** This indicates a higher number of citrulline modifications per peptide ion for the proteins in the pre-surgery sample of CD <2 patients (blue) compared with CD ≥2 patients (purple), this trend is similar for the post-operative biopsies (orange and green respectively). This type of analysis does not give statistical significance.

Citrullination is a PTM where arginine is converted to citrulline peptidylarginine deiminases[317]. There are different isoforms of peptidylarginine deiminases, depending on their tissue location[318]. Peptidylarginine deiminases 4 has been associated with tumorigenesis and immune function[317]. Despite the fact that patients in this cohort have cancer, there will be differences in

cancer biochemistry meaning that some patients have fewer post-operative complications and therefore differences in citrullination status of their proteins. This figure shows a slight trend for increased citrullination in the CD <2 group.

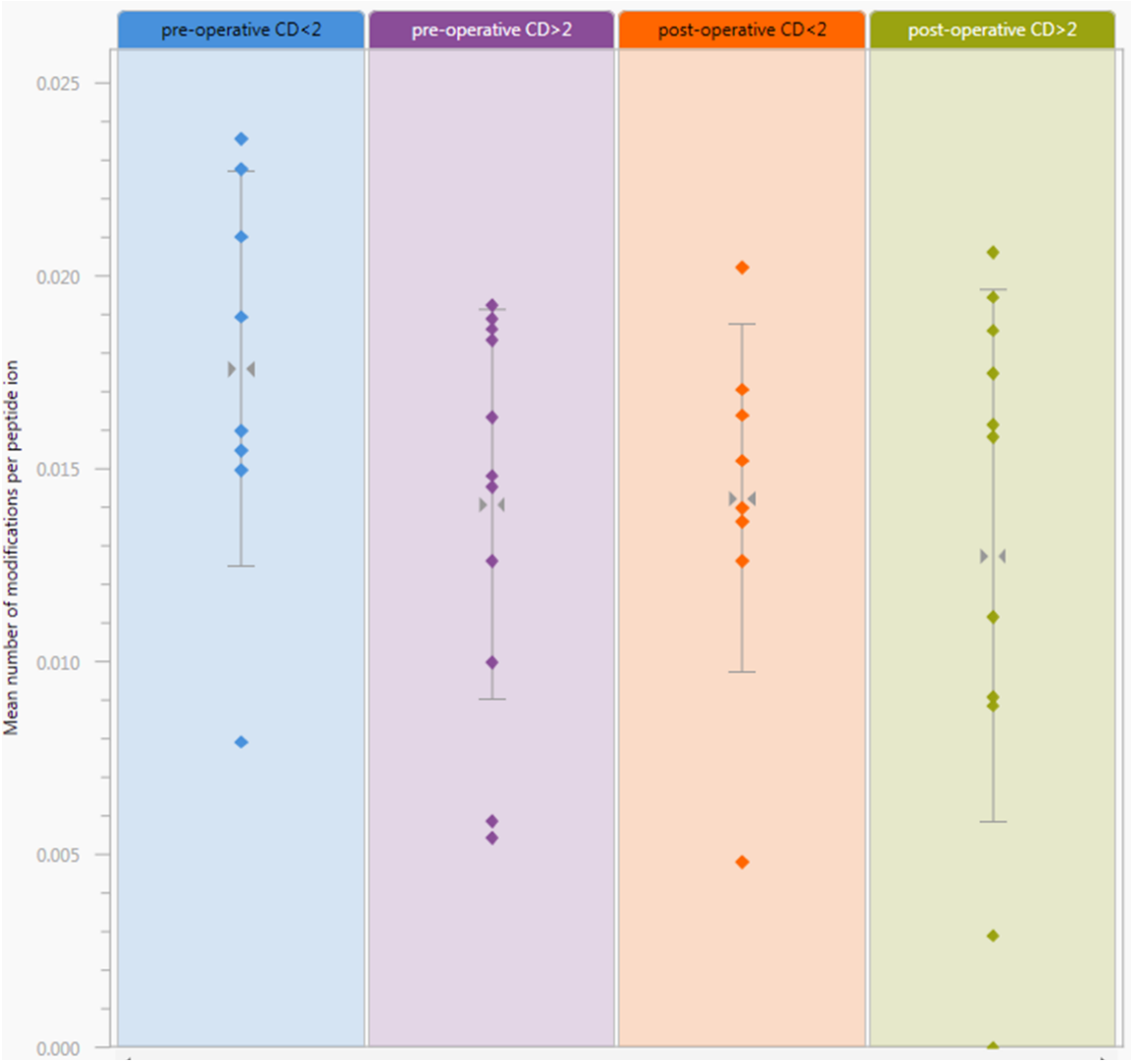

Figure 7.10. **Scatter plot illustrating the mean number of deamidated glutamine amino acid residues per peptide.** This shows a higher number of deamidated glutamine modifications per peptide ion for the proteins in the pre-surgery of CD <2 patients (blue) compared with CD ≥2 patients (purple), this trend is similar for the post-operative biopsies (orange and green respectively). This type of analysis does not give statistical significance.

Figure 7.10 shows changes in glutamine deamidation, this was also observed in Figure 6.17, deamidation is a PTM observed in ageing and age-related conditions[265; 266]. The results shown here could suggest an increased rate of protein turnover in the CD <2 patients compared with the CD ≥2 group. In this case, there is a suggestion that increased protein turnover is protective against post-operative morbidity.

7.6.2 Summary of the findings to investigate post-operative patient clinical outcomes

Our proteomic data revealed 47 proteins that were significantly differentially expressed between the two patient groups (Table 7.4). These proteins comprised enzymatic and structural proteins. Classification and pathway tools highlighted the catalytic, binding (Figure 7.5), cytoskeletal, oxidoreductase (Figure 7.6 and Figure 7.7) and immunological (Figure 7.8) differences. Further studies of PTMs revealed reduced citrullination and arginine deamidation in the CD ≥2 group of patients.

7.7 Biochemical predisposing factors for negative post-operative outcomes in high-risk surgical patients

The aim of this chapter was to biochemically analyse tissue samples from patient undergoing high-risk surgery, to determine factors associated with post-operative morbidity and with a view to using this data to review peri-operative care. This chapter focuses on two aspects: achievement or non-achievement of target oxygen saturation levels and post-operative complications. This was a unique study design designed to broaden our understanding of predictive risks of major surgery. This chapter has identified biochemical hallmarks associated with post-operative recovery.

7.7.1 Discussion of the results pertaining to the achievement of post-operative oxygen saturation levels

Section 7.5 of this chapter was based upon the theory that achievement of target oxygen saturation levels is a major contributing factor to reduction of post-operative morbidity[285; 319]. Thus by determining innate biochemical differences in individuals who did and did not achieve their target oxygen saturation levels, the relationship between post-operative oxygen saturation and morbidity could be probed and studied to identify whether pre-operative indicators of morbidity could be postulated. We identified differences in proteomic and PTM profiles between the two groups of patients (those that did achieve their post-operative oxygen saturation levels and those that did not). Further work is required, however, this work identifies differences in biochemical state between the groups that could be mined to improve patient outcomes.

Many of the proteins identified in Table 7.1 are signalling molecules and associated with cell turnover. Neither class were restricted to upregulation in one group, however the differences do suggest changes in pathways that could account for the observed clinical outcome differences. GA and major surgery are burdens on the body's homeostasis and subtle differences in the

underlying equilibrium would be of no clinical significance in health, but post-surgery may culminate in this divergence of clinical outcome. The focus of this section was tissue oxygen perfusion post-surgery, in order to quicken recovery of body tissues it is important that cells are able to regenerate quickly enough in the event of hypoxia, this could be why cell regeneration and proliferation capacities are shown to be different here.

Table 7.2 shows the pathways identified as being differentially expressed between the two groups. This table also suggests that hypoxia plays a key role. The PTM work (Figure 7.2, Figure 7.3 and Figure 7.4) shows an increase in modified peptides in the group of patients that did achieve their target oxygen saturation levels. The key PTMs shown were: carbonylation (Figure 7.2), hydroxylation (Figure 7.3) and methylation (Figure 7.4). Both carbonylation and hydroxylation are associated with oxidative stress and ROS, whilst hydroxylation and methylation regulate gene expression within the cell. Oxidative stress is largely reported as having negative effects pertaining to modifications of biological compounds, too little ROS can also have negative effects as suggested here.

Overall section 7.5 demonstrates biological differences between patients who achieve their target oxygen saturation levels and those that do not, with further work this data could be used to better manage peri-operative oxygen delivery.

7.7.2 Discussion of the results pertaining to post-operative morbidity

The second part of this chapter (section 7.6) probed other reasons for post-operative morbidity. Using the Clavien-Dindo classification system patients were assessed on post-surgery day 2 according to post-operative complications requiring intervention. Those classified as CD≥2 were suffered post-operative complications of a severe nature. The aim was to identify predisposing biochemical indicators of post-operative morbidity that could be used in the future as aids to reduce post-operative morbidity through patient-centred peri-operative management.

Forty-seven proteins were identified as significantly differentially expressed between the two groups of patients, listed in Table 7.4. Figure 7.5 shows the majority of those proteins were catalytic or binding proteins. There was also an oxidative stress component to the list of proteins, a common theme to both sections of this chapter. The PTM analysis identified more protein citrullination and deamidation in the CD <2 group. These modifications mimic previous findings of decreased cell turn-over and gene expression control in the CD ≥2 group, this could perhaps be due to reduced oxygenation of the cell.

Post-operative morbidity as described in this section is highly complex. Morbidity in this case can arise from infection, hypoxia, organ failure or co-morbidities. Not all patients in this cohort developed the same post-operative complication, some may have had multiple. The multi-faceted nature of post-operative morbidity renders the drawing a single conclusion for the cause near impossible. However, despite the overwhelming complexity of this topic there are some key features that have been brought to light whilst studying CD <2 and CD ≥2 patients. Most noteworthy being pathways pertaining to oxidative stress, regulation of gene expression and cell proliferation.

7.8 Conclusions

This chapter illustrates pathways and differences in the underlying biochemistry between groups of patients with different peri-operative outcomes. This work highlights the opportunity to pre-operatively assess patients in the future to predict surgical outcome and in turn appropriately modify treatment and management to reduce peri-operative morbidity. A combination of mass spectrometry-based proteomic techniques have been implemented to assess skin-based tissue responses to the impact of high-risk major surgery.

7.9 Further work

There is still considerable work required before conclusive results can be used to improve patient outcomes post-major surgery, however this chapter presents early evidence suggesting clear pre-operative indications of differences between patient groups linked to likelihood of reducing post-operative morbidity. In order to continue this work effectively it would be of merit to pursue the oxidative stress and gene regulation pathways. To identify whether there are environmental factors contributing to these differences and whether there are interventions that can safely be implemented in those patients that have lower levels of oxidative stress or gene regulation.

Chapter 8

Discussion

8 Discussion

Contents

The aims of this thesis were to validate protein biomarker expression in the skin of patients with atopic eczema (AE), to study the role of proteases and protease inhibitors as potential disease mechanisms in the skin, to develop methods to analyse protein expression in the skin and to apply these methods to disease. Chapters 3 to 7 present the major results from these investigations alongside discussions and conclusions pertaining to those specific chapters. This chapter will further expand on those results, find links between chapters and present the results in the wider context of theoretical and practical implications.

8.1 Validation of protein biomarkers in AE

The aim of chapter 3 was to use proteomic techniques to investigate roles of AE protein biomarkers in the skin. Biomarkers were identified using mass spectrometry (MS^E) (method 10.2.4) and literature searches. Immunohistochemistry was used to stain for proteins in health, AE and ichthyosis. The most striking staining difference was identified in CLP5 (Figure 3.7), where clear accumulation of CLP5 in the uppermost epidermal layer was observed in health and a sparser distribution in AE throughout the epidermis. CLP5 was shown to be a marker of keratinocyte differentiation in the skin and indicated that there could be disruption of the calcium ion gradient in AE contributing to poor trafficking of proteins required for correct keratinocyte differentiation and skin barrier maintenance.

In the introduction (chapter 1) challenges of managing diseases such as AE for the patient and the health service provider were discussed. There is no cure, nor known cause for AE this disease continues to be a social and financial burden. It is important to investigate and research the underlying disease mechanism and biochemical changes to contribute towards improved understanding of AE, why it is so common and in turn identify better treatment and care options for patients.

8.2 Alpha-1-acid glycoprotein (AGP), AE and the inflammatory response

The initial MS findings identified AGP expression in skin scrapings of AE patients as increased 14-fold compared with controls (Table 3.1). As detailed in section 3.5.1, AGP is a highly glycosylated, acute phase protein with anti-inflammatory and immunomodulatory properties[67]. Figure 3.1 shows images of AGP IHC staining in control, AE and ichthyosis. In controls staining was restricted to the cytoplasm and most pronounced in the stratum basale, in AE the staining was strongest in the nuclei of undifferentiated keratinocytes in the epidermis, throughout the epidermis. In ichthyosis staining more closely resembled the pattern observed in AE rather than controls, dark staining of keratinocyte nuclei throughout the epidermis with the exception of the stratum corneum. There is little literature concerning the localisation of AGP within cells and

even less within epithelial cells. However, it has been documented that nuclear AGP is increased during inflammation in rat livers. To produce more AGP, DNA in the nucleus will be translated to protein. Perhaps the increased staining peri-nucleus is not representing AGP within the nucleus, but AGP translation in AE and ichthyosis, surrounding the nucleus. AE is an inflammatory disease and both AE and ichthyosis present uncomfortable skin lesions which may be itchy of uncomfortable, scratching these lesions would illicit an immune response, in the absence of an increased baseline immunological activity in AE or ichthyosis.

AGP has not been linked with AE previously, this could be because AGP is an acute phase protein and due to the immunological aspect of AE it may not be surprising to see changes in its expression. However, the role of acute phase proteins has been documented in other diseases: heart disease[320], infectious disease[321] and cancer[322], but not AE. The glycosylation start of acute phase proteins is important in other inflammatory diseases[323], but not specifically AE. The results presented in section 3.5.1 indicate a role of acute phase proteins and more specifically AGP in AE that has perhaps been overlooked.

8.2.1 Calmodulin-like proteins and the calcium ion gradient in the skin

Chapter 3 also detailed results from the calmodulin-like group of proteins, more specifically CLP3 and CLP5. Initial MS results showed a respective decreased expression in the AE samples compared with controls of 16 and 3-fold (Table 3.1). Sections 3.5.3 and 3.5.4 present the IHC staining results for both these proteins (Figure 3.5 and Figure 3.7), CLP3 and CLP5 staining was similar, most pronounced differences were observed for CLP5. Dark condensed CLP5 staining was observed in controls in the stratum corneum, however, the staining was far more diffuse in AE with continued staining in the deeper epidermal layers. Ichthyosis staining was not confined to the stratum corneum either and there was staining in deeper epidermal layers.

CLP3 has not been described associated with AE. CLP5, however, has been associated with AE once. The study documents the discovery of protein biomarkers from the vernix (fluid covering the baby's body at birth) and compared the protein profile of children who developed AE at 2 years and those that did not. They quantified 203 proteins by LC-MS/MS and identified CLP5 and polyubiquitin-C as predictive markers of AE from the vernix.[324] Vernix is produced by sebaceous glands as well as being contributed to by squamous cells[325]. If we assume that CLP5 in the vernix comes from squamous cells of the upper epidermis this supports our findings that there is more CLP5 at the surface of the epidermis in health compared with AE. Together these pieces of research support each other illustrating that CLP5 has role in AE that can be determined at birth. This is of great importance as it shows innate biochemical differences in the

skin of children who are predisposed to develop AE. It illustrates that for some people the post-natal environment is not a sole contributing factor to AE susceptibility.

To use this knowledge to contribute towards understanding of AE disease mechanism and in turn provide better disease management and treatment we investigated other roles for CLP5 by studying proteins interactions in the skin (Table 3.2). These results highlighted the importance of CLP5 in skin as it interacts with a protease and two protease inhibitors (caspase-14, alpha-1-antitrypsin and serpin B5, respectively) and antimicrobial proteins (dermcidin, glyceraldehydr-3-phosphate dehydrogenase and galectin-3). In health we propose these proteins are required to travel together towards the stratum corneum to carry out their function. Near the surface of the skin is where antimicrobial proteins are required to control microbial infiltration and protease-protease inhibitor interactions are fundamental for normal desquamation of the skin. We hypothesise that the Ca^{2+} gradient across the epidermis encourages this movement of proteins towards the surface. The Ca^{2+} concentration is lowest in the basal layer and highest in the stratum corneum. Disturbances in the epidermal Ca^{2+} gradient been identified in other diseases such as psoriasis[326]. When the skin barrier is not maintained the Ca^{2+} gradient may not be maintained[327], also high Ca^{2+} concentrations in the stratum corneum initiates skin barrier recovery[328]. These two discoveries appear to be contradictory and perhaps highlight the uncertainty surrounding the extent to which the Ca^{2+} gradient maintains the skin barrier or whether the skin barrier maintains the Ca^{2+} gradient within the epidermis. The main role of the Ca^{2+} gradient is to initiate keratinocyte differentiation. Maturation of keratinocytes in AE is disturbed, illustrated in Figure 1.5. Fewer keratinocytes achieve complete differentiation in AE, together this information confirms the Ca^{2+} gradient warrants further interrogation.

8.3 Investigating proteases and protease inhibitors in the skin

Chapter 4 aimed to investigate the roles of proteases and proteases inhibitors in the skin and to identify protease-proteases inhibitor relationships that could be utilised for treatment of skin disease. The chapter focused on the use of protein 'bait' arrays to isolate proteins interacting with selected skin protease inhibitors. The most significant finding was that caspase-14 (protease) was identified as interacting with cystatin A and cystatin C (protease inhibitors).

8.3.1 Caspase-14 and the protease inhibitors LEKTI, cystatin A and cystatin C

Caspase-14 has roles in the epidermis including cleavage of filaggrin into monomers by citrullination[97]. Filaggrin is a Ca^{2+}-dependent protein in the skin, caspase-14 is a proteases that cleaves profilaggrin[95]. The staining work presented in chapter 3 showed minor differences in caspase-14 staining between controls and eczema samples (Figure 3.9). The staining illustrated

the protein distribution, however, does not account for caspase-14 activity. Caspase-14 is a binding partner for the protease inhibitor LEKTI in the skin[57] and this thesis shows its role as a binding partner for cystatin A and cystatin C (Table 4.5 and Table 4.6, respectively). This highlights the role that caspase-14 plays in correct differentiation and maturation of the skin barrier. There is currently no literature linking caspase-14 to either cystatin A or cystatin C[329].

No mutations in caspase-14 have been reported in human skin[330] this could suggest that if caspase-14 is involved in skin disease mechanisms it could mean other upstream proteins are dysregulated instead, similarly to the role of filaggrin in ichthyosis vulgaris and AE. We predict that dysregulation of cystatin A or cystatin C could have a downstream effect on the protease:protease inhibitor ratio with caspase-14. Cystatin A expression in skin keratinocytes is induced by Ca^{2+}[331], we have already described dysregulation of Ca^{2+}-dependent proteins in AE, perhaps there is also cystatin A dysregulation in these patients.

8.4 Optimisation of a sample preparation method for use when analysing skin tissue

In chapter 5 we developed a preparation method for the proteomic analysis of skin tissue, maximising protein solubilisation and incorporating MS analysis. This was achieved and the optimisation steps are presented in chapter 5 . As detailed in the introduction (chapter 1) we predicted skin tissue samples would be challenging to solubilise and analyse by mass spectrometry, due to the presence of many cross-linkage bonds and high lipid content. Despite the hurdles and limitations of analysing such a complex tissue such as skin the method (Figure 5.9) was optimised to achieve maximum protein coverage.

8.4.1 Homogenisation buffers for the solubilisation of skin tissue

Figure 5.5 shows the different number of proteins identified from the same tissue when it was homogenised in seven different homogenisation buffers. From that data we concluded that 50 mM AmBic, pH 7.8, containing 2% w/v ASB-14 solubilised most of the tissue proteins. Despite solubilising most skin proteins compared with the other six buffers, this homogenisation buffer is unlikely to solubilise all of the protein, after step 4 of Figure 5.9 an insolubilised pellet remained. Some of the insoluble matter will be lipids or small molecules, however, undoubtedly some will be insoluble protein matter.

As discussed at the end of chapter 5 proteins in complex tissues such as skin present a range of properties; different sizes, abundance and solubility. The range in solubility makes solubilisation in a single solution challenging. To overcome this we propose the use of more than one homogenisation buffer to accommodate for a wider range of solubilities to increase

protein detection by MS. Protein solubilisation for mass spectrometry has been extensively studied, conventional detergents are often not compatible with mass spectrometers[332]. Despite this, techniques are application-specific, for example using MS-compatible degradable surfactant enriches solubilisation of membrane proteins[333] and gel-separation first enriches for structural proteins[334]. In chapter 5 we designed a method to identify greatest number of different proteins within a sample, instead of enriching certain aspects of the proteome. It is challenging to assess to what extent the whole skin proteome is represented in the proteins we identified using our method detailed in chapter 5 without literature detailing the complete skin proteome. This method was applied to study disease and in chapter 6 it was noted (Figure 6.6) that the majority of proteins detected were intracellular. Proteins within the cell are more heterogeneous than extracellular proteins, however, it might reflect the relative solubilities of proteins in these two environments. Extracellular proteins may be more lipophilic and more extensively modified and cross-linked thus, hindering trypsin digestion.

8.5 Application of the skin preparation method to disease

The final aim of this thesis was to implement the developed sample preparation and MS technique to explore health and disease. Mass spectrometry is a powerful tool for biomarker discovery. We applied these methodologies to two clinical outcomes: hypertrophic scars and post-operative morbidity.

8.5.1 Application of the skin method to hypertrophic scarring

In chapter 6 we identified underlying biochemical differences in unscarred tissue of two distinct paediatric patient groups: those who would form a hypertrophic scar and those that would heal healthily post-surgical incision. We hypothesised that there would be physiological differences between the unscarred skin tissues of these patients. Further investigations could lead to the development of pre-surgical testing to predict scar outcome post-surgery. This precision medicine approach may lead to changes in patient management, such that treatment and management are tailored to the patient's physiology. Presented in chapter 6 are the results of this investigation where we identified protein, PTM and lipid differences in unscarred skin tissue.

8.5.1.1 TGF-ß and susceptibility to hypertrophic scarring

TGF-ß is an established component of skin healing[335], it has been implicated in abnormal wound healing, more specifically, keloid scars, where TGF-ß1 promotes keloid scar formation in fibroblasts[336]. We hypothesised that TGF-ß would be involved in hypertrophic scar formation as well. This hypothesis was supported by other research that identified a decreased expression of TGF-ß in hypertrophic scar fibroblasts[337] and that topical application of a TGF-ß1 inhibitor

improved hypertrophic scar outcomes[338]. No TGF-ß proteins were significantly differentially expressed in our study (Table 6.2), TGF-ß1 was detected but not significantly.

Most published studies investigating TGF-ß in hypertrophic scarring focus on hypertrophic scar cell lines and genetic expression of TGF-ß. The results presented here suggest genetic changes are only relevant to hypertrophic scar tissue itself and that unscarred tissue does not demonstrate the same TGF-ß changes. Perhaps there is an upstream component which initiates the switch between healthy scarring and hypertrophic scarring.

8.5.1.2 Protein expression and susceptibility to hypertrophic scarring

Table 6.2 lists the proteins identified as significantly differentially expressed between unscarred skin samples of patients who either scarred healthily or hypertrophically. This data identified structural, developmental and immunological differences between the tissues of the two groups. There is pre-existing evidence suggestive of structural differences between hypertrophic scars and healthy scars for example there is a structural collagen nodule in hypertrophic scars, not found in healthy scars.[339] There is also interest in the composition and structure of the extracellular matrix in abnormal scars[340]. The developmental component of the proteins identified as differentially expressed suggests that a component of the susceptibility for hypertrophic scar formation could be part of the underlying epidermal development. The epidermis is constantly renewing itself; the stratum basale contains progenitor cells which differentiate into keratinocytes progressing through the layers until they are fully differentiated corneocytes at stratum corneum, to be shed. There could be underlying developmental differences between that in health have no macroscopic clinical significance, yet when the system is traumatised the underlying differences may be exacerbated and lead to pathology. Finally the immunological component: HLA class I histocompatibility antigen, c-type lectin domain family and immunoglobulin gamma-2 were upregulated in the unscarred hypertrophic tissue (Table 6.2). No immunological proteins were upregulated in the control group. Immunological hypersensitivity has been suggestively linked to predisposition to hypertrophic scar formation[250; 341]. The mechanism of this association is unknown and raises queries about whether the observed differences are cause or consequence of the disease, but inflammatory mediators may play a role[342].

The implications of this work is reassurance that pre-operative biochemical differences between the unscarred tissues of individuals prone to develop a hypertrophic scar post-operatively can be detected. There is no conclusive evidence for a single cause, but given the complex nature of scarring it is perhaps unsurprising. However, these results support documented literature and provide insight into changes in unscarred tissue prior to disease. The uncertainty surrounding cause and consequence of changes in hypertrophic scar tissue and healthy scar tissue can be

broken down with study model such as the one used in this thesis. We have observed structural, developmental and immunological changes in unscarred skin samples. These changes therefore cannot be a consequence of hypertrophic scarring because no patients had a history of hypertrophic scarring. We cannot conclude that they are the cause but it is reasonable to eliminate them as sole consequences of the disease.

8.5.1.3 PTMs and susceptibility to post-operative hypertrophic scarring

Section 6.6.5 presents the results of PTM differences in unscarred skin tissue of patients that did and did not develop a post-operative hypertrophic scar. These results indicate increased oxidative stress, gene expression and protein ageing-related PTMs (Figure 6.15, Figure 6.16 and Figure 6.17) in patients that developed hypertrophic scars. Oxidative stress and ROS have been presented relating to cellular responses of fibroblast cells from hypertrophic scar tissue[343]. Gene expression and protein ageing changes could be linked to developmental aspect discussed in section 8.5.1.2 following on from the hypothesis that underlying changes in epidermal development could be exacerbated by trauma. In this case increasing gene expression and as a consequence increased protein degradation could lead to elevated cell turnover in the epidermis of no clinical consequence in health. However, when tissue has been damaged and the wound repair process is initiated, this underlying hyper-proliferation may lead to hypertrophic scar formation. If this is the case, further understanding of the underlying mechanism and causes of hypertrophic scarring will influence prevention, treatment and management in the future.

8.5.2 Application of the developed skin preparation method to post-operative morbidity and peri-operative oxygen delivery

The skin preparation method was applied to another cohort investigating post-operative morbidity and peri-operative oxygen delivery. In chapter 7 we endeavoured to understand more about the biochemistry underlying predisposition for a patient to achieve their target oxygen saturation levels and in turn reduce their chance of suffering post-operative morbidity.

8.5.2.1 Hypoxia and free radical damage associated with peri-operative morbidity

Table 7.1 and Table 7.4 list the proteins identified as significantly differentially expressed in the two experimental cohorts: achievement of target oxygen saturation levels and post-operative morbidity, respectively. These cohorts were analysed separately but are clinically linked, many

studies have investigated the effects of peri-operative oxygen saturation and morbidity. For example low pre-operative cerebral oxygen saturation[344] and discrepancies between central venous oxygen saturation (percentage of oxygen bound to haemoglobin returning to the right side of the heart from the upper body) and mixed venous oxygen saturation (percentage of total oxygen bound to haemoglobin returning to the right side of the heart)[345] have been associated with adverse post-operative outcomes. There is evidence to suggest that peri-operative decline in oxygen saturation is linked to post-operative morbidity such as stroke[346], cognitive decline[347] and organ dysfunction[348], however, the underlying causes of this remains unknown. By analysing these two patient cohorts investigating failure to achieve target oxygen saturation and post-operative morbidity we hoped to identify biochemical and metabolic predispositions to adverse post-operative outcomes.

One result that corroborates published work[344] is that prior to major surgery patients showing biochemical signs of tissue hypoxia are less likely to achieve their target oxygen saturation levels. We conclude that pre-operative hypoxia could reflect differences in basal metabolism. Some individuals will be in a continuous state of slight hypoxia and others a continuous state of slight hyperoxia, dictated by basal metabolic rate. In health these slight differences may be of no clinical significance, however, when under stress such as major surgery this could be exacerbated leading to post-operative morbidity, this theory is supported by findings associated with protein FAM213A, which is positively selected for in populations living at high altitude[304].

Oxidative stress was identified as a mechanism triggering post-operative atrial fibrillation[349; 350] and poor outcomes following coronary artery bypass surgery[351]. We identified indicators of oxidative stress and oxidoreductase activity, specifically a pre-operative increase in antioxidant proteins in the patients that did not develop post-operative morbidity. In a similar patient cohort administration of antioxidants reduced post-operative morbidity[352; 353], they improved immune recovery post-major surgery[352].

If our conclusions are correct we show that hypoxia and oxidative stress are pre-operative markers of post-operative morbidity. There are already approved interventions that could be tested to further understand this hypothesis such as pre-surgical oxygen delivery and the administration of antioxidants.

8.5.2.2 PTMs and peri-operative morbidity

Sections 7.5.2 and 7.6.1 investigate PTMs identified by MS, these results indicated an increase in modifications associated with gene expression, cell signalling and cell turnover. No literature available suggests that these PTMs have been studied with respect to post-operative morbidity. However, these results can be linked to findings discussed in the previous section (8.5.2.1) where hypoxia and oxidative stress were identified as predictive factors for the development of

post-operative morbidity. Carbonylation was identified as more prevalent in the patients that did not develop post-operative complications. Carbonylation is important in cell signalling, more specifically oxidant signalling. Proteins are carbonylated by ROS. ROS is vital for cell signalling, however, excess ROS can lead to damage of proteins, lipids and DNA with catastrophic consequences such as cancer.[354] There was a greater amount of carbonylated protein modifications alongside other cell signalling modifications (hydroxylation and methylation) in patients that did not develop post-operative complications. That would suggest that these modifications or pathways leading to their generation are preventative of peri-operative hypoxia and therefore post-operative morbidity. This knowledge, combined with the identification of increased antioxidant proteins suggests greater amounts of ROS in patients that do not develop post-operative morbidity, but at the same time increased amounts of antioxidant species. This supports the discussion points made in section 8.5.2.1 suggesting that oxidative stress and ROS could be intrinsic components susceptibility to post-operative morbidity.

Chapter 9

Conclusions

9 Conclusions

9.1 Major conclusion of this thesis

This thesis presents the work of a range of mass spectrometry techniques and has applied them to the study of human skin in health and disease. IHC staining of control and AE samples revealed CLP5 as demonstrating a significantly different staining pattern (Figure 3.7). Further investigations into CLP5 revealed its role as a marker of keratinocyte differentiation (section 3.6.2) and highlighted the importance of the Ca^{2+} gradient in the skin for correct transport of proteases, protease inhibitors and antimicrobial proteins. Protein "bait" arrays were used to identify new protease-protease inhibitor relationships that could be targeted for skin disease treatment, similarly to LEKTI and Netherton syndrome. A new relationship between cystatin A and cystatin C and the protease caspase-14 was identified and could be interrogated in skin diseases. Finally, a MS-compatible preparation method for the analysis of full-thickness skin tissue was developed and applied to two different clinical perspectives. Predisposition of paediatric patients to develop a hypertrophic scar post-operatively was investigated, a combination of structural, developmental and immunological aspects were identified. Similar changes have been observed in other studies. This was a novel study design with access to unscarred tissue pre-injury, so findings were able to confirm that differences identified were not a consequence of hypertrophic scar development, but associated with the underlying causes and predisposition to their manifestation. The second clinical outcome assessed was post-operative morbidity post-oesophagectomy in adult patients. In this chapter we identified pre-operative hypoxia, antioxidant levels and ROS as indicators of post-operative morbidity.

9.2 Implications of this thesis for future research

There is still considerable potential for further research into the topics investigated in this thesis. For example, Ca^{2+} gradients in the skin in diseases such as AE would be interesting to study and identify whether Ca^{2+} gradients are one of the underpinning factors contributing to AE and if so, whether that can be applied to treatment to encourage correct development of the epidermal Ca^{2+} gradient. Linked to the Ca^{2+} gradient in the skin was the discovery that caspase-14 interacts with cystatin A, which in keratinocytes is Ca^{2+}-dependent. It would be interesting to investigate the role of cystatin A in AE to identify whether that Ca^{2+}-dependent protein is also dysregulated in the same way as CLP5. Discussed in section 8.4.1 are the limitations of the homogenisation buffer used in the method developed in chapter 5 . Although there no alternatives have the potential to solubilise more proteins, further study and an array of buffers could increase the proteomic coverage. To further develop the work investigating predisposition to hypertrophic scarring targeted MS analysis such as MRM could be used to further scrutinise

the protein markers in Table 6.2. A targeted assay such as that could be used as a pre-operative panel test to assess patients' predisposition to scar hypertrophically. Finally, there is compelling evidence to suggest pre-operative hypoxia and oxidative stress are intrinsically involved in predisposition for post-operative complications following oesophagectomy. Interventions are available and could be implemented in a clinical trial situation to further assess whether pre-operative interventions to increase tissue oxygenation and antioxidant availability are able to reduce post-operative morbidity in susceptible patients identified from analysis of whole skin samples pre operatively.

Chapter 10

Materials and methods

10 Materials and methods

Contents

10.1 Materials

All reagents and materials were purchased from Sigma-Aldrich, Poole, UK, unless stated otherwise. Solvents were of ultrahigh performance liquid chromatography (UPLC) or higher grade specification.

10.2 Methods

Throughout this thesis methods have been altered and optimised, described here are the most recent versions and relevant previous versions will have been described in previous chapters.

10.2.1 Skin samples

Skin samples used in immunohisotchemistry (IHC) staining (chapter 3) were formalin-fixed paraffin-embedded archival samples. Skin samples for MS-based proteomics were excess tissue surgically removed for disposal with no linked clinical information, as stated in the ethics statement thus consent was not required. Research was carried out according to the ethical agreement REC reference: 12/LO/0905, approved by the London – Bloomsbury NRES Committee.[218]

10.2.2 Automated immunohistochemistry (IHC)

IHC was performed using a Leica biosystems BOND-MAX automated immunostainer, 4 µm sections were cut from cold blocks using a microtome (Sakura® Finatek, USA), sections were transferred to glass slides and allowed to dry at 37 °C overnight before being transferred to a 60 °C oven for 1 h. Slides were deparaffinised using Leica Novacastra Bond Dewax Solution. Depending on the antibody a different pre-treatment was used:

Antibody	Purchased from	Dilution factor	Antigen retrieval
alpha-1-acid glycoprotein	abcam®, ab58291	1 in 1000	HIER ER2, 20min
bleomycin hydrolase	santa cruz biotechnology® sc-166777	1 in 500	HIER ER2, 20min
calmodulin-like protein 3	abcam®, ab155130	1 in 250	Enzyme 1, 10min
calmodulin-like protein 5	abcam®, ab122665	1 in 4000	Enzyme 1, 10min
caspase 14	santa cruz biotechnology® sc-48336	1 in 1000	HIER ER1, 10min
cathepsin D	abcam®, ab75852	1 in 500	HIER ER1, 10min
dermcidin	abcam®, ab175519	1 in 100	HIER ER2, 20min

Table 10.1. **Table showing the automated immunohistochemistry techniques used for the different antibodies.** HIER: heat-induced epitope retrieval, ER1: epitope retrieval pre-made Leica solution, operated at pH 6 and ER2: operates at pH 9. The enzyme is a Leica pre-blended solution made up with 1 drop of enzyme to 7000 µL of Leica enzyme diluent.

Endogenous peroxidases were blocked by 150 µL hydrogen peroxide for 10 min. Slides were incubated in 150 µL of primary antibody for 15 min at RT. Incubation in 150 µL of secondary antibody for 8 min at RT followed. One hundred and fifty microlitres of dextrose polymer containing 12 horseradish peroxidase molecules was added for 8 min at room temperature (RT), this amplifies the signal 12-fold. A mixed 3, 3'-diaminobenzidine (DAB) refine detection kit was used and slides stained with haematoxylin for 5 min. Between the addition of each reagent 150 µL of Leica wash solution was applied. Reagents were supplied by Leica as part of the Novocastra Bind Polymer refine Detection Kit. Slides were dehydrated from water to 100% ethanol, to xylene and a coverslip added using a Leica CV5030 Autostainer XL, before visualisation on a microscope (Nikon Corporation).

10.2.3 Immobilisation of proteins to a solid magnetic support

Manufacturers' guidelines were followed: life technologies, Dynabeads® Co-Immunoprecipitation Kit (14321D, Thermo Fisher Scientific). For each experiment 1.5 mg of magnetic beads were used, the "Antibody Coupling Protocol" then "Co-IP Protocol for Western Blot or Silver Stain Analysis" were followed, beads were incubated in 100 µL of skin homogenate for 4 h at RT before collecting the interacting proteins.

10.2.4 Label-free quantitative mass spectrometry for proteins (MS^E)

Peptides were analysed using a nanoAcquity ultrahigh definition liquid chromatography (UPLC) system coupled to a quadrupole time-of-flight (QToF) Premier mass spectrometer (MS) (Waters Corporation, Manchester, UK). Peptides were trapped and desalted before reverse phase separation using a 5 mm x 300 µm Symmetry C18 5 µL, pre-column. Peptides were separated using a 15 cm x 75 µm C18 reverse phase analytical column and loaded onto the pre-column in

a 3% acetonitrile (ACN) and 0.1% formic acid (FA) in ultrapure water solution (Fluka) at a flow rate of 4 µL/min for 4 min. Peptides were eluted from and separated on the analytical column using a 3-40% ACN gradient containing 0.1% FA in ultrapure water over 30 min at a flow rate of 0.3 µL/min. The column was re-equilibrated to the starting conditions for 9 min, after removal of the non-polar and non-peptide material with 100% ACN containing 0.1% FA for 5 min at a flow rate of 0.4 µL/min. Columns were maintained at 35 °C and mass accuracy was maintained during the run using 0.3 nmol/L of [glutamic acid[1]]-fibrinopeptide B delivery through an auxiliary pump of the nanoAcquity at a flow rate of 0.3 µL/min[57; 355].

Peptides were analysed in positive ion mode using a QToF Premier (Waters Corporation, Manchester, UK), operated in V-mode, with a typical resolving power of 10000 fwhm. The ToF analyser was calibrated prior to analyses with [glutamic acid[1]]-fibrinopeptide B fragments over the mass range of 50-2000 m/z obtained using 25 eV of collision energy. Data files were mass-corrected every 30 s using the doubly charged [glutamic acid[1]]-fibrinopeptide B species (785.84262 m/z). Accurate mass LC-MS data were collected in a data independent and alternating, low and high collision energy mode. Each low/high acquisition was 1.5 s in duration with a 0.1 s inter-scan delay. Low energy data collections were performed at constant collision energy of 4 eV, high collision energy acquisitions were performed across a 15−40 eV ramp over 1.5 s and a complete low/high energy acquisition was achieved every 3.2 s.

10.2.5 Analysis and quantification of raw MS files (ProteinLynx GlobalServer)

Raw data were imported into Waters ProteinLynx GlobalServer version 3.0.1 to identify peptide masses corresponding to fragmentation ion data. Mass corrections was applied based on [glutamic acid1]-fibrinopeptide B delivered via an auxiliary pump. Processed spectra were merged prior to searching the UniProt reviewed human proteome. Search parameters were set to two fragment ions matched per peptide, four fragment ions per protein and two peptides per protein and one missed cleavage, fixed modifications were set to carbamidomethylation of cysteines and dynamic modifications of hydroxylation of aspartic acid, lysine, asparagine and proline and oxidation of methionine and the false discovery rate was 4 %.[218]

10.2.6 Removal of <3 kDa mass impurities using filtration for proteomic analysis

Amicon® Ultra-0.5 mL Centrifugal Filter Devices were used according to the manufacturer's guidelines (Merck Millipore, Merck KGaA, Germany). The filter unit was placed inside the provided microcentrifuge tubes, 500 µL of sample added and the cap closed. The filter device was centrifuged (Heraeus™ BIofuge Pico™, Thermo Scientific) at 14,000 *g* for 30 min. The filter

was then inverted and placed inside a fresh microcentrifuge tube and centrifuged at 1,000 *g* for 2 min. See Figure 5.1 steps 5-10 for a diagram.

10.2.7 Lipid extraction from skin samples

Lipids were extracted using a modified Folch extraction method, 1 mL of a 1:2 chloroform:methanol solution was added and the samples vortexed (Fisons plc., UK) and incubated at RT on a benchtop shaker (IKR, UK) for 1 h. Samples were centrifuged at 16,000 *g* for 10 min. Lipids were found in the liquid phase.

10.2.8 Bicinchoninic acid protein assay

A modified Lowry[356] protein assay was used. A seven point standard curve was made up to 10 µL of a 0-1 mg/mL concentration of bovine serum albumin in a 96-well flat-bottomed plate. Two microlitres of sample was added to different wells and made up to 10 µL with Milli-Q water (Merck Millipore, Merck KGaA, Germany). Two hundred microlitres of bicinchoninic acid was added to each well, the plate vortexed briefly and incubated at 37 °C for 10 min. Then 4 µL of a 4% w/v solution of copper sulphate solution was added, the plate vortexed briefly and incubated at 37 °C for 20 min. The absorption was measured at 555 nm.

10.2.9 Separation of proteins according to molecular weight using 1-dimensional gel electrophoresis

Polyacrylamide gel electrophoresis was used to separate proteins according to mass. Precast Any kDa™ Mini-PROTEAN® TGX™ gels were purchased from Bio-Rad. Loading buffer was made up in a 1:1:2 ratio of 4x sodium dodecyl sulphate Sample Buffer (Merck Millipore, Merck KGaA, Germany):300 mM DTE:Milli-Q water and 30 µL of this solution was added to freeze dried protein pellets, samples were vortexed and incubated at RT for 1 h, 4.5 µL of a 1.94 M 2-iodoacetamide solution was added, samples vortexed briefly and heated at 90 °C for 5 min. Samples were centrifuged at 16,000 *g* for 10 min and 20 µL of each sample added to separate wells of the gel. Four microlitres of GE Healthcare Rainbow Marker was used. Electrophoresis was performed at 200 V until the bromophenol blue line front was observed leaving the resolving gel (approximately 30-45 min). Gels were either Coomassie Brilliant Blue (Fisher Scientific, UK) stained immediately or stored in fixative.

The gel track was cut into 10 bands and digestion in separate eppendorfs as described in the literature[357; 358]. Gel bands were washed 3 times with 1 mL of 50 mM ammonium bicarbonate (AmBic), pH 7.8 solution and washes discarded. Five hundred microlitres of LC-MS grade ACN (Merck, Germany) was added to each gel piece and incubated on a benchtop shaker for 30 min,

further dehydration was carried out by centrifugal evaporation (Jouan, France) for 1-2 h. Gel pieces were digested with 60 µL of a 12.5 mg/mL trypsin solution in 50 mM AmBic and incubated at 37 °C overnight.

Peptides were extracted using an ACN gradient. Firstly 200 µL of 1% FA was added and the gel pieces incubated at RT on a benchtop shaker for 20 min. This was discarded, 300 µL of 50% ACN, containing 1% FA was then added, and the gel piece incubated at RT on a benchtop shaker for 20 min. This was removed and transferred to a clean eppendorf. This step was repeated with 200 µL of a 70% ACN, containing 1% FA solution to elute the final peptides. Peptides were dried using a centrifugal evaporator and reconstituted in 3% ACN, containing 0.1% trifluoroacetic acid (TFA) solution for MS analysis.

10.2.10 In-solution digestion of proteins

Fifty micrograms of protein solution was taken and lyophilised, reconstituted in 20 µL of 100 mmol/L tris, pH 7.8, containing 2 % w/v ASB-14, 6 mol/L urea and 2 mol/L thiourea. To this 1.5 µL of 1.94 mol/L DTE in 100 mmol/L tris, pH 7.8 was added, samples vortexed, centrifuged briefly and incubated on a platform shaker at RT for 1 h. Three microlitres of 1.94 mol/L 2-iodoacetamide in 100 mol/L tris, pH 7.8 was added, the sample vortexed, centrifuged briefly and incubated at RT on a platform shaker for 45 min. The reaction volume was made up to 190 µL with Milli-Q water. Ten microlitres of 0.1 mg/mL Sequencing Grade Modified Trypsin (Promega, Madison, USA) was added, samples vortexed briefly and incubated overnight at 37 °C.[218]

10.2.11 Separation of peptides according to polarity using high pH carbon-18 chromatography

Offline 2D-LC separation was carried out on ISOLUTE® C18 columns (Biotage) as described in the literature[359]. Columns were primed with 1 mL of 50% ACN containing 0.1% ammonia, followed by 2 mL of 0.1% ammonia solution. Peptides from an in-solution digest (method 3.12) were applied to the column and allowed to flow through, flow through was reapplied twice. Peptides were eluted into separate eppendorfs by increasing ACN concentrations containing 0.1% ammonium from 3-50% ACN. Peptides were dried using a centrifugal evaporator and peptides reconstituted in 3% ACN, containing 0.1% TFA solution before MS analysis.

10.2.12 Two-dimensional high pH fractionation of sample peptides, followed by low pH chromatographic separation using an online nanoACQUITY UHPLC system

Lypholised sample was reconstituted in 25 µL of 3 % v/v ACN containing 0.1 % v/v TFA and 50 pmol/µL enolase peptides standard (MassPREP™, Waters) solution, centrifuged at 16,000 g for 10 mins and the supernatant transferred to a vial (TruView™ LCMS Certified, Total Recovery Vial, Waters). The nanoACQUITY UPLC (Waters, Manchester) system was configured in 2D with dilution set-up to allow for the first dimension to online fractionate the sample using high pH mobile phases directly before individual fractions entered the second dimension of chromatographic separation using low pH mobile phases. The first dimension was performed at 2 µL/min flow on an XBridge Peptide ethylene bridged hybrid C18 NanoEase Column (130 Å, 5 µm, 300 µm X 50 mm, 1/pkg (PN: 186003682), Waters, Manchester) mobile phase A was a 20 mmol/L ammonium formate, pH 9 solution and mobile phase B was 100 % acetonitrile. At the start of the first dimension the sample solution was loaded onto the XBridge Peptide column in 3 % mobile phase B for 1 min before a 4 min gradient for each fraction after which the XBridge Peptide column is re-equilibrated at 3 % mobile phase B.

Number of Fractions	4	6	8
1	11.8%	10.1%	8.7%
2	15.3%	13.1%	11.8%
3	19.3%	15.3%	13.6%
4	50.0%	17.7%	15.3%
5		21.2%	17.1%
6		50.0%	19.3%
7			22.5%
8			50.0%

Table 10.2. **Table showing percentage composition of mobile phase B for each fraction.** Percentage composition of mobile phase B for each fraction, depending on the total number of fractions (4, 6 or 8).

After a fraction was eluted from the XBridge Peptide column it entered the second dimension constituting low pH reverse phase chromatographic separation at 400 nL/min flow on a ACQUITY UPLC Peptide ethylene bridged hybrid C18 nanoACQUITY Column (10 Kpsi, 130 Å, 1.7 µm, 75 µm X 150 mm (PN: 186003543), Waters, Manchester) maintained at 35 °C, mobile phase A was 0.1 % v/v formic acid with 5 % v/v dimethyl sulphoxide and mobile phase B was

0.1 % v/v formic acid in 100 % ACN with 5 % v/v dimethyl sulphoxide. Before peptides from the first dimension were chromatographically separated they were diluted 1:10 during trapping with mobile phase A from the second dimension (20 µL/min 0.1 % formic acid with 5 % v/v dimethyl sulphoxide), concentrated and further desalted onto a nanoACQUITY UPLC Symmetry C18 Trap Column (100 Å, 5 µm, 180 µm x 20 mm, 2G, V/M (PN:186006527), Waters, Manchester). The second dimension gradient started 20.5 min after the start of the first dimension at 3 % mobile phase B and increased to 40 % over 40 min, a further increase to 85 % mobile phase B occured over the next 2 min and was held there for 2 min further, before returning to starting conditions for 15 min of re-equilibration.[218]

10.2.13 Label-free ultrahigh definition label free (UDMS^E) mass spectrometry data acquisition

For each fraction a 60 min mass spectrometry analysis was performed on a SYNAPT G2-Si (Waters, Manchester) MS in UDMS^E, positive ion, electrospray ionisation (ESI) and operated in V-mode[360]. One second alternating high and low energy scans were performed at a capillary voltage of 3.0 kV, sampling cone voltage of 40 V, source temperature of 70 °C over a mass range of 50-2000 m/z in resolution analyser mode. Prior to fragmentation ion mobility separation (IMS) was performed at a wave velocity of 650 m/s and a wave height of 40 V. Low energy scans were performed at 0 V collision voltage and the high energy scans were on a gradient, from 0-20 ion mobility bins the collision voltage was 13.6 V increasing linearly to 49.1 V at 120 mobility bins, followed by another linear gradient to 54.1 V at 200 mobility bins. Every 60 s lock mass of [glutamic acid1]-fibrinopeptide B was delivered via an auxiliary pump at 300 nL/min.[218]

10.2.14 Skin preparation for mass spectrometry analysis

Skin tissue was washed with 1x PBS before being snap frozen in liquid nitrogen, embedded in optimum cutting temperature (Cell Path, Fisher Scientific), cryosectioned into 10 µm rolled tissue sections (Leica CM1860) and collected in a clean tube. Curls were suspended in 500 µL of 50 mmol/L AmBic containing 2 % w/v ASB-14. Curls and solution were transferred to a homogenisation vial (Precellys 0.5 mL tube containing 1.4 mm diameter ceramic beads, peqlab, VWR) and mechanically homogenised for 20 s at high power (Minilys®, Bertin Technologies). The solution was then transferred to ice for 1 min to stop thermal degradation. This was repeated twice. The vial was incubated on ice for 1 h before a further three cycles of homogenisation. The homogenate was transferred to a clean tube and sonicated for 10 s using a Soniprep 150 sonicator (MSE UK). Sample was centrifuged at 16,000 *g* for 10 min and the supernatant removed to a clean tube.[218]

10.2.15 Analysis and quantification of raw mass spectrometry files (Progenesis QI for proteomics)

Raw data were imported into Nonlinear Dynamics Progenesis QI for proteomics to identify peptide masses corresponding to the fragmentation ion data. Mass correction was based on [glutamic acid1]-fibrinopeptide B delivered via an auxiliary pump. Processed spectra were merged prior to searching the UniProt reviewed human proteome. Search parameters were set to two fragment ions matched per peptide, four fragment ions per protein and two peptides per protein and one missed cleavage, fixed modifications were carbamidomethylation of cysteines and dynamic modifications were hydroxylation of aspartic acid, lysine, asparagine and proline and oxidation of methionine and false discovery rate was 4 %.

10.2.16 Analysis and identification of post-translational modifications (PTMs)

Nonlinear Dynamics Progenesis QI for proteomics was used to search peptide masses acquired from UDMS^{E} mass spectrometry acquisition data to identify mass changes in peptides that could correlate with a PTM, mass changes shown in Table 10.3:

Modification	Applies to…	Mass change (Da)
Carbonylation	Arginine	-43.0537
	Lysine	-1.0316
	Proline	-43.0534
	Threonine	-2.0157
Citrullination	Arginine	0.9840
Deamidation	Asparagine	0.9840
	Glutamine	0.9840
Dimethylation	Arginine	28.0313
	Lysine	28.0100
Hydroxylation	Asparagine	15.9949
	Aspartic acid	15.9949
	Lysine	15.9949
	Proline	15.9949
Methylation	C-terminus	14.0156
	Asparagine	14.0156
	Aspartic acid	14.0156
	Arginine	14.0156
	Cysteine	14.0156
	Glutamic acid	14.0156
	Glutamine	14.0156
	Histidine	14.0156
	Lysine	14.0156
	N-terminus	14.0157
Nitrosylation	Cysteine	28.9902
	Tryptophan	28.9902
Sulphenylation	Cysteine	17.0073
Trimethylation	Lysine	42.0300

Table 10.3. **This table lists the mass changes for a selection of PTMs.** This table shows the mass changes used in this thesis to identify modified peptide sequences according to their mass from mass spectrometry data.

10.2.17 High performance liquid chromatography tandem mass spectrometry (HPLC-MS/MS) analysis of glycosphingolipids

Protein concentrations were determined using the bicinchoninic acid protein assay (section 10.2.8), 300 µg of protein was taken for glucosylceramide analysis. Compounds were extracted in 500 µL of chloroform:methanol solution (1:2 v/v) containing 200 ng/ml of d3-C16:0-glucosylceramide internal standard, synthesised in house[361]. Samples were shaken for 30 min at RT. After 10 min centrifugation at 16,000 *g* the liquid phase was collected and dried under nitrogen gas flow. Samples were reconstituted in 100 µL chloroform:methanol solution (1:2 v/v) and two 5 µl injections of each sample were introduced to the HPLC-MS/MS system. Glycosphingolipid reference standards (Matreya, USA) was analysed to confirm analyte identity.

Samples were injected onto Waters ACQUITY UPLC system (Manchester, UK) operated in partial loop mode and separated on Waters ACQUITY UPLC BEH C18 column (130Å, 1.7 µm, 2.1 mm X 50 mm) under the following gradient conditions:

Time (min)	Mobile Phase A (%)	Mobile Phase B (%)
0.00	80.0	20.0
0.20	80.0	20.0
5.00	0.1	99.9
9.00	0.1	99.9
9.01	80.0	20.0
11.00	80.0	20.0

Table 10.4. **Table detailing the mobile phase composition throughout the gradient.** Table detailing the relative compositions of mobile phase A and mobile phase B throughout the analytical gradient of this HPLC-MS/MS assay.

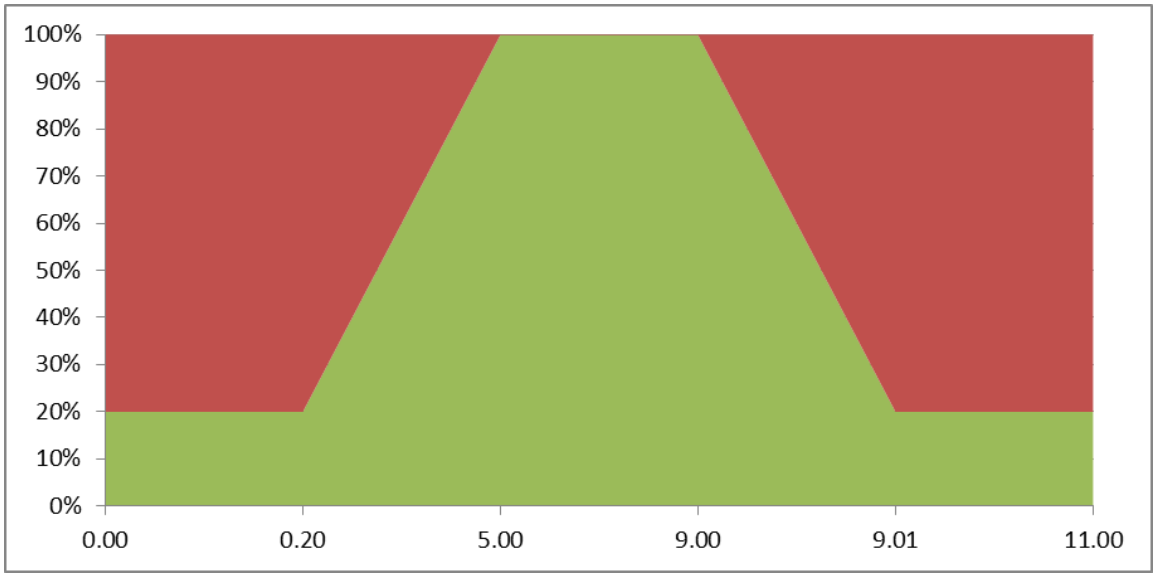

Figure 10.1. **Figure illustrating the 11 minute gradient used for the globotriaosylceramide HPLC-MS/MS.** Figure illustrating the composition of mobile phase A (red) and mobile phase B (green) over the 11 minute gradient of separation for the globotriaosylceramide isoforms.

Mobile phase A was water containing 0.1% FA, mobile phase B was methanol and the flow rate was 0.65 mL/min throughout. Column and sample temperatures were maintained at 40°C and 10°C respectively. Weak wash solvent was water containing 0.1% FA and strong wash solvent was acetonitrile:methanol:isopropanol:Milli-Q water (1:1:1:1 v/v). The eluting analytes were detected on a Waters XEVO TQ-S triple quadrupole mass spectrometer (Manchester, UK) which was equipped with ESI source and operated in multiple reaction monitoring (MRM) and positive ion mode (see Table 10.5 for MRM details) with the tune page parameters set to achieve the maximum sensitivity for glycosphingolipids as described previously[362]. The data was processed with MassLynx v4.1.

Globotriaosylceramide Isoform	Precursor Ion (m/z)	Fragment Ion (m/z)	Cone Voltage (V)	Collision Voltage (V)
C16:0	1046.60	884.60	40	40
C18:0	1074.70	912.70	40	42
d3-C18:0	1077.84	915.91	108	56
C20:0	1102.52	940.47	113	74
C22:1	1128.45	966.37	40	62
C22:0	1130.82	968.87	112	64
C22:0-OH	1144.45	982.37	130	64
C24:2	1154.83	992.92	128	62
C24:1	1156.45	994.37	40	62
C24:0	1158.45	996.37	40	62
C24:2-OH	1170.84	1008.79	130	62
C24:0-OH	1174.80	1012.87	130	62
C24:2-OOH	1186.83	1024.92	130	62
C26:0	1186.84	1024.77	130	64
C24:0-OH-OH	1190.80	1028.87	130	62

Table 10.5. **Table detailing the transition mass-to-charge ratio values for the globotriaosylceramide isoforms.** Precursor ion, fragment ion, cone voltage and collision voltage values for the globotriaosylceramide isoforms included in this MRM HPLC-MS/MS assay.

Chapter 11

References

11 References

1 DEMPSTER, A. J. The Passage of Slow Canal Rays through Hydrogen. **Proc Natl Acad Sci U S A,** v. 11, n. 9, p. 552-4, Sep 1925. ISSN 0027-8424. Disponível em: < http://www.ncbi.nlm.nih.gov/pubmed/16576916 >.

2 LAWRENCE, E. O.; SLOAN, D. H. The Production of High Speed Canal Rays without the Use of High Voltages. **Proc Natl Acad Sci U S A,** v. 17, n. 1, p. 64-70, Jan 1931. ISSN 0027-8424. Disponível em: < http://www.ncbi.nlm.nih.gov/pubmed/16577331 >.

3 THOMSON, J. J. Rays of positive electricity. **Proceedings of the Royal Society,** v. A, n. 89, p. 1-20, 1913.

4 NOBELPRIZE.ORG. The Nobel Prize in Physics 1906. **Physics Prizes**, p. https://www.nobelprize.org/nobel_prizes/physics/laureates/1906/, 2016. Acesso em: 25/05/2016.

5 YAMASHITA, M.; FENN, J. B. Electrospray ion source. Another variation on the free-jet theme. **The Journal of Physical Chemistry,** v. 88, n. 20, p. 4451-4459, 1984.

6 KUNGL VETENSKAPSAKADEMIEN, T. R. S. A. O. S. **Advanced information on the Nobel Prize in Chemistry 2002**. Mass spectrometry (MS) and nuclear magnetic resonance (NMR) applied to biological macromolecules**:** 13 p. 2002.

7 QUAN, L.; LIU, M. CID, ETD and HCD Fragmentation to Study Protein Post-Translational Modifications. **Modern Chemistry & Applications**, 2013.

8 MAY, J. C.; MCLEAN, J. A. Ion mobility-mass spectrometry: time-dispersive instrumentation. **Anal Chem,** v. 87, n. 3, p. 1422-36, Feb 2015. ISSN 1520-6882. Disponível em: < http://www.ncbi.nlm.nih.gov/pubmed/25526595 >.

9 LANUCARA, F. et al. The power of ion mobility-mass spectrometry for structural characterization and the study of conformational dynamics. **Nat Chem,** v. 6, n. 4, p. 281-94, Apr 2014. ISSN 1755-4349. Disponível em: < http://www.ncbi.nlm.nih.gov/pubmed/24651194 >.

10 PROKSCH, E.; BRANDNER, J. M.; JENSEN, J. M. The skin: an indispensable barrier. **Exp Dermatol,** v. 17, n. 12, p. 1063-72, Dec 2008. ISSN 0906-6705.

11 MADISON, K. C. Barrier Function of the Skin: [ldquo]La Raison d'Etre[rdquo] of the Epidermis. **J Investig Dermatol,** v. 121, n. 2, p. 231-241, 07/23/online 2003. ISSN 0022-202X. Disponível em: < http://dx.doi.org/10.1046/j.1523-1747.2003.12359.x >.

12 MARENHOLZ, I.; ESPARZA-GORDILLO, J.; LEE, Y. A. The genetics of the skin barrier in eczema and other allergic disorders. **Curr Opin Allergy Clin Immunol,** v. 15, n. 5, p. 426-34, Oct 2015. ISSN 1473-6322. Disponível em: < https://www.ncbi.nlm.nih.gov/pubmed/26226353 >.

13 BERENSON, G. S.; BURCH, G. E. Studies of Diffusion of Water Through Dead Human Skin: The Effect of Different Environmental States and of Chemical Alterations of the Epidermis. **The American Journal of Tropical Medicine and Hygiene,** v. s1-31, n. 6, p. 842-853, 1951. Disponível em: < http://www.ajtmh.org/content/s1-31/6/842.short >.

14 VAN SMEDEN, J. et al. Intercellular skin barrier lipid composition and organization in Netherton syndrome patients. **J Invest Dermatol,** v. 134, n. 5, p. 1238-45, May 2014. ISSN 1523-1747. Disponível em: < http://www.ncbi.nlm.nih.gov/pubmed/24292773 >.

15 DE BENEDETTO, A. et al. Histamine and Skin Barrier: Are Histamine Antagonists Useful for the Prevention or Treatment of Atopic Dermatitis? **J Clin Med,** v. 4, n. 4, p. 741-55, Apr 2015. Disponível em: < https://www.ncbi.nlm.nih.gov/pubmed/26239353 >.

16 ZHONG, W. et al. Linkage analysis suggests a locus of ichthyosis vulgaris on 1q22. **J Hum Genet,** v. 48, n. 7, p. 390-2, 2003. ISSN 1434-5161. Disponível em: < http://www.ncbi.nlm.nih.gov/pubmed/12838398 >.

17 DALE, B. A.; RESING, K. A.; LONSDALE-ECCLES, J. D. Filaggrin: a keratin filament associated protein. **Ann N Y Acad Sci,** v. 455, p. 330-42, 1985. ISSN 0077-8923. Disponível em: < http://www.ncbi.nlm.nih.gov/pubmed/2417519 >.

18 THYSSEN, J. P.; GODOY-GIJON, E.; ELIAS, P. M. Ichthyosis vulgaris: the filaggrin mutation disease. **Br J Dermatol,** v. 168, n. 6, p. 1155-66, Jun 2013. ISSN 1365-2133. Disponível em: < http://www.ncbi.nlm.nih.gov/pubmed/23301728 >.

19 CHAVANAS, S. et al. Mutations in SPINK5, encoding a serine protease inhibitor, cause Netherton syndrome. **Nat Genet,** v. 25, n. 2, p. 141-2, Jun 2000. ISSN 1061-4036. Disponível em: < http://www.ncbi.nlm.nih.gov/pubmed/10835624 >.

20 HACHEM, J. P. et al. Serine protease activity and residual LEKTI expression determine phenotype in Netherton syndrome. **J Invest Dermatol,** v. 126, n. 7, p. 1609-21, Jul 2006. ISSN 0022-202X. Disponível em: < http://www.ncbi.nlm.nih.gov/pubmed/16601670 >.

21 WERTZ, P. W. et al. Composition and morphology of epidermal cyst lipids. **J Invest Dermatol,** v. 89, n. 4, p. 419-25, Oct 1987. ISSN 0022-202X. Disponível em: < http://www.ncbi.nlm.nih.gov/pubmed/3668284 >.

22 WERTZ, P. W.; DOWNING, D. T. Stratum corneum: biological and biochemical considerations. **Transderm. Drug Deliv.,** v. 35, p. 1-22, 1989.

23 WERTZ, P. W. Current understanding of skin biology pertinent to skin penetration: skin biochemistry. **Skin Pharmacol Physiol,** v. 26, n. 4-6, p. 217-26, 2013. ISSN 1660-5535. Disponível em: < http://www.ncbi.nlm.nih.gov/pubmed/23921108 >.

24 KESSNER, D. et al. Arrangement of ceramide [EOS] in a stratum corneum lipid model matrix: new aspects revealed by neutron diffraction studies. **Eur Biophys J,** v. 37, n. 6, p. 989-99, Jul 2008. ISSN 0175-7571. Disponível em: < http://www.ncbi.nlm.nih.gov/pubmed/18427800 >.

[25] DI NARDO, A. et al. Ceramide and cholesterol composition of the skin of patients with atopic dermatitis. **Acta Derm Venereol,** v. 78, n. 1, p. 27-30, Jan 1998. ISSN 0001-5555. Disponível em: < http://www.ncbi.nlm.nih.gov/pubmed/9498022 >.

[26] LONG, S. A. et al. Human stratum corneum polar lipids and desquamation. **Arch Dermatol Res,** v. 277, n. 4, p. 284-7, 1985. ISSN 0340-3696. Disponível em: < http://www.ncbi.nlm.nih.gov/pubmed/4004327 >.

[27] JETTEN, A. M. et al. Increased cholesterol sulfate and cholesterol sulfotransferase activity in relation to the multi-step process of differentiation in human epidermal keratinocytes. **J Invest Dermatol,** v. 92, n. 2, p. 203-9, Feb 1989. ISSN 0022-202X. Disponível em: < http://www.ncbi.nlm.nih.gov/pubmed/2465352 >.

[28] KAWABE, S. et al. Cholesterol sulfate activates transcription of transglutaminase 1 gene in normal human keratinocytes. **J Invest Dermatol,** v. 111, n. 6, p. 1098-102, Dec 1998. ISSN 0022-202X. Disponível em: < http://www.ncbi.nlm.nih.gov/pubmed/9856823 >.

[29] STROTT, C. A.; HIGASHI, Y. Cholesterol sulfate in human physiology: what's it all about? **J Lipid Res,** v. 44, n. 7, p. 1268-78, Jul 2003. ISSN 0022-2275. Disponível em: < http://www.ncbi.nlm.nih.gov/pubmed/12730293 >.

[30] SATO, J. et al. Cholesterol sulfate inhibits proteases that are involved in desquamation of stratum corneum. **J Invest Dermatol,** v. 111, n. 2, p. 189-93, Aug 1998. ISSN 0022-202X. Disponível em: < http://www.ncbi.nlm.nih.gov/pubmed/9699715 >.

[31] YAMAMOTO, A. et al. Stratum corneum lipid abnormalities in atopic dermatitis. **Arch Dermatol Res,** v. 283, n. 4, p. 219-23, 1991. ISSN 0340-3696. Disponível em: < http://www.ncbi.nlm.nih.gov/pubmed/1929538 >.

[32] GREEN, C. et al. Clinical and cost-effectiveness of once-daily versus more frequent use of same potency topical corticosteroids for atopic eczema: a systematic review and economic evaluation. **Health Technol Assess,** v. 8, n. 47, p. iii,iv, 1-120, Nov 2004. ISSN 1366-5278. Disponível em: < https://www.ncbi.nlm.nih.gov/pubmed/15527669 >.

[33] Types of Eczema: National Eczema Society. Disponível em: < http://www.eczema.org/types-of-eczema >. Acesso em: 08/09/2014.

[34] PLÖTZ, S. G.; RING, J. What's new in atopic eczema? **Expert Opin Emerg Drugs,** v. 15, n. 2, p. 249-67, Jun 2010. ISSN 1744-7623. Disponível em: < http://www.ncbi.nlm.nih.gov/pubmed/20433363 >.

[35] WERNER, Y.; LINDBERG, M. Transepidermal water loss in dry and clinically normal skin in patients with atopic dermatitis. **Acta Derm Venereol,** v. 65, n. 2, p. 102-5, 1985. ISSN 0001-5555. Disponível em: < http://www.ncbi.nlm.nih.gov/pubmed/2408409 >.

[36] MATSUMOTO, M.; SUGIURA, H.; UEHARA, M. Skin barrier function in patients with completely healed atopic dermatitis. **J Dermatol Sci,** v. 23, n. 3, p. 178-82, Aug 2000. ISSN 0923-1811. Disponível em: < http://www.ncbi.nlm.nih.gov/pubmed/10959043 >.

[37] LÜBBE, J. Secondary infections in patients with atopic dermatitis. **Am J Clin Dermatol,** v. 4, n. 9, p. 641-54, 2003. ISSN 1175-0561. Disponível em: < http://www.ncbi.nlm.nih.gov/pubmed/12926982 >.

[38] RING, J. et al. Why are allergies increasing? **Curr Opin Immunol,** v. 13, n. 6, p. 701-8, Dec 2001. ISSN 0952-7915. Disponível em: < http://www.ncbi.nlm.nih.gov/pubmed/11677093 >.

[39] SANDILANDS, A. et al. Comprehensive analysis of the gene encoding filaggrin uncovers prevalent and rare mutations in ichthyosis vulgaris and atopic eczema. **Nat Genet,** v. 39, n. 5, p. 650-4, May 2007. ISSN 1061-4036. Disponível em: < https://www.ncbi.nlm.nih.gov/pubmed/17417636 >.

[40] RODRÍGUEZ, E. et al. Meta-analysis of filaggrin polymorphisms in eczema and asthma: robust risk factors in atopic disease. **J Allergy Clin Immunol,** v. 123, n. 6, p. 1361-70.e7, Jun 2009. ISSN 1097-6825. Disponível em: < https://www.ncbi.nlm.nih.gov/pubmed/19501237 >.

[41] BROWN, S. J. Molecular mechanisms in atopic eczema: insight gained from genetic studies. **J Pathol**, Sep 2016. ISSN 1096-9896. Disponível em: < https://www.ncbi.nlm.nih.gov/pubmed/27659773 >.

[42] ASSOCIATION, B. M. **2012-2013 BNF for children**. Tavistock Square, London, WC1H 9JP, UK: BMJ Publishing Group Ltd., 2012. ISBN 978 0 85711 033 6.

[43] TRAN, A. N.; KOO, J. Y. Risk of Systemic Toxicity With Topical Lidocaine/Prilocaine: A Review. **J Drugs Dermatol,** v. 13, n. 9, p. 1118-1122, Sep 2014. ISSN 1545-9616. Disponível em: < http://www.ncbi.nlm.nih.gov/pubmed/25226014 >.

[44] ACKLAND, G. L. et al. Individualised oxygen delivery targeted haemodynamic therapy in high-risk surgical patients: a multicentre, randomised, double-blind, controlled, mechanistic trial. **Lancet Respir Med,** v. 3, n. 1, p. 33-41, Jan 2015. ISSN 2213-2619. Disponível em: < http://www.ncbi.nlm.nih.gov/pubmed/25523407 >.

[45] DE VEER, S. J. et al. Proteases and proteomics: cutting to the core of human skin pathologies. **Proteomics Clin Appl,** v. 8, n. 5-6, p. 389-402, Jun 2014. ISSN 1862-8354. Disponível em: < http://www.ncbi.nlm.nih.gov/pubmed/24677727 >.

[46] HUANG, C. M. et al. Prospective highlights of functional skin proteomics. **Mass Spectrom Rev,** v. 24, n. 5, p. 647-60, 2005 Sep-Oct 2005. ISSN 0277-7037. Disponível em: < http://www.ncbi.nlm.nih.gov/pubmed/15376279 >.

[47] INFORMATION, N. C. F. B.; MEDICINE, U. S. N. L. O. PubMed Search for "liver AND proteomics". 2016. Disponível em: < http://www.ncbi.nlm.nih.gov/pubmed/?term=liver+AND+proteomics+AND+(Humans%5BMesh%5D) >. Acesso em: 27/04/2016.

[48] _____. PubMed Search for "blood AND proteomics". 2016. Disponível em: < http://www.ncbi.nlm.nih.gov/pubmed/?term=blood+AND+proteomics+AND+(Humans%5BMesh%5D) >. Acesso em: 27/04/2016.

[49] _____. PubMed Search for "skin AND proteomics". 2016. Disponível em: < http://www.ncbi.nlm.nih.gov/pubmed?term=skin+AND+proteomics+AND+(Humans%5BMesh%5D)&cmd=DetailsSearch >. Acesso em: 27/04/2016.

[50] LUNDBERG, K. C. et al. Proteomics of skin proteins in psoriasis: from discovery and verification in a mouse model to confirmation in humans. **Mol Cell Proteomics,** v. 14, n. 1, p. 109-19, Jan 2015. ISSN 1535-9484. Disponível em: < http://www.ncbi.nlm.nih.gov/pubmed/25351201 >.

[51] SCHNELL, G. et al. Discovery and targeted proteomics on cutaneous biopsies infected by borrelia to investigate lyme disease. **Mol Cell Proteomics,** v. 14, n. 5, p. 1254-64, May 2015. ISSN 1535-9484. Disponível em: < http://www.ncbi.nlm.nih.gov/pubmed/25713121 >.

[52] ZANIVAN, S. et al. In vivo SILAC-based proteomics reveals phosphoproteome changes during mouse skin carcinogenesis. **Cell Rep,** v. 3, n. 2, p. 552-66, Feb 2013. ISSN 2211-1247. Disponível em: < http://www.ncbi.nlm.nih.gov/pubmed/23375375 >.

[53] BURIAN, M. et al. Quantitative proteomics of the human skin secretome reveal a reduction in immune defense mediators in ectodermal dysplasia patients. **J Invest Dermatol,** v. 135, n. 3, p. 759-67, Mar 2015. ISSN 1523-1747. Disponível em: < http://www.ncbi.nlm.nih.gov/pubmed/25347115 >.

[54] HART, P. J. et al. MALDI-MS imaging of lipids in ex vivo human skin. **Anal Bioanal Chem,** v. 401, n. 1, p. 115-25, Jul 2011. ISSN 1618-2650. Disponível em: < http://www.ncbi.nlm.nih.gov/pubmed/21604167 >.

[55] KOISTINEN, K. M. et al. Quantitative lysophospholipidomics in human plasma and skin by LC-MS/MS. **Anal Bioanal Chem,** v. 407, n. 17, p. 5091-9, Jul 2015. ISSN 1618-2650. Disponível em: < http://www.ncbi.nlm.nih.gov/pubmed/25618760 >.

[56] VAN SMEDEN, J. et al. Combined LC/MS-platform for analysis of all major stratum corneum lipids, and the profiling of skin substitutes. **Biochim Biophys Acta,** v. 1841, n. 1, p. 70-9, Jan 2014. ISSN 0006-3002 (Print)

0006-3002.

[57] BENNETT, K. et al. New role for LEKTI in skin barrier formation: label-free quantitative proteomic identification of caspase 14 as a novel target for the protease inhibitor LEKTI. **J Proteome Res,** v. 9, n. 8, p. 4289-94, Aug 6 2010. ISSN 1535-3907 (Electronic) 1535-3893 (Linking). Disponível em: < http://www.ncbi.nlm.nih.gov/pubmed/20533828 >.

[58] _____. The identification of a new role for LEKTI in the skin: The use of protein 'bait' arrays to detect defective trafficking of dermcidin in the skin of patients with Netherton syndrome. **J Proteomics,** v. 75, n. 13, p. 3925-37, Jul 16 2012. ISSN 1876-7737 (Electronic).

[59] WALLACH, D.; TAÏEB, A. Atopic dermatitis/atopic eczema. **Chem Immunol Allergy,** v. 100, p. 81-96, 2014. ISSN 1662-2898. Disponível em: < http://www.ncbi.nlm.nih.gov/pubmed/24925387 >.

60 MUTGI, K.; KOO, J. Update on the role of systemic vitamin D in atopic dermatitis. **Pediatr Dermatol,** v. 30, n. 3, p. 303-7, 2013 May-Jun 2013. ISSN 1525-1470. Disponível em: < http://www.ncbi.nlm.nih.gov/pubmed/22957498 >.

61 HANIFIN, J. M.; CHAN, S. Biochemical and immunologic mechanisms in atopic dermatitis: new targets for emerging therapies. **J Am Acad Dermatol,** v. 41, n. 1, p. 72-7, Jul 1999. ISSN 0190-9622. Disponível em: < http://www.ncbi.nlm.nih.gov/pubmed/10411415 >.

62 MANCINI, A. J.; KAULBACK, K.; CHAMLIN, S. L. The socioeconomic impact of atopic dermatitis in the United States: a systematic review. **Pediatr Dermatol,** v. 25, n. 1, p. 1-6, 2008 Jan-Feb 2008. ISSN 1525-1470. Disponível em: < http://www.ncbi.nlm.nih.gov/pubmed/18304144 >.

63 WILLIAMS, H. et al. Worldwide variations in the prevalence of symptoms of atopic eczema in the International Study of Asthma and Allergies in Childhood. **J Allergy Clin Immunol,** v. 103, n. 1 Pt 1, p. 125-38, Jan 1999. ISSN 0091-6749. Disponível em: < http://www.ncbi.nlm.nih.gov/pubmed/9893196 >.

64 MITCHELL, A. E. et al. Childhood atopic dermatitis: a cross-sectional study of relationships between child and parent factors, atopic dermatitis management, and disease severity. **Int J Nurs Stud,** v. 52, n. 1, p. 216-28, Jan 2015. ISSN 1873-491X. Disponível em: < http://www.ncbi.nlm.nih.gov/pubmed/25441758 >.

65 MORTZ, C. G. et al. Atopic dermatitis from adolescence to adulthood in the TOACS cohort: prevalence, persistence and comorbidities. **Allergy,** v. 70, n. 7, p. 836-45, Jul 2015. ISSN 1398-9995. Disponível em: < http://www.ncbi.nlm.nih.gov/pubmed/25832131 >.

66 SCHMUTH, M. et al. Inherited ichthyoses/generalized Mendelian disorders of cornification. **Eur J Hum Genet,** v. 21, n. 2, p. 123-33, Feb 2013. ISSN 1476-5438. Disponível em: < https://www.ncbi.nlm.nih.gov/pubmed/22739337 >.

67 SAI, K. et al. Distal promoter regions are responsible for differential regulation of human orosomucoid-1 and -2 gene expression and acute phase responses. **Biol Pharm Bull,** v. 37, n. 1, p. 164-8, 2014. ISSN 1347-5215. Disponível em: < http://www.ncbi.nlm.nih.gov/pubmed/24389491 >.

68 OFOTOKUN, I. et al. Immune activation mediated change in alpha-1-acid glycoprotein: impact on total and free lopinavir plasma exposure. **J Clin Pharmacol,** v. 51, n. 11, p. 1539-48, Nov 2011. ISSN 1552-4604. Disponível em: < http://www.ncbi.nlm.nih.gov/pubmed/21209245 >.

69 BARROSO-SOUSA, R. et al. Decreased levels of alpha-1-acid glycoprotein are related to the mortality of septic patients in the emergency department. **Clinics (Sao Paulo),** v. 68, n. 8, p. 1134-9, 2013. ISSN 1980-5322. Disponível em: < http://www.ncbi.nlm.nih.gov/pubmed/24037010 >.

70 FERENS-SIECZKOWSKA, M. et al. Comparison of haptoglobin and alpha$_1$-acid glycoprotein glycosylation in the sera of small cell and non-small cell lung cancer

patients. **Postepy Hig Med Dosw (Online),** v. 67, p. 828-36, 2013. ISSN 1732-2693. Disponível em: < http://www.ncbi.nlm.nih.gov/pubmed/24018448 >.

71 MARTÌNEZ CORDERO, E. et al. Alpha-1-acid glycoprotein, its local production and immunopathological participation in experimental pulmonary tuberculosis. **Tuberculosis (Edinb),** v. 88, n. 3, p. 203-11, May 2008. ISSN 1472-9792. Disponível em: < http://www.ncbi.nlm.nih.gov/pubmed/18055265 >.

72 CHEN, Y. et al. Cleavage of bleomycin hydrolase by caspase-3 during apoptosis. **Oncol Rep,** v. 30, n. 2, p. 939-44, Aug 2013. ISSN 1791-2431. Disponível em: < http://www.ncbi.nlm.nih.gov/pubmed/23708668 >.

73 KAMATA, Y. et al. Neutral cysteine protease bleomycin hydrolase is essential for the breakdown of deiminated filaggrin into amino acids. **J Biol Chem,** v. 284, n. 19, p. 12829-36, May 2009. ISSN 0021-9258. Disponível em: < http://www.ncbi.nlm.nih.gov/pubmed/19286660 >.

74 _____. Expression of bleomycin hydrolase in keratinization disorders. **Arch Dermatol Res,** v. 304, n. 1, p. 31-8, Jan 2012. ISSN 1432-069X. Disponível em: < http://www.ncbi.nlm.nih.gov/pubmed/22037625 >.

75 The Human Protein Atlas. Disponível em: < http://www.proteinatlas.org/ENSG00000108578/subcellular >. Acesso em: 15/09/2014.

76 _____. Bleomycin hydrolase is regulated biphasically in a differentiation- and cytokine-dependent manner: relevance to atopic dermatitis. **J Biol Chem,** v. 286, n. 10, p. 8204-12, Mar 2011. ISSN 1083-351X. Disponível em: < http://www.ncbi.nlm.nih.gov/pubmed/21190945 >.

77 BENNETT, R. D.; STREHLER, E. E. Calmodulin-like protein enhances myosin-10 translation. **Biochem Biophys Res Commun,** v. 369, n. 2, p. 654-9, May 2008. ISSN 1090-2104. Disponível em: < http://www.ncbi.nlm.nih.gov/pubmed/18295593 >.

78 MÉHUL, B. et al. Identification and cloning of a new calmodulin-like protein from human epidermis. **J Biol Chem,** v. 275, n. 17, p. 12841-7, Apr 2000. ISSN 0021-9258. Disponível em: < http://www.ncbi.nlm.nih.gov/pubmed/10777582 >.

79 BENNETT, R. D. et al. Calmodulin-like protein upregulates myosin-10 in human keratinocytes and is regulated during epidermal wound healing in vivo. **J Invest Dermatol,** v. 129, n. 3, p. 765-9, Mar 2009. ISSN 1523-1747. Disponível em: < http://www.ncbi.nlm.nih.gov/pubmed/18818677 >.

80 BERG, J. S. et al. Myosin-X, a novel myosin with pleckstrin homology domains, associates with regions of dynamic actin. **J Cell Sci,** v. 113 Pt 19, p. 3439-51, Oct 2000. ISSN 0021-9533. Disponível em: < http://www.ncbi.nlm.nih.gov/pubmed/10984435 >.

81 HASHIMOTO, Y. et al. Secreted calmodulin-like skin protein inhibits neuronal death in cell-based Alzheimer's disease models via the heterotrimeric Humanin receptor. **Cell Death Dis,** v. 4, p. e555, 2013. ISSN 2041-4889. Disponível em: < http://www.ncbi.nlm.nih.gov/pubmed/23519124 >.

82 DEBALD, M. et al. Specific expression of k63-linked ubiquitination of calmodulin-like protein 5 in breast cancer of premenopausal patients. **J Cancer Res Clin Oncol,** v. 139, n. 12, p. 2125-32, Dec 2013. ISSN 1432-1335. Disponível em: < http://www.ncbi.nlm.nih.gov/pubmed/24146193 >.

83 WOLLINA, U. et al. Immunohistochemical localization of calmodulin in normal and psoriatic epidermis. **Arch Dermatol Res,** v. 280, n. 8, p. 497-8, 1989. ISSN 0340-3696. Disponível em: < http://www.ncbi.nlm.nih.gov/pubmed/2645837 >.

84 DURUSSEL, I. et al. Cation- and peptide-binding properties of human calmodulin-like skin protein. **Biochemistry,** v. 41, n. 17, p. 5439-48, Apr 2002. ISSN 0006-2960. Disponível em: < http://www.ncbi.nlm.nih.gov/pubmed/11969404 >.

85 MENON, G. K.; ELIAS, P. M. Ultrastructural localization of calcium in psoriatic and normal human epidermis. **Arch Dermatol,** v. 127, n. 1, p. 57-63, Jan 1991. ISSN 0003-987X. Disponível em: < http://www.ncbi.nlm.nih.gov/pubmed/1986708 >.

86 HENNINGS, H. et al. Calcium regulation of growth and differentiation of mouse epidermal cells in culture. **Cell,** v. 19, n. 1, p. 245-54, Jan 1980. ISSN 0092-8674. Disponível em: < http://www.ncbi.nlm.nih.gov/pubmed/6153576 >.

87 BOYCE, S. T.; HAM, R. G. Calcium-regulated differentiation of normal human epidermal keratinocytes in chemically defined clonal culture and serum-free serial culture. **J Invest Dermatol,** v. 81, n. 1 Suppl, p. 33s-40s, Jul 1983. ISSN 0022-202X. Disponível em: < http://www.ncbi.nlm.nih.gov/pubmed/6345690 >.

88 MÉHUL, B.; BERNARD, D.; SCHMIDT, R. Calmodulin-like skin protein: a new marker of keratinocyte differentiation. **J Invest Dermatol,** v. 116, n. 6, p. 905-9, Jun 2001. ISSN 0022-202X. Disponível em: < http://www.ncbi.nlm.nih.gov/pubmed/11407979 >.

89 DONOVAN, M. et al. Calmodulin-like skin protein level increases in the differentiated epidermal layers in atopic dermatitis. **Exp Dermatol,** v. 22, n. 12, p. 836-7, Dec 2013. ISSN 1600-0625. Disponível em: < http://www.ncbi.nlm.nih.gov/pubmed/24279918 >.

90 AHMAD, M. et al. Identification and characterization of murine caspase-14, a new member of the caspase family. **Cancer Res,** v. 58, n. 22, p. 5201-5, Nov 1998. ISSN 0008-5472. Disponível em: < http://www.ncbi.nlm.nih.gov/pubmed/9823333 >.

91 HVID, M. et al. Regulation of caspase 14 expression in keratinocytes by inflammatory cytokines--a possible link between reduced skin barrier function and inflammation? **Exp Dermatol,** v. 20, n. 8, p. 633-6, Aug 2011. ISSN 1600-0625. Disponível em: < http://www.ncbi.nlm.nih.gov/pubmed/21539619 >.

92 HOSTE, E. et al. Caspase-14-deficient mice are more prone to the development of parakeratosis. **J Invest Dermatol,** v. 133, n. 3, p. 742-50, Mar 2013. ISSN 1523-1747. Disponível em: < http://www.ncbi.nlm.nih.gov/pubmed/23014340 >.

93 DEMERJIAN, M. et al. Acute modulations in permeability barrier function regulate epidermal cornification: role of caspase-14 and the protease-activated receptor type 2.

Am J Pathol, v. 172, n. 1, p. 86-97, Jan 2008. ISSN 0002-9440. Disponível em: < http://www.ncbi.nlm.nih.gov/pubmed/18156206 >.

94 HOSTE, E. et al. Caspase-14 is required for filaggrin degradation to natural moisturizing factors in the skin. **J Invest Dermatol,** v. 131, n. 11, p. 2233-41, Nov 2011. ISSN 1523-1747. Disponível em: < http://www.ncbi.nlm.nih.gov/pubmed/21654840 >.

95 DENECKER, G. et al. Caspase-14 reveals its secrets. **J Cell Biol,** v. 180, n. 3, p. 451-8, Feb 2008. ISSN 1540-8140. Disponível em: < http://www.ncbi.nlm.nih.gov/pubmed/18250198 >.

96 BERGERON, L. et al. Skin presenting a higher level of caspase-14 is better protected from UVB irradiation according to in vitro and in vivo studies. **J Cosmet Dermatol,** v. 11, n. 2, p. 111-21, Jun 2012. ISSN 1473-2165. Disponível em: < http://www.ncbi.nlm.nih.gov/pubmed/22672275 >.

97 DENECKER, G. et al. Caspase-14 protects against epidermal UVB photodamage and water loss. **Nat Cell Biol,** v. 9, n. 6, p. 666-74, Jun 2007. ISSN 1465-7392. Disponível em: < http://www.ncbi.nlm.nih.gov/pubmed/17515931 >.

98 WALLEY, A. J. et al. Gene polymorphism in Netherton and common atopic disease. **Nat Genet,** v. 29, n. 2, p. 175-8, Oct 2001. ISSN 1061-4036. Disponível em: < http://www.ncbi.nlm.nih.gov/pubmed/11544479 >.

99 KATO, A. et al. Association of SPINK5 gene polymorphisms with atopic dermatitis in the Japanese population. **Br J Dermatol,** v. 148, n. 4, p. 665-9, Apr 2003. ISSN 0007-0963. Disponível em: < http://www.ncbi.nlm.nih.gov/pubmed/12752122 >.

100 NISHIO, Y. et al. Association between polymorphisms in the SPINK5 gene and atopic dermatitis in the Japanese. **Genes Immun,** v. 4, n. 7, p. 515-7, Oct 2003. ISSN 1466-4879. Disponível em: < http://www.ncbi.nlm.nih.gov/pubmed/14551605 >.

101 YAMAMOTO, M. et al. Quantification of activated and total caspase-14 with newly developed ELISA systems in normal and atopic skin. **J Dermatol Sci,** v. 61, n. 2, p. 110-7, Feb 2011. ISSN 1873-569X. Disponível em: < http://www.ncbi.nlm.nih.gov/pubmed/21183321 >.

102 TATTI, M. et al. Cathepsin-mediated regulation of autophagy in saposin C deficiency. **Autophagy,** v. 9, n. 2, p. 241-3, Feb 2013. ISSN 1554-8635. Disponível em: < http://www.ncbi.nlm.nih.gov/pubmed/23108186 >.

103 GOPALAKRISHNAN, M. M. et al. Purified recombinant human prosaposin forms oligomers that bind procathepsin D and affect its autoactivation. **Biochem J,** v. 383, n. Pt. 3, p. 507-15, Nov 2004. ISSN 1470-8728. Disponível em: < http://www.ncbi.nlm.nih.gov/pubmed/15255780 >.

104 TATTI, M. et al. Reduced cathepsins B and D cause impaired autophagic degradation that can be almost completely restored by overexpression of these two proteases in Sap C-deficient fibroblasts. **Hum Mol Genet,** v. 21, n. 23, p. 5159-73, Dec 2012. ISSN 1460-2083. Disponível em: < http://www.ncbi.nlm.nih.gov/pubmed/22949512 >.

105 HIRAIWA, M. et al. Lysosomal proteolysis of prosaposin, the precursor of saposins (sphingolipid activator proteins): its mechanism and inhibition by ganglioside. **Arch Biochem Biophys,** v. 341, n. 1, p. 17-24, May 1997. ISSN 0003-9861. Disponível em: < http://www.ncbi.nlm.nih.gov/pubmed/9143348 >.

106 KIM, H. Y. et al. Cathepsin D levels are reduced in patients with preeclampsia in Korean population. **Clin Biochem,** v. 46, n. 18, p. 1808-11, Dec 2013. ISSN 1873-2933. Disponível em: < http://www.ncbi.nlm.nih.gov/pubmed/23954850 >.

107 ACHOUR, O. et al. Cathepsin D activity and selectivity in the acidic conditions of a tumor microenvironment: Utilization in the development of a novel Cathepsin D substrate for simultaneous cancer diagnosis and therapy. **Biochimie,** v. 95, n. 11, p. 2010-7, Nov 2013. ISSN 1638-6183. Disponível em: < http://www.ncbi.nlm.nih.gov/pubmed/23871913 >.

108 ZHU, L. et al. Overexpression of cathepsin D in malignant melanoma. **Fukuoka Igaku Zasshi,** v. 104, n. 10, p. 370-5, Oct 2013. ISSN 0016-254X. Disponível em: < http://www.ncbi.nlm.nih.gov/pubmed/24511668 >.

109 MARKIĆEVIĆ, M. et al. Cathepsin D as an indicator of clinical outcome in early breast carcinoma during the first 3 years of follow-up. **Biomark Med,** v. 7, n. 5, p. 747-58, Oct 2013. ISSN 1752-0371. Disponível em: < http://www.ncbi.nlm.nih.gov/pubmed/24044567 >.

110 PARK, H. D. et al. Serum CA19-9, cathepsin D, and matrix metalloproteinase-7 as a diagnostic panel for pancreatic ductal adenocarcinoma. **Proteomics,** v. 12, n. 23-24, p. 3590-7, Dec 2012. ISSN 1615-9861. Disponível em: < http://www.ncbi.nlm.nih.gov/pubmed/23065739 >.

111 ZHENG, Y. et al. Expression of cathepsins in human skin photoaging. **Skin Pharmacol Physiol,** v. 24, n. 1, p. 10-21, 2011. ISSN 1660-5535. Disponível em: < http://www.ncbi.nlm.nih.gov/pubmed/20588086 >.

112 ROZHIN, J. et al. Pericellular pH affects distribution and secretion of cathepsin B in malignant cells. **Cancer Res,** v. 54, n. 24, p. 6517-25, Dec 1994. ISSN 0008-5472. Disponível em: < http://www.ncbi.nlm.nih.gov/pubmed/7987851 >.

113 LUEBBERDING, S.; KRUEGER, N.; KERSCHER, M. Skin physiology in men and women: in vivo evaluation of 300 people including TEWL, SC hydration, sebum content and skin surface pH. **Int J Cosmet Sci,** v. 35, n. 5, p. 477-83, Oct 2013. ISSN 1468-2494. Disponível em: < http://www.ncbi.nlm.nih.gov/pubmed/23713991 >.

114 Severity scoring of atopic dermatitis: the SCORAD index. Consensus Report of the European Task Force on Atopic Dermatitis. **Dermatology,** v. 186, n. 1, p. 23-31, 1993. ISSN 1018-8665. Disponível em: < http://www.ncbi.nlm.nih.gov/pubmed/8435513 >.

115 RIPPKE, F. et al. Stratum corneum pH in atopic dermatitis: impact on skin barrier function and colonization with Staphylococcus Aureus. **Am J Clin Dermatol,** v. 5, n. 4, p. 217-23, 2004. ISSN 1175-0561. Disponível em: < http://www.ncbi.nlm.nih.gov/pubmed/15301569 >.

116 LEE MOTOYAMA, J. P. et al. Identification of dermcidin in human gestational tissue and characterization of its proteolytic activity. **Biochem Biophys Res Commun,** v. 357, n. 4, p. 828-33, Jun 2007. ISSN 0006-291X. Disponível em: < http://www.ncbi.nlm.nih.gov/pubmed/17448443 >.

117 SCHITTEK, B. The multiple facets of dermcidin in cell survival and host defense. **J Innate Immun,** v. 4, n. 4, p. 349-60, 2012. ISSN 1662-8128. Disponível em: < http://www.ncbi.nlm.nih.gov/pubmed/22455996 >.

118 POWERS, J. C. et al. Proteases--structures, mechanism and inhibitors. **Agents Actions Suppl,** v. 42, p. 3-18, 1993. ISSN 0379-0363. Disponível em: < http://www.ncbi.nlm.nih.gov/pubmed/8356929 >.

119 SON, D. N. et al. Abundant expression of Kallikrein 1 gene in human keratinocytes was mediated by GATA3. **Gene,** v. 436, n. 1-2, p. 121-7, May 2009. ISSN 1879-0038. Disponível em: < http://www.ncbi.nlm.nih.gov/pubmed/19232384 >.

120 BAYANI, J.; DIAMANDIS, E. P. The physiology and pathobiology of human kallikrein-related peptidase 6 (KLK6). **Clin Chem Lab Med,** v. 50, n. 2, p. 211-33, Feb 2012. ISSN 1437-4331. Disponível em: < http://www.ncbi.nlm.nih.gov/pubmed/22047144 >.

121 EISSA, A. et al. Kallikrein-related peptidase-8 (KLK8) is an active serine protease in human epidermis and sweat and is involved in a skin barrier proteolytic cascade. **J Biol Chem,** v. 286, n. 1, p. 687-706, Jan 2011. ISSN 1083-351X. Disponível em: < http://www.ncbi.nlm.nih.gov/pubmed/20940292 >.

122 KOMATSU, N. et al. Expression and localization of tissue kallikrein mRNAs in human epidermis and appendages. **J Invest Dermatol,** v. 121, n. 3, p. 542-9, Sep 2003. ISSN 0022-202X. Disponível em: < http://www.ncbi.nlm.nih.gov/pubmed/12925213 >.

123 EMAMI, N.; DIAMANDIS, E. P. Human kallikrein-related peptidase 14 (KLK14) is a new activator component of the KLK proteolytic cascade. Possible function in seminal plasma and skin. **J Biol Chem,** v. 283, n. 6, p. 3031-41, Feb 2008. ISSN 0021-9258. Disponível em: < http://www.ncbi.nlm.nih.gov/pubmed/18056261 >.

124 KOSHIKAWA, N. et al. Expression of trypsin by epithelial cells of various tissues, leukocytes, and neurons in human and mouse. **Am J Pathol,** v. 153, n. 3, p. 937-44, Sep 1998. ISSN 0002-9440. Disponível em: < http://www.ncbi.nlm.nih.gov/pubmed/9736042 >.

125 BONNART, C. et al. Elastase 2 is expressed in human and mouse epidermis and impairs skin barrier function in Netherton syndrome through filaggrin and lipid misprocessing. **J Clin Invest,** v. 120, n. 3, p. 871-82, Mar 2010. ISSN 1558-8238. Disponível em: < http://www.ncbi.nlm.nih.gov/pubmed/20179351 >.

126 HALD, A. et al. Plasmin-driven fibrinolysis facilitates skin tumor growth in a gender-dependent manner. **FASEB J,** v. 26, n. 11, p. 4445-57, Nov 2012. ISSN 1530-6860. Disponível em: < http://www.ncbi.nlm.nih.gov/pubmed/22815383 >.

127 DONG, K. K. et al. UV-induced DNA damage initiates release of MMP-1 in human skin. **Exp Dermatol,** v. 17, n. 12, p. 1037-44, Dec 2008. ISSN 1600-0625. Disponível em: < http://www.ncbi.nlm.nih.gov/pubmed/18459971 >.

128 FRØSSING, S. et al. Skin wound healing in MMP2-deficient and MMP2 / plasminogen double-deficient mice. **Exp Dermatol,** v. 19, n. 8, p. e234-40, Aug 2010. ISSN 1600-0625. Disponível em: < http://www.ncbi.nlm.nih.gov/pubmed/20163454 >.

129 MCCAWLEY, L. J. et al. Keratinocyte expression of MMP3 enhances differentiation and prevents tumor establishment. **Am J Pathol,** v. 173, n. 5, p. 1528-39, Nov 2008. ISSN 1525-2191. Disponível em: < http://www.ncbi.nlm.nih.gov/pubmed/18832569 >.

130 BALBÍN, M. et al. Loss of collagenase-2 confers increased skin tumor susceptibility to male mice. **Nat Genet,** v. 35, n. 3, p. 252-7, Nov 2003. ISSN 1061-4036. Disponível em: < http://www.ncbi.nlm.nih.gov/pubmed/14517555 >.

131 THEWES, M. et al. Stromelysin-3 (ST-3): immunohistochemical characterization of the matrix metalloproteinase (MMP)-11 in benign and malignant skin tumours and other skin disorders. **Clin Exp Dermatol,** v. 24, n. 2, p. 122-6, Mar 1999. ISSN 0307-6938. Disponível em: < http://www.ncbi.nlm.nih.gov/pubmed/10233668 >.

132 VAALAMO, M. et al. Enhanced expression of human metalloelastase (MMP-12) in cutaneous granulomas and macrophage migration. **J Invest Dermatol,** v. 112, n. 4, p. 499-505, Apr 1999. ISSN 0022-202X. Disponível em: < http://www.ncbi.nlm.nih.gov/pubmed/10201535 >.

133 HATTORI, N. et al. MMP-13 plays a role in keratinocyte migration, angiogenesis, and contraction in mouse skin wound healing. **Am J Pathol,** v. 175, n. 2, p. 533-46, Aug 2009. ISSN 1525-2191. Disponível em: < http://www.ncbi.nlm.nih.gov/pubmed/19590036 >.

134 RODGERS, U. R. et al. Expression and function of matrix metalloproteinase (MMP)-28. **Matrix Biol,** v. 28, n. 5, p. 263-72, Jun 2009. ISSN 1569-1802. Disponível em: < http://www.ncbi.nlm.nih.gov/pubmed/19375502 >.

135 KRENGEL, S. et al. MMP-2, TIMP-2 and MT1-MMP are differentially expressed in lesional skin of melanocytic nevi and their expression is modulated by UVB-light. **J Cutan Pathol,** v. 29, n. 7, p. 390-6, Aug 2002. ISSN 0303-6987. Disponível em: < http://www.ncbi.nlm.nih.gov/pubmed/12139633 >.

136 OHNISHI, Y.; TAJIMA, S.; ISHIBASHI, A. Coordinate expression of membrane type-matrix metalloproteinases-2 and 3 (MT2-MMP and MT3-MMP) and matrix metalloproteinase-2 (MMP-2) in primary and metastatic melanoma cells. **Eur J Dermatol,** v. 11, n. 5, p. 420-3, 2001 Sep-Oct 2001. ISSN 1167-1122. Disponível em: < http://www.ncbi.nlm.nih.gov/pubmed/11525948 >.

137 TATTI, O. et al. Membrane-type-3 matrix metalloproteinase (MT3-MMP) functions as a matrix composition-dependent effector of melanoma cell invasion. **PLoS One,** v. 6, n. 12, p. e28325, 2011. ISSN 1932-6203. Disponível em: < http://www.ncbi.nlm.nih.gov/pubmed/22164270 >.

138 EGBERTS, F. et al. Cathepsin D is involved in the regulation of transglutaminase 1 and epidermal differentiation. **J Cell Sci,** v. 117, n. Pt 11, p. 2295-307, May 2004. ISSN 0021-9533. Disponível em: < http://www.ncbi.nlm.nih.gov/pubmed/15126630 >.

139 TSUKUBA, T. et al. Association of cathepsin E deficiency with development of atopic dermatitis. **J Biochem,** v. 134, n. 6, p. 893-902, Dec 2003. ISSN 0021-924X. Disponível em: < http://www.ncbi.nlm.nih.gov/pubmed/14769879 >.

140 BERNARD, D. et al. Identification and characterization of a novel retroviral-like aspartic protease specifically expressed in human epidermis. **J Invest Dermatol,** v. 125, n. 2, p. 278-87, Aug 2005. ISSN 0022-202X. Disponível em: < http://www.ncbi.nlm.nih.gov/pubmed/16098038 >.

141 IKEDA, K. et al. The expression of presenilin 1 mRNA in skin fibroblasts and brains from sporadic Alzheimer's disease. **Dement Geriatr Cogn Disord,** v. 11, n. 5, p. 245-50, 2000 Sep-Oct 2000. ISSN 1420-8008. Disponível em: < http://www.ncbi.nlm.nih.gov/pubmed/10940675 >.

142 BENAVIDES, F. et al. Protective role of cathepsin L in mouse skin carcinogenesis. **Mol Carcinog,** v. 51, n. 4, p. 352-61, Apr 2012. ISSN 1098-2744. Disponível em: < http://www.ncbi.nlm.nih.gov/pubmed/21538579 >.

143 RINNE, A. et al. Localization of cathepsin H and its inhibitor in the skin and other stratified epithelia. **Arch Dermatol Res,** v. 277, n. 3, p. 190-4, 1985. ISSN 0340-3696. Disponível em: < http://www.ncbi.nlm.nih.gov/pubmed/3848316 >.

144 HIRAI, T. et al. Cathepsin K is involved in development of psoriasis-like skin lesions through TLR-dependent Th17 activation. **J Immunol,** v. 190, n. 9, p. 4805-11, May 2013. ISSN 1550-6606. Disponível em: < http://www.ncbi.nlm.nih.gov/pubmed/23543761 >.

145 ZEEUWEN, P. L. et al. Evidence that unrestricted legumain activity is involved in disturbed epidermal cornification in cystatin M/E deficient mice. **Hum Mol Genet,** v. 13, n. 10, p. 1069-79, May 2004. ISSN 0964-6906. Disponível em: < http://www.ncbi.nlm.nih.gov/pubmed/15044380 >.

146 LIANG, D. Y. et al. Caspase-1 modulates incisional sensitization and inflammation. **Anesthesiology,** v. 113, n. 4, p. 945-56, Oct 2010. ISSN 1528-1175. Disponível em: < http://www.ncbi.nlm.nih.gov/pubmed/20823759 >.

147 SIMON, D. et al. Epidermal caspase-3 cleavage associated with interferon-gamma-expressing lymphocytes in acute atopic dermatitis lesions. **Exp Dermatol,** v. 15, n. 6, p. 441-6, Jun 2006. ISSN 0906-6705. Disponível em: < http://www.ncbi.nlm.nih.gov/pubmed/16689860 >.

148 SOLLBERGER, G. et al. Caspase-4 is required for activation of inflammasomes. **J Immunol,** v. 188, n. 4, p. 1992-2000, Feb 2012. ISSN 1550-6606. Disponível em: < http://www.ncbi.nlm.nih.gov/pubmed/22246630 >.

149 SALSKOV-IVERSEN, M. L. et al. Caspase-5 expression is upregulated in lesional psoriatic skin. **J Invest Dermatol,** v. 131, n. 3, p. 670-6, Mar 2011. ISSN 1523-1747. Disponível em: < http://www.ncbi.nlm.nih.gov/pubmed/21191419 >.

150 PENG, X.; GUAN, D. W.; WANG, Q. [A study on the time-dependent expression of caspase-6 during repair of skin contusion in rats]. **Fa Yi Xue Za Zhi,** v. 23, n. 5, p. 325-7, 331, Oct 2007. ISSN 1004-5619. Disponível em: < http://www.ncbi.nlm.nih.gov/pubmed/18175566 >.

151 CARTER, R.; SYKES, V.; LANNING, D. Scarless fetal mouse wound healing may initiate apoptosis through caspase 7 and cleavage of PARP. **J Surg Res,** v. 156, n. 1, p. 74-9, Sep 2009. ISSN 1095-8673. Disponível em: < http://www.ncbi.nlm.nih.gov/pubmed/19555972 >.

152 KOVALENKO, A. et al. Caspase-8 deficiency in epidermal keratinocytes triggers an inflammatory skin disease. **J Exp Med,** v. 206, n. 10, p. 2161-77, Sep 2009. ISSN 1540-9538. Disponível em: < http://www.ncbi.nlm.nih.gov/pubmed/19720838 >.

153 DE VEER, S. J. et al. Proteases: common culprits in human skin disorders. **Trends Mol Med,** v. 20, n. 3, p. 166-78, Mar 2014. ISSN 1471-499X. Disponível em: < http://www.ncbi.nlm.nih.gov/pubmed/24380647 >.

154 THOLEN, S. et al. Deletion of cysteine cathepsins B or L yields differential impacts on murine skin proteome and degradome. **Mol Cell Proteomics,** v. 12, n. 3, p. 611-25, Mar 2013. ISSN 1535-9484. Disponível em: < http://www.ncbi.nlm.nih.gov/pubmed/23233448 >.

155 RAWLINGS, A. V.; VOEGELI, R. Stratum corneum proteases and dry skin conditions. **Cell Tissue Res,** v. 351, n. 2, p. 217-35, Feb 2013. ISSN 1432-0878. Disponível em: < http://www.ncbi.nlm.nih.gov/pubmed/23053051 >.

156 BORGOÑO, C. A. et al. A potential role for multiple tissue kallikrein serine proteases in epidermal desquamation. **J Biol Chem,** v. 282, n. 6, p. 3640-52, Feb 2007. ISSN 0021-9258. Disponível em: < http://www.ncbi.nlm.nih.gov/pubmed/17158887 >.

157 NETZEL-ARNETT, S. et al. Evidence for a matriptase-prostasin proteolytic cascade regulating terminal epidermal differentiation. **J Biol Chem,** v. 281, n. 44, p. 32941-5, Nov 2006. ISSN 0021-9258. Disponível em: < http://www.ncbi.nlm.nih.gov/pubmed/16980306 >.

158 ZEEUWEN, P. L. et al. The cystatin M/E-cathepsin L balance is essential for tissue homeostasis in epidermis, hair follicles, and cornea. **FASEB J,** v. 24, n. 10, p. 3744-55, Oct 2010. ISSN 1530-6860. Disponível em: < http://www.ncbi.nlm.nih.gov/pubmed/20495178 >.

159 WEBER, S. et al. The disintegrin/metalloproteinase Adam10 is essential for epidermal integrity and Notch-mediated signaling. **Development,** v. 138, n. 3, p. 495-505, Feb 2011. ISSN 1477-9129. Disponível em: < http://www.ncbi.nlm.nih.gov/pubmed/21205794 >.

160 MARETZKY, T. et al. ADAM10 mediates E-cadherin shedding and regulates epithelial cell-cell adhesion, migration, and beta-catenin translocation. **Proc Natl Acad Sci U S A,** v. 102, n. 26, p. 9182-7, Jun 2005. ISSN 0027-8424. Disponível em: < http://www.ncbi.nlm.nih.gov/pubmed/15958533 >.

161 SAHIN, U. et al. Distinct roles for ADAM10 and ADAM17 in ectodomain shedding of six EGFR ligands. **J Cell Biol,** v. 164, n. 5, p. 769-79, Mar 2004. ISSN 0021-9525. Disponível em: < http://www.ncbi.nlm.nih.gov/pubmed/14993236 >.

162 FRANZKE, C. W. et al. Epidermal ADAM17 maintains the skin barrier by regulating EGFR ligand-dependent terminal keratinocyte differentiation. **J Exp Med,** v. 209, n. 6, p. 1105-19, Jun 2012. ISSN 1540-9538. Disponível em: < http://www.ncbi.nlm.nih.gov/pubmed/22565824 >.

163 MARETZKY, T. et al. iRhom2 controls the substrate selectivity of stimulated ADAM17-dependent ectodomain shedding. **Proc Natl Acad Sci U S A,** v. 110, n. 28, p. 11433-8, Jul 2013. ISSN 1091-6490. Disponível em: < http://www.ncbi.nlm.nih.gov/pubmed/23801765 >.

164 DENNEMÄRKER, J. et al. Deficiency for the cysteine protease cathepsin L promotes tumor progression in mouse epidermis. **Oncogene,** v. 29, n. 11, p. 1611-21, Mar 2010. ISSN 1476-5594. Disponível em: < http://www.ncbi.nlm.nih.gov/pubmed/20023699 >.

165 DERAISON, C. et al. LEKTI fragments specifically inhibit KLK5, KLK7, and KLK14 and control desquamation through a pH-dependent interaction. **Mol Biol Cell,** v. 18, n. 9, p. 3607-19, Sep 2007. ISSN 1059-1524. Disponível em: < http://www.ncbi.nlm.nih.gov/pubmed/17596512 >.

166 WALRAVEN, M.; BEELEN, R. H.; ULRICH, M. M. Transforming growth factor-β (TGF-β) signaling in healthy human fetal skin: a descriptive study. **J Dermatol Sci,** v. 78, n. 2, p. 117-24, May 2015. ISSN 1873-569X. Disponível em: < http://www.ncbi.nlm.nih.gov/pubmed/25795202 >.

167 KONO, M. et al. Whole-exome sequencing identifies ADAM10 mutations as a cause of reticulate acropigmentation of Kitamura, a clinical entity distinct from Dowling-Degos disease. **Hum Mol Genet,** v. 22, n. 17, p. 3524-33, Sep 2013. ISSN 1460-2083. Disponível em: < http://www.ncbi.nlm.nih.gov/pubmed/23666529 >.

168 VASUDEVAN, B. et al. A case of reticulate acropigmentation of kitamura: dowling degos disease overlap with unusual clinical manifestations. **Indian J Dermatol,** v. 59, n. 3, p. 290-2, May 2014. ISSN 1998-3611. Disponível em: < http://www.ncbi.nlm.nih.gov/pubmed/24891663 >.

169 GRIFFITHS, W. A. Reticulate acropigmentation of Kitamura. **Br J Dermatol,** v. 95, n. 4, p. 437-43, Oct 1976. ISSN 0007-0963. Disponível em: < http://www.ncbi.nlm.nih.gov/pubmed/823955 >.

170 BLAYDON, D. C. et al. Inflammatory skin and bowel disease linked to ADAM17 deletion. **N Engl J Med,** v. 365, n. 16, p. 1502-8, Oct 2011. ISSN 1533-4406. Disponível em: < http://www.ncbi.nlm.nih.gov/pubmed/22010916 >.

171 PESCHON, J. J. et al. An essential role for ectodomain shedding in mammalian development. **Science,** v. 282, n. 5392, p. 1281-4, Nov 1998. ISSN 0036-8075. Disponível em: < http://www.ncbi.nlm.nih.gov/pubmed/9812885 >.

172 TOOMES, C. et al. Loss-of-function mutations in the cathepsin C gene result in periodontal disease and palmoplantar keratosis. **Nat Genet,** v. 23, n. 4, p. 421-4, Dec 1999. ISSN 1061-4036. Disponível em: < http://www.ncbi.nlm.nih.gov/pubmed/10581027 >.

173 RAO, N. V.; RAO, G. V.; HOIDAL, J. R. Human dipeptidyl-peptidase I. Gene characterization, localization, and expression. **J Biol Chem,** v. 272, n. 15, p. 10260-5, Apr 1997. ISSN 0021-9258. Disponível em: < http://www.ncbi.nlm.nih.gov/pubmed/9092576 >.

174 PALMER, C. N. et al. Common loss-of-function variants of the epidermal barrier protein filaggrin are a major predisposing factor for atopic dermatitis. **Nat Genet,** v. 38, n. 4, p. 441-6, Apr 2006. ISSN 1061-4036. Disponível em: < http://www.ncbi.nlm.nih.gov/pubmed/16550169 >.

175 KATO, T. et al. Cystatin A inhibits IL-8 production by keratinocytes stimulated with Der p 1 and Der f 1: biochemical skin barrier against mite cysteine proteases. **J Allergy Clin Immunol,** v. 116, n. 1, p. 169-76, Jul 2005. ISSN 0091-6749. Disponível em: < http://www.ncbi.nlm.nih.gov/pubmed/15990791 >.

176 CHENG, T. et al. Cystatin M/E is a high affinity inhibitor of cathepsin V and cathepsin L by a reactive site that is distinct from the legumain-binding site. A novel clue for the role of cystatin M/E in epidermal cornification. **J Biol Chem,** v. 281, n. 23, p. 15893-9, Jun 2006. ISSN 0021-9258. Disponível em: < http://www.ncbi.nlm.nih.gov/pubmed/16565075 >.

177 BLAYDON, D. C. et al. Mutations in CSTA, encoding Cystatin A, underlie exfoliative ichthyosis and reveal a role for this protease inhibitor in cell-cell adhesion. **Am J Hum Genet,** v. 89, n. 4, p. 564-71, Oct 2011. ISSN 1537-6605. Disponível em: < http://www.ncbi.nlm.nih.gov/pubmed/21944047 >.

178 KRUNIC, A. L. et al. Acral peeling skin syndrome resulting from a homozygous nonsense mutation in the CSTA gene encoding cystatin A. **Pediatr Dermatol,** v. 30, n. 5, p. e87-8, 2013 Sep-Oct 2013. ISSN 1525-1470. Disponível em: < http://www.ncbi.nlm.nih.gov/pubmed/23534700 >.

179 YANG, T. et al. Epidermal detachment, desmosomal dissociation, and destabilization of corneodesmosin in Spink5-/- mice. **Genes Dev,** v. 18, n. 19, p. 2354-8, Oct 2004. ISSN 0890-9369. Disponível em: < http://www.ncbi.nlm.nih.gov/pubmed/15466487 >.

180 DESCARGUES, P. et al. Spink5-deficient mice mimic Netherton syndrome through degradation of desmoglein 1 by epidermal protease hyperactivity. **Nat Genet,** v. 37, n. 1, p. 56-65, Jan 2005. ISSN 1061-4036. Disponível em: < http://www.ncbi.nlm.nih.gov/pubmed/15619623 >.

181 DEMENTIEV, A.; DOBÓ, J.; GETTINS, P. G. Active site distortion is sufficient for proteinase inhibition by serpins: structure of the covalent complex of alpha1-proteinase

inhibitor with porcine pancreatic elastase. **J Biol Chem,** v. 281, n. 6, p. 3452-7, Feb 2006. ISSN 0021-9258. Disponível em: < http://www.ncbi.nlm.nih.gov/pubmed/16321984 >.

182 PUBMED. PubMed - NCBI search for "suprabasin[Title]". p. http://www.ncbi.nlm.nih.gov/pubmed/?term=suprabasin%5BTitle%5D&cmd=DetailsSearch, 2016. Acesso em: 16/06/2016.

183 PARK, G. T. et al. Suprabasin, a novel epidermal differentiation marker and potential cornified envelope precursor. **J Biol Chem,** v. 277, n. 47, p. 45195-202, Nov 2002. ISSN 0021-9258. Disponível em: < http://www.ncbi.nlm.nih.gov/pubmed/12228223 >.

184 SHAO, C. et al. Suprabasin is hypomethylated and associated with metastasis in salivary adenoid cystic carcinoma. **PLoS One,** v. 7, n. 11, p. e48582, 2012. ISSN 1932-6203. Disponível em: < http://www.ncbi.nlm.nih.gov/pubmed/23144906 >.

185 ALAM, M. T. et al. Suprabasin as a novel tumor endothelial cell marker. **Cancer Sci,** v. 105, n. 12, p. 1533-40, Dec 2014. ISSN 1349-7006. Disponível em: < http://www.ncbi.nlm.nih.gov/pubmed/25283635 >.

186 ZHU, J. et al. Overexpression of Suprabasin is Associated with Proliferation and Tumorigenicity of Esophageal Squamous Cell Carcinoma. **Sci Rep,** v. 6, p. 21549, 2016. ISSN 2045-2322. Disponível em: < http://www.ncbi.nlm.nih.gov/pubmed/26899563 >.

187 KENAGY, R. D. et al. Scavenger receptor class A member 5 (SCARA5) and suprabasin (SBSN) are hub genes of coexpression network modules associated with peripheral vein graft patency. **J Vasc Surg**, Apr 2015. ISSN 1097-6809. Disponível em: < http://www.ncbi.nlm.nih.gov/pubmed/25935274 >.

188 UNIPROT. Alignment. 2016. Disponível em: < http://www.uniprot.org/align/A201603149C9P4AT15H >. Acesso em: 14/03/2016.

189 ZHOU, M. et al. An investigation into the human serum "interactome". **Electrophoresis,** v. 25, n. 9, p. 1289-98, May 2004. ISSN 0173-0835. Disponível em: < http://www.ncbi.nlm.nih.gov/pubmed/15174051 >.

190 CARUSO, J. A. et al. The serine protease inhibitor elafin maintains normal growth control by opposing the mitogenic effects of neutrophil elastase. **Oncogene,** v. 34, n. 27, p. 3556-67, Jul 2015. ISSN 1476-5594. Disponível em: < http://www.ncbi.nlm.nih.gov/pubmed/25195861 >.

191 LIM, J. et al. A protein-protein interaction network for human inherited ataxias and disorders of Purkinje cell degeneration. **Cell,** v. 125, n. 4, p. 801-14, May 2006. ISSN 0092-8674. Disponível em: < http://www.ncbi.nlm.nih.gov/pubmed/16713569 >.

192 ECKHART, L. et al. Terminal differentiation of human keratinocytes and stratum corneum formation is associated with caspase-14 activation. **J Invest Dermatol,** v. 115, n. 6, p. 1148-51, Dec 2000. ISSN 0022-202X. Disponível em: < http://www.ncbi.nlm.nih.gov/pubmed/11121154 >.

193 WALSH, D. S. et al. Psoriasis is characterized by altered epidermal expression of caspase 14, a novel regulator of keratinocyte terminal differentiation and barrier formation. **J Dermatol Sci,** v. 37, n. 1, p. 61-3, Jan 2005. ISSN 0923-1811. Disponível em: < http://www.ncbi.nlm.nih.gov/pubmed/15619438 >.

194 WOLF, R.; RUZICKA, T.; YUSPA, S. H. Novel S100A7 (psoriasin)/S100A15 (koebnerisin) subfamily: highly homologous but distinct in regulation and function. **Amino Acids,** v. 41, n. 4, p. 789-96, Oct 2011. ISSN 1438-2199. Disponível em: < https://www.ncbi.nlm.nih.gov/pubmed/20596736 >.

195 CHEN, L. M. et al. Differential interactions of human kallikrein-binding protein and alpha 1-antitrypsin with human tissue kallikrein. **Biochem J,** v. 267, n. 1, p. 79-84, Apr 1990. ISSN 0264-6021. Disponível em: < http://www.ncbi.nlm.nih.gov/pubmed/2327990 >.

196 OVAERE, P. et al. The emerging roles of serine protease cascades in the epidermis. **Trends Biochem Sci,** v. 34, n. 9, p. 453-63, Sep 2009. ISSN 0968-0004. Disponível em: < http://www.ncbi.nlm.nih.gov/pubmed/19726197 >.

197 BRÜGGEN, M. C. et al. Epidermal elafin expression is an indicator of poor prognosis in cutaneous graft-versus-host disease. **J Invest Dermatol,** v. 135, n. 4, p. 999-1006, Apr 2015. ISSN 1523-1747. Disponível em: < http://www.ncbi.nlm.nih.gov/pubmed/25405322 >.

198 WIEDOW, O. et al. Elafin: an elastase-specific inhibitor of human skin. Purification, characterization, and complete amino acid sequence. **J Biol Chem,** v. 265, n. 25, p. 14791-5, Sep 1990. ISSN 0021-9258. Disponível em: < http://www.ncbi.nlm.nih.gov/pubmed/2394696 >.

199 KORKMAZ, B.; MOREAU, T.; GAUTHIER, F. Neutrophil elastase, proteinase 3 and cathepsin G: physicochemical properties, activity and physiopathological functions. **Biochimie,** v. 90, n. 2, p. 227-42, Feb 2008. ISSN 0300-9084. Disponível em: < http://www.ncbi.nlm.nih.gov/pubmed/18021746 >.

200 SIMPSON, A. J. et al. Adenoviral augmentation of elafin protects the lung against acute injury mediated by activated neutrophils and bacterial infection. **J Immunol,** v. 167, n. 3, p. 1778-86, Aug 2001. ISSN 0022-1767. Disponível em: < http://www.ncbi.nlm.nih.gov/pubmed/11466403 >.

201 IQBAL, S. M. et al. Elevated elafin/trappin-2 in the female genital tract is associated with protection against HIV acquisition. **AIDS,** v. 23, n. 13, p. 1669-77, Aug 2009. ISSN 1473-5571. Disponível em: < http://www.ncbi.nlm.nih.gov/pubmed/19553806 >.

202 SIMPSON, A. J. et al. Elafin (elastase-specific inhibitor) has anti-microbial activity against gram-positive and gram-negative respiratory pathogens. **FEBS Lett,** v. 452, n. 3, p. 309-13, Jun 1999. ISSN 0014-5793. Disponível em: < http://www.ncbi.nlm.nih.gov/pubmed/10386612 >.

203 WILKINSON, T. S. et al. Trappin-2 promotes early clearance of Pseudomonas aeruginosa through CD14-dependent macrophage activation and neutrophil

recruitment. **Am J Pathol,** v. 174, n. 4, p. 1338-46, Apr 2009. ISSN 1525-2191. Disponível em: < http://www.ncbi.nlm.nih.gov/pubmed/19264904 >.

204 BARANGER, K. et al. The antibacterial and antifungal properties of trappin-2 (pre-elafin) do not depend on its protease inhibitory function. **FEBS J,** v. 275, n. 9, p. 2008-20, May 2008. ISSN 1742-464X. Disponível em: < http://www.ncbi.nlm.nih.gov/pubmed/18341586 >.

205 SANDILANDS, A. et al. Filaggrin in the frontline: role in skin barrier function and disease. **J Cell Sci,** v. 122, n. Pt 9, p. 1285-94, May 2009. ISSN 0021-9533. Disponível em: < http://www.ncbi.nlm.nih.gov/pubmed/19386895 >.

206 RIEG, S. et al. Dermcidin is constitutively produced by eccrine sweat glands and is not induced in epidermal cells under inflammatory skin conditions. **Br J Dermatol,** v. 151, n. 3, p. 534-9, Sep 2004. ISSN 0007-0963. Disponível em: < http://www.ncbi.nlm.nih.gov/pubmed/15377337 >.

207 SCHITTEK, B. et al. Dermcidin: a novel human antibiotic peptide secreted by sweat glands. **Nat Immunol,** v. 2, n. 12, p. 1133-7, Dec 2001. ISSN 1529-2908. Disponível em: < http://www.ncbi.nlm.nih.gov/pubmed/11694882 >.

208 NIYONSABA, F. et al. The human antimicrobial peptide dermcidin activates normal human keratinocytes. **Br J Dermatol,** v. 160, n. 2, p. 243-9, Feb 2009. ISSN 1365-2133. Disponível em: < http://www.ncbi.nlm.nih.gov/pubmed/19014393 >.

209 RIEG, S. et al. Deficiency of dermcidin-derived antimicrobial peptides in sweat of patients with atopic dermatitis correlates with an impaired innate defense of human skin in vivo. **J Immunol,** v. 174, n. 12, p. 8003-10, Jun 2005. ISSN 0022-1767. Disponível em: < http://www.ncbi.nlm.nih.gov/pubmed/15944307 >.

210 PUBMED. PubMed Search: ("cystatin a"[Title] AND "atopic dermatitis"[Title]). PubMed.gov, p. http://www.ncbi.nlm.nih.gov/pubmed/?term=(%22cystatin%20a%22%5BTitle%5D%20AND%20%22atopic%20dermatitis%22%5BTitle%5D)&cmd=DetailsSearch, 2016. Acesso em: 19/06/2016.

211 VASILOPOULOS, Y. et al. A nonsynonymous substitution of cystatin A, a cysteine protease inhibitor of house dust mite protease, leads to decreased mRNA stability and shows a significant association with atopic dermatitis. **Allergy,** v. 62, n. 5, p. 514-9, May 2007. ISSN 0105-4538. Disponível em: < http://www.ncbi.nlm.nih.gov/pubmed/17441792 >.

212 FOLCH, J.; LEES, M.; SLOANE STANLEY, G. H. A simple method for the isolation and purification of total lipides from animal tissues. **J Biol Chem,** v. 226, n. 1, p. 497-509, May 1957. ISSN 0021-9258. Disponível em: < http://www.ncbi.nlm.nih.gov/pubmed/13428781 >.

213 MALÁKOVÁ, J. et al. High-performance liquid chromatographic method with UV photodiode-array, fluorescence and mass spectrometric detection for simultaneous determination of galantamine and its phase I metabolites in biological samples. **J**

Chromatogr B Analyt Technol Biomed Life Sci, v. 853, n. 1-2, p. 265-74, Jun 2007. ISSN 1570-0232. Disponível em: < http://www.ncbi.nlm.nih.gov/pubmed/17416214 >.

214 LEROY, P. et al. Determination of josamycin residues in porcine tissues using high-performance liquid chromatography with pre-column derivatization and spectrofluorimetric detection. **Analyst,** v. 119, n. 12, p. 2743-7, Dec 1994. ISSN 0003-2654. Disponível em: < http://www.ncbi.nlm.nih.gov/pubmed/7879887 >.

215 SHLIAHA, P. V. et al. Effects of traveling wave ion mobility separation on data independent acquisition in proteomics studies. **J Proteome Res,** v. 12, n. 6, p. 2323-39, Jun 2013. ISSN 1535-3907. Disponível em: < http://www.ncbi.nlm.nih.gov/pubmed/23514362 >.

216 BLONDER, J. et al. A detergent- and cyanogen bromide-free method for integral membrane proteomics: application to Halobacterium purple membranes and the human epidermal membrane proteome. **Proteomics,** v. 4, n. 1, p. 31-45, Jan 2004. ISSN 1615-9853. Disponível em: < http://www.ncbi.nlm.nih.gov/pubmed/14730670 >.

217 _____. A proteomic characterization of the plasma membrane of human epidermis by high-throughput mass spectrometry. **J Invest Dermatol,** v. 123, n. 4, p. 691-9, Oct 2004. ISSN 0022-202X. Disponível em: < http://www.ncbi.nlm.nih.gov/pubmed/15373774 >.

218 BLISS, E. et al. An optimised method for the proteomic profiling of full thickness human skin. **Biol Proced Online,** v. 18, p. 15, 2016. ISSN 1480-9222. Disponível em: < https://www.ncbi.nlm.nih.gov/pubmed/27445641 >.

219 VANWIJCK, R. [Surgical biology of wound healing]. **Bull Mem Acad R Med Belg,** v. 156, n. 3-4, p. 175-84; discussion 185, 2001. ISSN 0377-8231. Disponível em: < http://www.ncbi.nlm.nih.gov/pubmed/11789398 >.

220 HART, J. Inflammation. 1: Its role in the healing of acute wounds. **J Wound Care,** v. 11, n. 6, p. 205-9, Jun 2002. ISSN 0969-0700. Disponível em: < http://www.ncbi.nlm.nih.gov/pubmed/12096576 >.

221 SIEGGREEN, M. Y. Healing of physical wounds. **Nurs Clin North Am,** v. 22, n. 2, p. 439-47, Jun 1987. ISSN 0029-6465. Disponível em: < http://www.ncbi.nlm.nih.gov/pubmed/3646670 >.

222 VELNAR, T.; BAILEY, T.; SMRKOLJ, V. The wound healing process: an overview of the cellular and molecular mechanisms. **J Int Med Res,** v. 37, n. 5, p. 1528-42, 2009 Sep-Oct 2009. ISSN 0300-0605. Disponível em: < http://www.ncbi.nlm.nih.gov/pubmed/19930861 >.

223 RAMASASTRY, S. S. Acute wounds. **Clin Plast Surg,** v. 32, n. 2, p. 195-208, Apr 2005. ISSN 0094-1298. Disponível em: < http://www.ncbi.nlm.nih.gov/pubmed/15814117 >.

224 SERVOLD, S. A. Growth factor impact on wound healing. **Clin Podiatr Med Surg,** v. 8, n. 4, p. 937-53, Oct 1991. ISSN 0891-8422. Disponível em: < http://www.ncbi.nlm.nih.gov/pubmed/1933739 >.

225 KIRSNER, R. S.; EAGLSTEIN, W. H. The wound healing process. **Dermatol Clin,** v. 11, n. 4, p. 629-40, Oct 1993. ISSN 0733-8635. Disponível em: < http://www.ncbi.nlm.nih.gov/pubmed/8222347 >.

226 TRUST, D. N. Z. Wound healing. Abnormal wound healing. p. http://www.dermnetnz.org/doctors/wound-healing/abnormal-healing.html, 2014. Disponível em: < http://www.dermnetnz.org/doctors/wound-healing/abnormal-healing.html >. Acesso em: 05/01/2016.

227 SON, D.; HARIJAN, A. Overview of surgical scar prevention and management. **J Korean Med Sci,** v. 29, n. 6, p. 751-7, Jun 2014. ISSN 1598-6357. Disponível em: < http://www.ncbi.nlm.nih.gov/pubmed/24932073 >.

228 KISCHER, C. W. et al. Increased fibronectin production by cell lines from hypertrophic scar and keloid. **Connect Tissue Res,** v. 23, n. 4, p. 279-88, 1989. ISSN 0300-8207. Disponível em: < http://www.ncbi.nlm.nih.gov/pubmed/2630174 >.

229 ISHIDA, Y.; GAO, J. L.; MURPHY, P. M. Chemokine receptor CX3CR1 mediates skin wound healing by promoting macrophage and fibroblast accumulation and function. **J Immunol,** v. 180, n. 1, p. 569-79, Jan 2008. ISSN 0022-1767. Disponível em: < http://www.ncbi.nlm.nih.gov/pubmed/18097059 >.

230 BOCK, O. et al. Studies of transforming growth factors beta 1-3 and their receptors I and II in fibroblast of keloids and hypertrophic scars. **Acta Derm Venereol,** v. 85, n. 3, p. 216-20, 2005. ISSN 0001-5555. Disponível em: < http://www.ncbi.nlm.nih.gov/pubmed/16040405 >.

231 SHAH, M.; FOREMAN, D. M.; FERGUSON, M. W. Neutralisation of TGF-beta 1 and TGF-beta 2 or exogenous addition of TGF-beta 3 to cutaneous rat wounds reduces scarring. **J Cell Sci,** v. 108 (Pt 3), p. 985-1002, Mar 1995. ISSN 0021-9533. Disponível em: < http://www.ncbi.nlm.nih.gov/pubmed/7542672 >.

232 WANG, R. et al. Hypertrophic scar tissues and fibroblasts produce more transforming growth factor-beta1 mRNA and protein than normal skin and cells. **Wound Repair Regen,** v. 8, n. 2, p. 128-37, 2000 Mar-Apr 2000. ISSN 1067-1927. Disponível em: < http://www.ncbi.nlm.nih.gov/pubmed/10810039 >.

233 COWIN, A. J. et al. Expression of TGF-beta and its receptors in murine fetal and adult dermal wounds. **Eur J Dermatol,** v. 11, n. 5, p. 424-31, 2001 Sep-Oct 2001. ISSN 1167-1122. Disponível em: < http://www.ncbi.nlm.nih.gov/pubmed/11525949 >.

234 SULLIVAN, K. M. et al. A model of scarless human fetal wound repair is deficient in transforming growth factor beta. **J Pediatr Surg,** v. 30, n. 2, p. 198-202; discussion 202-3, Feb 1995. ISSN 0022-3468. Disponível em: < http://www.ncbi.nlm.nih.gov/pubmed/7738738 >.

235 SOO, C. et al. Differential expression of fibromodulin, a transforming growth factor-beta modulator, in fetal skin development and scarless repair. **Am J Pathol,** v. 157, n. 2, p. 423-33, Aug 2000. ISSN 0002-9440. Disponível em: < http://www.ncbi.nlm.nih.gov/pubmed/10934147 >.

236 COULOMBE, P. A. Wound epithelialization: accelerating the pace of discovery. **J Invest Dermatol,** v. 121, n. 2, p. 219-30, Aug 2003. ISSN 0022-202X. Disponível em: < http://www.ncbi.nlm.nih.gov/pubmed/12880412 >.

237 MACHESNEY, M. et al. Activated keratinocytes in the epidermis of hypertrophic scars. **Am J Pathol,** v. 152, n. 5, p. 1133-41, May 1998. ISSN 0002-9440. Disponível em: < http://www.ncbi.nlm.nih.gov/pubmed/9588880 >.

238 ANDRIESSEN, M. P. et al. Hypertrophic scarring is associated with epidermal abnormalities: an immunohistochemical study. **J Pathol,** v. 186, n. 2, p. 192-200, Oct 1998. ISSN 0022-3417. Disponível em: < http://www.ncbi.nlm.nih.gov/pubmed/9924436 >.

239 HUANG, C.; OGAWA, R. The link between hypertension and pathological scarring: does hypertension cause or promote keloid and hypertrophic scar pathogenesis? **Wound Repair Regen,** v. 22, n. 4, p. 462-6, 2014 Jul-Aug 2014. ISSN 1524-475X. Disponível em: < http://www.ncbi.nlm.nih.gov/pubmed/24899409 >.

240 ARAKAWA, M. et al. Reduced collagenase gene expression in fibroblasts from hypertrophic scar tissue. **Br J Dermatol,** v. 134, n. 5, p. 863-8, May 1996. ISSN 0007-0963. Disponível em: < http://www.ncbi.nlm.nih.gov/pubmed/8736326 >.

241 WAN, K. C.; EVANS, J. H. Free radical involvement in hypertrophic scar formation. **Free Radic Biol Med,** v. 26, n. 5-6, p. 603-8, Mar 1999. ISSN 0891-5849. Disponível em: < http://www.ncbi.nlm.nih.gov/pubmed/10218648 >.

242 GILMAN, T. H. Silicone sheet for treatment and prevention of hypertrophic scar: a new proposal for the mechanism of efficacy. **Wound Repair Regen,** v. 11, n. 3, p. 235-6, 2003 May-Jun 2003. ISSN 1067-1927. Disponível em: < http://www.ncbi.nlm.nih.gov/pubmed/12753606 >.

243 NIESSEN, F. B. et al. The use of silicone occlusive sheeting (Sil-K) and silicone occlusive gel (Epiderm) in the prevention of hypertrophic scar formation. **Plast Reconstr Surg,** v. 102, n. 6, p. 1962-72, Nov 1998. ISSN 0032-1052. Disponível em: < http://www.ncbi.nlm.nih.gov/pubmed/9810992 >.

244 SO, K. et al. Effects of enhanced patient education on compliance with silicone gel sheeting and burn scar outcome: a randomized prospective study. **J Burn Care Rehabil,** v. 24, n. 6, p. 411-7; discussion 410, 2003 Nov-Dec 2003. ISSN 0273-8481. Disponível em: < http://www.ncbi.nlm.nih.gov/pubmed/14610432 >.

245 VAN DEN KERCKHOVE, E. et al. Silicones in the rehabilitation of burns: a review and overview. **Burns,** v. 27, n. 3, p. 205-14, May 2001. ISSN 0305-4179. Disponível em: < http://www.ncbi.nlm.nih.gov/pubmed/11311512 >.

246 KARAGOZ, H. et al. Comparison of efficacy of silicone gel, silicone gel sheeting, and topical onion extract including heparin and allantoin for the treatment of postburn hypertrophic scars. **Burns,** v. 35, n. 8, p. 1097-103, Dec 2009. ISSN 1879-1409. Disponível em: < http://www.ncbi.nlm.nih.gov/pubmed/19766399 >.

247 RABELLO, F. B.; SOUZA, C. D.; FARINA JÚNIOR, J. A. Update on hypertrophic scar treatment. **Clinics (Sao Paulo),** v. 69, n. 8, p. 565-73, Aug 2014. ISSN 1980-5322. Disponível em: < http://www.ncbi.nlm.nih.gov/pubmed/25141117 >.

248 MANUSKIATTI, W.; FITZPATRICK, R. E. Treatment response of keloidal and hypertrophic sternotomy scars: comparison among intralesional corticosteroid, 5-fluorouracil, and 585-nm flashlamp-pumped pulsed-dye laser treatments. **Arch Dermatol,** v. 138, n. 9, p. 1149-55, Sep 2002. ISSN 0003-987X. Disponível em: < http://www.ncbi.nlm.nih.gov/pubmed/12224975 >.

249 EDRISS, A. S.; MESTÁK, J. Management of keloid and hypertrophic scars. **Ann Burns Fire Disasters,** v. 18, n. 4, p. 202-10, Dec 2005. ISSN 1592-9558. Disponível em: < http://www.ncbi.nlm.nih.gov/pubmed/21991008 >.

250 VAN DER VEER, W. M. et al. Potential cellular and molecular causes of hypertrophic scar formation. **Burns,** v. 35, n. 1, p. 15-29, Feb 2009. ISSN 1879-1409. Disponível em: < http://www.ncbi.nlm.nih.gov/pubmed/18952381 >.

251 ALASTI, F.; VAN CAMP, G. Genetics of microtia and associated syndromes. **J Med Genet,** v. 46, n. 6, p. 361-9, Jun 2009. ISSN 1468-6244. Disponível em: < http://www.ncbi.nlm.nih.gov/pubmed/19293168 >.

252 LUQUETTI, D. V. et al. Microtia: epidemiology and genetics. **Am J Med Genet A,** v. 158A, n. 1, p. 124-39, Jan 2012. ISSN 1552-4833. Disponível em: < http://www.ncbi.nlm.nih.gov/pubmed/22106030 >.

253 BALUCH, N. et al. Auricular reconstruction for microtia: A review of available methods. **Plast Surg (Oakv),** v. 22, n. 1, p. 39-43, 2014. ISSN 2292-5503. Disponível em: < http://www.ncbi.nlm.nih.gov/pubmed/25152646 >.

254 SOLTANI, A. M. et al. Hypertrophic scarring in cleft lip repair: a comparison of incidence among ethnic groups. **Clin Epidemiol,** v. 4, p. 187-91, 2012. ISSN 1179-1349. Disponível em: < https://www.ncbi.nlm.nih.gov/pubmed/22879780 >.

255 TENTORI, L. et al. Poly(ADP-ribose) glycohydrolase inhibitor as chemosensitiser of malignant melanoma for temozolomide. **Eur J Cancer,** v. 41, n. 18, p. 2948-57, Dec 2005. ISSN 0959-8049. Disponível em: < https://www.ncbi.nlm.nih.gov/pubmed/16288862 >.

256 CHANG, P.; JACOBSON, M. K.; MITCHISON, T. J. Poly(ADP-ribose) is required for spindle assembly and structure. **Nature,** v. 432, n. 7017, p. 645-9, Dec 2004. ISSN 1476-4687. Disponível em: < https://www.ncbi.nlm.nih.gov/pubmed/15577915 >.

257 YING, W. et al. Poly(ADP-ribose) glycohydrolase mediates oxidative and excitotoxic neuronal death. **Proc Natl Acad Sci U S A,** v. 98, n. 21, p. 12227-32, Oct 2001. ISSN 0027-8424. Disponível em: < https://www.ncbi.nlm.nih.gov/pubmed/11593040 >.

258 DAVIDOVIC, L. et al. Importance of poly(ADP-ribose) glycohydrolase in the control of poly(ADP-ribose) metabolism. **Exp Cell Res,** v. 268, n. 1, p. 7-13, Aug 2001. ISSN 0014-4827. Disponível em: < https://www.ncbi.nlm.nih.gov/pubmed/11461113 >.

259 NADER, H. B. et al. Heparan sulfates and heparins: similar compounds performing the same functions in vertebrates and invertebrates? **Braz J Med Biol Res,** v. 32, n. 5, p. 529-38, May 1999. ISSN 0100-879X. Disponível em: < http://www.ncbi.nlm.nih.gov/pubmed/10412563 >.

260 NGOKA, L. C. Dramatic down-regulation of oxidoreductases in human hepatocellular carcinoma hepG2 cells: proteomics and gene ontology unveiling new frontiers in cancer enzymology. **Proteome Sci,** v. 6, p. 29, 2008. ISSN 1477-5956. Disponível em: < http://www.ncbi.nlm.nih.gov/pubmed/18950483 >.

261 DE WITTE, L. et al. Langerin is a natural barrier to HIV-1 transmission by Langerhans cells. **Nat Med,** v. 13, n. 3, p. 367-71, Mar 2007. ISSN 1078-8956. Disponível em: < http://www.ncbi.nlm.nih.gov/pubmed/17334373 >.

262 GOULD, N. et al. Regulation of protein function and signaling by reversible cysteine S-nitrosylation. **J Biol Chem,** v. 288, n. 37, p. 26473-9, Sep 2013. ISSN 1083-351X. Disponível em: < http://www.ncbi.nlm.nih.gov/pubmed/23861393 >.

263 DAZE, K. D.; HOF, F. The cation-π interaction at protein-protein interaction interfaces: developing and learning from synthetic mimics of proteins that bind methylated lysines. **Acc Chem Res,** v. 46, n. 4, p. 937-45, Apr 2013. ISSN 1520-4898. Disponível em: < http://www.ncbi.nlm.nih.gov/pubmed/22724379 >.

264 DAMBACHER, S.; HAHN, M.; SCHOTTA, G. Epigenetic regulation of development by histone lysine methylation. **Heredity (Edinb),** v. 105, n. 1, p. 24-37, Jul 2010. ISSN 1365-2540. Disponível em: < http://www.ncbi.nlm.nih.gov/pubmed/20442736 >.

265 VAN DOORN, N. L. et al. Site-specific deamidation of glutamine: a new marker of bone collagen deterioration. **Rapid Commun Mass Spectrom,** v. 26, n. 19, p. 2319-27, Oct 2012. ISSN 1097-0231. Disponível em: < http://www.ncbi.nlm.nih.gov/pubmed/22956324 >.

266 ROBINSON, N. E.; ROBINSON, A. B. Deamidation of human proteins. **Proc Natl Acad Sci U S A,** v. 98, n. 22, p. 12409-13, Oct 2001. ISSN 0027-8424. Disponível em: < http://www.ncbi.nlm.nih.gov/pubmed/11606750 >.

267 DE LA MORA-DE LA MORA, I. et al. Structural effects of protein aging: terminal marking by deamidation in human triosephosphate isomerase. **PLoS One,** v. 10, n. 4, p. e0123379, 2015. ISSN 1932-6203. Disponível em: < http://www.ncbi.nlm.nih.gov/pubmed/25884638 >.

268 KOSSIAKOFF, A. A. Tertiary structure is a principal determinant to protein deamidation. **Science,** v. 240, n. 4849, p. 191-4, Apr 1988. ISSN 0036-8075. Disponível em: < http://www.ncbi.nlm.nih.gov/pubmed/3353715 >.

269 LAPKO, V. N. et al. Deamidation in human gamma S-crystallin from cataractous lenses is influenced by surface exposure. **Biochemistry,** v. 41, n. 27, p. 8638-48, Jul 2002. ISSN 0006-2960. Disponível em: < http://www.ncbi.nlm.nih.gov/pubmed/12093281 >.

270 STRATTON, L. P. et al. Controlling deamidation rates in a model peptide: effects of temperature, peptide concentration, and additives. **J Pharm Sci,** v. 90, n. 12, p. 2141-8, Dec 2001. ISSN 0022-3549. Disponível em: < http://www.ncbi.nlm.nih.gov/pubmed/11745773 >.

271 HAO, P. et al. Detection, evaluation and minimization of nonenzymatic deamidation in proteomic sample preparation. **Mol Cell Proteomics,** v. 10, n. 10, p. O111.009381, Oct 2011. ISSN 1535-9484. Disponível em: < http://www.ncbi.nlm.nih.gov/pubmed/21784994 >.

272 SCHIEBER, M.; CHANDEL, N. S. ROS function in redox signaling and oxidative stress. **Curr Biol,** v. 24, n. 10, p. R453-62, May 2014. ISSN 1879-0445. Disponível em: < http://www.ncbi.nlm.nih.gov/pubmed/24845678 >.

273 FINKEL, T. Signal transduction by reactive oxygen species. **J Cell Biol,** v. 194, n. 1, p. 7-15, Jul 2011. ISSN 1540-8140. Disponível em: < http://www.ncbi.nlm.nih.gov/pubmed/21746850 >.

274 CROSS, C. E. et al. Oxygen radicals and human disease. **Ann Intern Med,** v. 107, n. 4, p. 526-45, Oct 1987. ISSN 0003-4819. Disponível em: < http://www.ncbi.nlm.nih.gov/pubmed/3307585 >.

275 MAEHRE, H. K. et al. ω-3 Fatty Acids and Cardiovascular Diseases: Effects, Mechanisms and Dietary Relevance. **Int J Mol Sci,** v. 16, n. 9, p. 22636-61, 2015. ISSN 1422-0067. Disponível em: < http://www.ncbi.nlm.nih.gov/pubmed/26393581 >.

276 GROEN, D. et al. In vitro model systems for studying the impact of organic chemicals on the skin barrier lipids. **Biochim Biophys Acta,** v. 1838, n. 1 Pt B, p. 310-8, Jan 2014. ISSN 0006-3002. Disponível em: < http://www.ncbi.nlm.nih.gov/pubmed/24125684 >.

277 WERTZ, P. W.; VAN DEN BERGH, B. The physical, chemical and functional properties of lipids in the skin and other biological barriers. **Chem Phys Lipids,** v. 91, n. 2, p. 85-96, Feb 1998. ISSN 0009-3084. Disponível em: < http://www.ncbi.nlm.nih.gov/pubmed/9569614 >.

278 IMOKAWA, G.; HATTORI, M. A possible function of structural lipids in the water-holding properties of the stratum corneum. **J Invest Dermatol,** v. 84, n. 4, p. 282-4, Apr 1985. ISSN 0022-202X. Disponível em: < http://www.ncbi.nlm.nih.gov/pubmed/3981042 >.

279 PARKER, C. E. et al. **Neuroproteomics - Chapter 6 Mass Spectrometry for Post-Translational Modifications**. Boca Raton, Florida: CRC Press/Taylor & Francis Group, 2010.

280 KIM, M. S. et al. Systematic evaluation of alternating CID and ETD fragmentation for phosphorylated peptides. **Proteomics,** v. 11, n. 12, p. 2568-72, Jun 2011. ISSN 1615-9861. Disponível em: < http://www.ncbi.nlm.nih.gov/pubmed/21598390 >.

281 DEVA, D. P. et al. Cardiovascular magnetic resonance demonstration of the spectrum of morphological phenotypes and patterns of myocardial scarring in Anderson-Fabry

disease. **J Cardiovasc Magn Reson,** v. 18, p. 14, 2016. ISSN 1532-429X. Disponível em: < http://www.ncbi.nlm.nih.gov/pubmed/27036375 >.

282 TOYOOKA, K. Fabry disease. **Curr Opin Neurol,** v. 24, n. 5, p. 463-8, Oct 2011. ISSN 1473-6551. Disponível em: < http://www.ncbi.nlm.nih.gov/pubmed/21825987 >.

283 CENTRE, H. S. C. I. Provisional Monthly Hospital Episode Statistics for Admitted Patient Care, Outpatients and Accident and Emergency Data - April 2015 to February 2016. 2016. Disponível em: < http://www.hscic.gov.uk/searchcatalogue?productid=20809&q=HES+proceedures+and+interventions&sort=Most+recent&size=10&page=1#top >. Acesso em: 28/04/2016.

284 BODENHAM, A. R.; HOWELL, S. J. General anaesthesia vs local anaesthesia: an ongoing story. **Br J Anaesth,** v. 103, n. 6, p. 785-9, Dec 2009. ISSN 1471-6771. Disponível em: < https://www.ncbi.nlm.nih.gov/pubmed/19918020 >.

285 ACKLAND, G. L.; EDWARDS, M. Defining higher-risk surgery. **Curr Opin Crit Care,** v. 16, n. 4, p. 339-46, Aug 2010. ISSN 1531-7072. Disponível em: < http://www.ncbi.nlm.nih.gov/pubmed/20489608 >.

286 KHURI, S. F. et al. Determinants of long-term survival after major surgery and the adverse effect of postoperative complications. **Ann Surg,** v. 242, n. 3, p. 326-41; discussion 341-3, Sep 2005. ISSN 0003-4932. Disponível em: < http://www.ncbi.nlm.nih.gov/pubmed/16135919 >.

287 DIMICK, J. B. et al. Complications and costs after high-risk surgery: where should we focus quality improvement initiatives? **J Am Coll Surg,** v. 196, n. 5, p. 671-8, May 2003. ISSN 1072-7515. Disponível em: < http://www.ncbi.nlm.nih.gov/pubmed/12742194 >.

288 GROCOTT, M. P. et al. The Postoperative Morbidity Survey was validated and used to describe morbidity after major surgery. **J Clin Epidemiol,** v. 60, n. 9, p. 919-28, Sep 2007. ISSN 0895-4356. Disponível em: < http://www.ncbi.nlm.nih.gov/pubmed/17689808 >.

289 BENNETT-GUERRERO, E. et al. The use of a postoperative morbidity survey to evaluate patients with prolonged hospitalization after routine, moderate-risk, elective surgery. **Anesth Analg,** v. 89, n. 2, p. 514-9, Aug 1999. ISSN 0003-2999. Disponível em: < http://www.ncbi.nlm.nih.gov/pubmed/10439777 >.

290 SHOEMAKER, W. C. et al. Clinical trial of survivors' cardiorespiratory patterns as therapeutic goals in critically ill postoperative patients. **Crit Care Med,** v. 10, n. 6, p. 398-403, Jun 1982. ISSN 0090-3493. Disponível em: < http://www.ncbi.nlm.nih.gov/pubmed/7042206 >.

291 SHOEMAKER, W. C.; APPEL, P. L.; KRAM, H. B. Hemodynamic and oxygen transport responses in survivors and nonsurvivors of high-risk surgery. **Crit Care Med,** v. 21, n. 7, p. 977-90, Jul 1993. ISSN 0090-3493. Disponível em: < http://www.ncbi.nlm.nih.gov/pubmed/8319478 >.

292 _____. Measurement of tissue perfusion by oxygen transport patterns in experimental shock and in high-risk surgical patients. **Intensive Care Med,** v. 16 Suppl 2, p. S135-44, 1990. ISSN 0342-4642. Disponível em: < http://www.ncbi.nlm.nih.gov/pubmed/2289979 >.

293 SHOEMAKER, W. C. et al. Prospective trial of supranormal values of survivors as therapeutic goals in high-risk surgical patients. **Chest,** v. 94, n. 6, p. 1176-86, Dec 1988. ISSN 0012-3692. Disponível em: < http://www.ncbi.nlm.nih.gov/pubmed/3191758 >.

294 KERN, J. W.; SHOEMAKER, W. C. Meta-analysis of hemodynamic optimization in high-risk patients. **Crit Care Med,** v. 30, n. 8, p. 1686-92, Aug 2002. ISSN 0090-3493. Disponível em: < http://www.ncbi.nlm.nih.gov/pubmed/12163777 >.

295 PEARSE, R. M. et al. Effect of a perioperative, cardiac output-guided hemodynamic therapy algorithm on outcomes following major gastrointestinal surgery: a randomized clinical trial and systematic review. **JAMA,** v. 311, n. 21, p. 2181-90, Jun 2014. ISSN 1538-3598. Disponível em: < http://www.ncbi.nlm.nih.gov/pubmed/24842135 >.

296 CONTE, B. et al. Perioperative Optimization of Oxygen Delivery. **Transfusion Alternatives in Transfusion Medicine,** v. 11, n. 3, p. 22-29, 2010.

297 CLOWES, G. H.; DEL GUERCIO, L. R. Circulatory response to trauma of surgical operations. **Metabolism,** v. 9, p. 67-81, Jan 1960. ISSN 0026-0495. Disponível em: < http://www.ncbi.nlm.nih.gov/pubmed/13810744 >.

298 BOYD, A. D. et al. Estimation of cardiac output soon after intracardiac surgery with cardiopulmonary bypass. **Ann Surg,** v. 150, p. 613-26, Oct 1959. ISSN 0003-4932. Disponível em: < http://www.ncbi.nlm.nih.gov/pubmed/13803517 >.

299 GROCOTT, M. P. et al. Perioperative increase in global blood flow to explicit defined goals and outcomes after surgery: a Cochrane Systematic Review. **Br J Anaesth,** v. 111, n. 4, p. 535-48, Oct 2013. ISSN 1471-6771. Disponível em: < http://www.ncbi.nlm.nih.gov/pubmed/23661403 >.

300 DAWES, K. **Oesophagectomy, Gastrointestinal Services Division**. https://www.uclh.nhs.uk/PandV/PIL/Patient%20information%20leaflets/Oesophagectomy.pdf. TRUST, U. C. L. H. N. F.: Medical Illustration RNTNEH. UCLH/S&G/GI/OESOPGTMY/3 2014.

301 GARCÍA-MÁRQUEZ, A. et al. Defective Guanine Nucleotide Exchange in the Elongation Factor-like 1 (EFL1) GTPase by Mutations in the Shwachman-Diamond Syndrome Protein. **J Biol Chem,** v. 290, n. 29, p. 17669-78, Jul 2015. ISSN 1083-351X. Disponível em: < https://www.ncbi.nlm.nih.gov/pubmed/25991726 >.

302 LEVIN, T. L. et al. Shwachman-Bodian-Diamond syndrome: metaphyseal chondrodysplasia in children with pancreatic insufficiency and neutropenia. **Pediatr Radiol,** v. 45, n. 7, p. 1066-71, Jul 2015. ISSN 1432-1998. Disponível em: < https://www.ncbi.nlm.nih.gov/pubmed/25416932 >.

303 KOHR, M. J. et al. S-nitrosylation of TRIM72 at cysteine 144 is critical for protection against oxidation-induced protein degradation and cell death. **J Mol Cell Cardiol,** v. 69, p. 67-74, Apr 2014. ISSN 1095-8584. Disponível em: < https://www.ncbi.nlm.nih.gov/pubmed/24487118 >.

304 VALVERDE, G. et al. A novel candidate region for genetic adaptation to high altitude in Andean populations. **PLoS One,** v. 10, n. 5, p. e0125444, 2015. ISSN 1932-6203. Disponível em: < https://www.ncbi.nlm.nih.gov/pubmed/25961286 >.

305 ANWAR, S. L. et al. Caveolin-1 in Breast Cancer: Single Molecule Regulation of Multiple Key Signaling Pathways. **Asian Pac J Cancer Prev,** v. 16, n. 16, p. 6803-12, 2015. ISSN 1513-7368. Disponível em: < https://www.ncbi.nlm.nih.gov/pubmed/26514450 >.

306 PARADOWSKA-GORYCKA, A. et al. Relationship between VEGF Gene Polymorphisms and Serum VEGF Protein Levels in Patients with Rheumatoid Arthritis. **PLoS One,** v. 11, n. 8, p. e0160769, 2016 2016. ISSN 1932-6203. Disponível em: < https://www.ncbi.nlm.nih.gov/pubmed/27513931 >.

307 TANAKA, T. et al. Negative pressure wound therapy induces early wound healing by increased and accelerated expression of vascular endothelial growth factor receptors. **Eur J Plast Surg,** v. 39, p. 247-256, 2016 2016. ISSN 0930-343X. Disponível em: < https://www.ncbi.nlm.nih.gov/pubmed/27512293 >.

308 MIYAMOTO, D. et al. Increased serum levels of vascular endothelial growth factor in pemphigus foliaceus patients with erythroderma. **J Eur Acad Dermatol Venereol**, Aug 2016. ISSN 1468-3083. Disponível em: < https://www.ncbi.nlm.nih.gov/pubmed/27510449 >.

309 VENCES-CATALÁN, F. et al. Tetraspanin CD81, a modulator of immune suppression in cancer and metastasis. **Oncoimmunology,** v. 5, n. 5, p. e1120399, May 2016. ISSN 2162-4011. Disponível em: < https://www.ncbi.nlm.nih.gov/pubmed/27467918 >.

310 QIAN, X. J. et al. Trachelogenin, a novel inhibitor of hepatitis C virus entry through CD81. **J Gen Virol,** v. 97, n. 5, p. 1134-44, May 2016. ISSN 1465-2099. Disponível em: < https://www.ncbi.nlm.nih.gov/pubmed/26879209 >.

311 KAMBUROV, A. et al. Integrated pathway-level analysis of transcriptomics and metabolomics data with IMPaLA. **Bioinformatics,** v. 27, n. 20, p. 2917-8, Oct 2011. ISSN 1367-4811. Disponível em: < http://www.ncbi.nlm.nih.gov/pubmed/21893519 >.

312 SUZUKI, Y. J.; CARINI, M.; BUTTERFIELD, D. A. Protein carbonylation. **Antioxid Redox Signal,** v. 12, n. 3, p. 323-5, Mar 2010. ISSN 1557-7716. Disponível em: < http://www.ncbi.nlm.nih.gov/pubmed/19743917 >.

313 WONG, C. M. et al. Protein carbonylation as a novel mechanism in redox signaling. **Circ Res,** v. 102, n. 3, p. 310-8, Feb 2008. ISSN 1524-4571. Disponível em: < http://www.ncbi.nlm.nih.gov/pubmed/18079412 >.

314 _____. Cell signaling by protein carbonylation and decarbonylation. **Antioxid Redox Signal,** v. 12, n. 3, p. 393-404, Mar 2010. ISSN 1557-7716. Disponível em: < http://www.ncbi.nlm.nih.gov/pubmed/19686045 >.

315 PLOUMAKIS, A.; COLEMAN, M. L. OH, the Places You'll Go! Hydroxylation, Gene Expression, and Cancer. **Mol Cell,** v. 58, n. 5, p. 729-41, Jun 2015. ISSN 1097-4164. Disponível em: < http://www.ncbi.nlm.nih.gov/pubmed/26046647 >.

316 DONG, X. et al. Aspartate β-Hydroxylase expression promotes a malignant pancreatic cellular phenotype. **Oncotarget,** v. 6, n. 2, p. 1231-48, Jan 2015. ISSN 1949-2553. Disponível em: < http://www.ncbi.nlm.nih.gov/pubmed/25483102 >.

317 BAKA, Z. et al. Citrullination under physiological and pathological conditions. **Joint Bone Spine,** v. 79, n. 5, p. 431-6, Oct 2012. ISSN 1778-7254. Disponível em: < http://www.ncbi.nlm.nih.gov/pubmed/22366145 >.

318 VOSSENAAR, E. R. et al. PAD, a growing family of citrullinating enzymes: genes, features and involvement in disease. **Bioessays,** v. 25, n. 11, p. 1106-18, Nov 2003. ISSN 0265-9247. Disponível em: < http://www.ncbi.nlm.nih.gov/pubmed/14579251 >.

319 CHAUDRY, I. H. et al. Hemorrhage and resuscitation: immunological aspects. **Am J Physiol,** v. 259, n. 4 Pt 2, p. R663-78, Oct 1990. ISSN 0002-9513. Disponível em: < http://www.ncbi.nlm.nih.gov/pubmed/2145776 >.

320 CORREALE, M. et al. Acute phase proteins in acute coronary syndrome: an up-to-date. **Cardiovasc Hematol Agents Med Chem,** v. 10, n. 4, p. 352-61, Dec 2012. ISSN 1875-6182. Disponível em: < http://www.ncbi.nlm.nih.gov/pubmed/22721440 >.

321 RAY, S. et al. Differential expression of serum/plasma proteins in various infectious diseases: specific or nonspecific signatures. **Proteomics Clin Appl,** v. 8, n. 1-2, p. 53-72, Feb 2014. ISSN 1862-8354. Disponível em: < http://www.ncbi.nlm.nih.gov/pubmed/24293340 >.

322 DEMPSEY, E.; RUDD, P. M. Acute phase glycoproteins: bystanders or participants in carcinogenesis? **Ann N Y Acad Sci,** v. 1253, p. 122-32, Apr 2012. ISSN 1749-6632. Disponível em: < http://www.ncbi.nlm.nih.gov/pubmed/22352780 >.

323 MCCARTHY, C. et al. The role and importance of glycosylation of acute phase proteins with focus on alpha-1 antitrypsin in acute and chronic inflammatory conditions. **J Proteome Res,** v. 13, n. 7, p. 3131-43, Jul 2014. ISSN 1535-3907. Disponível em: < http://www.ncbi.nlm.nih.gov/pubmed/24892502 >.

324 HOLM, T. et al. Protein biomarkers in vernix with potential to predict the development of atopic eczema in early childhood. **Allergy,** v. 69, n. 1, p. 104-12, Jan 2014. ISSN 1398-9995. Disponível em: < http://www.ncbi.nlm.nih.gov/pubmed/24205894 >.

325 HOATH, S. B.; PICKENS, W. L.; VISSCHER, M. O. The biology of vernix caseosa. **Int J Cosmet Sci,** v. 28, n. 5, p. 319-33, Oct 2006. ISSN 1468-2494. Disponível em: < http://www.ncbi.nlm.nih.gov/pubmed/18489296 >.

326 MENON, G. K.; ELIAS, P. M.; FEINGOLD, K. R. Integrity of the permeability barrier is crucial for maintenance of the epidermal calcium gradient. **Br J Dermatol,** v. 130, n. 2, p. 139-47, Feb 1994. ISSN 0007-0963. Disponível em: < http://www.ncbi.nlm.nih.gov/pubmed/8123567 >.

327 JIANG, S.; KOO, S. W.; LEE, S. H. The morphologic changes in lamellar bodies and intercorneocyte lipids after tape stripping and occlusion with a water vapor-impermeable membrane. **Arch Dermatol Res,** v. 290, n. 3, p. 145-51, Mar 1998. ISSN 0340-3696. Disponível em: < http://www.ncbi.nlm.nih.gov/pubmed/9558490 >.

328 HWANG, S. M. et al. Basis of occlusive therapy in psoriasis: correcting defects in permeability barrier and calcium gradient. **Int J Dermatol,** v. 40, n. 3, p. 223-31, Mar 2001. ISSN 0011-9059. Disponível em: < http://www.ncbi.nlm.nih.gov/pubmed/11422532 >.

329 PUBMED. PubMed Search: "cystatin C" AND "caspase 14". p. http://www.ncbi.nlm.nih.gov/pubmed/?term=%22cystatin+C%22+AND+%22caspase+14%22, 2016. Acesso em: 11/07/2016.

330 BROCKLEHURST, K.; PHILPOTT, M. P. Cysteine proteases: mode of action and role in epidermal differentiation. **Cell Tissue Res,** v. 351, n. 2, p. 237-44, Feb 2013. ISSN 1432-0878. Disponível em: < https://www.ncbi.nlm.nih.gov/pubmed/23344364 >.

331 TAKAHASHI, H. et al. Cloning of human keratolinin cDNA: keratolinin is identical with a cysteine proteinase inhibitor, cystatin A, and is regulated by Ca2+, TPA, and cAMP. **J Invest Dermatol,** v. 108, n. 6, p. 843-7, Jun 1997. ISSN 0022-202X. Disponível em: < https://www.ncbi.nlm.nih.gov/pubmed/9182808 >.

332 KACHUK, C.; STEPHEN, K.; DOUCETTE, A. Comparison of sodium dodecyl sulfate depletion techniques for proteome analysis by mass spectrometry. **J Chromatogr A,** v. 1418, p. 158-66, Oct 2015. ISSN 1873-3778. Disponível em: < https://www.ncbi.nlm.nih.gov/pubmed/26422304 >.

333 CHANG, Y. H. et al. New mass-spectrometry-compatible degradable surfactant for tissue proteomics. **J Proteome Res,** v. 14, n. 3, p. 1587-99, Mar 2015. ISSN 1535-3907. Disponível em: < https://www.ncbi.nlm.nih.gov/pubmed/25589168 >.

334 HOPKINSON, A. et al. Optimised two-dimensional electrophoresis procedures for the protein characterisation of structural tissues. **Proteomics,** v. 5, n. 7, p. 1967-79, May 2005. ISSN 1615-9853. Disponível em: < https://www.ncbi.nlm.nih.gov/pubmed/15816006 >.

335 WALRAVEN, M. et al. Altered TGF-β signaling in fetal fibroblasts: what is known about the underlying mechanisms? **Wound Repair Regen,** v. 22, n. 1, p. 3-13, 2014 Jan-Feb 2014. ISSN 1524-475X. Disponível em: < https://www.ncbi.nlm.nih.gov/pubmed/24134669 >.

336 BETTINGER, D. A. et al. The effect of TGF-beta on keloid fibroblast proliferation and collagen synthesis. **Plast Reconstr Surg,** v. 98, n. 5, p. 827-33, Oct 1996. ISSN 0032-1052. Disponível em: < https://www.ncbi.nlm.nih.gov/pubmed/8823022 >.

337 CHEN, R. et al. Focal adhesion kinase (FAK) siRNA inhibits human hypertrophic scar by suppressing integrin α, TGF-β and α-SMA. **Cell Biol Int,** v. 38, n. 7, p. 803-8, Jul 2014. ISSN 1095-8355. Disponível em: < https://www.ncbi.nlm.nih.gov/pubmed/24523242 >.

338 QIU, S. S.; DOTOR, J.; HONTANILLA, B. Effect of P144® (Anti-TGF-β) in an "In Vivo" Human Hypertrophic Scar Model in Nude Mice. **PLoS One,** v. 10, n. 12, p. e0144489, 2015. ISSN 1932-6203. Disponível em: < https://www.ncbi.nlm.nih.gov/pubmed/26720517 >.

339 KISCHER, C. W.; BRODY, G. S. Structure of the collagen nodule from hypertrophic scars and keloids. **Scan Electron Microsc**, n. Pt 3, p. 371-6, 1981. ISSN 0586-5581. Disponível em: < https://www.ncbi.nlm.nih.gov/pubmed/7330586 >.

340 XUE, M.; JACKSON, C. J. Extracellular Matrix Reorganization During Wound Healing and Its Impact on Abnormal Scarring. **Adv Wound Care (New Rochelle),** v. 4, n. 3, p. 119-136, Mar 2015. ISSN 2162-1918. Disponível em: < https://www.ncbi.nlm.nih.gov/pubmed/25785236 >.

341 SMITH, C. J.; SMITH, J. C.; FINN, M. C. The possible role of mast cells (allergy) in the production of keloid and hypertrophic scarring. **J Burn Care Rehabil,** v. 8, n. 2, p. 126-31, 1987 Mar-Apr 1987. ISSN 0273-8481. Disponível em: < https://www.ncbi.nlm.nih.gov/pubmed/3647037 >.

342 BUTZELAAR, L. et al. Currently known risk factors for hypertrophic skin scarring: A review. **J Plast Reconstr Aesthet Surg,** v. 69, n. 2, p. 163-9, Feb 2016. ISSN 1878-0539. Disponível em: < https://www.ncbi.nlm.nih.gov/pubmed/26776348 >.

343 BARROW, R. E.; DASU, M. R. Oxidative and heat stress gene changes in hypertrophic scar fibroblasts stimulated with interleukin-1beta. **J Surg Res,** v. 126, n. 1, p. 59-65, Jun 2005. ISSN 0022-4804. Disponível em: < https://www.ncbi.nlm.nih.gov/pubmed/15916976 >.

344 SUN, X. et al. Mortality predicted by preinduction cerebral oxygen saturation after cardiac operation. **Ann Thorac Surg,** v. 98, n. 1, p. 91-6, Jul 2014. ISSN 1552-6259. Disponível em: < https://www.ncbi.nlm.nih.gov/pubmed/24815908 >.

345 SUEHIRO, K. et al. Discrepancy between superior vena cava oxygen saturation and mixed venous oxygen saturation can predict postoperative complications in cardiac surgery patients. **J Cardiothorac Vasc Anesth,** v. 28, n. 3, p. 528-33, Jun 2014. ISSN 1532-8422. Disponível em: < https://www.ncbi.nlm.nih.gov/pubmed/23972741 >.

346 GOLDMAN, S. et al. Optimizing intraoperative cerebral oxygen delivery using noninvasive cerebral oximetry decreases the incidence of stroke for cardiac surgical patients. **Heart Surg Forum,** v. 7, n. 5, p. E376-81, 2004. ISSN 1522-6662. Disponível em: < https://www.ncbi.nlm.nih.gov/pubmed/15799908 >.

347 YAO, F. S. et al. Cerebral oxygen desaturation is associated with early postoperative neuropsychological dysfunction in patients undergoing cardiac surgery. **J Cardiothorac Vasc Anesth,** v. 18, n. 5, p. 552-8, Oct 2004. ISSN 1053-0770. Disponível em: < https://www.ncbi.nlm.nih.gov/pubmed/15578464 >.

348 MURKIN, J. M. et al. Monitoring brain oxygen saturation during coronary bypass surgery: a randomized, prospective study. **Anesth Analg,** v. 104, n. 1, p. 51-8, Jan 2007. ISSN 1526-7598. Disponível em: < https://www.ncbi.nlm.nih.gov/pubmed/17179242 >.

349 WU, J. H. et al. Oxidative Stress Biomarkers and Incidence of Postoperative Atrial Fibrillation in the Omega-3 Fatty Acids for Prevention of Postoperative Atrial Fibrillation (OPERA) Trial. **J Am Heart Assoc,** v. 4, n. 5, May 2015. ISSN 2047-9980. Disponível em: < https://www.ncbi.nlm.nih.gov/pubmed/25994442 >.

350 NEGI, S.; SOVARI, A. A.; DUDLEY, S. C. Atrial fibrillation: the emerging role of inflammation and oxidative stress. **Cardiovasc Hematol Disord Drug Targets,** v. 10, n. 4, p. 262-8, Dec 2010. ISSN 2212-4063. Disponível em: < https://www.ncbi.nlm.nih.gov/pubmed/20932266 >.

351 PLICNER, D. et al. Asymmetric dimethylarginine and oxidative stress following coronary artery bypass grafting: associations with postoperative outcome. **Eur J Cardiothorac Surg,** v. 45, n. 5, p. e136-41, May 2014. ISSN 1873-734X. Disponível em: < https://www.ncbi.nlm.nih.gov/pubmed/24523493 >.

352 AIKO, S. et al. Effects of an immuno-enhanced diet containing antioxidants in esophageal cancer surgery following neoadjuvant therapy. **Dis Esophagus,** v. 25, n. 2, p. 137-45, Feb 2012. ISSN 1442-2050. Disponível em: < https://www.ncbi.nlm.nih.gov/pubmed/21762279 >.

353 FUKUDA, T. et al. Can immune-enhancing nutrients reduce postoperative complications in patients undergoing esophageal surgery? **Dis Esophagus,** v. 21, n. 8, p. 708-11, 2008. ISSN 1442-2050. Disponível em: < https://www.ncbi.nlm.nih.gov/pubmed/18847452 >.

354 WONG, C. M.; ZHANG, Y.; HUANG, Y. Bone morphogenic protein-4-induced oxidant signaling via protein carbonylation for endothelial dysfunction. **Free Radic Biol Med,** v. 75, p. 178-90, Oct 2014. ISSN 1873-4596. Disponível em: < https://www.ncbi.nlm.nih.gov/pubmed/25091895 >.

355 MANWARING, V. et al. The identification of new biomarkers for identifying and monitoring kidney disease and their translation into a rapid mass spectrometry-based test: evidence of presymptomatic kidney disease in pediatric Fabry and type-I diabetic patients. **J Proteome Res,** v. 12, n. 5, p. 2013-21, May 2013. ISSN 1535-3907. Disponível em: < http://www.ncbi.nlm.nih.gov/pubmed/23464927 >.

356 LOWRY, O. H. et al. Protein measurement with the Folin phenol reagent. **J Biol Chem,** v. 193, n. 1, p. 265-75, Nov 1951. ISSN 0021-9258. Disponível em: < http://www.ncbi.nlm.nih.gov/pubmed/14907713 >.

357 MILLS, P. B. et al. Analysis by matrix assisted laser desorption/ionisation-time of flight mass spectrometry of the post-translational modifications of alpha 1-antitrypsin isoforms separated by two-dimensional polyacrylamide gel electrophoresis. **Proteomics,** v. 1, n. 6, p. 778-86, Jun 2001. ISSN 1615-9853. Disponível em: < http://www.ncbi.nlm.nih.gov/pubmed/11677785 >.

[358] SHEVCHENKO, A. et al. Mass spectrometric sequencing of proteins silver-stained polyacrylamide gels. **Anal Chem,** v. 68, n. 5, p. 850-8, Mar 1996. ISSN 0003-2700. Disponível em: < http://www.ncbi.nlm.nih.gov/pubmed/8779443 >.

[359] MILLS, K. et al. A strategy for the identification of site-specific glycosylation in glycoproteins using MALDI TOF MS. **Tetrahedron: Asymmetry,** v. 11, n. 1, p. 75-93, 1/28/ 2000. ISSN 0957-4166. Disponível em: < http://www.sciencedirect.com/science/article/pii/S0957416699005455 >.

[360] DISTLER, U. et al. Drift time-specific collision energies enable deep-coverage data-independent acquisition proteomics. **Nat Methods,** v. 11, n. 2, p. 167-70, Feb 2014. ISSN 1548-7105. Disponível em: < http://www.ncbi.nlm.nih.gov/pubmed/24336358 >.

[361] MILLS, K. et al. The synthesis of internal standards for the quantitative determination of sphingolipids by tandem mass spectrometry. **Rapid Commun Mass Spectrom,** v. 19, n. 12, p. 1739-48, 2005. ISSN 0951-4198. Disponível em: < http://www.ncbi.nlm.nih.gov/pubmed/15909321 >.

[362] AURAY-BLAIS, C. et al. Urinary biomarker investigation in children with Fabry disease using tandem mass spectrometry. **Clin Chim Acta,** v. 438, p. 195-204, Jan 2015. ISSN 1873-3492. Disponível em: < http://www.ncbi.nlm.nih.gov/pubmed/25149322 >.

Chapter 12

Appendices

12 Appendices

Contents

12.1 Full MS data for the 42 proteins identified as interacting with CLP5, presented in Table 3.2

Protein entry and accession number are unique identifiers for each protein. Protein score is a software generated value taking into account the quality of the data used to identify that protein. Matched peptides to protein details the number of peptides detected in the sample mixture for that specific protein. Amount of protein indicates the relative abundance of each protein compared with a standard peptide spiked into the mixture.

Protein Entry	Protein Accession Number	Protein Full Name	Protein Score	Average Protein Mass (Da)	Matched Peptides to Protein	Protein Sequence Coverage (%)	Amount of Protein (fmol)
1433E_HUMAN	P62258	14-3-3 protein epsilon	905	29345.0493	7	32.2	0.671
1433S_HUMAN	P31947	14-3-3 protein sigma	2144	27888.1757	6	21.8	5.302
1433Z_HUMAN	P63104	14-3-3 protein zeta/delta	3311	27916.2394	6	23.7	3.583
A1AT_HUMAN	P01009	Alpha-1-antitrypsin	1024	46907.7136	8	29.7	2.113
ACTB_HUMAN	P60709	Actin_ cytoplasmic 1	3455	42079.017	15	56.0	6.522
ACTC_HUMAN	P68032	Actin_ alpha cardiac muscle 1	1969	42361.2493	9	27.9	0.390
ALBU_HUMAN	P02768	Serum albumin	4636	71362.7109	28	51.2	12.006
ANXA1_HUMAN	P04083	Annexin A1	802	38942.4262	9	37.3	0.861
ANXA2_HUMAN	P07355	Annexin A2	4384	38832.2204	22	51.9	6.374
ANXA5_HUMAN	P08758	Annexin A5	1347	35993.8588	8	29.4	1.675
ARGI1_HUMAN	P05089	Arginase-1	631	34906.0649	5	26.1	1.748
CALL3_HUMAN	P27482	Calmodulin-like protein 3	680	16947.7959	4	31.5	0.473
CASPE_HUMAN	P31944	Caspase-14	1131	27964.7122	7	26.0	1.719
CO1A1_HUMAN	P02452	Collagen alpha-1(I) chain	708	139968.1403	34	26.2	8.502
CO1A2_HUMAN	P08123	Collagen alpha-2(I) chain	537	129827.2687	31	31.3	4.296
CO6A3_HUMAN	P12111	Collagen alpha-3(VI) chain	514	345380.5637	46	19.4	2.619
DCD_HUMAN	P81605	Dermcidin	6404	11397.9338	4	24.6	2.206
ENOA_HUMAN	P06733	Alpha-enolase	2808	47511.201	16	41.0	3.568
FABP5_HUMAN	Q01469	Fatty acid-binding protein_ epidermal	2338	15506.6309	5	25.2	1.805
G3P_HUMAN	P04406	Glyceraldehyde-3-phosphate dehydrogenase	3418	36224.3681	12	41.5	5.870
GSTP1_HUMAN	P09211	Glutathione S-transferase P	2085	23583.9696	7	47.1	2.903
H2A1A_HUMAN	Q96QV6	Histone H2A type 1-A	3072	14233.5231	5	56.5	4.929
H2B1C_HUMAN	P62807	Histone H2B type 1-C/E/F/G/I	1670	13906.1627	4	27.0	2.565
H31T_HUMAN	Q16695	Histone H3.1t	1180	15622.3388	3	16.9	3.336
H4_HUMAN	P62805	Histone H4	10602	11367.3627	9	56.3	7.174
HBG2_HUMAN	P69892	Hemoglobin subunit gamma-2	12129	16183.4933	6	51.7	6.737
IGHG1_HUMAN	P01857	Ig gamma-1 chain C region	1756	36619.1863	6	21.8	1.983
K1H2_HUMAN	Q14532	Keratin_ type I cuticular Ha2	1339	51825.8233	5	29.5	0.841
KPYM_HUMAN	P14618	Pyruvate kinase PKM	1146	58507.2826	15	37.7	2.148
LDHA_HUMAN	P00338	L-lactate dehydrogenase A chain	3674	36973.9299	12	35.5	3.464
LEG3_HUMAN	P17931	Galectin-3	729	26209.3917	4	21.2	1.061
LUM_HUMAN	P51884	Lumican	1646	38771.222	9	26.9	4.434
PPIA_HUMAN	P62937	Peptidyl-prolyl cis-trans isomerase A	4106	18240.6427	10	59.4	3.527
PRDX1_HUMAN	Q06830	Peroxiredoxin-1	1137	22338.4925	6	25.6	0.963
PRDX2_HUMAN	P32119	Peroxiredoxin-2	1905	22063.0168	5	29.3	1.123
PROF1_HUMAN	P07737	Profilin-1	2639	15225.3488	7	50.7	1.608
S10A6_HUMAN	P06703	Protein S100-A6	697	10236.7832	3	24.4	4.396
S10AA_HUMAN	P60903	Protein S100-A10	565	11317.2115	2	35.1	1.234
SPB5_HUMAN	P36952	Serpin B5	576	42556.5983	11	40.0	1.048
TRFE_HUMAN	P02787	Serotransferrin	716	79345.0824	10	17.6	1.657
VIME_HUMAN	P08670	Vimentin	1798	53708.7907	14	33.1	2.057

12.2 Full MS data for the 35 proteins identified as interacting with alpha-1-antitrypsin, presented in Table 4.4

Protein entry and accession number are unique identifiers for each protein. Protein score is a software generated value taking into account the quality of the data used to identify that protein. Matched peptides to protein details the number of peptides detected in the sample mixture for that specific protein. Amount of protein indicates the relative abundance of each protein compared with a standard peptide spiked into the mixture.

Protein Entry	Protein Accession Number	Protein Full Name	Protein Score	Average Protein Mass (Da)	Matched Peptides to Protein	Protein Sequence Coverage (%)	Amount of Protein (fmol)
1433B_HUMAN	P31946	14-3-3 protein beta/alpha	665	28196.5102	2	5.3	4.491
1433E_HUMAN	P62258	14-3-3 protein epsilon	508	29345.0493	1	3.1	4.491
1433F_HUMAN	Q04917	14-3-3 protein eta	665	28389.8608	2	5.3	4.491
1433G_HUMAN	P61981	14-3-3 protein gamma	665	28473.7251	2	5.3	4.491
1433S_HUMAN	P31947	14-3-3 protein sigma	665	27888.1757	2	5.2	4.491
1433T_HUMAN	P27348	14-3-3 protein theta	665	28049.4331	2	5.3	4.491
1433Z_HUMAN	P63104	14-3-3 protein zeta/delta	1502	27916.2394	5	18.8	4.491
ANXA2_HUMAN	P07355	Annexin A2	1323	38832.2204	9	28.9	5.150
ANXA5_HUMAN	P08758	Annexin A5	358	35993.8588	2	13.1	2.475
AXA2L_HUMAN	A6NMY6	Putative annexin A2-like protein	1145	38830.1648	7	23.6	5.150
CALL3_HUMAN	P27482	Calmodulin-like protein 3	179	16947.7959	6	47.7	0.598
CALL5_HUMAN	Q9NZT1	Calmodulin-like protein 5	1084	15892.5388	5	39.7	2.485
CALM_HUMAN	P62158	Calmodulin	578	16837.6523	4	26.9	2.799
ENOA_HUMAN	P06733	Alpha-enolase	350	47511.2010	7	18.2	3.096
G3P_HUMAN	P04406	Glyceraldehyde-3-phosphate dehydrogenase	567	36224.3681	7	39.1	3.125
GRP78_HUMAN	P11021	78 kDa glucose-regulated protein	176	72447.1105	4	6.3	2.866
GSTP1_HUMAN	P09211	Glutathione S-transferase P	952	23583.9696	5	43.3	1.639
HBAZ_HUMAN	P02008	Hemoglobin subunit zeta	1184	15694.0702	1	4.9	0.265
HS71L_HUMAN	P34931	Heat shock 70 kDa protein 1-like	208	70774.3427	3	5.6	2.866
HSP71_HUMAN	P08107	Heat shock 70 kDa protein 1A/1B	205	70337.4552	2	3.7	2.866
HSP72_HUMAN	P54652	Heat shock-related 70 kDa protein 2	205	70306.2015	2	3.8	2.866
HSP7C_HUMAN	P11142	Heat shock cognate 71 kDa protein	220	71126.3096	4	5.4	2.866
IGHG1_HUMAN	P01857	Ig gamma-1 chain C region	140	36619.1863	3	14.9	2.079
MDHC_HUMAN	P40925	Malate dehydrogenase_ cytoplasmic	485	36654.3026	2	9.6	1.550
PAL4A_HUMAN	Q9Y536	Peptidyl-prolyl cis-trans isomerase A-like 4A/B/C	670	18409.9414	1	4.3	2.383
PAL4D_HUMAN	F5H284	Peptidyl-prolyl cis-trans isomerase A-like 4D	670	18394.8625	1	4.3	2.383
PAL4G_HUMAN	A2BFH1	Peptidyl-prolyl cis-trans isomerase A-like 4G	670	18393.8522	1	4.3	2.383
PGK1_HUMAN	P00558	Phosphoglycerate kinase 1	648	45013.9805	3	12.0	1.991
PGK2_HUMAN	P07205	Phosphoglycerate kinase 2	616	45195.4213	1	3.6	1.991
PPIA_HUMAN	P62937	Peptidyl-prolyl cis-trans isomerase A	1194	18240.6427	5	32.1	2.383
PROF1_HUMAN	P07737	Profilin-1	1166	15225.3488	3	28.6	1.701
RAB44_HUMAN	Q7Z6P3	Ras-related protein Rab-44	147	78037.3847	7	21.3	7.953
SBSN_HUMAN	Q6UWP8	Suprabasin	125	60597.9204	3	9.2	3.321
SH3L3_HUMAN	Q9H299	SH3 domain-binding glutamic acid-rich-like protein 3	401	10494.7603	1	20.4	0.827
TRFE_HUMAN	P02787	Serotransferrin	177	79345.0824	7	14.3	1.715

12.3 Full MS data for the 71 proteins identified as interacting with cystatin A, presented in Table 4.5

Protein entry and accession number are unique identifiers for each protein. Protein score is a software generated value taking into account the quality of the data used to identify that protein. Matched peptides to protein details the number of peptides detected in the sample mixture for that specific protein. Amount of protein indicates the relative abundance of each protein compared with a standard peptide spiked into the mixture.

Protein Entry	Protein Accession Number	Protein Full Name	Protein Score	Average Protein Mass (Da)	Matched Peptides to Protein	Protein Sequence Coverage (%)	Amount of Protein (fmol)
1433B_HUMAN	P31946	14-3-3 protein beta/alpha	1870	28196.5102	7	25.20	1.677
1433E_HUMAN	P62258	14-3-3 protein epsilon	1854	29345.0493	3	12.16	1.588
1433S_HUMAN	P31947	14-3-3 protein sigma	4192	27888.1757	6	18.15	7.121
1433Z_HUMAN	P63104	14-3-3 protein zeta/delta	5325	27916.2394	6	23.67	5.620
A1AT_HUMAN	P01009	Alpha-1-antitrypsin	1173	46907.7136	8	18.66	3.480
ACTB_HUMAN	P60709	Actin_ cytoplasmic 1	4992	42079.0170	15	54.40	7.547
AL1A1_HUMAN	P00352	Retinal dehydrogenase 1	210	55489.2213	6	11.58	1.537
ALBU_HUMAN	P02768	Serum albumin	17793	71362.7109	49	73.56	30.299
ALDOA_HUMAN	P04075	Fructose-bisphosphate aldolase A	338	39876.2787	6	22.80	1.773
ANXA1_HUMAN	P04083	Annexin A1	2318	38942.4262	14	44.51	1.848
ANXA2_HUMAN	P07355	Annexin A2	9120	38832.2204	24	54.57	6.777
ANXA4_HUMAN	P09525	Annexin A4	457	36110.9082	8	29.47	0.746
ANXA5_HUMAN	P08758	Annexin A5	1941	35993.8588	11	28.13	3.047
ANXA6_HUMAN	P08133	Annexin A6	198	76215.5931	6	8.92	0.627
ARGI1_HUMAN	P05089	Arginase-1	1565	34906.0649	6	25.16	1.697
ATPA_HUMAN	P25705	ATP synthase subunit alpha_ mitochondrial	377	59864.7823	9	14.47	0.708
CALL3_HUMAN	P27482	Calmodulin-like protein 3	1678	16947.7959	3	20.13	0.602
CALL5_HUMAN	Q9NZT1	Calmodulin-like protein 5	3232	15892.5388	8	69.18	2.171
CALM_HUMAN	P62158	Calmodulin	1743	16837.6523	4	32.89	1.756
CASPE_HUMAN	P31944	Caspase-14	316	27964.7122	5	20.25	0.869
CD44_HUMAN	P16070	CD44 antigen	137	82050.9837	2	2.83	1.382
CO1A1_HUMAN	P02452	Collagen alpha-1(I) chain	890	139968.1403	41	29.58	6.775
CO1A2_HUMAN	P08123	Collagen alpha-2(I) chain	534	129827.2687	32	34.99	4.229
CO6A1_HUMAN	P12109	Collagen alpha-1(VI) chain	564	109670.0622	11	17.32	1.799
CO6A2_HUMAN	P12110	Collagen alpha-2(VI) chain	514	109777.1344	11	12.37	1.350
CO6A3_HUMAN	P12111	Collagen alpha-3(VI) chain	1092	345380.5637	62	24.33	3.436
COEA1_HUMAN	Q05707	Collagen alpha-1(XIV) chain	252	194599.2742	21	15.37	1.197
DCD_HUMAN	P81605	Dermcidin	2399	11397.9338	4	23.64	1.493
DHE3_HUMAN	P00367	Glutamate dehydrogenase 1_ mitochondrial	606	61740.1428	12	27.06	0.745
ENOA_HUMAN	P06733	Alpha-enolase	4075	47511.2010	17	43.09	5.275
FABP5_HUMAN	Q01469	Fatty acid-binding protein_ epidermal	2534	15506.6309	5	31.11	2.325
FIBB_HUMAN	P02675	Fibrinogen beta chain	172	56612.6167	6	11.20	0.624
FIBG_HUMAN	P02679	Fibrinogen gamma chain	263	52139.0338	6	15.67	0.853
GDIB_HUMAN	P50395	Rab GDP dissociation inhibitor beta	212	51119.5596	9	17.30	1.015
GELS_HUMAN	P06396	Gelsolin	492	86096.8228	11	14.32	1.099
GRP78_HUMAN	P11021	78 kDa glucose-regulated protein	515	72447.1105	12	23.55	1.215
GSTP1_HUMAN	P09211	Glutathione S-transferase P	4464	23583.9696	9	53.33	4.071
H12_HUMAN	P16403	Histone H1.2	628	21364.7689	3	9.86	0.777
HNRPK_HUMAN	P61978	Heterogeneous nuclear ribonucleoprotein K	461	51261.4781	6	16.63	0.959
HPT_HUMAN	P00738	Haptoglobin	2896	45889.6837	10	41.13	4.299
HS90A_HUMAN	P07900	Heat shock protein HSP 90-alpha	644	85059.0572	12	13.25	2.700
HSP71_HUMAN	P08107	Heat shock 70 kDa protein 1A/1B	1541	70337.4552	17	37.13	1.582
HSP7C_HUMAN	P11142	Heat shock cognate 71 kDa protein	1082	71126.3096	18	29.72	1.021
IGHG1_HUMAN	P01857	Ig gamma-1 chain C region	964	36619.1863	10	40.91	2.148
KPYM_HUMAN	P14618	Pyruvate kinase PKM	2592	58507.2826	19	44.63	3.436
LDHA_HUMAN	P00338	L-lactate dehydrogenase A chain	3289	36973.9299	11	30.42	3.562
LMNA_HUMAN	P02545	Prelamin-A/C	284	74424.7180	13	23.64	0.862
LRIQ3_HUMAN	A6PVS8	Leucine-rich repeat and IQ domain-containing protein 3	193	74302.4365	6	10.26	4.772
LUM_HUMAN	P51884	Lumican	2564	38771.2220	11	32.54	6.388
MDHC_HUMAN	P40925	Malate dehydrogenase_ cytoplasmic	610	36654.3026	6	20.36	1.109
MDHM_HUMAN	P40926	Malate dehydrogenase_ mitochondrial	245	35959.5534	7	24.85	1.025
PDIA1_HUMAN	P07237	Protein disulfide-isomerase	1204	57515.6095	19	37.99	2.004
PDIA3_HUMAN	P30101	Protein disulfide-isomerase A3	731	57181.6493	12	26.73	1.051
PGAM1_HUMAN	P18669	Phosphoglycerate mutase 1	804	28918.0363	6	25.59	0.934
PGK1_HUMAN	P00558	Phosphoglycerate kinase 1	1847	45013.9805	18	50.36	11.372
PGS2_HUMAN	P07585	Decorin	518	40088.9951	5	19.50	1.069
PLST_HUMAN	P13797	Plastin-3	369	71324.4032	5	10.95	1.288
PPIA_HUMAN	P62937	Peptidyl-prolyl cis-trans isomerase A	2214	18240.6427	7	33.94	4.043
PRDX1_HUMAN	Q06830	Peroxiredoxin-1	1935	22338.4925	8	34.17	1.586

Continued overleaf

PRDX2_HUMAN	P32119	Peroxiredoxin-2	2159	22063.0168	6	24.75	1.105
PRDX6_HUMAN	P30041	Peroxiredoxin-6	444	25149.0747	5	26.79	0.745
PROF1_HUMAN	P07737	Profilin-1	4658	15225.3488	7	50.71	2.435
S10A6_HUMAN	P06703	Protein S100-A6	6124	10236.7832	4	33.33	8.391
SBSN_HUMAN	Q6UWP8	Suprabasin	522	60597.9204	6	23.73	2.390
SPB5_HUMAN	P36952	Serpin B5	1976	42556.5983	13	42.40	2.220
TAGL2_HUMAN	P37802	Transgelin-2	2390	22562.5876	6	29.15	1.525
TALDO_HUMAN	P37837	Transaldolase	330	37711.2783	4	12.76	1.039
TPM4_HUMAN	P67936	Tropomyosin alpha-4 chain	420	28635.9130	4	17.74	0.639
TRFE_HUMAN	P02787	Serotransferrin	1675	79345.0824	14	29.23	3.595
VIME_HUMAN	P08670	Vimentin	2379	53708.7907	15	27.47	2.366
VTDB_HUMAN	P02774	Vitamin D-binding protein	199	54560.4875	4	7.17	0.916

12.4 Full MS data for the 30 proteins identified as interacting with cystatin C, presented in Table 4.6

Protein entry and accession number are unique identifiers for each protein. Protein score is a software generated value taking into account the quality of the data used to identify that protein. Matched peptides to protein details the number of peptides detected in the sample mixture for that specific protein. Amount of protein indicates the relative abundance of each protein compared with a standard peptide spiked into the mixture.

Protein Entry	Protein Accession Number	Protein Full Name	Protein Score	Average Protein Mass (Da)	Matched Peptides to Protein	Protein Sequence Coverage (%)	Amount of Protein (fmol)
1433B_HUMAN	P31946	14-3-3 protein beta/alpha	247	28196.5102	4	14.2	1.2027
1433F_HUMAN	Q04917	14-3-3 protein eta	228	28389.8608	3	5.3	1.2027
1433G_HUMAN	P61981	14-3-3 protein gamma	228	28473.7251	3	5.3	1.2027
1433S_HUMAN	P31947	14-3-3 protein sigma	324	27888.1757	4	8.9	1.2027
1433T_HUMAN	P27348	14-3-3 protein theta	228	28049.4331	3	5.3	1.2027
1433Z_HUMAN	P63104	14-3-3 protein zeta/delta	337	27916.2394	6	17.6	1.1835
ACTA_HUMAN	P62736	Actin_ aortic smooth muscle	325	42408.2561	3	8.0	4.1512
ACTB_HUMAN	P60709	Actin_ cytoplasmic 1	1065	42079.0170	7	24.3	4.1512
ACTC_HUMAN	P68032	Actin_ alpha cardiac muscle 1	325	42361.2493	3	8.0	4.1512
ACTG_HUMAN	P63261	Actin_ cytoplasmic 2	1065	42135.1246	7	24.3	4.1512
ACTH_HUMAN	P63267	Actin_ gamma-enteric smooth muscle	325	42276.1803	3	8.0	4.1512
ACTS_HUMAN	P68133	Actin_ alpha skeletal muscle	325	42393.3153	3	8.0	4.1512
ALBU_HUMAN	P02768	Serum albumin	4228	71362.7109	20	34.8	7.9415
ANXA2_HUMAN	P07355	Annexin A2	2020	38832.2204	10	26.8	2.2724
ARGI1_HUMAN	P05089	Arginase-1	386	34906.0649	3	16.5	0.5413
AXA2L_HUMAN	A6NMY6	Putative annexin A2-like protein	1938	38830.1648	9	24.2	2.2724
CASPE_HUMAN	P31944	Caspase-14	335	27964.7122	3	15.3	1.1752
CO1A1_HUMAN	P02452	Collagen alpha-1(I) chain	332	139968.1403	25	20.8	5.513
ENOA_HUMAN	P06733	Alpha-enolase	578	47511.2010	5	15.2	1.3589
FIBG_HUMAN	P02679	Fibrinogen gamma chain	181	52139.0338	7	22.1	1.2147
G3P_HUMAN	P04406	Glyceraldehyde-3-phosphate dehydrogenase	645	36224.3681	10	47.8	1.821
H31_HUMAN	P68431	Histone H3.1	651	15518.1658	3	14.7	0.7786
H31T_HUMAN	Q16695	Histone H3.1t	651	15622.3388	3	14.7	0.7786
H32_HUMAN	Q71DI3	Histone H3.2	651	15445.0777	3	14.7	0.7786
H33_HUMAN	P84243	Histone H3.3	651	15384.9580	3	14.7	0.7786
HBAZ_HUMAN	P02008	Hemoglobin subunit zeta	778	15694.0702	1	4.9	7.8943
NIT2_HUMAN	Q9NQR4	Omega-amidase NIT2	286	31007.1910	4	21.4	3.4661
PPIA_HUMAN	P62937	Peptidyl-prolyl cis-trans isomerase A	920	18240.6427	2	12.1	1.1193
PRDX2_HUMAN	P32119	Peroxiredoxin-2	264	22063.0168	3	29.3	0.7174
PROF1_HUMAN	P07737	Profilin-1	365	15225.3488	2	22.9	0.5894

12.5 Full MS data for the 24 proteins identified as interacting with elafin, presented in Table 4.7

Protein entry and accession number are unique identifiers for each protein. Protein score is a software generated value taking into account the quality of the data used to identify that protein. Matched peptides to protein details the number of peptides detected in the sample mixture for that specific protein. Amount of protein indicates the relative abundance of each protein compared with a standard peptide spiked into the mixture.

Protein Entry	Protein Accession Number	Protein Full Name	Protein Score	Average Protein Mass (Da)	Matched Peptides to Protein	Protein Sequence Coverage (%)	Amount of Protein (fmol)
1433S_HUMAN	P31947	14-3-3 protein sigma	1014	27888.1757	6	16.5	10.791
ACTA_HUMAN	P62736	Actin_ aortic smooth muscle	258	42408.2561	5	11.1	3.796
ACTB_HUMAN	P60709	Actin_ cytoplasmic 1	269	42079.0170	8	25.9	3.796
ACTC_HUMAN	P68032	Actin_ alpha cardiac muscle 1	258	42361.2493	5	11.1	3.796
ACTG_HUMAN	P63261	Actin_ cytoplasmic 2	269	42135.1246	8	25.9	3.796
ACTH_HUMAN	P63267	Actin_ gamma-enteric smooth muscle	258	42276.1803	5	11.2	3.796
ACTS_HUMAN	P68133	Actin_ alpha skeletal muscle	258	42393.3153	5	11.1	3.796
ALBU_HUMAN	P02768	Serum albumin	1370	71362.7109	14	17.4	50.253
ANXA2_HUMAN	P07355	Annexin A2	470	38832.2204	4	9.4	7.016
AXA2L_HUMAN	A6NMY6	Putative annexin A2-like protein	470	38830.1648	4	9.4	7.016
CO1A1_HUMAN	P02452	Collagen alpha-1(I) chain	86	139968.1403	7	6.5	19.299
ENOA_HUMAN	P06733	Alpha-enolase	501	47511.2010	5	7.6	4.198
FABP5_HUMAN	Q01469	Fatty acid-binding protein_ epidermal	459	15506.6309	2	20.0	3.793
GSTP1_HUMAN	P09211	Glutathione S-transferase P	209	23583.9696	2	11.0	3.869
H31_HUMAN	P68431	Histone H3.1	263	15518.1658	2	10.3	1.779
H31T_HUMAN	Q16695	Histone H3.1t	263	15622.3388	2	10.3	1.779
H32_HUMAN	Q71DI3	Histone H3.2	263	15445.0777	2	10.3	1.779
H33_HUMAN	P84243	Histone H3.3	263	15384.9580	2	10.3	1.779
MON1A_HUMAN	Q86VX9	Vacuolar fusion protein MON1 homolog A	106	62473.6958	3	9.4	4.009
PAL4A_HUMAN	Q9Y536	Peptidyl-prolyl cis-trans isomerase A-like 4A/B/C	459	18409.9414	2	7.9	6.641
PAL4D_HUMAN	F5H284	Peptidyl-prolyl cis-trans isomerase A-like 4D	459	18394.8625	2	7.9	6.641
PAL4G_HUMAN	A2BFH1	Peptidyl-prolyl cis-trans isomerase A-like 4G	459	18393.8522	2	7.9	6.641
PPIA_HUMAN	P62937	Peptidyl-prolyl cis-trans isomerase A	495	18240.6427	4	29.7	6.641
PROF1_HUMAN	P07737	Profilin-1	240	15225.3488	2	14.3	1.270

12.6 Full mass spectrometry data for the 89 proteins identified as being significantly differentially expressed in unscarred control compared with unscarred hypertrophic tissue

Protein accession number is a unique identifier for each protein. Peptide count details the total number of peptides detected for that protein and unique peptides refers to the peptides that can only have come from that specific protein. Confidence score is a software generated value taking into account the quality of the data used to identify that protein. Maximum fold change is the greatest value difference between a single control and hypertrophic scar sample. Proteins highlighted in green were upregulated in the control samples and those that are highlighted in red were upregulated in the hypertrophic scar samples.

Protein Accession	Description	Peptide count	Unique peptides	Confidence score	ANOVA (p-value)	Maximum fold change	Detected in which fractions?
Q9X697	VdcC protein	3	1	15	0.0489	Infinity	4
Q56703	Polar flagellin A	2	1	9	0.0325	17443.7	4
O75616	GTPase Era, mitochondrial	1	1	5	0.0303	265.8	8
P52521	U4 protein	1	1	3	0.0464	157.3	4
P44933	Glutathione-regulated potassium-efflux system protein	1	1	4	0.0348	37.0	4
Q9NX46	Poly(ADP-ribose) glycohydrolase ARH3	10	2	58	0.0129	33.7	1;2;3
Q58084	Hypothetical protein MJ0670	3	1	13	0.0353	19.5	4
O94856	Neurofascin	3	3	20	0.0236	9.2	6
Q9UDW1	Cytochrome b-c1 complex subunit 9	4	2	29	0.0235	9.0	2;4
P11048	Lamin A	34	4	236	0.0281	8.7	4
P38367	Outer membrane protein class 4 precursor	1	1	0	0.0458	7.4	4
O53677	Cobyric acid synthase	2	1	5	0.0211	7.3	4
O43405	Cochlin	3	1	15	0.0222	6.4	5
P02304	Histone H4	7	3	55	0.0477	6.0	4
Q9ULM3	YEATS domain-containing protein 2	3	2	22	0.0194	4.3	6
Q96RG2	PAS domain-containing serine/threonine-protein kinase	5	1	26	0.0229	4.1	6
P19012	Keratin, type I cytoskeletal 15	121	38	778	0.0027	4.1	1;2;3;4;5;6;7;8
P08236	Beta-glucuronidase	4	1	16	0.0402	3.8	5
Q9RN18	Hypothetical protein pXO2-14	8	6	37	0.0471	3.5	4
P61626	Lysozyme C	4	1	22	0.0340	3.3	5;6;7
O60888	Protein CutA	3	2	17	0.0496	3.2	2;3;5;6
P13646	Keratin, type I cytoskeletal 13	75	10	493	0.0002	3.1	1;2;3;4;5;6;7
P36969	Phospholipid hydroperoxide glutathione peroxidase, mitochondrial	11	4	64	0.0019	3.0	1;2;3;4;5
Q15366	Poly(rC)-binding protein 2	19	2	101	0.0019	2.9	1;2;3;4;5;7;8
P10589	COUP transcription factor 1	4	1	31	0.0024	2.9	7;8
Q08380	Galectin-3-binding protein	11	4	54	0.0114	2.7	2;3;5;6
P02533	Keratin, type I cytoskeletal 14	167	40	1070	0.0342	2.5	1;2;3;4;5;6;7;8
P55809	Succinyl-CoA:3-ketoacid coenzyme A transferase 1, mitochondrial	6	3	29	0.0320	2.5	2;6
Q5T6V5	UPF0553 protein C9orf64	8	1	50	0.0166	2.5	2;3
Q6FI81	Anamorsin	1	1	5	0.0409	2.5	7
Q9Y2E4	Disco-interacting protein 2 homolog C	4	1	20	0.0087	2.4	3
P55058	Phospholipid transfer protein	6	2	37	0.0103	2.3	4;5
Q04695	Keratin, type I cytoskeletal 17	105	15	743	0.0007	2.3	1;2;3;4;5;6;7
P62136	Serine/threonine-protein phosphatase PP1-alpha catalytic subunit	16	3	118	0.0240	2.3	2;5;6;7
Q9BXJ9	N-alpha-acetyltransferase 15, NatA auxiliary subunit	5	3	17	0.0489	2.2	2;3
Q14203	Dynactin subunit 1	56	16	316	0.0472	2.1	1;2;3;4;5;6
P62158	Calmodulin	16	6	113	0.0323	2.0	1;2;3;4;5;6
P01111	GTPase NRas	5	2	31	0.0121	2.0	5;7
P01859	Ig gamma-2 chain C region	108	24	693	0.0437	2.1	1;2;3;4;5;6;7;8
P13807	Glycogen [starch] synthase, muscle	4	1	21	0.0165	2.1	5
Q5VU43	Myomegalin	9	1	36	0.0329	2.1	2;3
Q53GQ0	Estradiol 17-beta-dehydrogenase 12	13	2	74	0.0212	2.2	6;7;8
P01611	Ig kappa chain V-I region Wes	3	2	29	0.0446	2.2	2;3;4;5;6
P27348	14-3-3 protein theta	36	9	279	0.0419	2.2	1;2;3;4;5;6;7;8
Q15363	Transmembrane emp24 domain-containing protein 2	7	6	51	0.0412	2.3	5;6;7
O14980	Exportin-1	24	7	115	0.0443	2.3	2;5
P54802	Alpha-N-acetylglucosaminidase	9	1	38	0.0433	2.3	2;3;7
P39023	60S ribosomal protein L3	12	9	69	0.0371	2.5	1;2;5;6;7
Q6P1W5	Uncharacterized protein C1orf94	2	2	16	0.0236	2.6	6
P55084	Trifunctional enzyme subunit beta, mitochondrial	46	26	331	0.0201	2.6	1;2;3;4;5;6;7;8
Q9C035	Tripartite motif-containing protein 5	5	1	30	0.0375	2.6	3;8
Q9UJ71	C-type lectin domain family 4 member K	9	3	55	0.0051	2.7	5;6
Q96L46	Calpain small subunit 2	7	4	45	0.0484	2.8	2;3;5
P16083	Ribosyldihydronicotinamide dehydrogenase	9	6	56	0.0379	2.9	2;3;4;5
Q9BY32	Inosine triphosphate pyrophosphatase	3	2	16	0.0425	2.9	5;7
P09486	SPARC	11	9	68	0.0033	2.9	1;2;3;4;5;6
Q99538	Legumain	16	5	95	0.0357	3.0	4;5;6
Q5JSJ4	Protein DDX26B	2	1	11	0.0032	3.4	6
P04196	Histidine-rich glycoprotein	35	18	270	0.0365	3.4	1;2;3;4;5;6;7
Q13838	Spliceosome RNA helicase DDX39B	31	8	219	0.0328	3.6	1;2;3;4;5;6;7;8
Q8IU60	m7GpppN-mRNA hydrolase	1	1	4	0.0036	3.8	7
P12709	Glucose-6-phosphate isomerase	15	7	103	0.0210	4.2	4
Q96283	Ras-related protein Rab11A	4	1	38	0.0244	4.4	4
Q8N998	Coiled-coil domain-containing protein 89	2	2	19	0.0190	4.5	1
P35203	Centromere DNA-binding protein complex CBF3	3	1	15	0.0465	4.6	4
Q8TB36	Ganglioside-induced differentiation-associated protein 1	3	1	20	0.0388	4.8	5
Q6WCQ1	Myosin phosphatase Rho-interacting protein	5	1	24	0.0475	5.0	2
Q04941	Proteolipid protein 2	3	2	27	0.0057	5.1	1;2;7;8
Q14767	Latent-transforming growth factor beta-binding protein 2	2	1	8	0.0437	5.6	2
Q96AX2	Ras-related protein Rab-37	6	2	30	0.0304	5.7	1;2;3;4;5;6;7
Q6ZVC0	Neuronal tyrosine-phosphorylated phosphoinositide-3-kinase adapter 1	3	1	14	0.0424	6.5	5
A2RUR9	Coiled-coil domain-containing protein 144A	16	2	78	0.0223	6.7	2;3
Q14161	ARF GTPase-activating protein GIT2	3	1	13	0.0243	7.5	5
Q9NR48	Histone-lysine N-methyltransferase ASH1L	9	2	30	0.0149	7.6	1
Q96QU1	Protocadherin-15	5	1	17	0.0443	10.4	3
P25246	Hypothetical 21.8 kDa protein in RNA2	2	2	8	0.0220	10.4	4

Continued overleaf

O94973	AP-2 complex subunit alpha-2	30	10	220	0.0498	10.5	2;5;6;7;8
Q8IUI4	Putative protein SNX29P2	2	1	9	0.0142	12.0	6
Q00042	Putative transposon gamma-delta 80.3 kDa protein	3	1	14	0.0281	12.6	4
Q31612	HLA class I histocompatibility antigen, B-73 alpha chain	10	1	77	0.0360	12.6	1;2;3;5;6;7
Q96JB8	MAGUK p55 subfamily member 4	1	1	10	0.0324	21.6	5
Q86YS7	C2 domain-containing protein 5	2	1	10	0.0117	22.8	7
P71384	Fumarate hydratase class II	4	1	19	0.0187	31.6	4
O75781	Paralemmin-1	7	1	39	0.0257	43.1	1;2;5
Q92917	G patch domain and KOW motifs-containing protein	2	1	10	0.0218	54.8	7
P16403	Histone H1.2	28	1	223	0.0183	118.9	1;2;3;4;5;6;7
Q8WXW3	Progesterone-induced-blocking factor 1	6	1	27	0.0081	Infinity	3
Q9H6D8	Fibronectin type III domain-containing protein 4	3	1	14	0.0073	Infinity	2

12.7 Full MS data for the 30 proteins identified as being significantly differentially expressed in unscarred control compared with unscarred hypertrophic tissue, presented in Table 6.2, selected from the longer list of 89 proteins

Protein accession number is a unique identifier for each protein. Peptide count details the total number of peptides detected for that protein and unique peptides refers to the peptides that can only have come from that specific protein. Confidence score is a software generated value taking into account the quality of the data used to identify that protein. Maximum fold change is the greatest value difference between a single control and hypertrophic scar sample. Proteins highlighted in green were upregulated in the control samples and those that are highlighted in red were upregulated in the hypertrophic scar samples.

Protein Accession	Description	Peptide count	Unique peptides	Confidence score	ANOVA (p-value)	Maximum fold change	Detected in which fractions?
Q9NX46	Poly(ADP-ribose) glycohydrolase ARH3	10	2	58	0.0129	33.7	1;2;3
P02545	Lamin A.	34	4	236	0.0281	8.7	4
P19012	Keratin, type I cytoskeletal 15	121	38	778	0.0027	4.1	1;2;3;4;5;6;7;8
P13646	Keratin, type I cytoskeletal 13	75	10	493	0.0002	3.1	1;2;3;4;5;6;7
P36969	Phospholipid hydroperoxide glutathione peroxidase, mitochondrial	11	4	64	0.0019	3.0	1;2;3;4;5
Q15366	Poly(rC)-binding protein 2	19	2	101	0.0019	2.9	1;2;3;4;5;7;8
Q08380	Galectin-3-binding protein	11	4	54	0.0114	2.7	2;3;5;6
P02533	Keratin, type I cytoskeletal 14	167	40	1070	0.0342	2.5	1;2;3;4;5;6;7;8
Q04695	Keratin, type I cytoskeletal 17	105	15	743	0.0007	2.3	1;2;3;4;5;6;7
P62136	Serine/threonine-protein phosphatase PP1-alpha catalytic subunit	16	3	118	0.0240	2.3	2;5;6;7
Q14203	Dynactin subunit 1	56	16	316	0.0472	2.1	1;2;3;4;5;6
P62158	Calmodulin	16	6	113	0.0323	2.0	1;2;3;4;5;6
P01859	Ig gamma-2 chain C region	108	24	693	0.0437	2.1	1;2;3;4;5;6;7;8
Q53GQ0	Estradiol 17-beta-dehydrogenase 12	13	2	74	0.0212	2.2	6;7;8
P27348	14-3-3 protein theta	36	9	279	0.0419	2.2	1;2;3;4;5;6;7;8
Q15363	Transmembrane emp24 domain-containing protein 2	7	6	51	0.0412	2.3	5;6;7
O14980	Exportin-1	24	7	115	0.0443	2.3	2;5
P39023	60S ribosomal protein L3	12	9	69	0.0371	2.5	1;2;5;6;7
P55084	Trifunctional enzyme subunit beta, mitochondrial	46	26	331	0.0201	2.6	1;2;3;4;5;6;7;8
Q9UJ71	C-type lectin domain family 4 member K	9	3	55	0.0051	2.7	5;6
P16083	Ribosyldihydronicotinamide dehydrogenase	9	6	56	0.0379	2.9	2;3;4;5
P09486	SPARC	11	9	68	0.0033	2.9	1;2;3;4;5;6
Q99538	Legumain	16	5	95	0.0357	3.0	4;5;6
P04196	Histidine-rich glycoprotein	35	18	270	0.0365	3.4	1;2;3;4;5;6;7
Q13838	Spliceosome RNA helicase DDX39B	31	8	219	0.0328	3.6	1;2;3;4;5;6;7;8
P06744	Glucose-6-phosphate isomerase	15	7	103	0.0210	4.2	4
A2RUR9	Coiled-coil domain-containing protein 144A	16	2	78	0.0223	6.7	2;3
O94973	AP-2 complex subunit alpha-2	30	10	220	0.0498	10.5	2;5;6;7;8
Q31612	HLA class I histocompatibility antigen, B-73 alpha chain	10	1	77	0.0360	12.6	1;2;3;5;6;7
P16403	Histone H1.2	28	1	223	0.0183	118.9	1;2;3;4;5;6;7

12.8 Full MS data for the 17 proteins significantly differentially expressed between the achievers and non-achievers of pre-surgery oxygen saturation levels, presented in Table 7.1

Protein accession number is a unique identifier for each protein. Maximum fold change is the greatest value difference between a single control and hypertrophic scar sample. Peptide count details the total number of peptides detected for that protein and unique peptides refers to the peptides that can only have come from that specific protein. Confidence score is a software generated value taking into account the quality of the data used to identify that protein. Proteins highlighted in blue were upregulated in the samples that did achieve their pre-operative oxygen saturation levels and those that are highlighted in red were upregulated in those that did not achieve their pre-operative oxygen saturation levels.

Protein Accession Number	ANOVA (p-value)	Maximum Fold Change	Protein Full Name	Peptide Count	Unique Peptides	Confidence Score	Detected in which fractions?
Q2TBE0	0.0236	13.6	CWF19-like protein 2	5	3	24	1;3
Q7Z2Z2	0.0478	3.2	Elongation factor Tu GTP-binding domain-containing protein 1	5	2	33	2
Q6ZMU5	0.0339	3.0	Tripartite motif-containing protein 72	3	1	20	3;4
Q9BRX8	0.0353	2.7	Redox-regulatory protein FAM213A	2	1	15	2;4
Q9BUH8	0.0380	2.3	Brain-enriched guanylate kinase-associated protein	4	2	19	2;3
Q14141	0.0286	2.1	Septin-6	25	4	162	1;2;3;4
P51451	0.0376	2.2	Tyrosine-protein kinase Blk	6	1	32	2;3;4
P27448	0.0259	2.3	MAP/microtubule affinity-regulating kinase 3	6	3	32	1
P04259	0.0289	2.4	Keratin, type II cytoskeletal 6B	64	2	487	1;2;3;4
Q6P3W2	0.0364	2.5	DnaJ homolog subfamily C member 24	3	2	15	2;3;4
Q96AC1	0.0167	2.6	Fermitin family homolog 2	6	4	35	1;2;3
Q03135	0.0277	3.2	Caveolin-1	8	2	68	1;2;3;4
P35968	0.0356	3.4	Vascular endothelial growth factor receptor 2	24	4	120	1;2;3;4
P18859	0.0330	3.7	ATP synthase-coupling factor 6, mitochondrial	3	3	28	1;2
Q9H3G5	0.0435	6.6	Probable serine carboxypeptidase CPVL	3	2	18	1;2;3
Q5SQN1	0.0241	45.4	Synaptosomal-associated protein 47	8	1	40	1;2;3;4
P60033	0.0234	55.8	CD81 antigen	3	1	17	4

12.9 Full MS data for the 47 proteins significantly differentially expressed between the CD <2 and the CD ≥2 groups, presented in Table 7.4

Protein accession number is a unique identifier for each protein. Maximum fold change is the greatest value difference between a single control and hypertrophic scar sample. Peptide count details the total number of peptides detected for that protein and unique peptides refers to the peptides that can only have come from that specific protein. Confidence score is a software generated value taking into account the quality of the data used to identify that protein. Proteins highlighted in blue were upregulated in the samples that had minimal post-operative complications and those that are highlighted in red had serious post-operative complications.

Protein Accession Number	ANOVA (p-value)	Maximum Fold Change	Protein Full Name	Peptide Count	Unique Peptides	Confidence Score	Detected in which fractions?
Q29960	0.00502	205.5	HLA class I histocompatibility antigen, Cw-16 alpha chain	9	1	67	1;2;3;4
Q15019	0.00763	45.4	Septin-2	10	2	68	1;2;3;4
A6NNZ2	0.00721	38.1	Tubulin beta-8 chain-like protein LOC260334	12	1	78	1;2;3;4
Q9NR30	0.03653	24.6	Nucleolar RNA helicase 2	11	4	58	1;2;3;4
Q13561	0.03865	15.7	Dynactin subunit 2	9	3	51	1;2;3;4
Q96MM6	0.02799	15.5	Heat shock 70 kDa protein 12B	8	2	53	1;3;4
P60903	0.00333	12.4	Protein S100-A10	9	2	65	2;3;4
P11413	0.02505	11.5	Glucose-6-phosphate 1-dehydrogenase	8	2	56	1;2;3;4
O75083	0.04586	6.4	WD repeat-containing protein 1	39	14	268	1;2;3;4
Q9NZN3	0.00207	5.8	EH domain-containing protein 3	12	3	74	1;2;3;4
P61604	0.02986	5.7	10 kDa heat shock protein, mitochondrial	17	11	152	1;2;3;4
P10721	0.03171	5.1	Mast/stem cell growth factor receptor Kit	21	3	122	2;3;4
Q15751	0.02800	5.0	Probable E3 ubiquitin-protein ligase HERC1	15	4	78	1;3
Q96AX2	0.04342	4.7	Ras-related protein Rab-37	9	1	62	1;2;3;4
Q9NVA2	0.02440	4.3	Septin-11	24	4	155	1;2;3;4
H7BZ55	0.00525	4.2	Putative ciliary rootlet coiled-coil protein-like 3 protein	33	15	162	1;2;3;4
P49419	0.01810	4.0	Alpha-aminoadipic semialdehyde dehydrogenase	16	5	101	2;3;4
P68871	0.03064	3.6	Hemoglobin subunit beta	57	22	324	1;2;3;4
O60240	0.02075	3.5	Perilipin-1	19	8	145	1;2;3;4
P07476	0.00327	3.4	Involucrin	21	7	145	1;2;3;4
Q9P2J3	0.02985	3.4	Kelch-like protein 9	14	1	81	1;2;3;4
P25311	0.04823	3.3	Zinc-alpha-2-glycoprotein	26	18	247	1;2;3;4
Q5VTR2	0.02421	2.8	E3 ubiquitin-protein ligase BRE1A	16	4	79	1;2;3;4
Q13228	0.03472	2.7	Selenium-binding protein 1	25	12	175	1;2;3;4
P00915	0.04038	2.6	Carbonic anhydrase 1	32	27	241	1;2;3;4
P69891	0.00816	2.6	Hemoglobin subunit gamma-1	11	2	67	1;2;3;4
P31948	0.01867	2.4	Stress-induced-phosphoprotein 1	26	13	151	1;2;3;4
P39019	0.00622	2.4	40S ribosomal protein S19	6	2	58	1;2;3;4
Q00610	0.04951	2.4	Clathrin heavy chain 1	66	29	393	1;2;3;4
P32119	0.03136	2.3	Peroxiredoxin-2	24	13	174	1;2;3;4
P04040	0.01111	2.2	Catalase	46	21	351	1;2;3;4
Q8NCM8	0.01132	2.1	Cytoplasmic dynein 2 heavy chain 1	44	13	204	2;3;4
P32926	0.03068	2.3	Desmoglein-3	14	4	78	1;2;3;4
P16070	0.01762	2.5	CD44 antigen	14	8	101	1;2;3;4
Q03135	0.03293	2.5	Caveolin-1	8	2	68	1;2;3;4
Q13418	0.00689	2.5	Integrin-linked protein kinase	23	9	146	2;3;4
P78527	0.00561	2.7	DNA-dependent protein kinase catalytic subunit	17	2	89	1;2;4
Q8IZD2	0.00827	2.7	Histone-lysine N-methyltransferase 2E	12	4	63	1;2;3;4
P00352	0.00021	2.7	Retinal dehydrogenase 1	32	13	207	1;2;3;4
Q14141	0.00551	2.8	Septin-6	25	4	162	1;2;3;4
Q6ZQQ6	0.00563	3.0	WD repeat-containing protein 87	85	21	447	1;2;3;4
Q96M02	0.00110	3.2	Centrosomal protein C10orf90	11	1	70	2;4
Q9NZM1	0.04435	3.8	Myoferlin	45	20	225	1;2;3;4
P35968	0.00024	5.0	Vascular endothelial growth factor receptor 2	24	4	120	1;2;3;4
P14868	0.03443	5.5	Aspartate--tRNA ligase, cytoplasmic	13	6	64	1;2;3;4
P58107	0.00067	5.6	Epiplakin	113	40	691	1;2;3;4
Q7L576	0.00708	11.3	Cytoplasmic FMR1-interacting protein 1	20	5	99	1;2;3;4